On a Mechanism of Spalling of Concrete Under Fire Conditions.

Sertmehmetoglu, Y

ON A MECHANISM OF SPALLING OF CONCRETE UNDER FIRE CONDITIONS

Thesis submitted to the University of London

for the degree of Doctor of Philosophy

by

Yavuz Sertmehmetoglu

Department of Civil Engineering

University of London, King's College

Strand

London WC2

July 1977

ABSTRACT

Spalling in fire conditions may be defined as the removal of surface material from concrete exposed to excessive heat.

This type of failure is generally unpredictable , occurs at early stages of exposure to heat, and may substantially reduce the fire resistance of members by exposing the reinforcement to direct heat.

This thesis is concerned with the cause of spalling.

Existing theories are reviewed.It has been pointed out that none of these theories are satisfactory.

A mechanism for spalling of concrete,first introduced by Dougill(I.I8),has been considered.In this,it is suggested that spalling may be caused by steam pressures , inside cracks parallel to the heated surface ,causing failure of the material between the crack and the heated surface. It has also been pointed out that such cracks may be expected to form under biaxial state of stresses.

The pressures necessary to cause failure in such circumstances are found experimentally.The steam pressures actually generated in test specimens exposed to heat are also measured.

The results showed that the mechanism is plausible.

As a preventive measure biaxial compression is suggested to be avoided.

ACKNOWLEDGEMENTS

Firstly,I wish to acknowledge the guidance and considerable help given to me by my supervisor,Prof.J.W.Dougill of King's College,London.

My thanks are due to Fire Research Station which financially supported this research project,in particular to Mr.H.L.Malhotra,Head of the Station,for allowing me to use the facilities of the station,to Mr.A.Morris and Mr. J. Hopkinson for their valuable advice and assistance.

My thanks are also due to Mr.A.W.Blake,the chief technician, Mr.R.Earll,Mr.C.Blakey,and other members of King's College Civil Engineering workshop,who were involved in making and assembling the apparatus,to Mr.R.Hunt who took the photos.

I also acknowledge the useful suggestions given by Dr.J.Newman,from Imperial College,London,who allowed me to carry out some of my tests at Imperial College , and assistance given by Mr.R.Glenn during these tests.

TABLE OF CONTENTS

NOMENCLATURE

N.B. In addition to the list below all symbols are defined where they first appear.

ε	Effective porosity
ϕ	Original moisture content by volume
δ	fraction of vapour readsorbed
Λ	thickness of moisture clog
q	heat flux
T_f	furnace temperature
T_s	surface temperature
T_ℓ	temperature at the interface
λ	coefficient of thermal conductivity
Q	isosteric heat of adsorption
h	heat transfer coefficient
ρ	density
v_1	rate of progression of the interface CD caused solely by the removal of water by evaporation
v_c	rate of progression of the interface CD caused solely by the pressure
v_{CD}	rate of progression of the interface CD
	tensile strength of concrete
K	permeability
P_1	pressure at a distance l from the interface
l	distance from the heated surface to the interface
	shear stress on the walls of the capillaries

v_{av} average velocity

v_v velocity of vapour

r radius of capillary

v_{100} velocity of 100 C evaporation front

A_p area of pores per unit area of concrete

R drag force on a capillary tube

A_1 number of pores per unit area of concrete

$\sigma_{c_1}^{c}$ stress due to thermal gradient

$\sigma_{c_1}^{H}$ stress due to external loading

volume increase factor (ratio of volume of vapour to the volume of water of the same weight)

K_w permeability of concrete to water

K_v permeability of concrete to vapour

η_w dynamic viscosity of water

η_v dynamic viscosity of vapour

n_b volume porosity

n_s surface porosity

R specific gas constant

E Modulus of elasticity

ν Poisson's ratio

v_a actual velocity

v_d discharge velocity

Chapter I

INTRODUCTION

1·1 Background material

Although calcined gypsum was used as cement by the Egyptians and calcined limestone by both Greeks and Romans, the first dependable hydraulic cement was made by Joseph Aspdin, an English mason, in 1824. His product was called Portland cement because it resembled a building stone that was quarried on the Isle of Portland off the coast of Dorset.

Reinforced concrete was first developed by such people as W.B.Wilkinson of Newcastle-on-Tyne in 1854, and the Frenchmen, J.L.Lambot in 1855, F.Coignet in 1851. By the turn of the century forty-three patents had been granted on reinforced concrete. Most of its basic properties had been examined and methods had been established for design and detailing.

As a construction material good reinforced concrete appeared to be more attractive economically than other construction materials used previously, including cast and wrought iron, steel, wood, masonery etc.. This was mainly due to its flexibility in construction and its inherent durability leading to minimum maintenance. However, more important than these aspects in providing an incentive for the use of reinforced concrete was the idea that concrete construction was 'fire proof'. This was a particularly attractive feature when the material was compared with traditional construction in timber or cast iron and was also a selling point in the battle with the new rival, structural steelwork.

Maybe as a result of this competition between materials

and also because of a growing history of fire losses, the British Fire Prevention Committee was formed in 1897 to represent the interests of various insurance bodies and to advise architects and engineers in their choice of fire resisting materials. In 1899 the committee opened its first testing station near Regent's Park, London. In 1903 the International Fire Prevention Congress was held in London. It was agreed not to use the term 'Fire proof', which could be misleading and contentious, and to substitute for it the term 'Fire resisting', since this described more correctly the varying qualities of the different materials, and structures intended to resist the effect of fire for shorter or longer periods, at high or low temperatures, as the case may be.

The first British Standard on fire resistance tests was issued in 1932 (1·1). Since then, British Standard 476 has been revised three times, in 1953, 1972 and 1975. The second revision deals only with fire resistance tests (1·2) and reflects the growing harmonization between different national codes by incorporating most of the recommendations given in ISO/R834 (1·3) produced by International Organisation for Standardization in 1968.

Almost without exception, the various standards define 'fire resistance' in terms of the performance of structural elements or members in furnace tests using a standard heating regime.

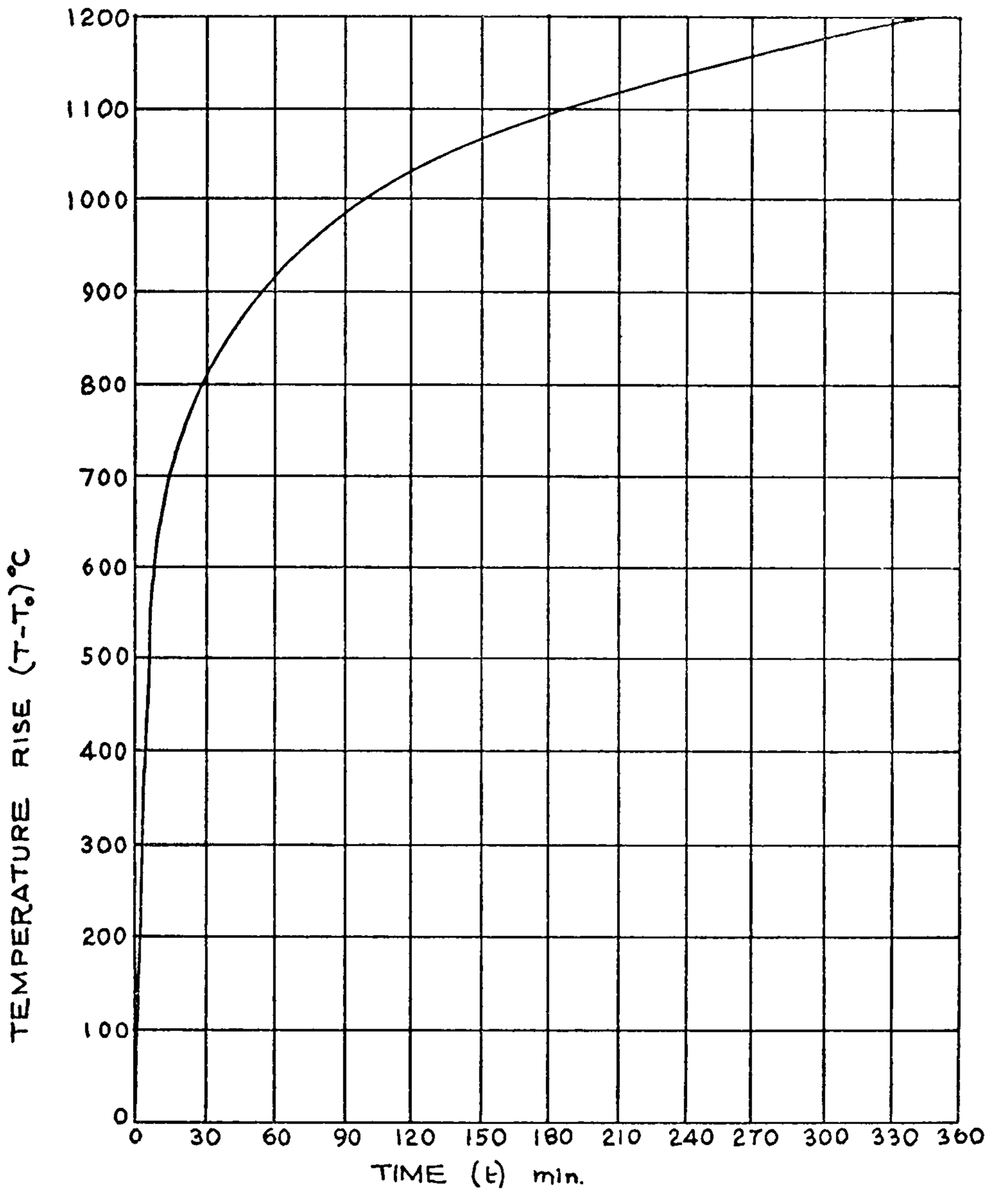

FIG. 1.1 STANDARD TIME-TEMPERATURE CURVE

[BS 476, (1.9)]

These tests, termed 'Standard Fire Resistance Tests', provide information on the relative performance of the individual members by the exposure of the test specimens to the specified condition of heating called the 'Standard exposure condition.' (Fig.1·1). The latter is expressed in the form of a time/ambient temperature relationship, and, even before the introduction of ISO (1·3), this relationship differed only slightly between different national standards.

As defined by ISO (1·3), fire resistance is the time expressed in hours and minutes from commencement of the test until failure occurs. This might be collapse or excessive deformation in which case failure is said to be due to loss of stability. Alternatively, failure may be due to the formation of holes or fissures that allow the passage of flame (loss of integrity), or, by excessive heat transfer (i.e. too little insulation.)

The definition of fire resistance is convenient in providing a basis for fire test procedures, but, clearly, lacks precision when used in relation to a complete building subject to fire. Underlying the fire test philosophy is the implication that if an element performs satisfactorily in a fire test, a similar element will do so as part of a structure exposed to fire. This is not necessarily so. Thus, although the standard exposure curve is based on an early appraisal of the results of burn-out tests by Ingberg(1·4), the exposure conditions that obtain in any particular fire might be very far from standard . In addition,

the manner in which a member is loaded or connected within a structure could provide boundary conditions more complex than any that are included in current fire test procedures.

Both these difficulties are recognised in current work on fire resistance. Attempts are in hand to predict the likely exposure conditions in actual structures, and, relate these to the results of fire tests (1·4). In addition, the behaviour of continuous+ structures has been studied extensively for a number of years at the PCA laboratories (Carlson et al.(1·5), Selvaggio et al (1·6)) and elsewhere, and this has led to the concept of 'Rational Design for Fire Resistance' which was recently taken up in the report of the Joint Committee of the Institution of Structural Engineers and the Concrete Society on Fire Resistance of Concrete Structures (1·7). However, neither of these developments are likely to produce major changes in the practice of design for fire resistance for some years. In the meantime, regulations and design will remain based on empirical evidence derived from tests on individual members and the relation to complete structures will remain arbitrary.

Clearly, there is the danger that this approach may become less acceptable and could produce unsafe structures, as design procedures for loadings other than fire aim at greater precision, and load factors are reduced.

Footnote

+ See Appendix I

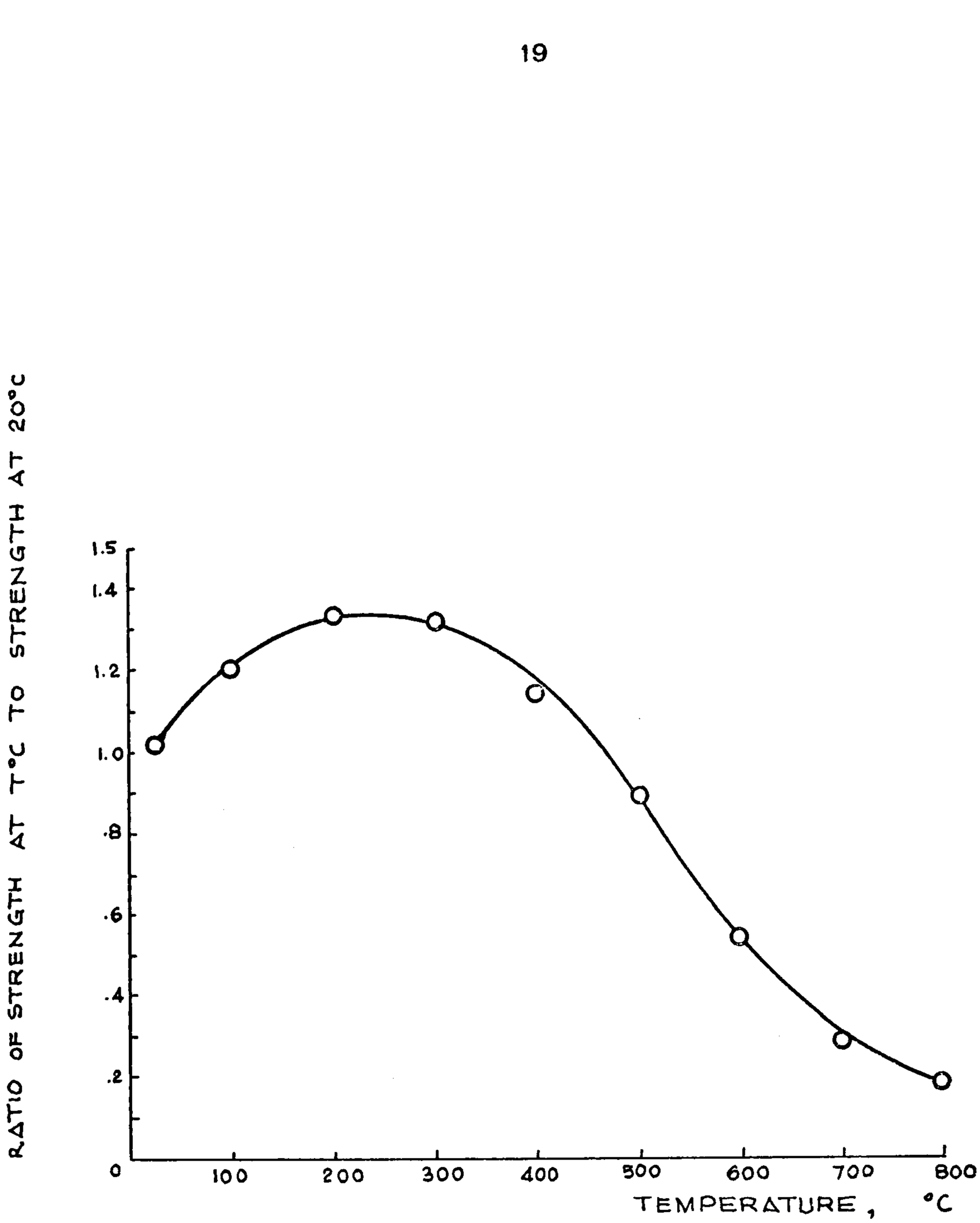

FIG. 1.2 TYPICAL STRENGTH OF STEEL BARS TESTED AT ELEVATED TEMPERATURES

[AFTER CORSON, (1.19)]

Ignoring these possible future trends, past experience of reinforced concrete construction suggests a general view that, provided the reinforcement cover is maintained and sections are not too slender, behaviour of members in fire tests is usually stable and predictable. However, there are circumstances when local failure occurs by the removal of the surface material exposed to fire. This form of failure, called 'spalling' may occur within only the first 30 minutes of a standard fire test and invariably results in a reduction in fire resistance (1·8).

In this context the following types of failure should be considered:

1) Due to spalling, part of reinforcement essential to structural stability may be exposed to fire, resulting in rapid heating of the steel and reduction of its tensile strength (Fig.1·2)to the applied stress level. In statically determinate structures failure will be comprehensive. The effects may not be so serious in continuous structures although there is again the possibility that the occurrence of spalling could lead to an early development of a mechanism sufficient for collapse.

2) Spalling may reduce the concrete cross section so that the member may no longer perform its load-bearing and fire-separating functions. Failure of this type is mostly observed in thin members, such

as slender columns, thin floor slabs, thin webs of T and I - beams, especially when loaded in compression. Here again the effects of continuity may be important. As discussed in the Appendix I, restraint from adjoining members may lead to high compression stresses and so influence the occurrence of spalling.

3) Spalling may produce holes in space-enclosing members without substantially altering their load-bearing capacity. Nevertheless, failure could be considered to have occurred by loss of integrity according to BS 476 (1·2) as the formation of holes would allow the passage of flame. Clearly, not all types of spalling cause the same extent of damage. It is therefore up to the designer to decide whether spalling should be prevented at all costs or whether some degree of spalling is permissible, depending on the particular situation, thus establishing a compromise between safety and economy. Such a decision, on the other hand, requires a full understanding of the cause of spalling leading to practical and economical counter measures.

At present, spalling still remains relatively unpredictable, even under carefully controlled laboratory conditions (1·9). Knowledge about the relation between spalling and the factors which affect it, is still inadequate to give a quantitative explanation of its

mechanism. This uncertainty seriously undermines any effort to provide a theoretical approach to structural fire resistance, particularly for compression members, and is met only by the inclusion of additional reinforcement or insulation in a wholesale manner.

Clearly, research on spalling could have considerable value for safety and economy if it provides a means of recognizing where spalling is likely to occur and also suggests methods of minimising its effect. To do this it is necessary to understand how spalling occurs, that is, to obtain a comprehensive view of the mechanism of spalling, so that, the effects of all the various influential factors can be anticipated in some way. In broad terms this is the object of the current work which is however directed particularly to one form of spalling only. Before dealing with this it is convenient to discuss the various forms in which spalling occurs or has been observed.

1·2 Spalling of Concrete

It has already been suggested that there are different mechanisms of failure causing local damages in fire. Therefore, for a systematic study, it is helpful to distinguish between these different types of breakdown.

One such distinction is suggested by Harmathy (1·10) between 'Thermal Spalling' and 'Moisture Spalling' depending on the probable cause of breakdown. This classification, however, is rather misleading, as there

TABLE 1·1 (after Dougill (1·11))

Types of Spalling

1. General or Destructive Spalling

This is of a violent nature and occurs at an early stage of heating. This form of spalling causes extensive damage. If it occurs in a fire test it marks the end of the test.

2. Local Spalling

Surface Spalling

This involves local removal of surface material . Sometimes violent.

Aggregate Splitting

Failure of aggregate near the surface causing small surface spallings.

Corner Separation

Removal of external corners from beams and columns . Occasionally violent.

3. Sloughing off

Gradual progressive mode of breakdown, involving partial separation of layers of surface material from the member.

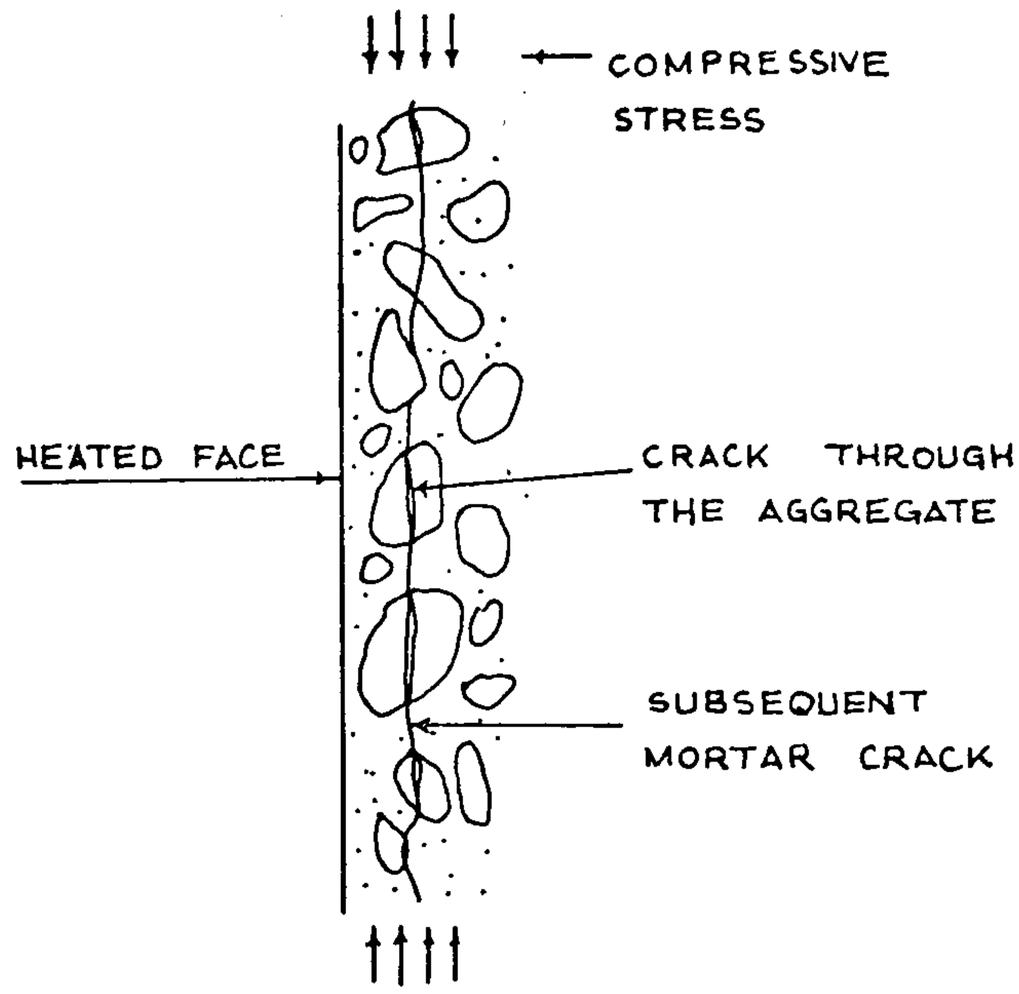

FIG. 1.3 AGGREGATE SPLITTING

[AFTER DOUGILL, (1.7)(1.11)]

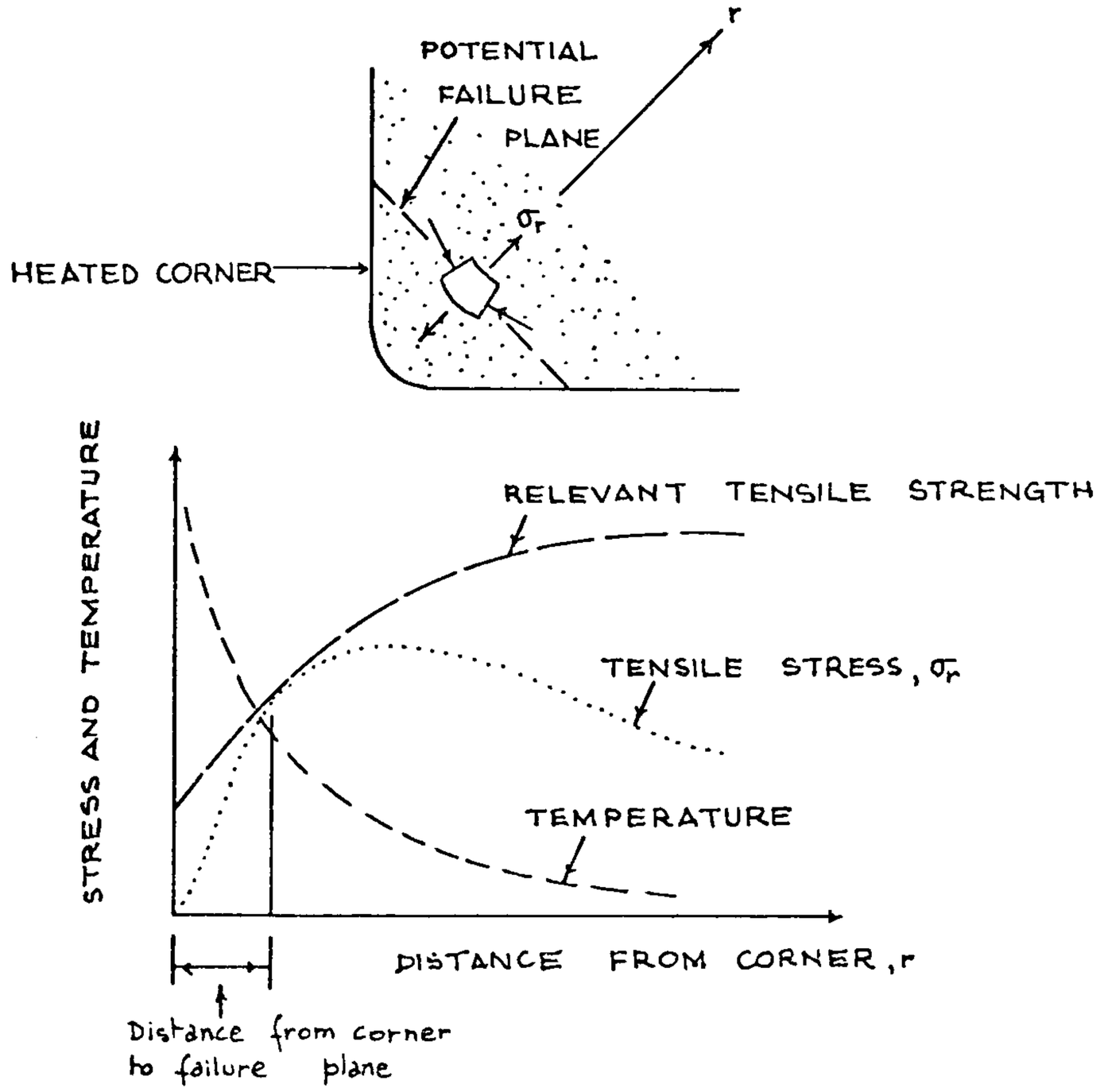

FIG. 1.4 DIAGRAMMATIC REPRESENTATION OF CONDITIONS AT START OF CORNER SEPARATION

[DOUGILL, (1.7)(1.11)]

still is not agreement on the exact cause of spalling. The classification based on the observed features, suggested by Dougill (1·11) and similar to that used independently by Meyer-Ottens (1·12), seems more useful in practical applications. (Table 1·1).

Plausible mechanism for aggregate splitting, corner separation, and general spalling have already been proposed (1·7) Dougill (1·11) These mechanisms can be briefly summarized as follows:

a) Aggregate splitting

Here it seems that the mechanism of failure is somewhat similar to the manner in which concrete specimens, subjected to a compression load fail in the Brazillian test. During heating, thermal stresses close to the surface of a member will be predomimantly compressive in directions parallel to the heated surface. The aggregate thus splits in this direction as indicated in Fig.1·3.

b) Corner Separation

This type of failure appears to be due to a component of tensile stress, which causes splitting across the corner. A typical situation at failure is shown in Fig. 1·4 in which the stress induced by heating is equal to the strength of the material in tension + at a section some distance away from the heated corner.

Footnote

+ Actually the stress is nearer shear than pure tension because of the tangential compression. (Fig.1·4)

c) General Spalling

A view of this type of spalling has been provided by Dougill (1·11) as a type of instability which would be possible in slender members under high compression loading or restraint. In essence this approach focuses attention on the behaviour of concrete in compression after the peak stress or strength has been achieved and can be regarded as an extension or refinement of Saito's (1·13) view of spalling due to compressive stress.

Surface Spalling

There remains, however conflicting views as to the cause of surface spalling. The main difference of opinion is whether the thermal stress (Saito 1·13) or pore pressure due to steam (Shorter and Harmathy 1·14) (Harmathy 1·10) is the most significant variable.

Saito (1·13) suggests that explosive spalling is a compressive failure due to non-linear temperature distribution across its section. The author apparently rejects the possibility of steam pressures causing failure as suggested by other workers.

Saito assumes concrete to be a linear elastic, brittle material with temperature dependent properties. On this basis it follows that for a reinforced concrete section subjected to standard furnace test, stresses develop consisting of compressive stresses acting both on the heated and on the unexposed faces, with tensile stresses acting in the middle portion. The analysis

suggests that the compressive stress at the surface is increased by longitudinal restraint (or prestress) but is reduced by internal tensile cracking. This pattern is modified by the effects of prestress or axial load which would both tend to put the whole section in compression and increase the compressive stresses at the heated face. Saito considers spalling to occur when the compressive stress in the outer fibres reaches a limiting value. Thus his theory apparently accounts for the effects of axial restraint, prestress and longitudinal loading. However Saito considers the effects of moisture to be merely due to the difference in temperature gradient which results in a different moisture content.

There are, however, some important deficiencies in Saito's theory. As Dougill (1·11) noted, these arise because concrete is not a linear material and failure does not necessarily occur when the compressive stress at a point reaches a maximum value. Also, the theory fails to explain why the failure is sudden.

Furthermore, the theory suggests that explosive spalling should occur most frequently in members of very large cross-section, which is contrary to usual experience.

Finally, the experimental work reported by Akhtaruzzaman and Sullivan (1·15) and the tests described in Chapter 6 of the present work clearly indicate that spalling occurs much more frequently

in water cured specimens as opposed to moist cured ones. However, the theory proposed by Saito seems to be in contradiction with this experimental observation in the sense that the theory would predict an improved fire resistance for water cured specimens which would undoubtedly have a stronger layer near the surface due to more complete hydration.

At the other extreme a number of research workers (Shorter and Harmathy (1·14), Harmathy (1·10) and Meyer-Ottens (1·12)) believe that spalling is due to steam pressures generated in concrete during heating. A detailed view of this concept was first provided by Shorter and Harmathy (1·14) and subsequently by Harmathy (1·10). The type of spalling envisaged was termed 'Moisture Clog Spalling' and will be discussed in detail in Chapter 3.

According to Shorter and Harmathy (1·14), if the surface of a concrete member is heated, desorption of moisture occurs in a thin layer next to the heated surface. Some of the vapour released escapes to the atmosphere through the heated face. The remainder of the vapour moves inwards, towards the cooler material, and may be reabsorbed. Movement of the steam and condensation in the cooler regions lead to free water saturating some capillaries and causing a complete blockage or 'Moisture Clog' to further movement of steam into the member. Shorter and Harmathy (1·14) concentrate their attention on this effect whereas both Waubke (1·16) and Meyer-Ottens (1·12) base their

Table I.2 Summary of experimental work on estimation of pore pressures generated during heating of concrete.	Steam pressure $MN/_m^2$	Temperature °C
I. Thelandersson (2.21) tested I500 x I50 x I50 mm mortar prisms under torsional loading ,exposed to transient heating.He obtained explosive spalling after I hour heating at a rate of 8°C/min increase.The pressure recorded at the time of spalling at the centre of the specimen was 0.65 $MN/_m^2$, and the temperature,less than I50°C.	0.65	I50
2. Nekrasov et al.(2.20) slowly heated large blocks of refractory concrete from one side and measured the pore pressure generated at various depths. The maximum pressure recorded was 0.70 $MN/_m^2$ and the temperature I40°C.	0.70	I40
3. Dougill (1.11) heated planks of different grades of concrete from one side, and measured the temperature variation with time at various points through the depth of the specimens.Because of heat required for desorption,the rate of temperature rise was very much reduced at any point during vaporization. This effect showed itself as a step in a graph of temperature against time. Maximum temperature at which vaporization occurred ,determined this way by Dougill was around I50°C.No spalling occurred.	—	I50
4. Tests carried out by Meyer-Ottens (1.12),where reinforced concrete specimens were heated from both sides showed that spalling occurred when temperature of the interface was less than I50°C.No pressure measurement was made.	—	I50

assessement of the pressures induced on the resistance, to flow of vapour arising directly from drag forces on the walls of the capillaries. As will be discussed in Chapter 3, there are many approximations used in either approach. However, it appears that the pressure generated within the steam in the concrete pores is likely to be appreciably less than the tensile strength of concrete, at least for the rates of heating used in standard fire tests. This view is supported by experimental evidence in that steam is normally formed at temperatures less than 150° C in fire tests, the temperature being marked by a depression in the rate of temperature rise at points within the concrete where heat is being used to vaporize water. There have also been attempts to measure the pore pressure generated in heated concrete, although the rates of temperature rise have been usually less than in the standard test. These results are summarized in Table1.2 which shows that spalling did occur in some instances but that the pressures recorded were all significantly lower than the tensile strength of concrete. These results suggest that it is not sufficient to consider pore pressure to be the sole cause of surface spalling even though experience from fire tests indicates that the moisture condition is an important variable.

The defficiencies in the two extreme views of spalling suggest that an alternative view is required. Some workers have suggested that surface spalling may

be due to a combination of pore pressure and thermal stress rather than either influence alone and a Dutch group (1·17) has proposed a programme of research based on this idea and their experience of the results of fire tests in their own laboratory.

The object of the present work is to investigate a mechanism for spalling which would account for its local character and its dependence on both pore pressure and applied stress. A mechanism of this sort was originally proposed by Dougill in a report to the Fire Research Station (1·18). This suggested the form of the mechanism but provided no direct evidence as whether it would work in the manner supposed, and also be relevant to the magnitudes of pressures actually generated in concrete structures. Accordingly experiments have been planned and undertaken to investigate both these aspects. The experiments comprised two series of tests described in Chapters 5,6 and 8. These deal with the pressure developed in concrete during heating (Chapter 5), and the pressure necessary to 'break out' the material outside a subsurface crack under various conditions of loading and heating (Chapters 6 and 8). The description of the experimental work is preceded by a review of experimental evidence on spalling in Chapter 2, and an account of theoretical work aimed at assessing pore pressures in heated concrete (Chapter 3). Chapter 4 provides a description of the proposed mechanism for spalling and deals with the design of the experimental

programme. Conclusions from the work are brought together in a final Chapter. (Chapter 9).

Chapter 2

EXPERIMENTAL EVIDENCE RELATED TO SPALLING

2.1 Introduction

In Chapter I it was pointed out that standard fire resistance tests are performed in an idealised fashion and that their main objective is to obtain information on the relative behaviour of different structural members under standard exposure conditions. It was also noted that such standardization of information is necessary among fire research laboratories and other related organizations on national and international level. However, a recent international survey on spalling of concrete carried out by CIB Commission (2.1) showed that there were conflicting views on spalling among many research laboratories. This is partly due to the different laboratory conditions and specimen preparation techniques adopted, which are either not included in International Standards, or, although stated, are difficult to apply. For instance, although restraining and conditioning, among other factors, are known to affect spalling, the CIB survey showed that only 3 out of 12 laboratories possessed special conditioning facilities, and that, others kept the specimens in the laboratories until the moisture content was acceptable. Similarly, only 3 out of 12 laboratories possessed restraining facilities, although ISO (2.2) clearly indicates that the methods adopted for supporting and restraining the ends of a test specimen during a test should be similar in nature to those which would be applied to a similar element in service.

Nevertheless, there are some general trends concerning spalling observed in fire tests on which there is agreement. These are:

1. Spalling occurs only within the first half hour or so after the start of the standard fire test. (CIB report (2.1), Barends (2.3), Kordina (2.4)).
2. Thin sections are more liable to spalling than thick ones. (Ashton and Bate (2.5), Davey and Ashton (2.6) Meyer-Ottens (2.7))
3. Siliceous aggregate is more liable to cause spalling in concrete than calcareous aggregate (CIB report (2.1), Davey and Ashton (2.6)).
4. External corners are particularly susceptible to spalling. (Meyer-Ottens (2.7))
5. No spalling occurs below certain moisture content level. (Meyer-Ottens (2.7,2.8) Christian e et al (2.9)

In short, experience on spalling gained from fire tests seems to be of only a superficial nature, and, clearly, experiments specifically designed to obtain information on the cause and occurrence of spalling are required.

2.2 Meyer-Ottens' Tests

The most comprehensive spalling tests carried out for this purpose are by Meyer-Ottens (2.7, 2.8,2.IO-2.I3).The author investigated the effect of aggregate type, concrete quality, thermal stresses, amount and arrangement of reinforcement, shape of the member, moisture content,

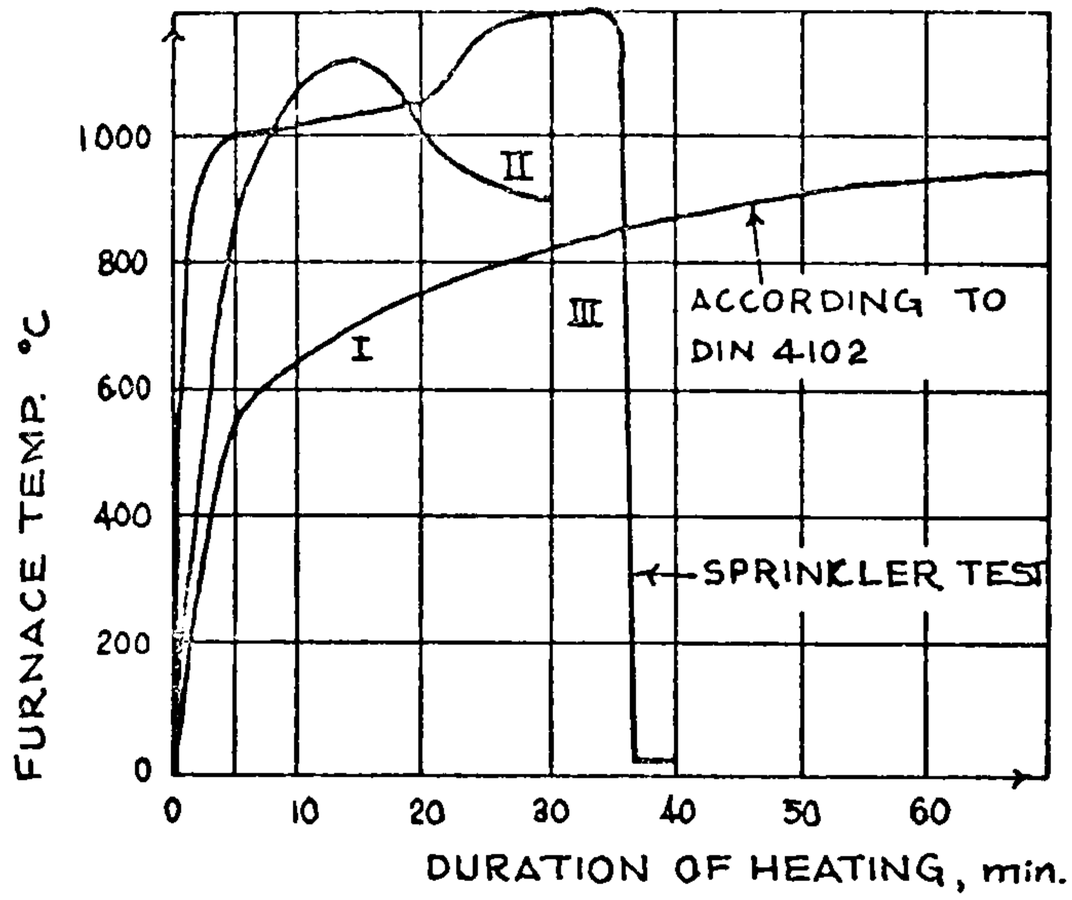

FIG. 2.1 HEATING RATES USED BY MEYER-OTTENS

[AFTER MEYER-OTTENS, (2.8)]

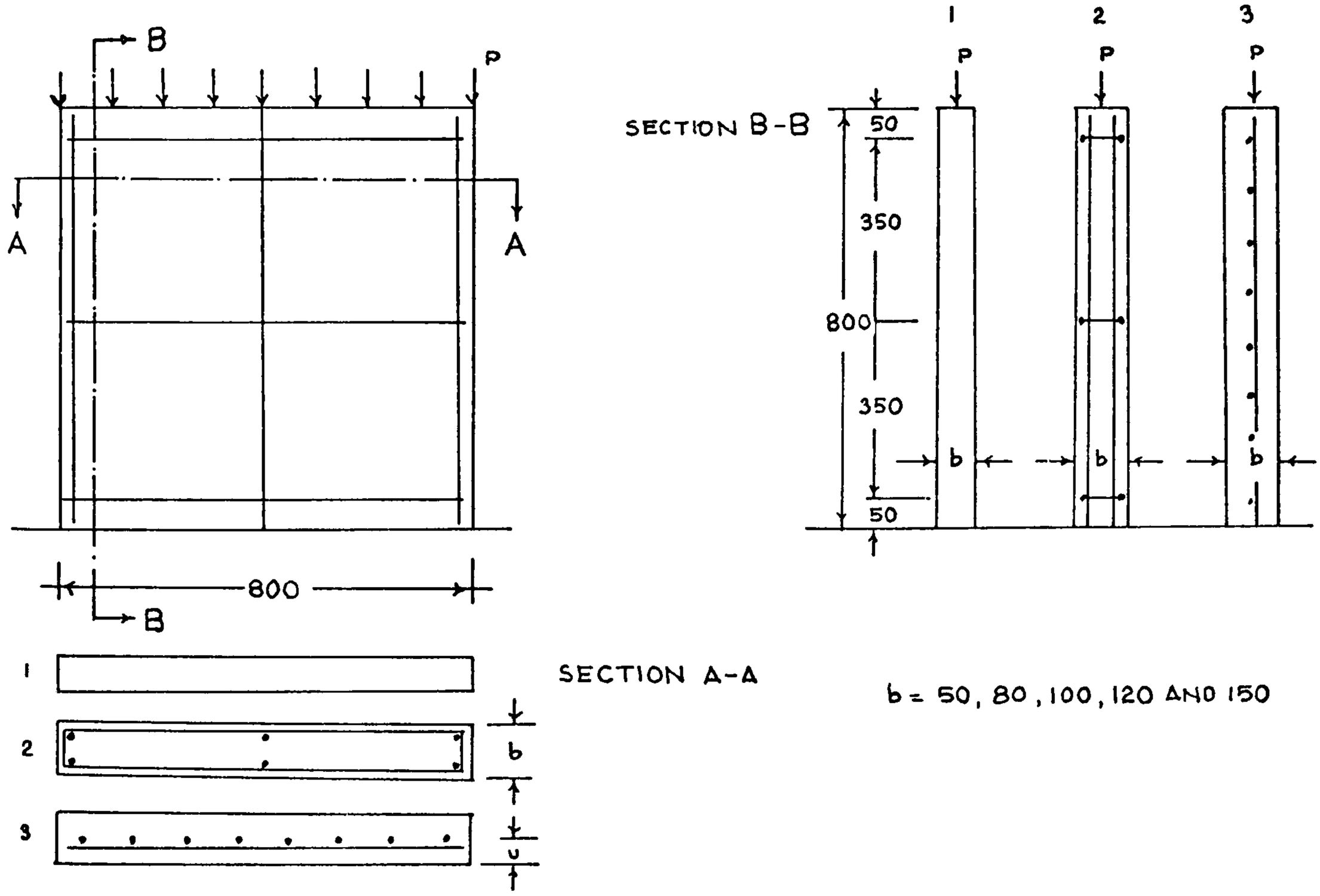

FIG. 2.2 DIMENSIONS AND REINFORCEMENT DETAIL OF THE TEST SPECIMENS DESCRIBED IN TABLES 2.8 - 2.11

[AFTER MEYER-OTTENS, (2.8)]

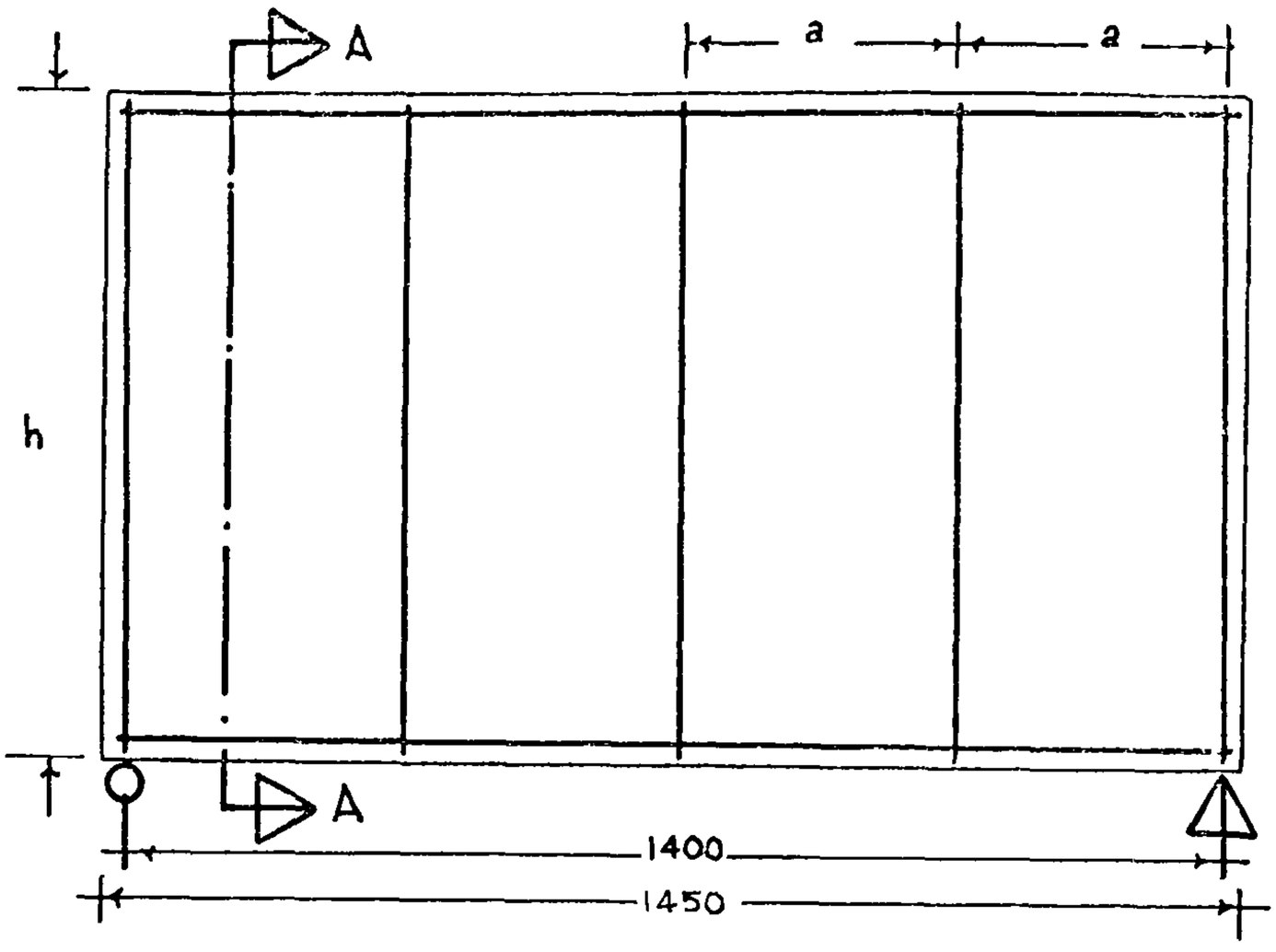

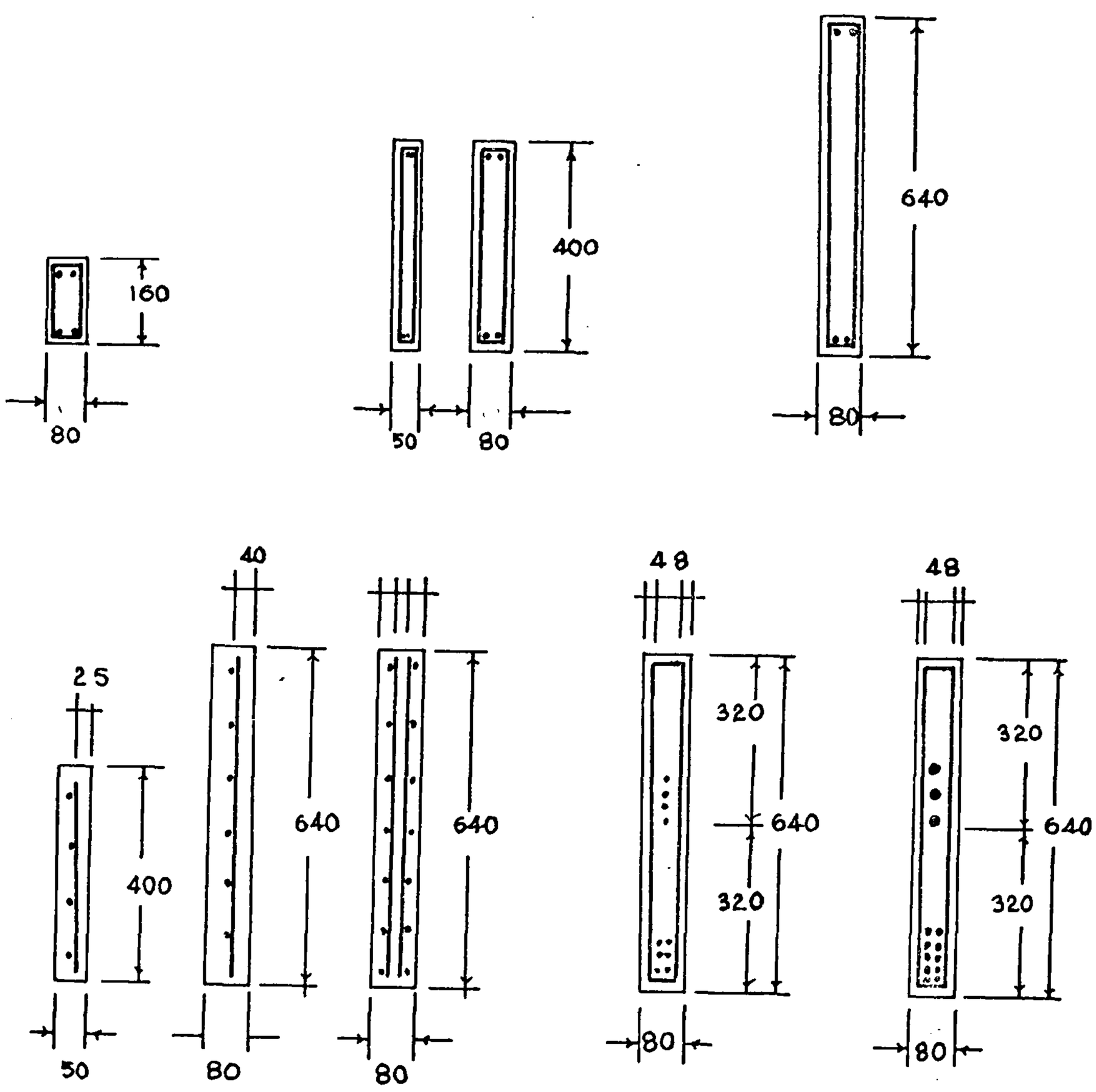

FIG. 2.3 DIMENSIONS AND REINFORCEMENT DETAIL OF SPECIMENS HEATED FROM THREE SIDES DESCRIBED IN TABLES 2.5 - 2.7

[AFTER MEYER-OTTENS, (2.8)]

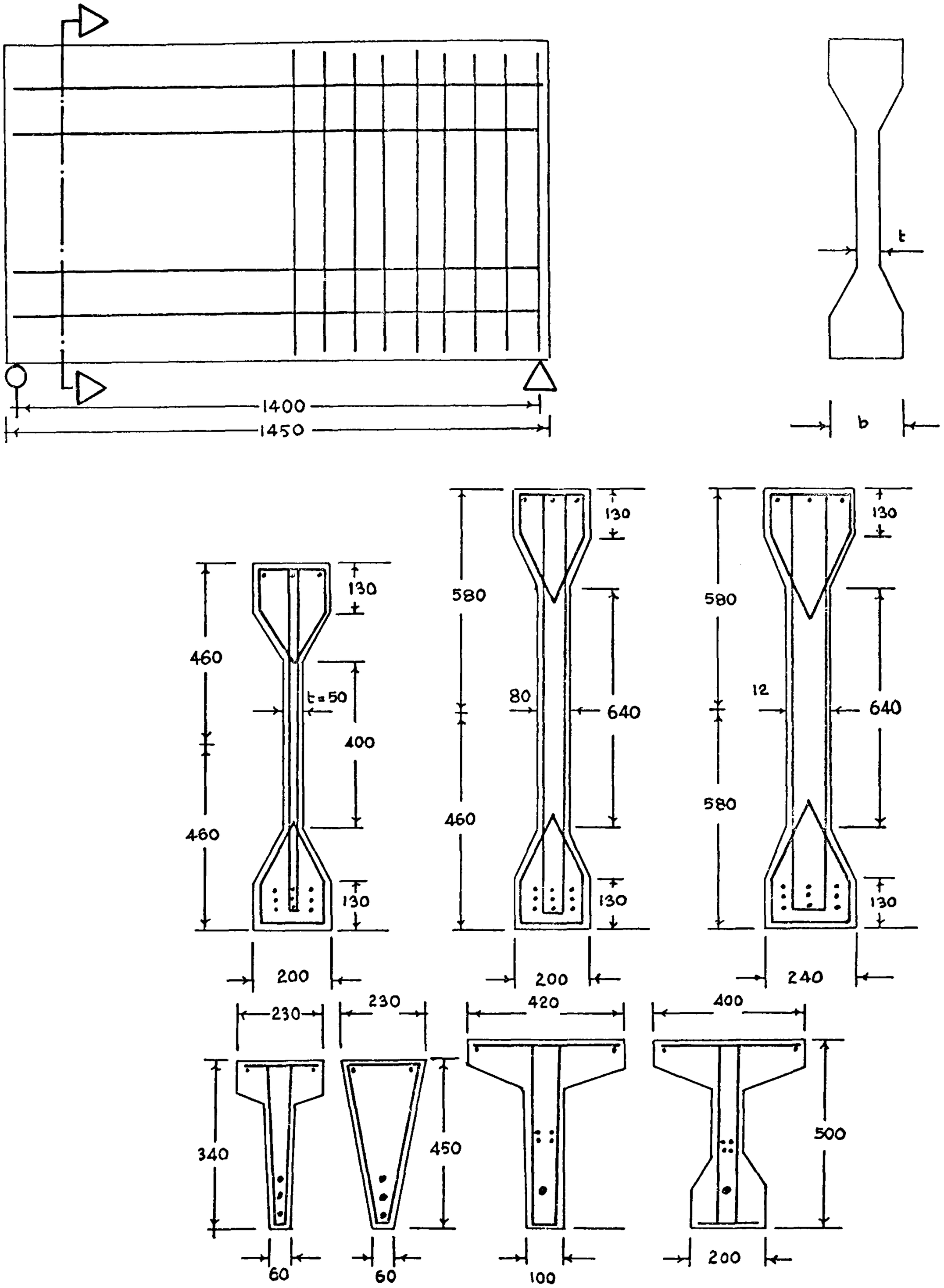

FIG. 2.4 DIMENSIONS AND REINFORCEMENT DETAIL OF THE SPECIMENS DESCRIBED IN TABLES 2.1 , 2.2

[AFTER MEYER-OTTENS, (2.8)]

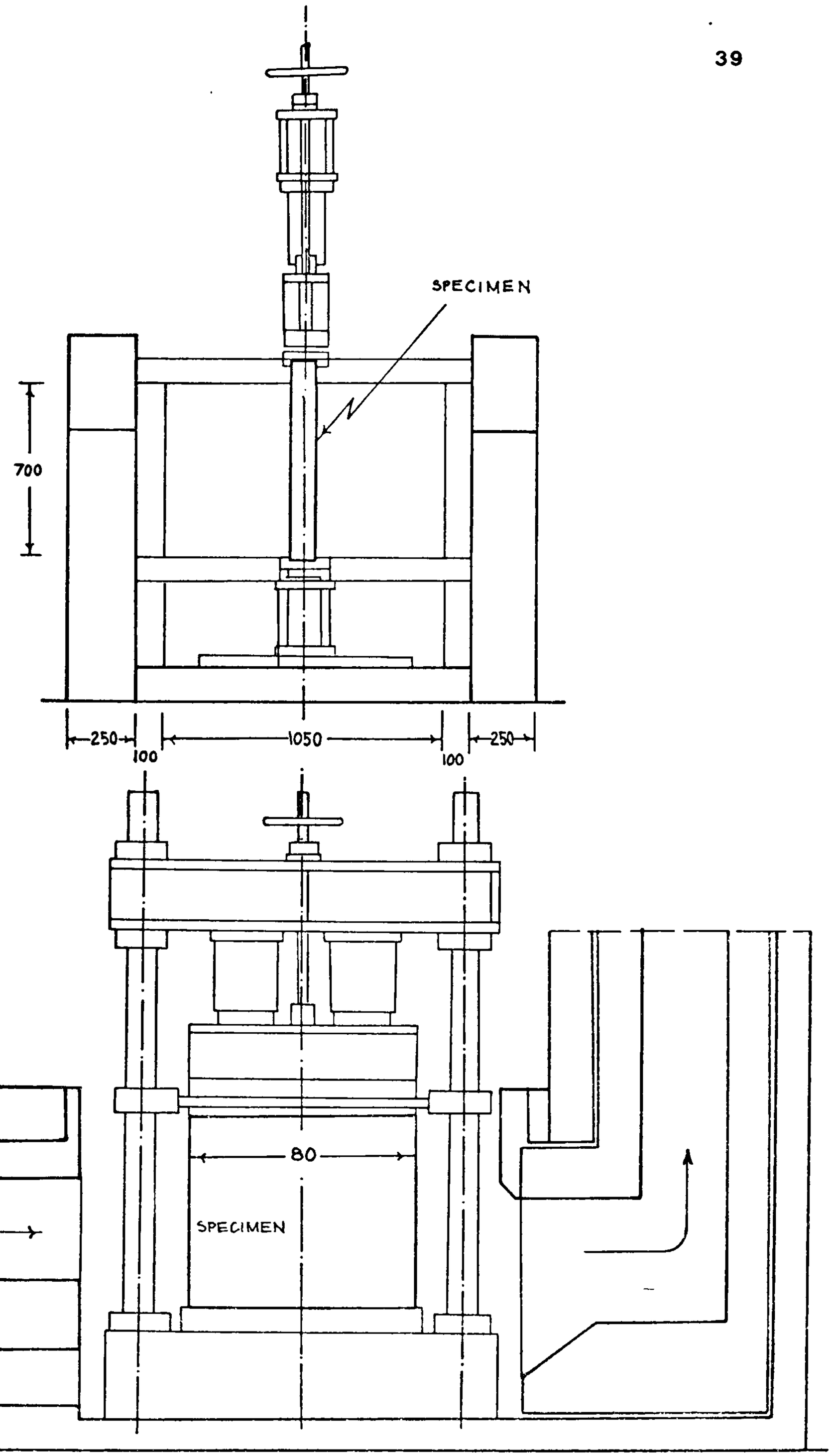

FIG. 2.5 LOADING ARRANGEMENT AND FURNACE USED BY MEYER-OTTENS (2.8)

and compressive stresses on spalling by testing conventi onally reinforced and prestressed concrete members of various sizes and shapes.

In these tests three different mixes corresponding to three different compressive strengths, 22·5 MN/m^2, 45 MN/m^2, and 60 MN/m^2 have been used. Also, three different heating rates were used in order to obtain different distribution of thermal stress.

These were, rate I as proposed in DIN 4102 (2.14), and rate II and rate III being somewhat higher. Furnace tests where rate III were applied were ended by a sprinkler test. (Fig.2.1)

Members were either conventionally reinforced or prestressed. The effect of additional reinforcement in mid plane of slabs heated from both sides was also investigated. (Fig.2.2 and Fig,2.3)

Members which were not loaded externally were simply supported over a single span. No continuous members could be tested due to technical limitations. For the same reason, the length of the members was kept constant at 1450mm, with the exception of the 800 x 800mm panels, but different cross sections including rectangular, trapezoidal shapes, I-sections and T-sections of various thickness were tested (Fig.2.4).

Compressive stresses were induced by dead weight, prestressing, or in the case of 800 x 800mm panels, by the application of an external load using the loading arrangement shown in Fig.2.5.

Table 2.I Effect of cross-section, dimensions, and reinforcement on spalling.

Cross-section mm x mm	Reinforcement	Stirrup spacing mm	Loading	Mix	Concrete quality	Concrete moisture content %	Application of heating	Heating rate	Remarks
50x400		350	g	M2	B450	5-6	3 sides		no spalling
50x400	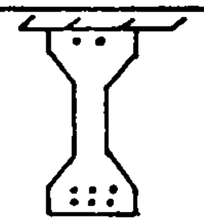 3ø6 ø6 9ø6	200 100 50 100						I II	explosive surface spalling
80x160 80x400 80x640	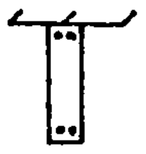 2ø6 2ø6	350		MI				I	small surface spalling specially with heating rate II
80x640	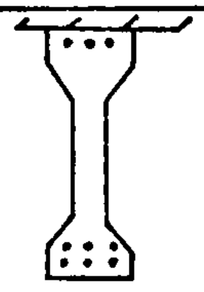 3ø6 9ø6	200 100 100 100 50		M2	B450	5-6		II I	
120x960 120x640		350 50		MI M2				II	

Table 2.2 Effect of cross-section, dimensions, and reinforcement on spalling.

Dimensions and reinforcement	Stirrup spacing mm	Loading MN/m^2	Mix	Concrete quality	Concrete moisture content %	Application of heating	Heating rate	Remarks
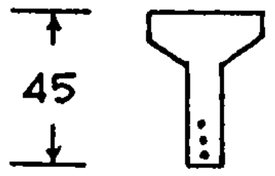 45 — 2 ϕ6, 3 ϕ24	50	0	MIa	B450	5-7	3 sides	I	surface spalling
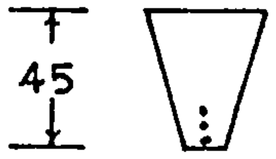 45 — 2 ϕ6, 3 ϕ24	50	0						no spalling
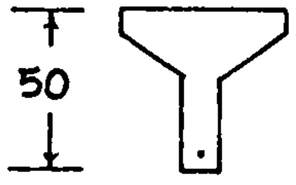 50 — 4 ϕ8, 4 ϕ8	200	10.9						explosive surface spalling
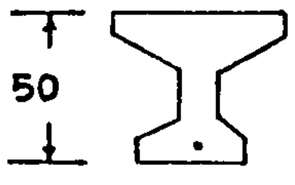 50 — 4 ϕ8, 2 ϕ8	200	7.5						no spalling
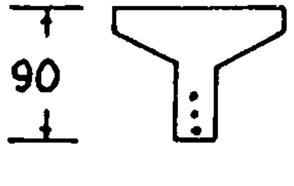 90 — 4 ϕ8, 12 ϕ8	200	17.6						explosive surface spalling
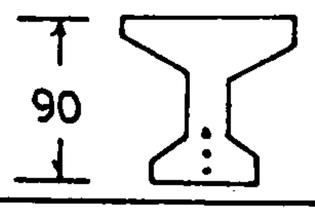 90 — 4 ϕ8, 12 ϕ8	200	11.4						explosive surface spalling

Table 2.3 Effect of cross-section, dimensions, and reinforcement on spalling. Rectangular members with various reinforcement arrangement.

Cross-section mm x mm		Stirrup spacing mm	Loading	Mix	Concrete quality	Concrete moisture content %	Application of heating	Heating rate	Remarks
50 x 400 80 x 640	2φ6 2φ6	350	g	MI	B450	5-7	3 sides	I	no spalling
50 x 400	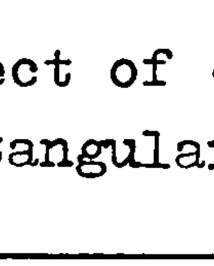	-						I	explosive spalling
800 x 640		-						II	surface spalling with heating rate II
800 x 640		-						I II	
800 x 640	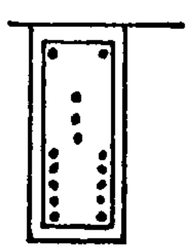 2φ6 3φ26 10 φ16	350 200 I00 50		M2				I	explosive spalling reinforcement exposed
I20 x 960		350		M4	B225				

Table 2.4 Spalling due to one side heating.

Remarks	no spalling			surface spalling			deep surface spalling reinforcement exposed
Heating rate	I						II
Application of heating	one side heated						
Concrete moisture content %	3.2	2.6	3.1	3.1	4.2	3.9	4.1
Concrete quality	B450						
Mix	MI						
Loading MN/m^2	14						
Reinforcement	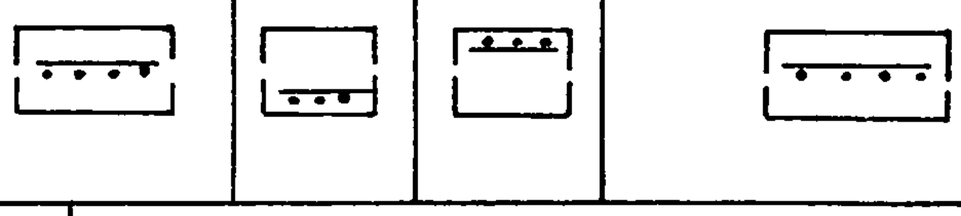						
Cross-section mm x mm	80 x 800	50 x 800					

Tests on 1450mm long members were carried out to investigate the effect of amount and arrangement of reinforcement. The results of such tests are summarized in Table 2.1 where it is shown that 50mm by 400mm I-sections spalled in a destructive way under type I as well as type II heating (Fig.2.1), while larger I-sections (80 x 640mm) with exactly the same amount of reinforcement as the 50 x 400mm ones showed only insignificant surface spalling and that only under type II heating. Results of the same sort for T-sections (Table 2.2), and rectangular sections (Table 2.3) lead to the conclusion that thin specimens with closely spaced reinforcement are more liable to spall than thick specimens with little or no reinforcement. This tendency seems to be more pronounced in prestressed concrete specimens than in conventionally reinforced ones (Table 2.2).

The effect of compressive stresses, whether induced internally or externally, will be discussed in Chapter 4 of the present work. However, it is interesting to note here, that higher compressive stresses due to prestressing or reduction of cross-sectional area in Meyer -Ottens' tests increased the occurrence of spalling.

In fact a similar conclusion can be drawn from Table 2.4 which shows that reinforcement near the heated face seemed to cause spalling while the same amount of reinforcement placed close to the cool side did not cause spalling. This is apparently due to the

Table 2.5 Effect of concrete quality and heating rate on spalling.

Cross-section mm x mm	80 x 640															
Reinforcement	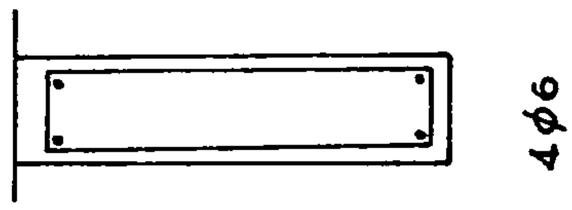 4φ6															
Loading	g															
Mix	MI	M2	M3	M4	MI	M2	M3	M4	MI	M2	M3	M4	MI	M2	M3	M4
Concrete quality	B450		B225		B450		B225		B450		B225					
Concrete moisture content %	5–7															
Application of heat	3 sides												3 sides			
Heating rate	I				II				III							
Remarks	none or only minor surface spalling				"				surface spalling 400 mm in diameter and 5 to 10 mm deep, specially with mix M2							

Table 2.6 Effect of moisture content on spalling. b= 50 mm.

Remarks	explosive surface spalling reinforcement exposed spalling depth, b/2	no spalling	explosive surface spalling	no spalling	
Heating rate	I				
Application of heat	3 sides				
Concrete moisture content %	5.7 5.5 5.4 5.5 4.4 3.3	3.3 3.3 3.2 2.9 0.8	7.2	0.5	
Concrete quality	B450				
Mix	MI				
Loading	g				
Reinforcement			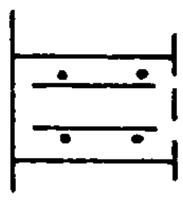		
Cross-section mm x mm	50 x 400				

restriction to the thermal expansion in the former case, thus causing additional compressive stresses.

To investigate the effect of moisture content, Meyer-Ottens tested lightly reinforced as well as heavily reinforced members for various moisture contents in the range 0·8 - 7·0% by weight.

Lightly reinforced specimens of various concrete qualities, heated from 3 sides, with 5 to 7% by weight moisture content did not spall under the heating rate I which is the standard rate described in DIN 4102 (2.14). However, similar specimens exhibited surface spalling up to 400mm diameter and 5 to 10mm depth under type II and type III heating but otherwise similar test conditions (Table 2.5).

These results clearly show that spalling is significantly affected by the heating regime. Care must therefore be exercised when predictions of a wider application involving an actual fire, are required.

However, no matter what the applied heating rate was, none of the lightly reinforced specimens described above spalled explosively. On the other hand, specimens containing central reinforcement mat spalled at moisture contents in excess of 3·3% by weight (Table 2.6) presumably due to the additional compressive stresses induced by the relatively cool central reinforcement restricting the expansion of the warmer concrete closer to the heated surface.

This is in agreement with Dougill (2.15) who

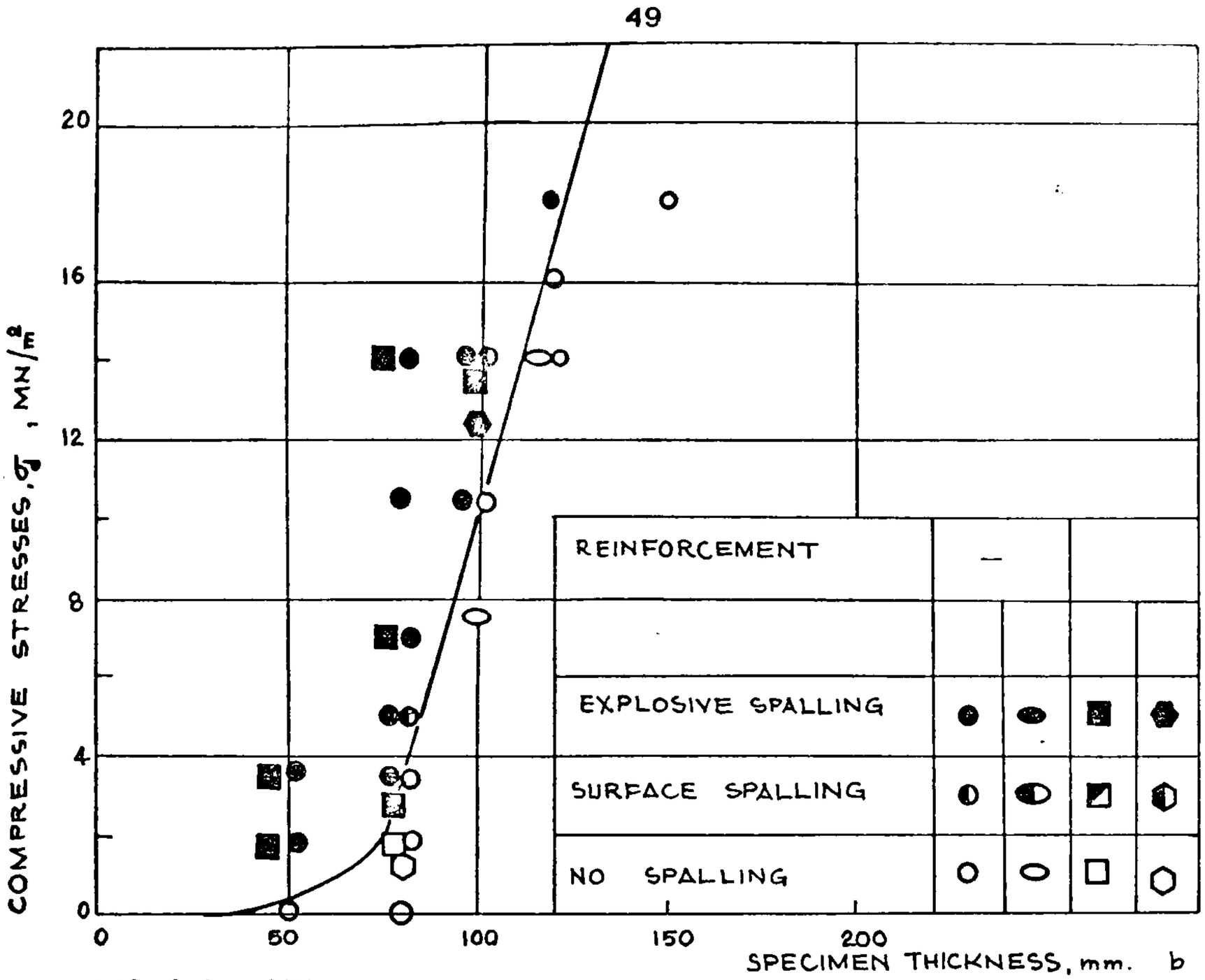

FIG. 2.6 SPALLING OF SPECIMEN UNDER COMPRESSIVE STRESSES HEATED FROM TWO SIDES [AFTER MEYER-OTTENS, (2.8)]

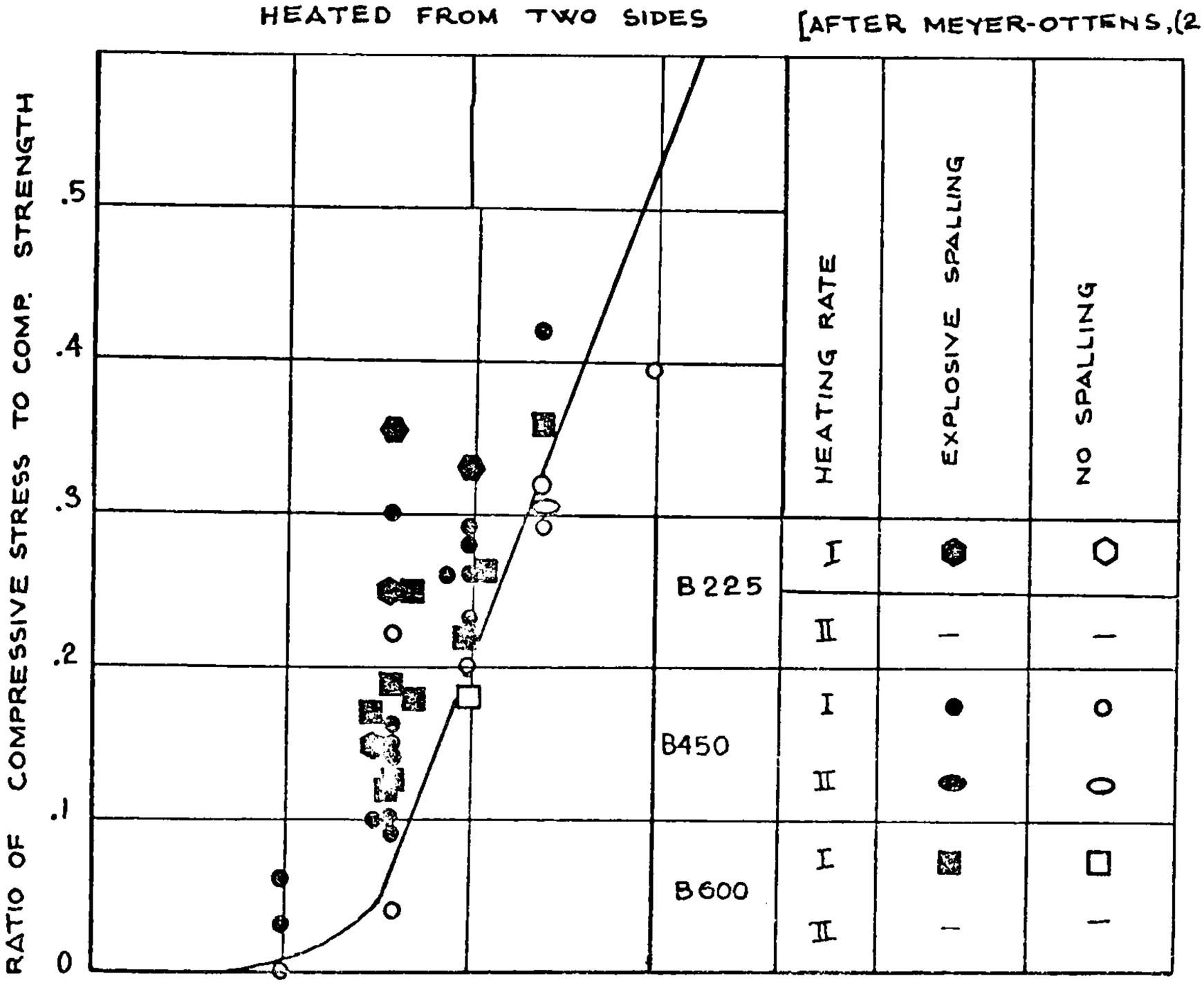

FIG. 2.7 SPALLING OF SPECIMEN UNDER COMPRESSIVE STRESSES HEATED FROM TWO SIDES [AFTER MEYER-OTTENS, (2.8)]

stated that if a concrete panel is heated from both sides, shortly after the start of heating the interior of the panel will be in tension and the surfaces in compression. Obviously, heavy reinforcement close to the axis of symmetry would increase the compressive stresses. Furthermore such a reinforcement arrangement would limit the development of cracking as pointed out by Dougill (2.16), and, therefore, the compressive stresses would be even higher than could be achieved without the reinforcement.

Perhaps the most important contribution of Meyer-Ottens is his tests carried out to demonstrate the effect of compressive stresses on spalling. These results are summarized in Fig.2.6 where the applied compressive stress is plotted against specimen thickness. The results suggest that there is a limit of compressive stress for a specimen of a certain thickness, below which no spalling is likely to occur and above which spalling can be expected. It should be noted that Fig.2.6 represent test results concerning concrete B 450. A more general representation of the results is given in Fig.2.7 where the ratio σ_d/β_w, where σ_d is the compressive stress induced, and β_w, the compressive strength of the concrete, is plotted against the thickness of the member. However, it should be remembered that these compressive stresses were induced either by prestressing 1400mm long members or by uniaxial loading of 800 x 800mm panels. The stresses due to prestressing are not therefore exactly comparable to those caused by end

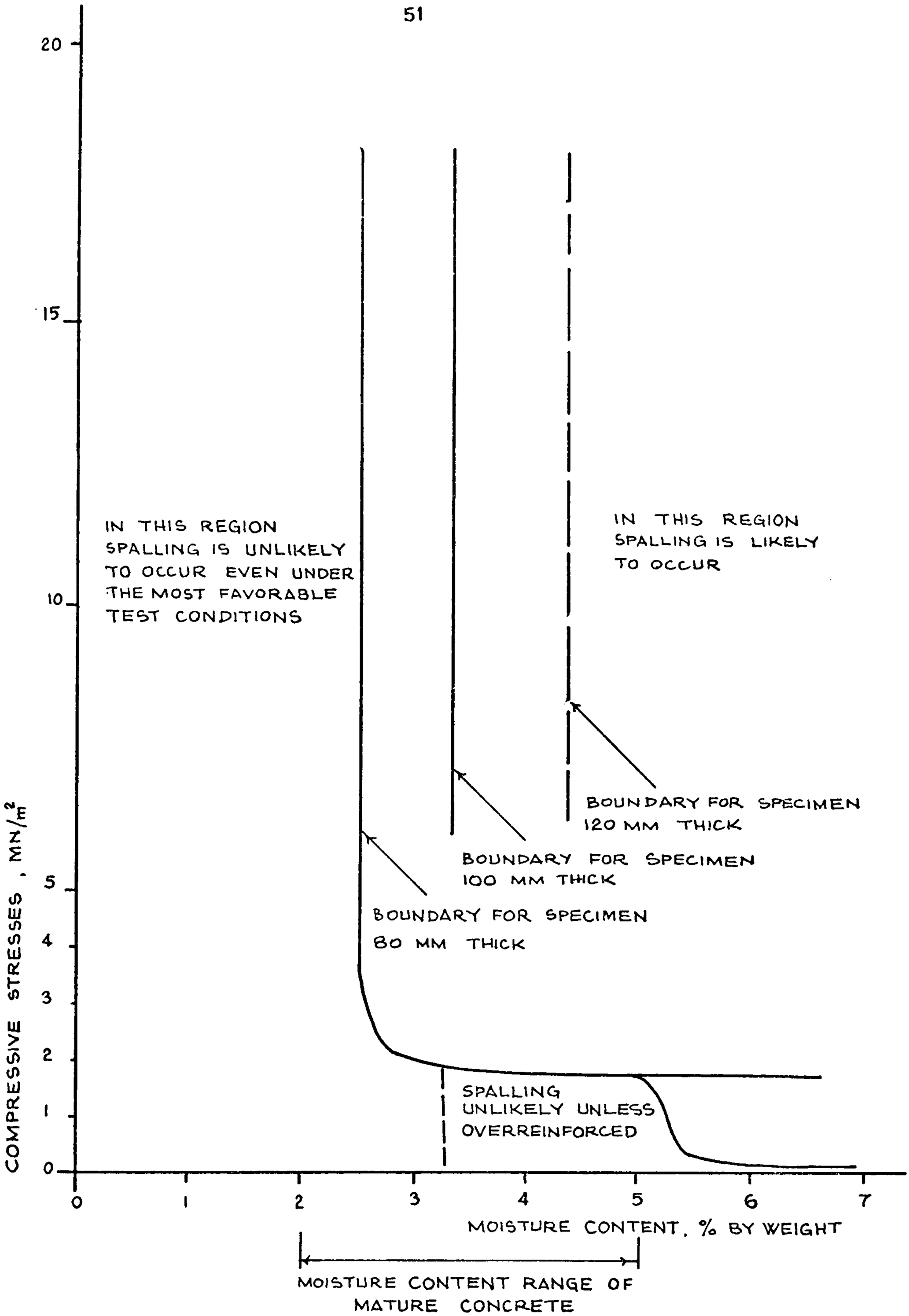

FIG. 2.8 SUMMARY OF MEYER-OTTENS' TEST RESULTS

Table 2.7 Effect of moisture content on spalling. b=80 mm.

Cross-section mm x mm	Reinforcement	Loading	Mix	Concrete quality	Moisture content %	Application of heat	Heating rate	Remarks
80 x 640	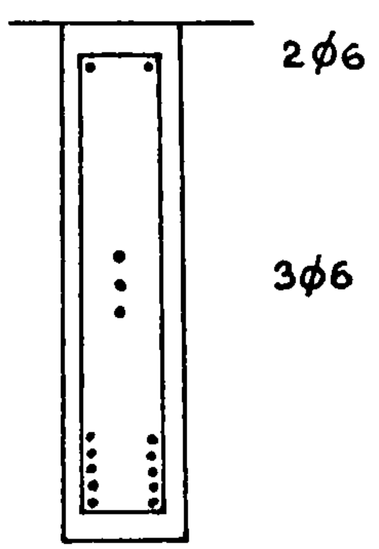 2φ6 3φ6	g	M2	B450	7.2	3 sides	I	explosive surface spalling
			M4	B225	7.0			
			M2	B450	5.3			
					4.7			smaller surface spalling down to I0 mm
					4.5			
					I.2			no spalling
					0.8			
	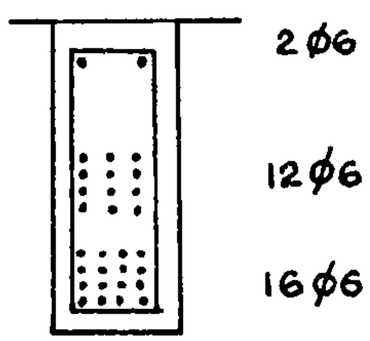 2φ6 12φ6 16φ6				7.5			explosive surface spalling
			M4	B225	6.8			
			M2	B450	4.8			no spalling
					3.2			
					I.3			

Table 2.8 Effect of moisture content on spalling. Loading g+v or g+p .

Cross-section mm x mm	Reinforcement	Loading MN/m^2	Mix	Concrete quality	Moisture content %	Aggregate type	Application of heating	Heating rate	Remarks
100 x 900	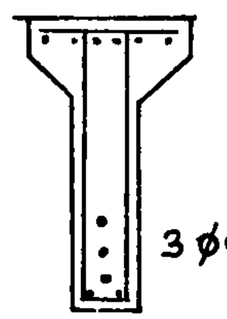	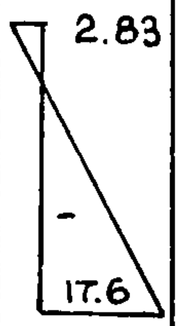	MIa	B450	5.1 3.4 2.9 2.3	Quartz Calc.	3 sides	I	explosive spalling reinforcement exposed
					0.5				no spalling
500 x 800	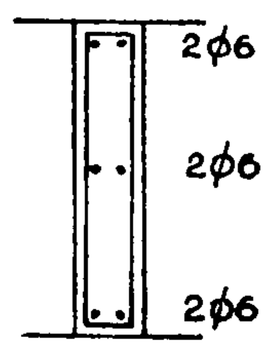	3.5 1.7 7.0 10.5 14.0	MI	B450	2.5 2.0	sand gravel	2	I	explosive spalling
					.8 .3 .2				no spalling
		14.0	MI	B450	2.5 1.6		2	I	
80 x 800		10.5			.4 .4				no spalling

Table 2.9 Effect of compressive stresses on spalling.
Unreinforced specimens.

Cross-section mm x mm	Reinforcement	Loading, MN/m^2	Mix	Concrete quality	Moisture content %	Application of heat	Heating rate	Number of tests	Explosive spalling	Surface spalling
50 x 800	-	.35	MI	B450	3.1	2 sides	I	I	I	-
		.18			3.1			I	I	-
		.0			2.5			I	-	-
80 x 800	-	1.40			3.1			I	I	-
		1.05			2.7			I	I	-
		.70			3.1, 3.3			2	2	-
		.50			3.2			I	-	I
		.35			3.6, 2.6, 3.9			3	I	-
		.17			3.6, 4.2			2	-	-
		.0			3.6			I	-	-
100 x 800	-	1.40			3.1, 3.4, 3.4			3	2	I
		1.05			3.2			I	-	-
120 x 800	-	1.80			3.6			I	I	-
		1.60			4.2			I	-	-
150 x 800	-	1.80			2.9			I	-	-
800 x 80		.50			3.		II	I	I	-
100 x 800		1.05			3.9			I	I	-
100 x 800		.75			3.9			I	-	-
120 x 800		1.40			2.9, 3.0			2	-	-

Table 2.IO Effect of compressive stresses on spalling.
Reinforced concrete specimens. B450

Cross-section mm x mm	Reinforcement	Loading, MN/m^2	Mix	Concrete quality	Moisture content, %	Application of heat		Heating rate	Number of tests	Explosive spalling
50 x 800	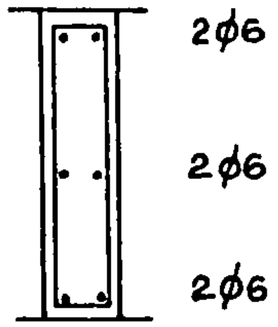	3.5	MI	B450	2.5	2 sides		I	I	I
		1.7			2.				I	I
80 x 800		14.0			2.5			I	I	I
		7.0			2.9, 3.5				2	2
		1.5			2.8, 3.4				2	I
		1.7			2.8, 3.I				2	-
		1.7			3.6			II	I	-
I00 x 800		14.0			3.9			I	I	I
		12.5			3.8			II	I	I
I00 x 900	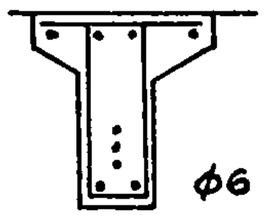	I7.5	MIa	B450	2.9	3 sides		I	I	I
		I3.3			2.3				I	I
		8.9			2.8				I	-
		4.4			2.7			II	I	I
		0.0			2.7				I	I

Table 2.II Effect of compressive stresses on spalling.
Reinforced concrete specimens . B225 and B600.

Surface spalling	Explosive spalling	Number of tests	Heating rate	Application of heat	Moisture content, %	Concrete quality	Mix	Loading, MN/m^2	Reinforcement	Cross-section mm x mm
-	I	I	I	2 sides	2.5	B225	M3	9.0	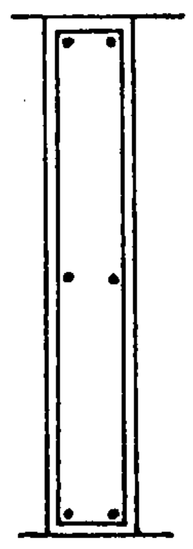	80 x 800
-	I	I	2		2.8			6.7		
-	2	2			2.6,2.7			4.5		
-	-	2			2.2,3.5			3.0		
-	I	I			2.6			9.0		I00 x 800
-	-	I			2.6			7.0		
-	I	I			4.2		MI	16.0		80 x 800
-	I	I			3.9			12.0		
-	2	2			4.0,3.9			10.5		
I	-	I			3.8	B600		8.0		
-	-	I			3.8			7.0		
-	I	I			4.2			16.0		I00 x 800
-	I	I			4.3			13.0		
-	-	I			4.3			10.5		
-	I	I			3.9			21.0		I20 x 800

restraint. Also, it is believed that most concrete wall panels in fire are under biaxial compression, and that the behaviour of such panels may be substantially different from the ones tested with additional uniaxial compression for reasons discussed in Chapter 4.

Furthermore, in Fig.2.7 the effect of the moisture content clearly shown in Tables 2.6 - 2.10 is ignored. Possibly a more satisfactory representation of the results is that given in Fig.2.8 where the effect of compressive stresses, moisture content and dimension and shape of the specimen are taken into account.

Fig.2.8 suggests that:

a) If no compressive stresses exist, no spalling occurred below 3·3% by weight moisture content, even under unfavourable test conditions. In the 3·3% - 7% by weight moisture content range spalling is likely to take place only if the member is heavily reinforced, and/or, axially reinforced, and/or, the section is thin (less than 80mm).

b) If compressive stresses up to 20 Kg/cm^2 (2 MN/m^2) are present, no spalling is likely to occur with moisture contents up to 3·3%. However with moisture contents in the range 3·3 - 5% by weight, spalling is likely to occur if the properties of the member are favourable to spalling. With moisture contents 5 - 7% spalling is always likely to occur.

c) If compressive stresses larger than 20 kg/cm^2 (2 MN/m^2) are induced, spalling is unlikely under any compressive stress within the range of the test, if the moisture content is below 2% by weight. However at higher moisture contents spalling can be expected.

In summary, Fig.2.8 suggests that any combination of compressive stress above 2 MN/m^2 (20 kg/cm^2) and moisture content above 3·3% by weight, makes spalling likely to occur, while higher compressive stresses alone or higher moisture contents alone are not sufficient to cause spalling under the sort of exposure conditions that obtained in the tests.

It could be argued that 0 - 7% by weight range of moisture content is too narrow compared with the wider range considered by Harmathy (2.17) (0-30% by volume, 0-13% by weight). However a 2200 kg/m^3 dry weight concrete contains 150 to 225 l/m^3 water, corresponding to 7 to 10% by weight of moisture. Considering hydration and drying out of free water, a range of moisture content of 2 to 5% by weight is obtained. This falls well within the range studied by Meyer-Ottens.

Bearing in mind the limits of the range of possible moisture contents for mature concrete, Fig.2.8 indicates that compressive stresses rather than moisture content are likely to be the governing factor in causing spalling in practical situations.

Further refinement could be brought into diagrams

like Fig.2.8 by including the effect of aggregate type. In fact it is known that siliceous aggregate is more liable to cause spalling than calcareous aggregate, as, the former undergoes physical changes at high temperatures. The most important of these is α to β transformation occuring at 575°C accompanied by a 0·4% increase in volume. However, more specific results concerning the effect of aggregate are necessary, as, although some researchers suggest that the type of aggregate and its behaviour may contribute significantly to spalling (CIB (2.1)), some others do not seem to observe any marked effect of aggregate type. In fact, Meyer-Ottens (2.7) tested 1400 x 640 80mm simply supported members with calcareous or siliceous aggregate, containing 2·75 - 5·3% moisture at the day of the test, under heating type I or type II. He observed some aggregate splitting in all specimens but no surface spalling except where clay was mixed with siliceous aggregate.

Thus, in agreement with Gustaferro and Carlson (2.18), Meyer-Ottens concluded that the effect of aggregate type is of minor importance in the occurrence of spalling.

2.3 Tests in Holland

Clearly, Meyer-Ottens' spalling tests give useful information on the effect of various test conditions or specimen properties on spalling of concrete. This information together with results of their own tests on lightweight concrete members persuaded Christiaange

Table 2.I2 Spalling test results. After Christiaange et al.(2.9).

	severe spalling	normal spalling	no spalling	no spalling
Moisture	8% (vol.)	5-6 (vol.)	4% (vol.)	I0% (vol.)
Prestress	I $MN/_m^2$	I $MN/_m^2$	I $MN/_m^2$	-
Furnace temperature	500 °C	500 °C	500 °C	500 °C

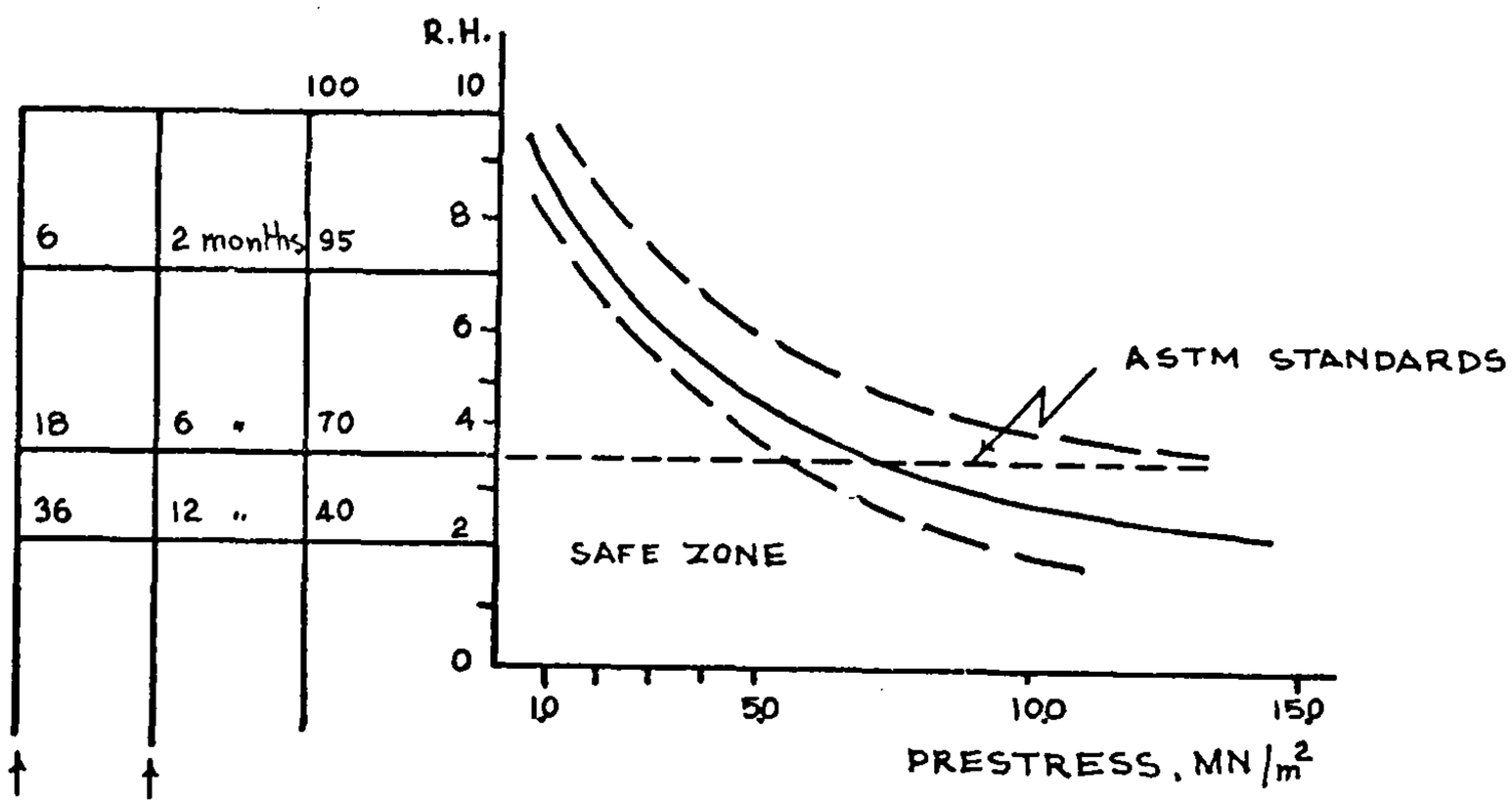

FIG. 2.9 EXAMPLE OF SAFE-ENVELOPE DIAGRAM

[AFTER CHRISTIAANGE ET AL., (2.9)]

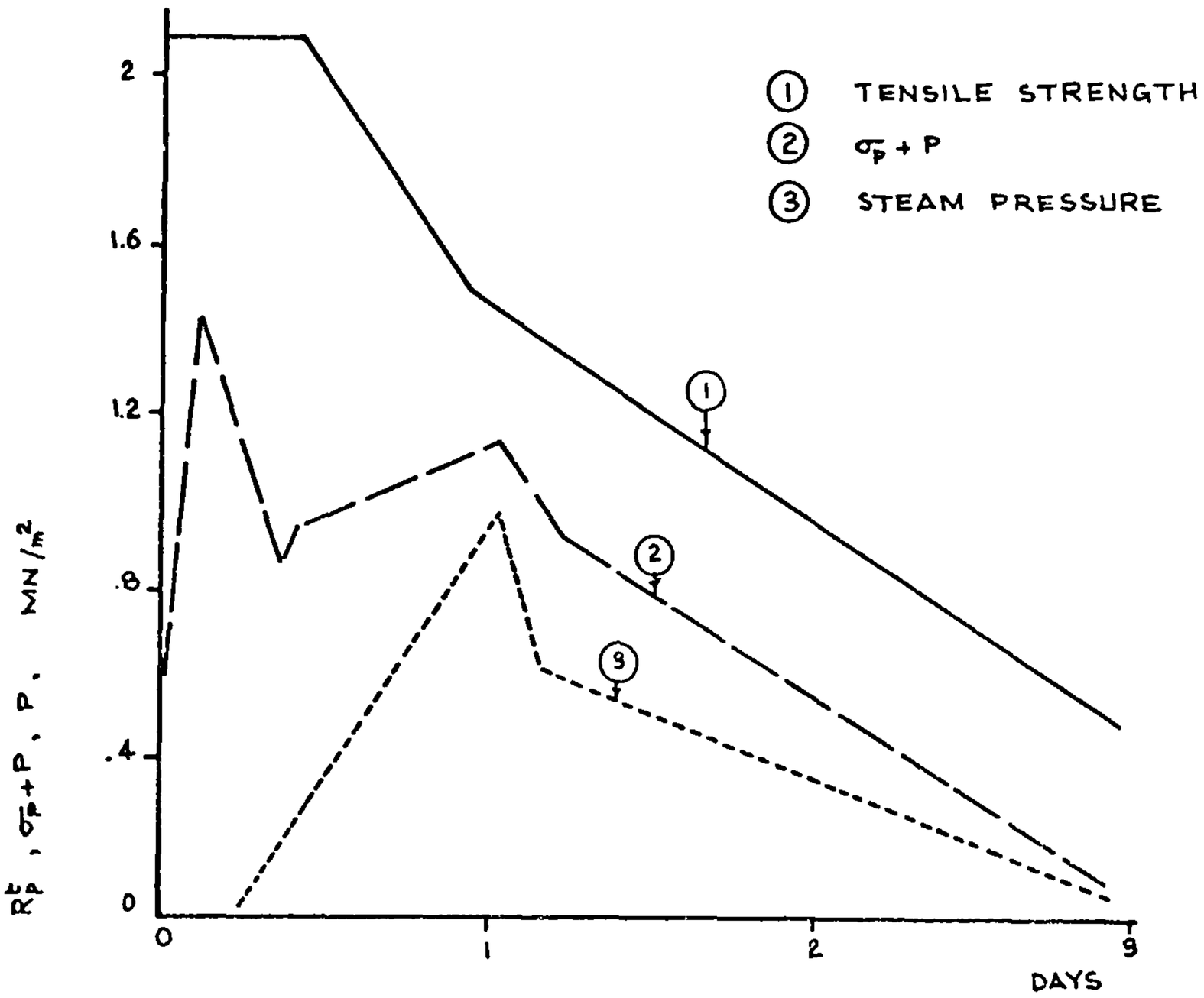

FIG. 2.10 VARIATION OF R_p^t, $\sigma_p + P$, AND STEAM PRESSURE P DURING HEATING OF A CONCRETE BLOCK

[AFTER NEKRASOV ET AL., (2.20)]

et al. (2.9) that spalling might be caused by the compression-high moisture content combination. Although these authors carried out no test on dense concrete, their tests performed on three weeks old, double T, lightweight aggregate elements did support the idea that compression-high moisture content combination may cause spalling (Table 2.12). They stated that a safe zone in a compressive stress-moisture content diagram, where no spalling would be expected to occur, could be defined. For this purpose they suggested a diagram of the type shown in Fig.2.9 which is similar in general form to Fig.2.8 derived from Meyer-Ottens' results.

However, to be of any real use, diagrams of this type should be obtained from tests on life size specimens, with and without restraint[x], for various test conditions simulating the conditions encountered in practical application.

Dutch tests, like Meyer-Ottens' tests, do not seem to be planned to investigate why and how compressive stresses or the combination of compressive stresses and moisture content cause spalling. It is interesting to note, here, that although Meyer-Ottens' test results underline the importance of compressive stresses, the effect of such stresses seems to be ignored in the theoretical work presented by the author. (2.7, 2.13).

Footnote

x See Appendix I for effect of restraint on spalling.

In this, only the escape of vapour, under pressure gradient, through the capillaries, is considered. (See Chapter 3)

Furthermore in neither Meyer-Ottens' tests nor in Dutch tests (2.9) has an attempt been made to measure this pressure.

2.4 Pore Pressure - Tests at Imperial College, London.

The possible effect of pressure is, however recognised by Akhtaruzzaman and Sullivan (2.19) who suggested that concrete, when exposed to fire, can be considered to behave like a hollow sphere under internal pressure. The authors measured moisture loss in 840 x 75 x 50mm plain or reinforced prismatic specimens under transient heating and observed explosive spalling in some of the tests. However, no comparison of the moisture loss data between moist cured and water cured specimens has been made, although such a comparison would mean a denser shell in water cured specimens due to hydration products, leading to a slower rate of moisture loss under heating. A denser shell, or a slower rate of moisture loss would in turn suggest the presence of high pressures in concrete which, in extreme cases, could be capable of causing spalling.

They noted, however, that water cured specimens were significantly more susceptible to explosive spalling than moist cured specimens.

Similar observations are made in the present work (See Chapter 5) where water cured specimens spalled

violently while specimens kept in the curing room at 94% average relative humidity following a 7 day water curing did not spall.

This behaviour is believed to be due to the formation of a denser and less permeable layer of hydration products close to the surface, thus partly preventing the escape of the vapour to the atmosphere and so assisting pressure generation. However these conclusions were arrived at without knowledge of the actual pore pressures involved. Ideally the experiments should have included measurement of pore pressure, but this was left for others.

2.5 Pore Pressure Measurements

The pore pressure generated in concrete exposed to high temperatures was measured by Nekrasov et al. (2.20) and subsequently by Thelandersson (2.21) using the same technique.

Nekrasov et al. investigated the safe heating rate of large blocks (1050 x 1450 x 500mm and 1050 x 1450 x 200mm) of refractory concrete heated from one side up to 800°C. The pressure was measured using a 2mm internal diameter copper tube cast in concrete. The other end of the tube was connected to a spring manometer. They considered that the main cause of destruction of concrete is increased pressure and temperature-moisture stresses. Thus, for concrete to survive without cracking they suggested the condition that

$$(P+\sigma)K < R_p^t \qquad (2.1)$$

or, equivalently,

$$\left[\frac{P}{E_b^t} + \varepsilon\right] K < \varepsilon_p^t \qquad (2.2)$$

where, P = pressure of steam in concrete

σ = tensile stress

R_p^t = tensile strength of the hot concrete

ε = strain due to thermal stress in the concrete

E_b^t = elastic modulus of the hot concrete

ε_p^t = deformation limit of the heated concrete due to the tensile stresses.

and, K = a coefficient introduced merely in order to enable the prediction of the formulae to be matched to experimental observations.

The highest pressure obtained by the authors was 700 KN/m^2 at a depth of 150mm. However, Fig.2.10 shows that $\sigma + P$ is still about 20% lower than the tensile strength of the concrete at the temperature considered.

No failure was observed in these tests probably because the rate of heating was too slow. The peak pressure was reached after 30 hours heating when the surface temperature was only 400°C and the temperature at the point where the peak pressure occurred was only 140°C. Thus, it is possible that a higher rate of heating could cause a pressure of a magnitude sufficient for failure.

Thelandersson (2.21) used the same technique as Nekrasov et al. to measure steam pressure when investigating the behaviour of 1500 x 150 x 150mm mortar specimens under transient heating and torsional

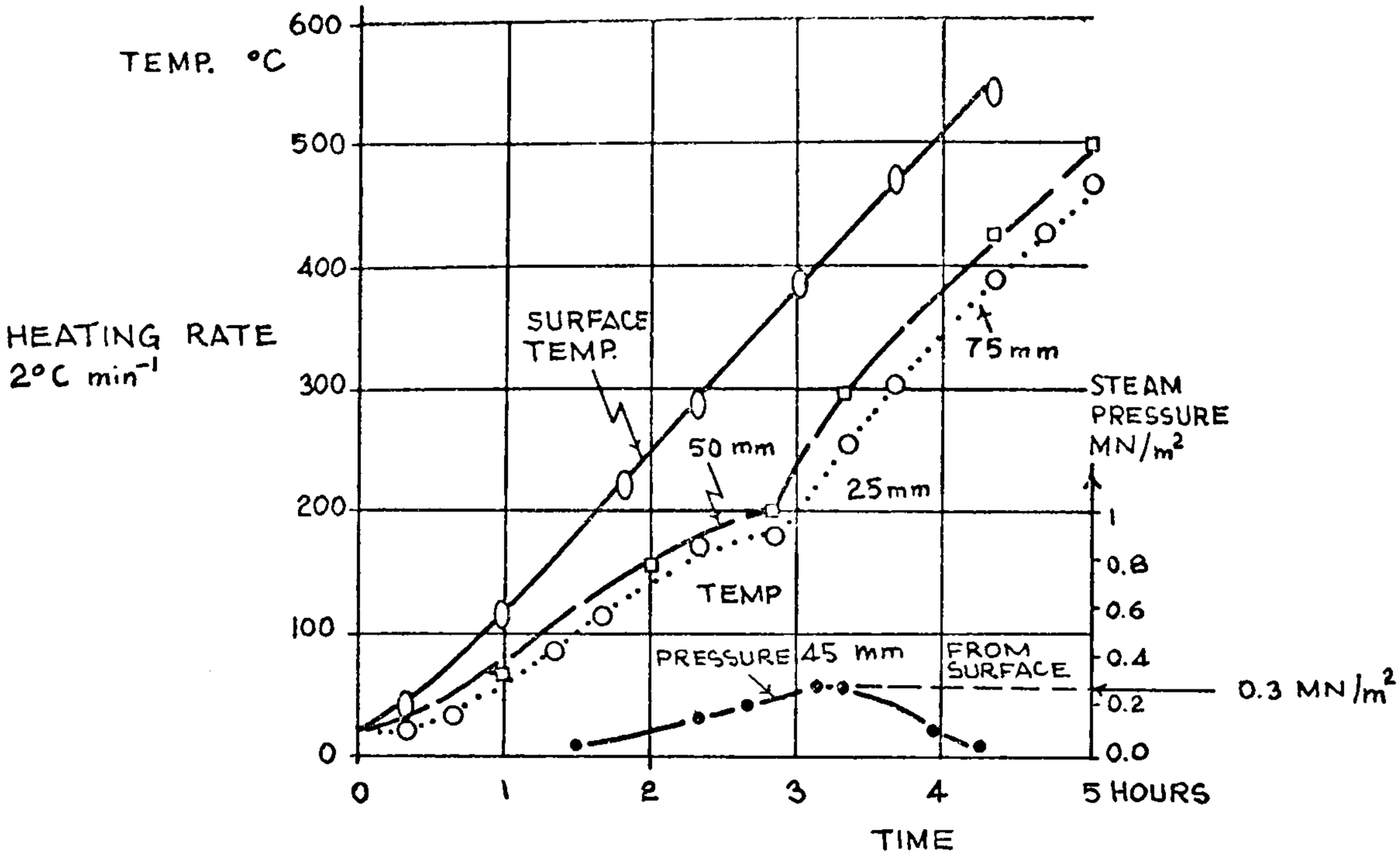

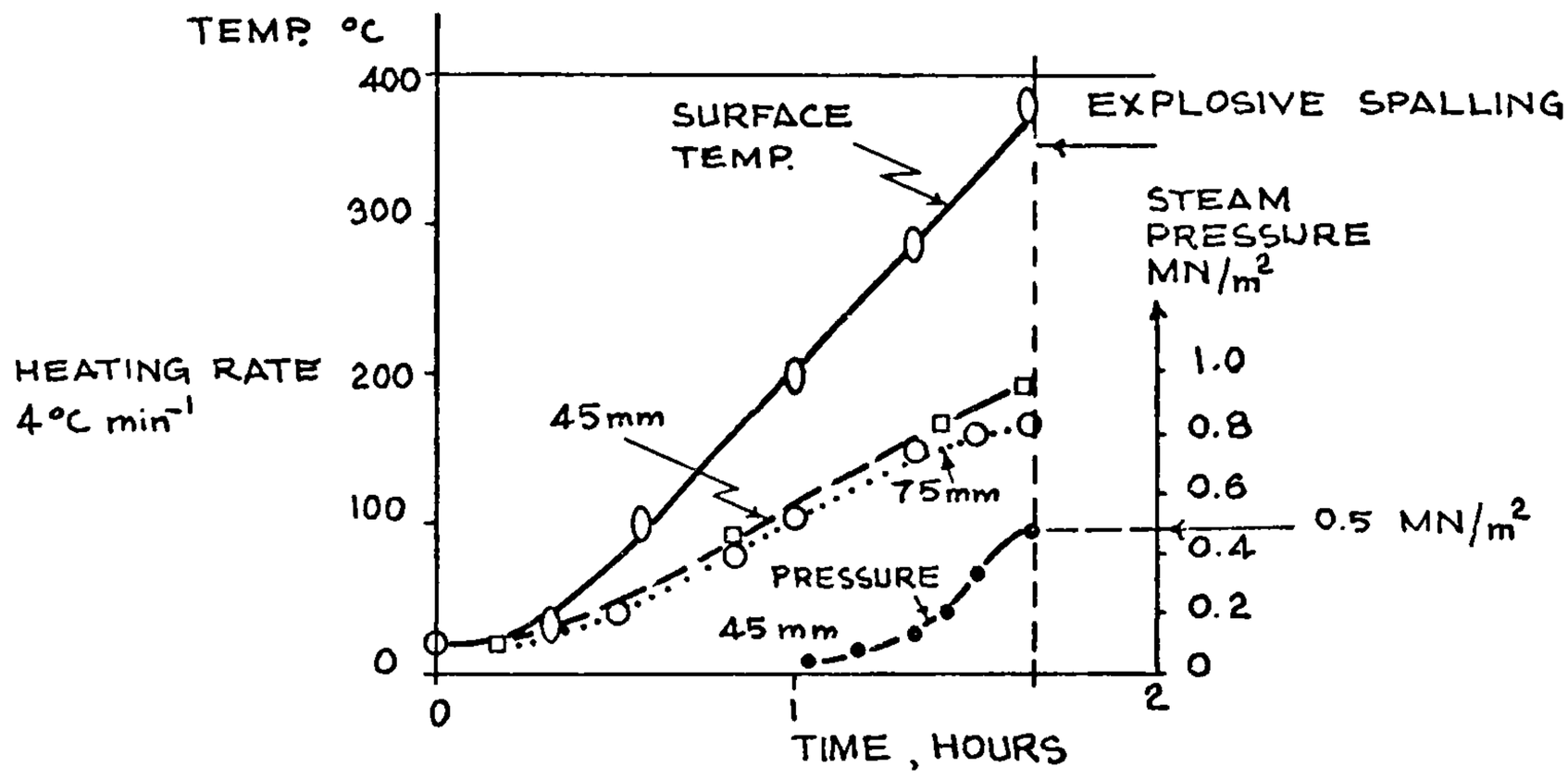

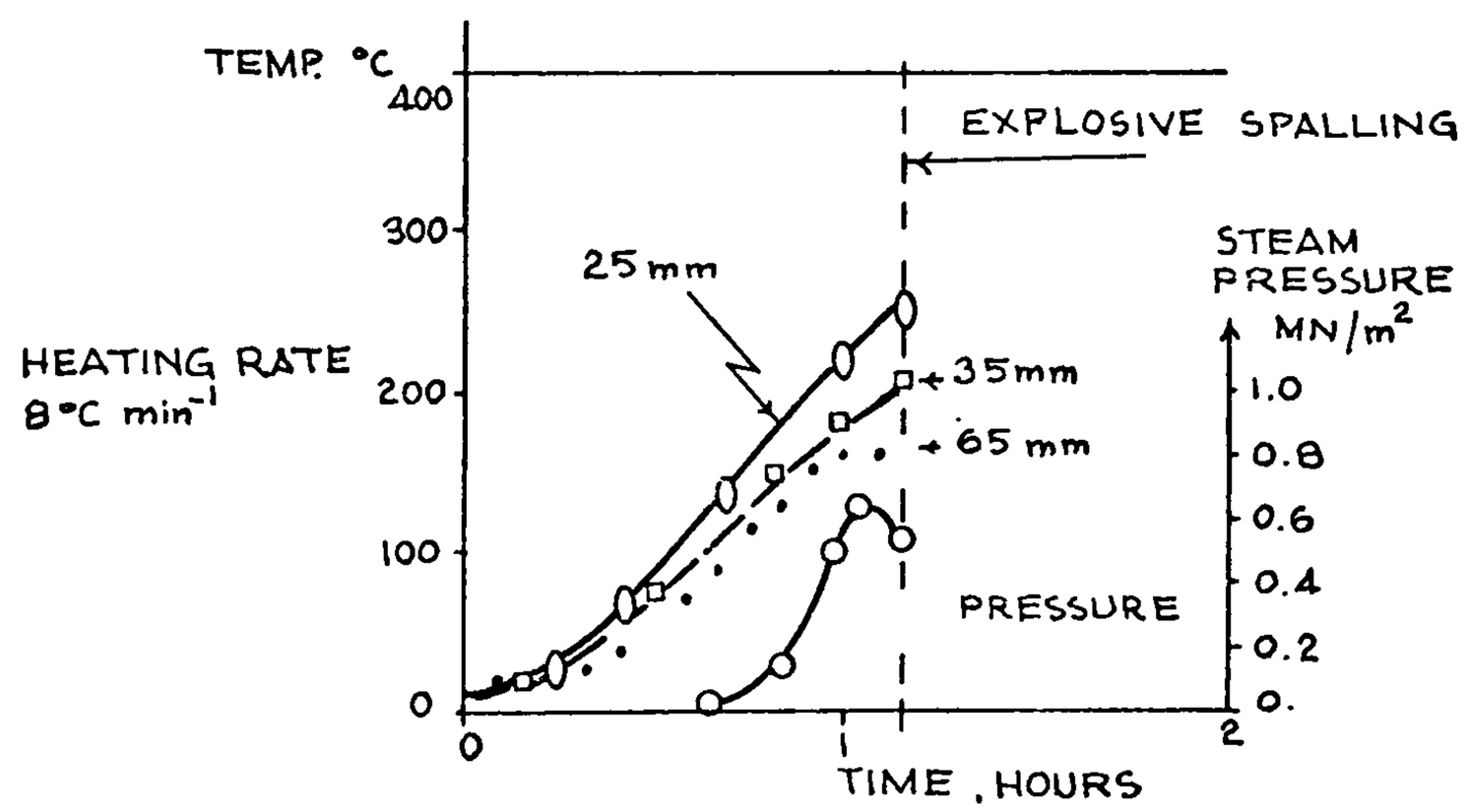

FIG. 2.11 TEMPERATURE AND STEAM PRESSURES MEASURED AT DIFFERENT POINTS IN THE SPECIMENS AS A FUNCTION OF TIME

[AFTER THELANDERSSON, (2.21)]

	LOADING	HEATING	CROSS-SECTION
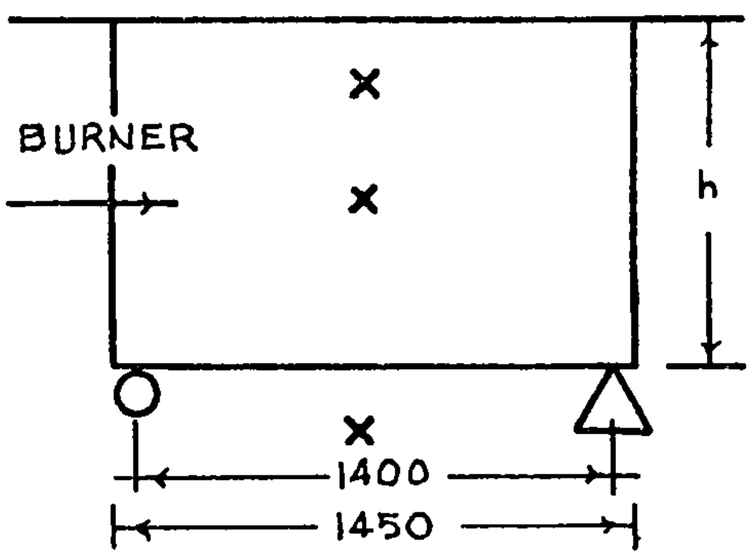	SELF WEIGHT g	3 SIDES	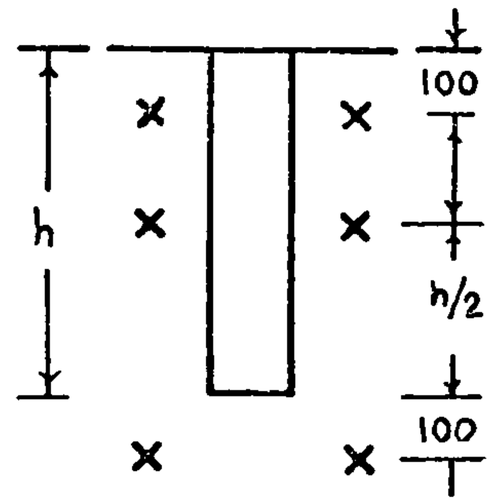
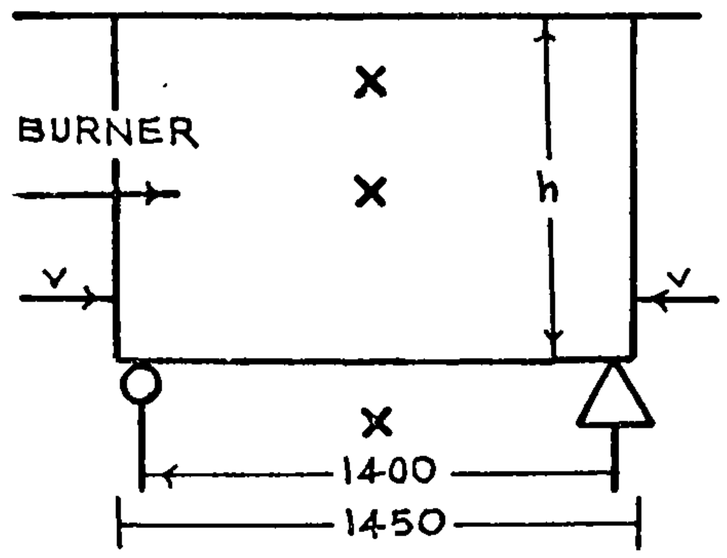	g+v v = PRESTRESS	3 SIDES	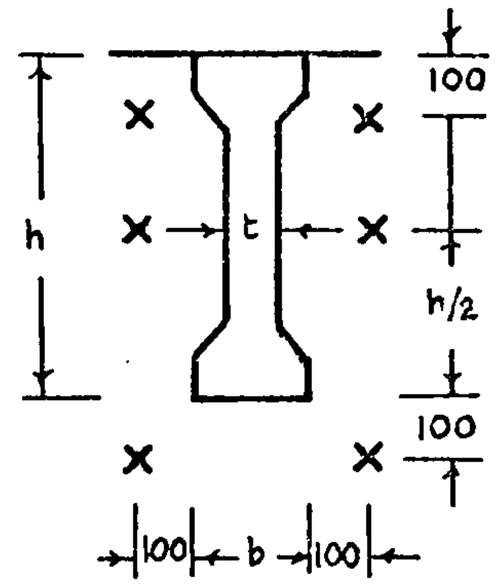
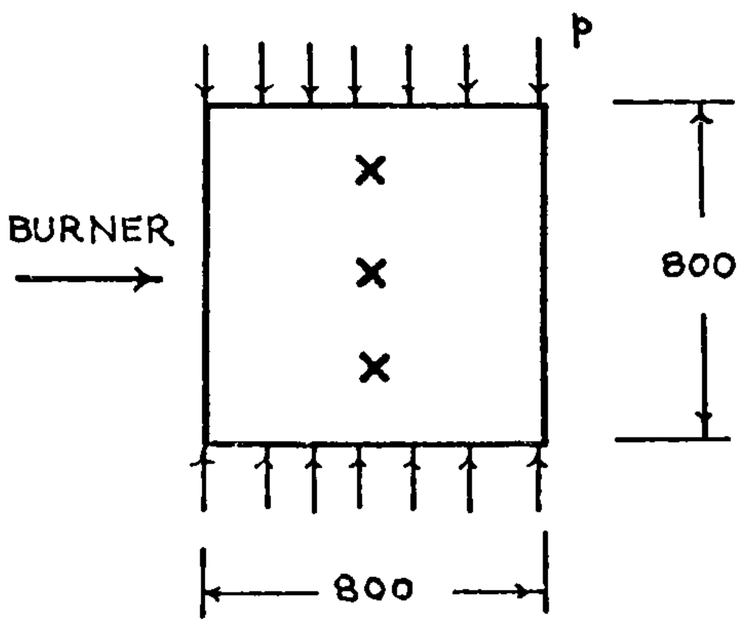	g+p p = EXTER. LOADING	ONE OR TWO SIDES	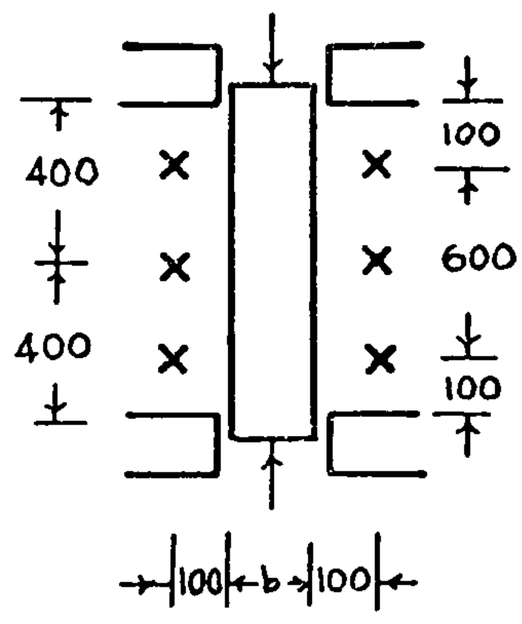

FIG. 2.12 LOADING AND HEATING CONDITIONS IN MEYER-OTTENS' (2.8) TESTS

loading. Although the author tried three different rates of heating (Fig.2.11) they all fell below the standard time/temperature curve heating rate, thus suggesting that the highest pressure obtained, 0·65 MN/m^2, could be raised under different heating conditions. Nevertheless with heating rates of 4°C/min and 8°C/min Thelandersson observed explosive spalling at pressures of 0·5 MN/m^2 and 0·65 MN/m^2 respectively.

2.6 Concluding Remarks

The results of the spalling tests discussed in this chapter suggest that spalling is encouraged by the presence of compressive stresses and moisture in concrete. Meyer-Ottens' test results indicate that either influence alone is unlikely to cause spalling in practical situations. However, the reasonably high steam pressures obtained by Nekrasov et al. (2.20) and Thelandersson (2.21) suggest that under certain rather unusual conditions pore pressures alone may cause spalling.

Chapter 3

THEORETICAL ASPECTS OF PRESSURE DEVELOPMENT

3.1 The Moisture Clog Concept

As Shorter and Harmathy (3.1) pointed out, soon after concrete is exposed to heat, a thin layer of moisture is lost from the layers nearest to the surface by 'desorption'. Part of this water, in vapour form, escapes to the atmosphere through the interconnected pores, part of it stays in the pores and causes an increase of pore pressure. The rest is probably readsorbed by the colder solid wall, further away from the heated surface by the process of condensation.

Harmathy (3.2) states that when heat begins to penetrate into a concrete slab, desorption of moisture starts in a thin layer adjoining the surface exposed to fire. A significant portion of the vapour released leaves towards the cooler regions and becomes readsorbed in the pores of some neighbouring layer. As the thickness of the dry layer gradually increases, a completely saturated layer of considerable thickness builds up at some distance from the exposed surface. A little later, a sharply defined front[x] forms between the dry and saturated layers. (Fig.3.1) This evaporation front, however, may not be as sharp as mentioned above,

Footnote

x Harmathy's account represents a simplification. The interface may not perhaps be so sharply defined because various types of water held in concrete evaporate at different temperatures.

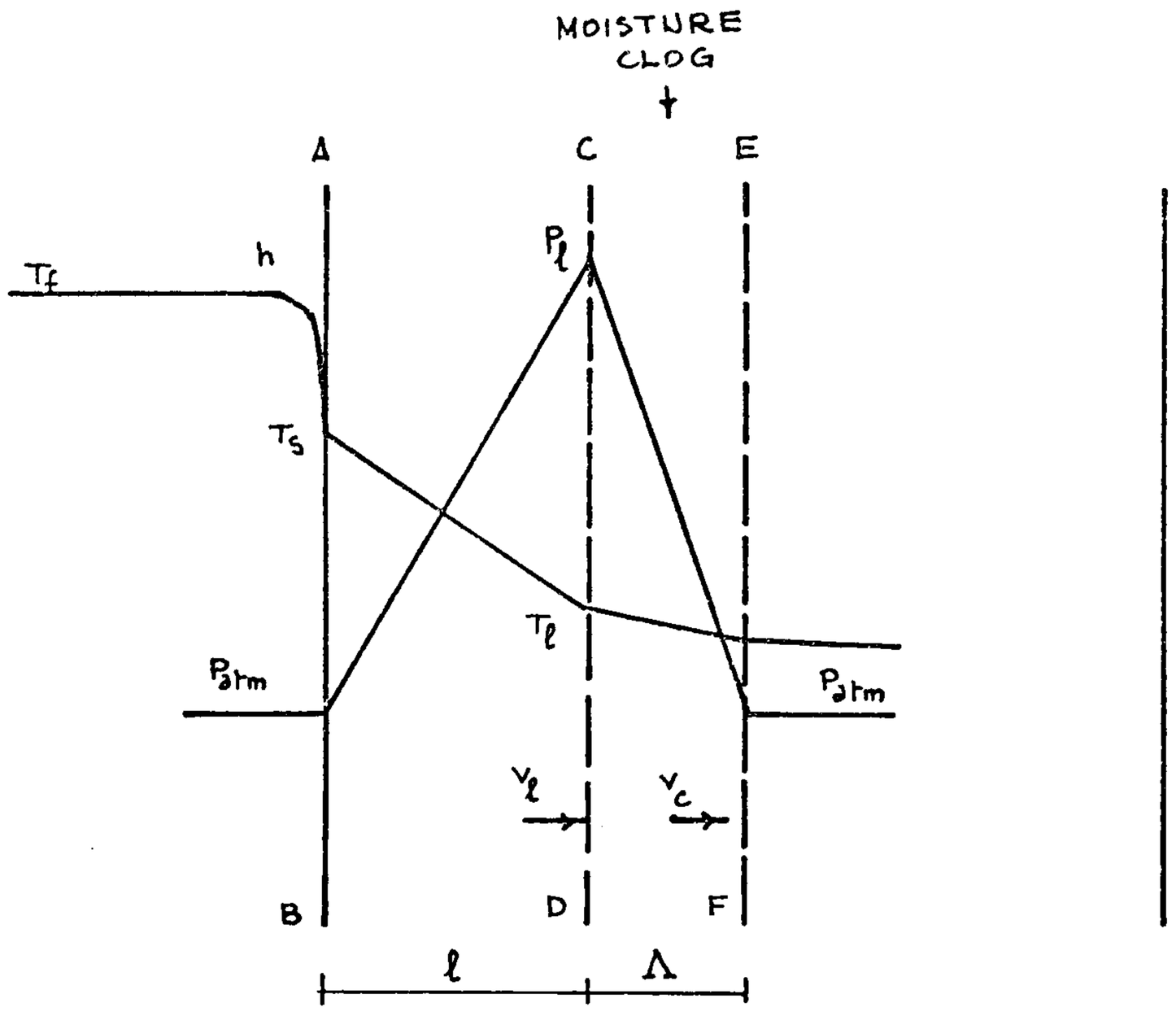

FIG. 3.1 DIAGRAM SHOWING MOISTURE CLOG MOVEMENT

[AFTER HARMATHY, (3.2)]

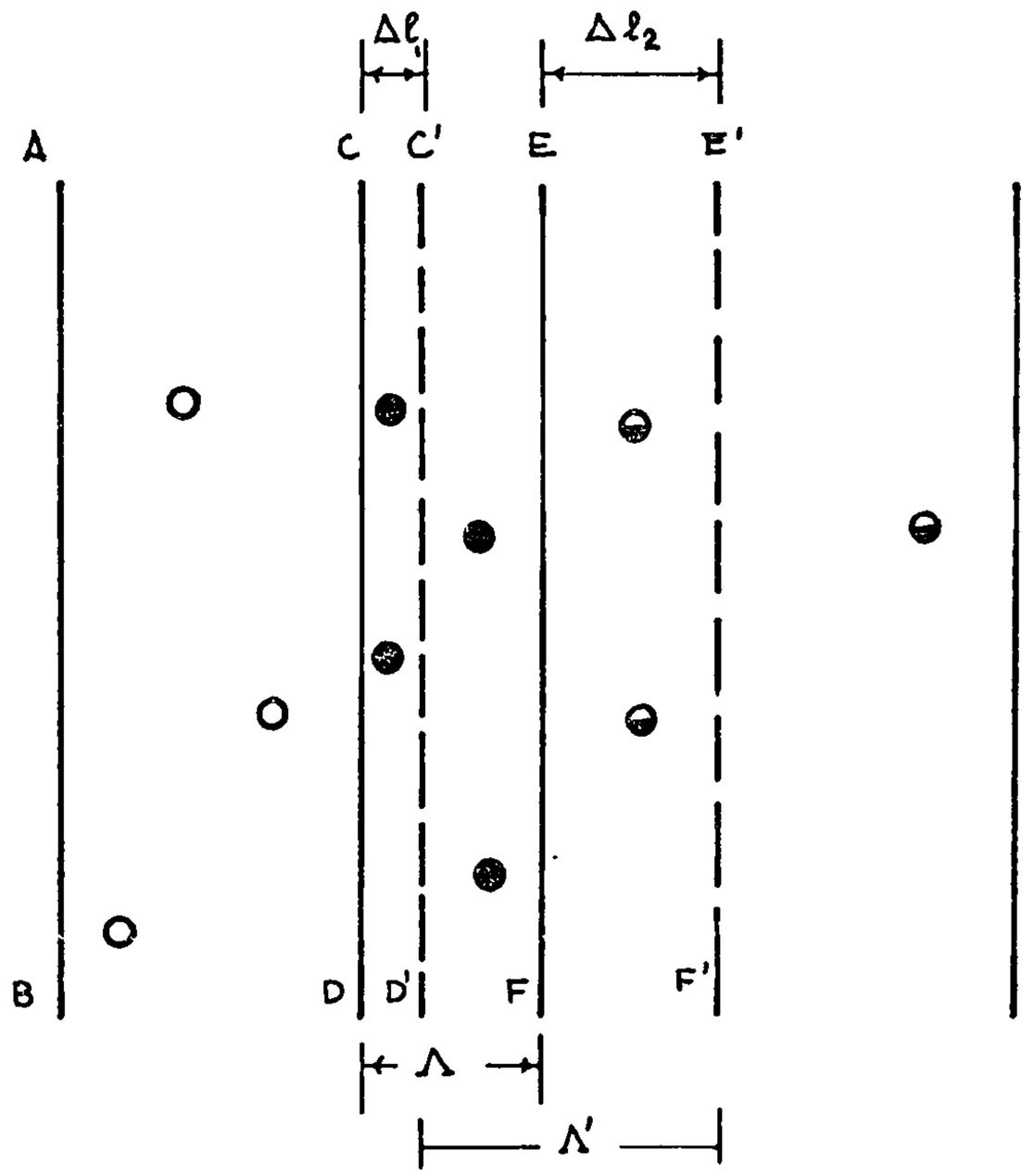

FIG. 3.3 DIAGRAM SHOWING INCRESE IN MOISTURE CLOG THICKNESS DUE TO MOVEMENT OF THE CLOG

because vaporization and condensation occur at changing rates due to the fluctuating pressure.

Shorter and Harmathy (3.1) pointed out that during the evaporation from front CD, the temperature of the exposed surface keeps rising and a very steep temperature gradient develops across the dry layer, resulting in high heat flow and intensified desorption at the CD plane. The vapour escaping through the dry layer encounters more and more resistance due to the increasing temperature along the path, causing expansion of vapour and increase of pressure. Cracks may have been formed at this stage but, the horizontal cracks responsible for decrease in permeability are probably prevented from propagating due to compressive stresses in the hot regions.

In Harmathy's opinion if the permeability of concrete is low and the rate of vaporization high, the pressure will continue to increase till it reaches the tensile strength of the concrete. At this stage a layer will separate from the material. Spalling thus occurs due to generation of pore pressure.

During this process the evaporation front CD will move towards the cooler region due to:

1. the vapour pressure acting on the moisture clog,

and, 2. the water in the clog becomes evaporated so reducing the thickness of the moisture clog.

3.1.1 Harmathy's Analysis

Considering Fig.3.1 Harmathy assumed that a fraction of the moisture which has been desorbed from the

region ABCD has been absorbed by the layer CDEF, the volume of the voids in the moisture clog region being equal to the original moisture plus the volume of moisture coming from the region ABCD.

Considering unit area,

$$\varepsilon \Lambda = \phi + \delta l \phi \tag{3.1}$$

where ε is the porisity and ϕ the original moisture content by volume.

Hence,

$$\Lambda = \frac{\delta l \phi}{\varepsilon - \phi} \tag{3.2}$$

On the other hand, assuming a quasi-steady state condition in the region ABCD, and considering the heat conduction through the dry region, we have the heat flux,

$$q = \lambda \frac{dT}{dx} = \lambda \frac{(T_s - T_L)}{l} \tag{3.3}$$

where λ is the thermal conductivity of the dry concrete.

Now, considering the heat transferred across the heated surface AB to depend on a surface heat transfer coefficient 'h',

$$q = h(T_f - T_s) \tag{3.4}$$

and applying heat balance to the surface AB, so that, on equating the expressions for the heat flux we obtain,

$$T_s = \frac{T_l + \frac{hl}{\lambda} T_f}{1 + hl/\lambda} \tag{3.5}$$

On combining equations 3.4 and 3.5

$$q = \frac{h\,(T_f - T_l)}{1 + hl/\lambda} \tag{3.6}$$

The weight of water evaporated per unit time for unit cross-section is q/Q, where Q is the heat of absorption.

Thus the volume of water evaporated per unit time, for unit cross-section is $q/Q\rho_w$

The volume of saturated concrete that would contain this volume of water is,

$$\frac{q}{Q\rho_w}\,\frac{1}{\varepsilon} \tag{3.7}$$

so that,

$$v_l = \frac{q}{Q\rho_w\varepsilon} \tag{3.8}$$

where,

v_l = the rate of progression of the interface CD caused solely by the removal of the water by evaporation.

The velocity of the moisture clog due to pressure only, v_c, can be obtained using Darcy's law,

$$v_c = \frac{K}{\eta_w}\,\frac{P_l - P_{atm}}{\Lambda} \tag{3.9}$$

where K is the permeability, and η_w is the dynamic viscosity of the water.

Harmathy (3.2) assumes that if $v_c > v_l$ the moisture clog must be moving faster that the surface CD, thus allowing space for the vapour to expand into with consequent reduction in pressure. On the other hand,

if $v_c < v_l$, an ever increasing rate of vaporization would apparently occur from the surface CD, which would cause a pressure build-up. Thus, Harmathy's assumption leads to the condition that spalling must eventually occur if $v_c < v_l$. However it turns out on further examination, (see section 3.1.2.1) that the motivation for comparing v_c and v_l is based on incorrect view of the boundary conditions in the moisture clog and can not be justified.

However ignoring this error for the moment and using Harmathy's assumption that the concrete would fail if,

$$P_l - P_{atm} = \sigma_f \qquad (3.10)$$

where σ_f is an appropriate value for the strength of the material, and also his assumption that,

$v_c < v_l$ at failure,

Harmathy obtains the following expression for failure:

$$\frac{\phi}{\varepsilon} > \frac{1}{1+(A/\varepsilon K\sigma_f)[\lambda/(\lambda+B)}} \qquad (3.11)$$

where,

$$A = \frac{\delta l \eta_w h (T_f - T_s)}{Q \rho_w}$$

and,

$$B = hl$$

For any value of the permeability K, equation 3.11 provides a limiting value of the saturation ratio ϕ/ε below which spalling is unlikely to occur. Some results

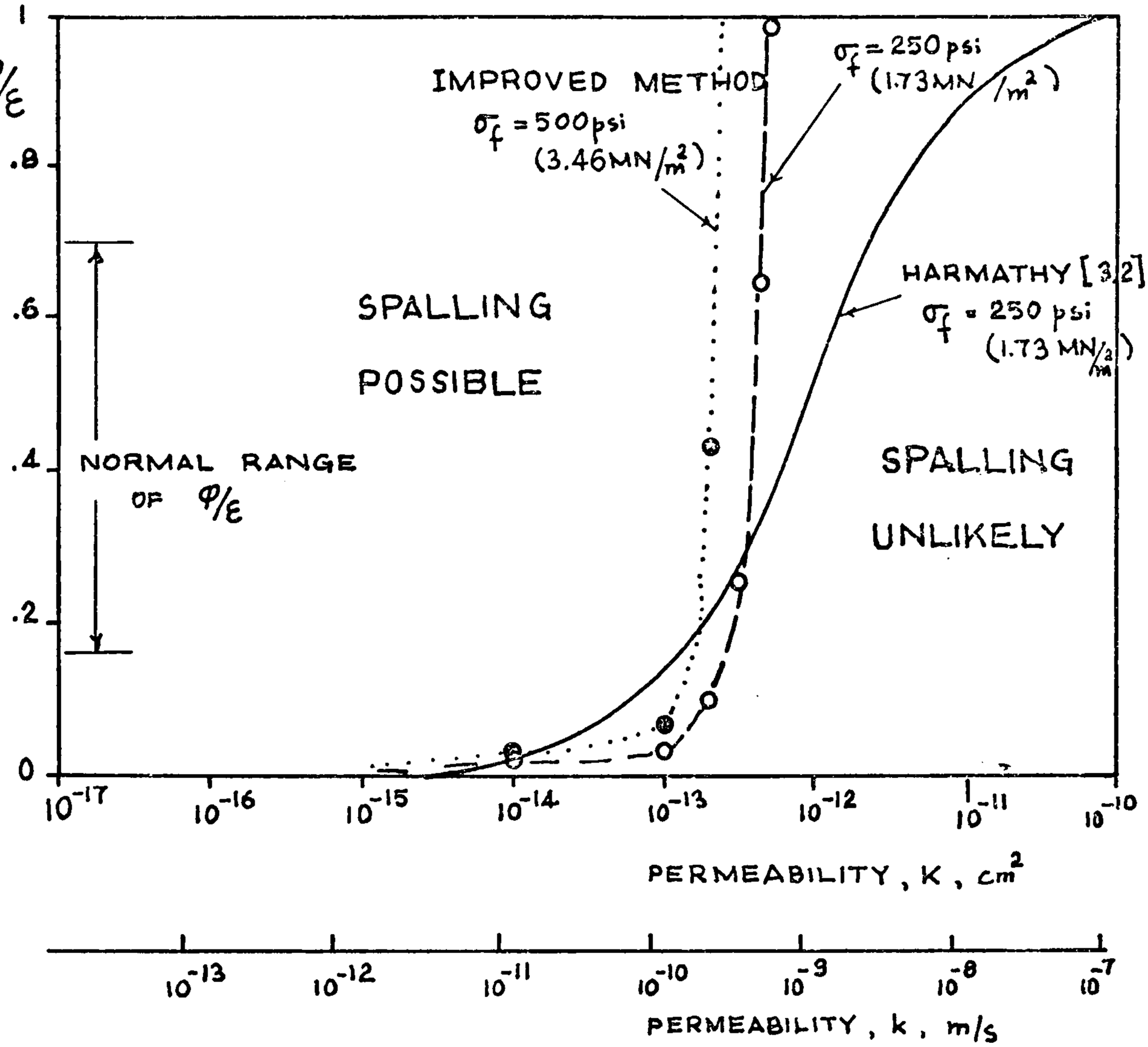

ASSUMED PROPERTIES

$\varepsilon = 0.3$

$\sigma_f = 1.73\ MN/m^2$ (250 psi)

$t = 20$ min

FIG. 3.2 DIFFERENT SPALLING LIABILITY CURVES

calculated from this equation are shown in Fig.3.2 for an assumed constant value of δ and with the tensile strength σ_f taken to be 1·72 MN/m^2 (250psi). Results of this sort could be informative as to a material's susceptability to spalling if reservations on the derivation of equation 3.11 could be reduced. Thus there is some incentive to try to improve Harmathy's approach.

3.1.2 Moisture Clog Theory: Modified Approach

In attempting to improve the analysis of the moisture clog situation it seems that we can,

a) adopt a more realistic criterion for the conditions for pressure build up,

and, b) take a more complete view of the effect of movement of the moisture clog and vaporization on the size of the saturated zone with a view to eliminating the need to make an arbitrary and uninformed choice for the value of the parameter δ in Harmathy's theory.

3.1.2.1 A Revised Criterion for Pressure Build-Up

It is in the spirit of Harmathy's approach to suggest that the pressure will continue to increase at the front CD if vapour is evaporated faster than space is made available for it at the same pressure. In these terms, space is made available by vapour leaving the front at velocity v_v to pass through the dry zone, and by movement of the front CD towards the cooler region. The velocity of this front is the sum of the velocities

of the water in the saturated pores v_c (which can be considered to be the velocity of the front due to the effects of pressure alone) and the rate v_l that the front is advanced due to evaporation. Thus if we take the volume of the vapour formed from unit volume of liquad to be α, the condition for an increase in pressure to occur is

$$(\alpha - 1)v_l - v_c > v_v \qquad (3.12)$$

in which $\alpha > 1$ and depends on the precise conditions at the front CD. This replaces Harmathy's condition for pressure build up. It will be noted that even if the velocity of escaping vapour can be neglected, Harmathy's expression omits effects due to α and gives a totally incorrect view of the conditions for pressure increase.

In order to use the revised criterion we need expressions for the velocities v_l, v_c and v_v. These are derived in the next sections.

3.1.2.2 The Velocity Components

As an approximation we assume laminar flow of vapour in the capillaries and take the pressure gradient to be constant within the dry zone so that

$$v_v = \frac{K_v}{\eta_v} \frac{P_l - P_{atm}}{L} \qquad (3.13)$$

where K_v is the permeability of the dry concrete to vapour, and η_v is the dynamic viscosity of the vapour.

Next, we adopt Harmathy's expressions for the heat flux q (equation 3.6) and for the velocity v_l (equation 3.8)

to obtain:

$$v_l = \frac{h(T_f - T_l)}{\left[1 + \frac{\lambda L}{K}\right] Q \rho_\omega \varepsilon} \qquad (3.14)$$

There is some error in this result due to the assumption of steady state conditions and the consequent neglect of the heat used in raising the temperature within the dry zone. This error connot be avoided without a fuller analysis and leads to an over-estimate of the velocity v_l.

Harmathy also gives an expression for the velocity v_c, the velocity of front CD due to the effects of pressure alone (see equation 3.9). This expression is:

$$v_c = \frac{K_\omega}{\eta_\omega} \frac{P_l - P_{atm}}{\Lambda} \qquad (3.15)$$

in which Λ , the thickness of the moisture clog, needs to be known before the velocity v_c can be calculated. In order to do this Harmathy introduced the quantity which was later arbitrarily given a constant value. Clearly, it would be an improvement if this device could be avoided.

3.1.2.3 The Moisture Clog Thickness Λ

Changes in the thickness of the moisture clog occur in two ways. Without evaporation, the clog would increase in size as it is pushed into the cool regions as it encounters material with pores already partly filled. (Fig.3.3) In the practical case, this effect must be taken together with the reduction in thickness caused by evaporation at the front CD. The two effects

are considered separately in the following sections.

a. Thickness Λ_1 , of Moisture Clog in the Absence of Evaporation

Consider the situation shown in Fig.3.3

Water lost in the region $CDC'D' = v_c \varepsilon$ (3.16)

Water gained in the region $EFE'F' = (v_c + x)(\varepsilon - \phi)$ (3.17)

where, 'x' is the increase in velocity between C'D'and E'F'.

Equating equations 3.16 and 3.17,

$$v_c \phi = x(\varepsilon - \phi) \tag{3.18}$$

and, therefore,

$$x = v_c \frac{\phi}{\varepsilon - \phi} \tag{3.19}$$

where 'x' should be interpreted as the additional distance travelled by E'F' when compared with the distance travelled by C'D', per unit time.

Considering Λ , as the sum of all 'x' up to the time t during which CD travelled a distance l_p, we obtain,

$$\Lambda_1 = l_p \frac{\phi}{\varepsilon - \phi} \tag{3.20}$$

b. Thickness of the Layer Lost Through Evaporation

Let,

$\Lambda_2 = l_v$ = the thickness of the layer lost by evaporation only, during the time t.

Assuming the velocity of front CD as being constant, we have,

$$t = \frac{l}{v_{CD}} \tag{3.21}$$

where,

$l = l_v + l_p$ = total change in the thickness of the moisture clog during the time 't',

and, v_{CD} = velocity of the front CD.

Similarly, by assuming constant rate of evaporation and pressure increase, we have:

$$t = \frac{l_v}{v_l} \qquad \text{and} \qquad t = \frac{l_p}{v_c} \tag{3.22}$$

Combining equations 3.21 and 3.22 we obtain,

$$l_p = l \frac{v_c}{v_{CD}} \tag{3.23}$$

and,

$$l_v = l \frac{v_l}{v_{CD}} \tag{3.24}$$

On the other hand, combining equations 3.20 and 3.23 and also considering that:

Final thickness of the moisture clog = (Final thickness if no evaporation had occurred) - (thickness lost due to evaporation),

we have,

$$\Lambda = \Lambda_1 - \Lambda_2 = l_p \frac{\phi}{\varepsilon - \phi} - l_v \tag{3.25}$$

$$\Lambda = l \frac{v_c}{v_{CD}} \frac{\phi}{\varepsilon - \phi} - l \frac{v_l}{v_{CD}} \tag{3.26}$$

$$\Lambda = \frac{l}{v_{CD}} \left(v_c \frac{\phi}{\varepsilon - \phi} - v_l \right) \tag{3.27}$$

where, v_{CD} is the velocity of the interface CD.

Substituting the values of Λ in the equation 3.15 we obtain,

$$v_c = \frac{K_w}{\eta_w} \frac{P_l - P_{atm}}{\frac{L}{v_{CD}} \left(v_{CD} \frac{\phi}{\varepsilon - \phi} - v_l \right)} \tag{3.28}$$

Also,

(Total velocity of the front CD) = (Velocity of the front CD due to pressure only) + (Velocity of the front CD due to vaporization only)

Thus,

$$v_{CD} = v_c + v_l \tag{3.29}$$

where, v_{CD} is the total velocity of the front CD.

Hence, equation 3.29 becomes,

$$v_c = \frac{K_w}{\eta_w} \frac{\Delta P}{\left(\frac{L v_c}{v_c + v_l} \frac{\phi}{\varepsilon - \phi} \right) - \left(\frac{L v_l}{v_c + v_l} \right)} \tag{3.30}$$

or,

$$\frac{v_c^2 L}{v_c + v_l} \frac{\phi}{\varepsilon - \phi} - \frac{L v_l v_c}{v_c + v_l} = \frac{K_w}{\eta_w} \Delta P \tag{3.31}$$

Assuming that,

$$\frac{v_c}{v_l} = A \qquad \text{and} \qquad \frac{\phi}{\varepsilon} = B$$

we obtain,

$$v_c L \left[\left(\frac{A}{A+1} \right) \left(\frac{B}{1-B} \right) - \left(\frac{1}{A+1} \right) \right] = \frac{K_w}{\eta_w} \Delta P \tag{3.32}$$

Using plausible values for q, Q, ε, ρ_w, η_w and K_w

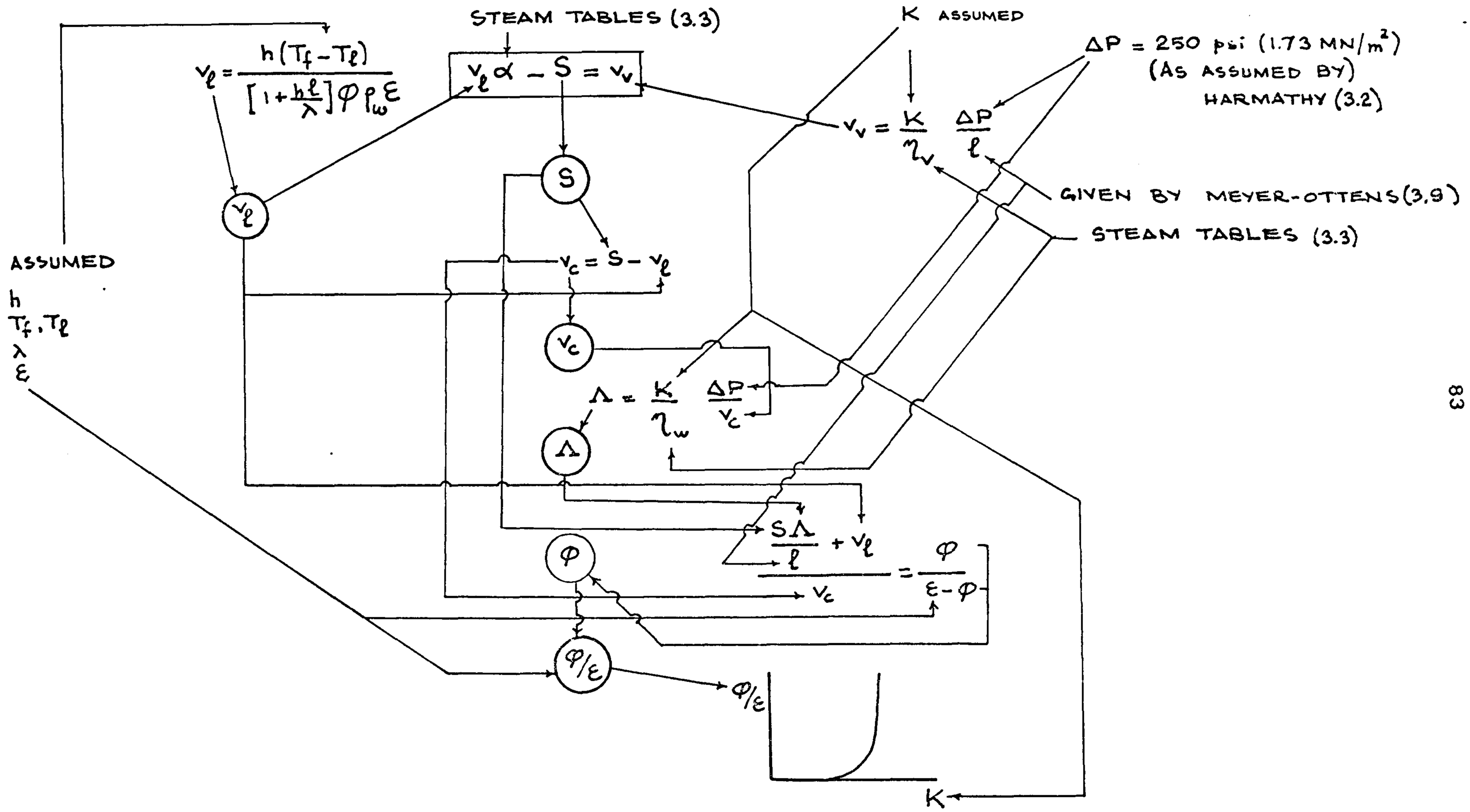

FIG. 3.4 DIAGRAM SHOWING THE STEPS TO OBTAIN FIG. 3.2

83

in the equation 3.32 and following the numerical procedure shown in Fig.3.4, results shown in Fig.3.2 are obtained.

3.1.2.4 Concluding Remarks

A more realistic spalling liability curve taking into account the escape of vapour through the dry layer is presented in Fig.3.2.

In the usual range of permeability (10^{-14} - 10^{-12}) and normal range of moisture content (5·5% - 12·5% by volume) Fig.3.2 suggests that permeability itself rather than permeability and moisture content combination is the governing factor in spalling.

It appears that there is a clear cut limit of permeability below which spalling is likely to occur. This limit depends basically on the porosity, the tensile strength, the rate of heating, rather than on the moisture content.

If this assumption is correct, explosive spalling observed in some tests on specimens with a high moisture content could be related to the low permeability due to more complete hydration at high moisture content level, rather than directly to high moisture content making larger amount of water available for the evaporation.

This argument does not, of course, apply to materials such as bricks where hydration is not so important. For such materials, although moisture content and permeability are still the governing factors

for pore pressure generation, these two factors are not interdependent. Such materials should therefore be studied separately.

3.2 Effective Stress Approach

3.2.1 Introduction

In the previous section it has been assumed that concrete fails if:

a. the space made available for the vapour is less than the increase in volume due to the phase change of water vapour.

and (according to Harmathy),

b. if the excess pore pressure above atmospheric thus created is greater than the tensile strength of the concrete.

Condition 'a' suggests an increase in pressure, but may not necessarily be considered the condition for failure unless coupled with 'b', because the increase of pressure at relatively low levels of pressure need not cause a failure.

However, there seems to be no straightforward relationship like the one expressed in 'b', between the tensile strength and the pore pressure, simply because measured tensile strength can be considered as a stress or force upon a unit area including solid portion as well as voids, and pressure is only applied within the pores.

Comparison of the total due to the pore pressure, with the force necessary to break the material could

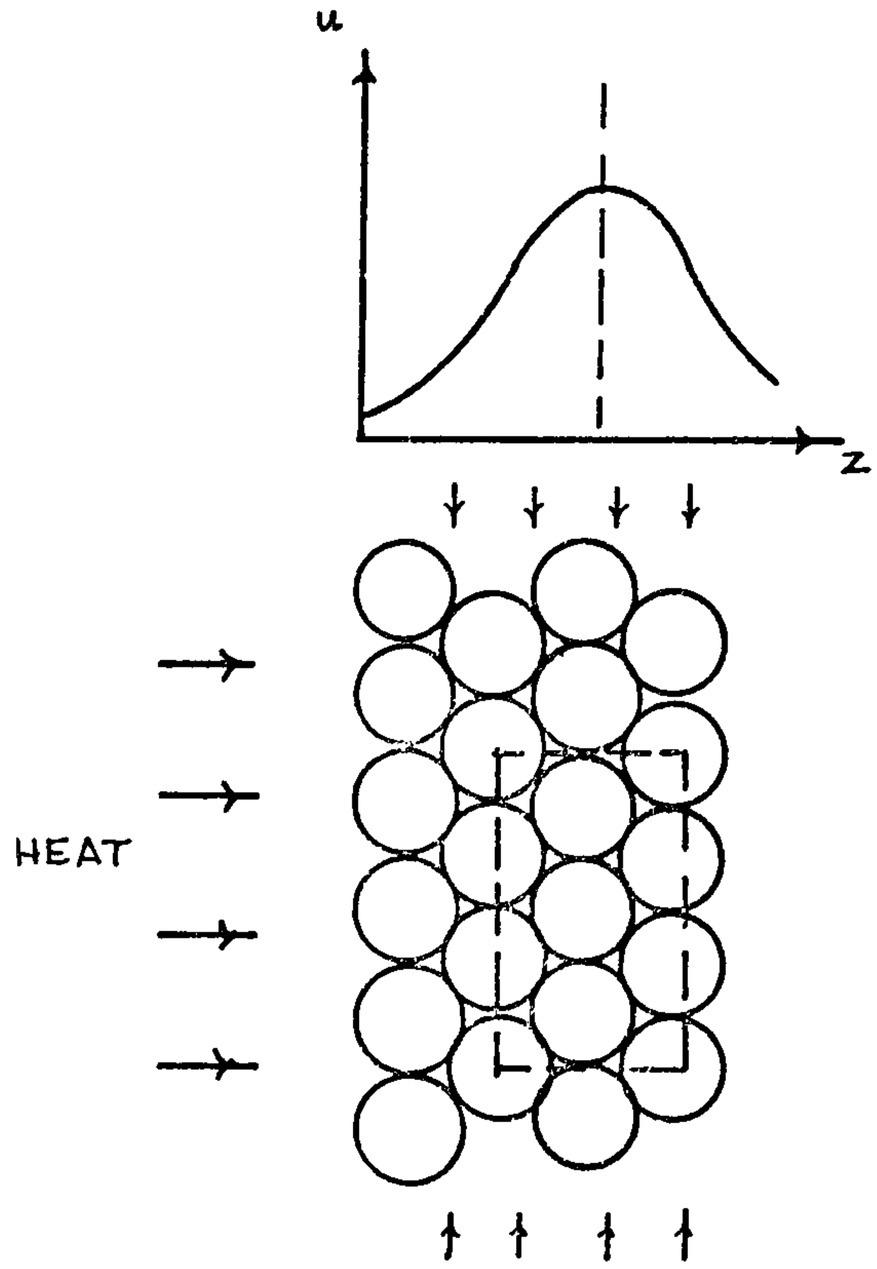

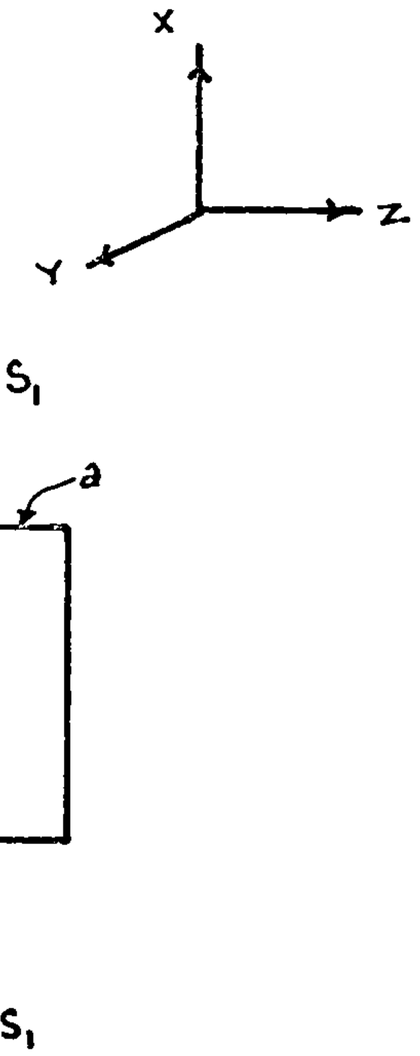

FIG. 3.5 CONCRETE EXPOSED TO HEAT

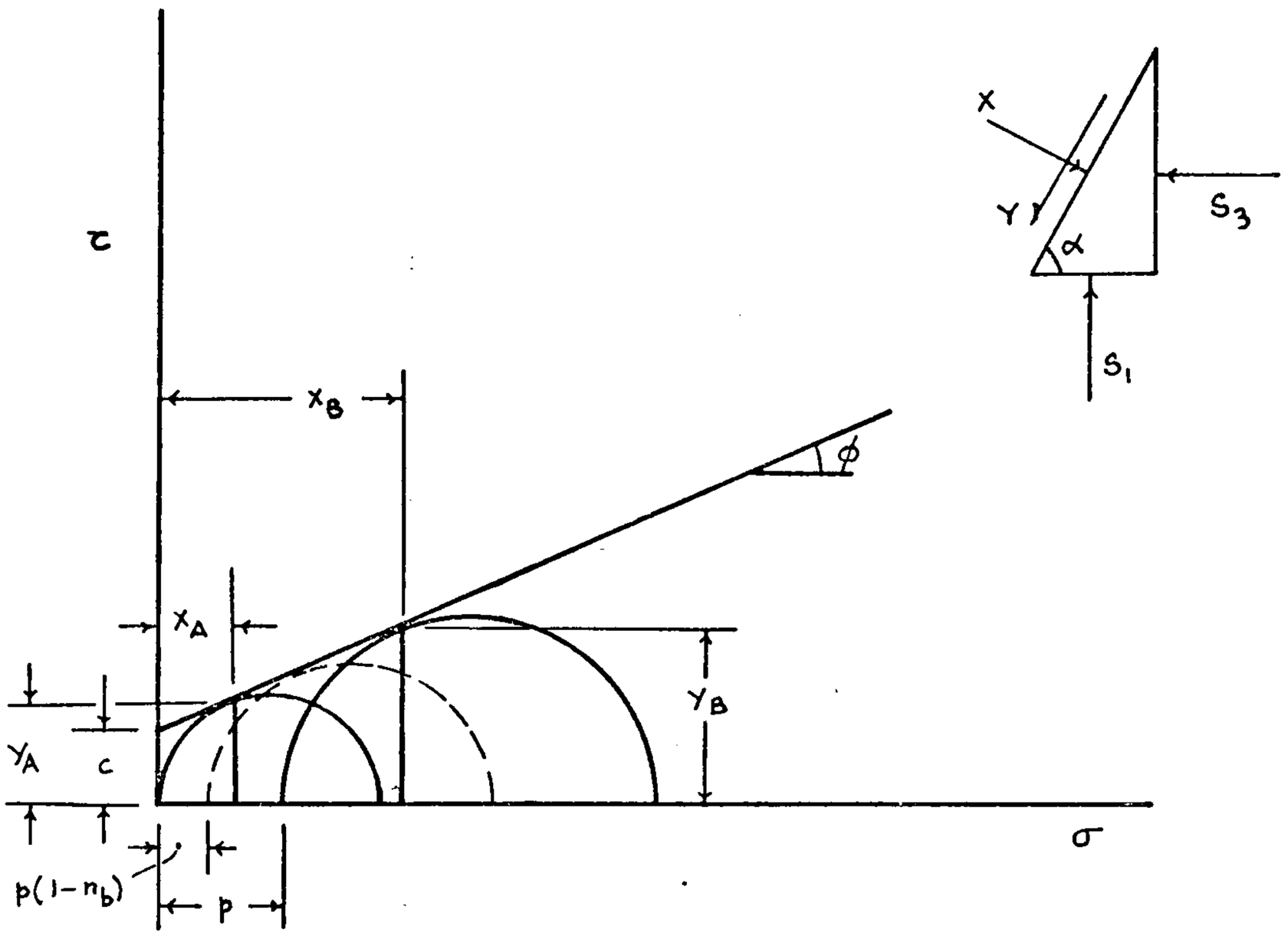

FIG. 3.6 MOHR CIRCLE RELATED TO TRIAXIAL TESTS

perhaps constitute a more realistic criterion than the comparison of the pore pressure with the tensile strength.

Furthermore, there is experimental evidence that spalling occurs in a fire test when saturated steam is at about 150°C (see Chapter I). Vaporization at this temperature suggests the presence of 0·63 MN/m^2 (Arnold 3.3) steam pressure which is substantially less than the lower estimate of the tensile strength of concrete which is 2·0 MN/m^2.

Therefore, direct comparison of the pore pressure with the tensile strength of the concrete at that temperature may not provide a suitable failure criterion as failure is generally observed at pressures less than the tensile strength of concrete.

An alternative mechanism by which failure can be induced by pore pressures less than the tensile strength of concrete will be presented in the next section.

3,2,2 Effective Stress Principle Applied to Concrete

Let us assume the concrete to be granular in nature, with the grains bonded by a cementive medium.

When exposed to heat such a material would:

a. be under compressive stresses due to restrained thermal expansion (Fig.3.5)

b. be affected by internal steam pressure due to vaporization. (Fig.3.5)

Let us now consider a smaller section of the material where maximum pressure 'p' at failure occurs, and, assume that the thickness 'a' of the section is small enough to allow 'p' to be considered uniform throughout.

If the pores contain fluid under pressure, as it is the case here, part of the load must be carried by the fluid, thus reducing the compressive stresses which act in the direction of the load on the solid material.

We therefore have

$$\sigma' = \sigma - u \qquad (3.33)$$

where, σ' is the effective stress on the solid particles, σ, is the total stress, and 'u' is the pore pressure.

One implication is that the presence of the pore pressure increases the compressive strength of the concrete.

Such a result can be demonstrated for instance using the Mohr-Coulomb theory where failure is assumed to occur at the weakest plane under a certain combination of normal and shear stresses. Calling the normal and shear stresses on the failure plane, X and Y respectively, and, constructing the Mohr circles corresponding to the cases with and without pore pressure Fig.3.6 is obtained, where X_B, the normal stress on the failure plane A-A in case where pore pressure exists, is greater than X_A, the normal stress on the failure plane in case where no pore pressure is considered to be present.

Such a decrease in total stress was expected by Dougill (3.4) in studying the effective stresses in thick slabs restrained from thermal expansion in two dimensions and heated from the third face. The author noted that the effect of pore pressure would be to

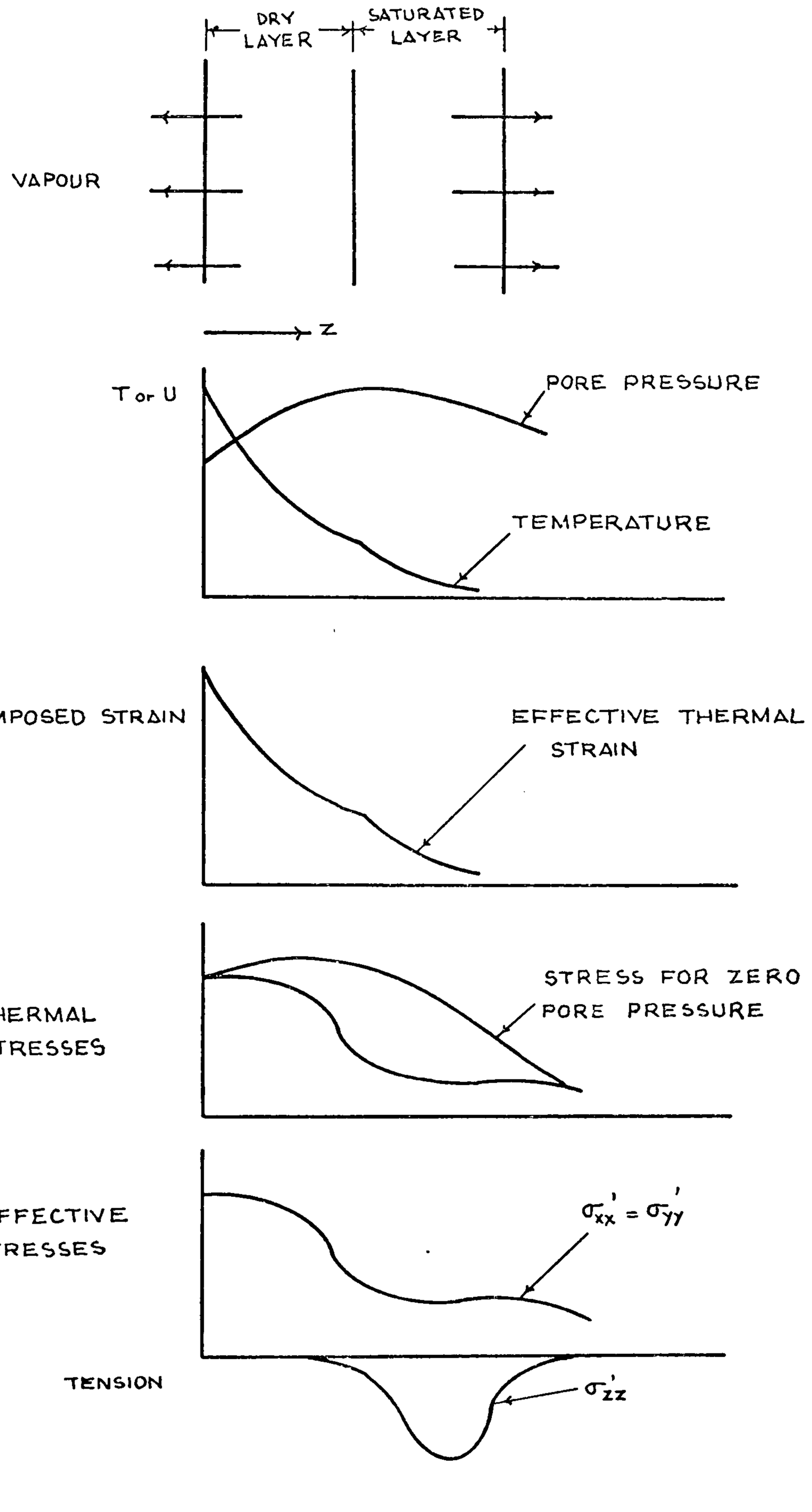

FIG. 3.7 DEVELOPMENT OF EFFECTIVE STRESSES

[AFTER DOUGILL (3.4)]

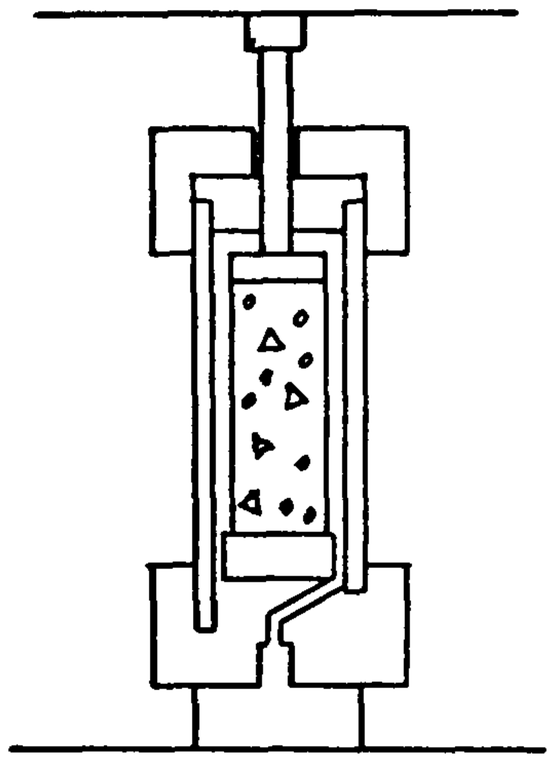

FIG. 3.8 TRIAXIAL TEST ARRANGEMENT

[AFTER TERZAGHI, (3.6)]

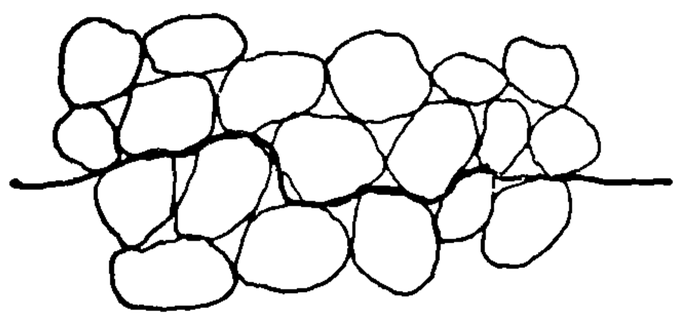

FIG. 3.9 CONCRETE CROSS-SECTION

[AFTER TERZAGHI, (3.6)]

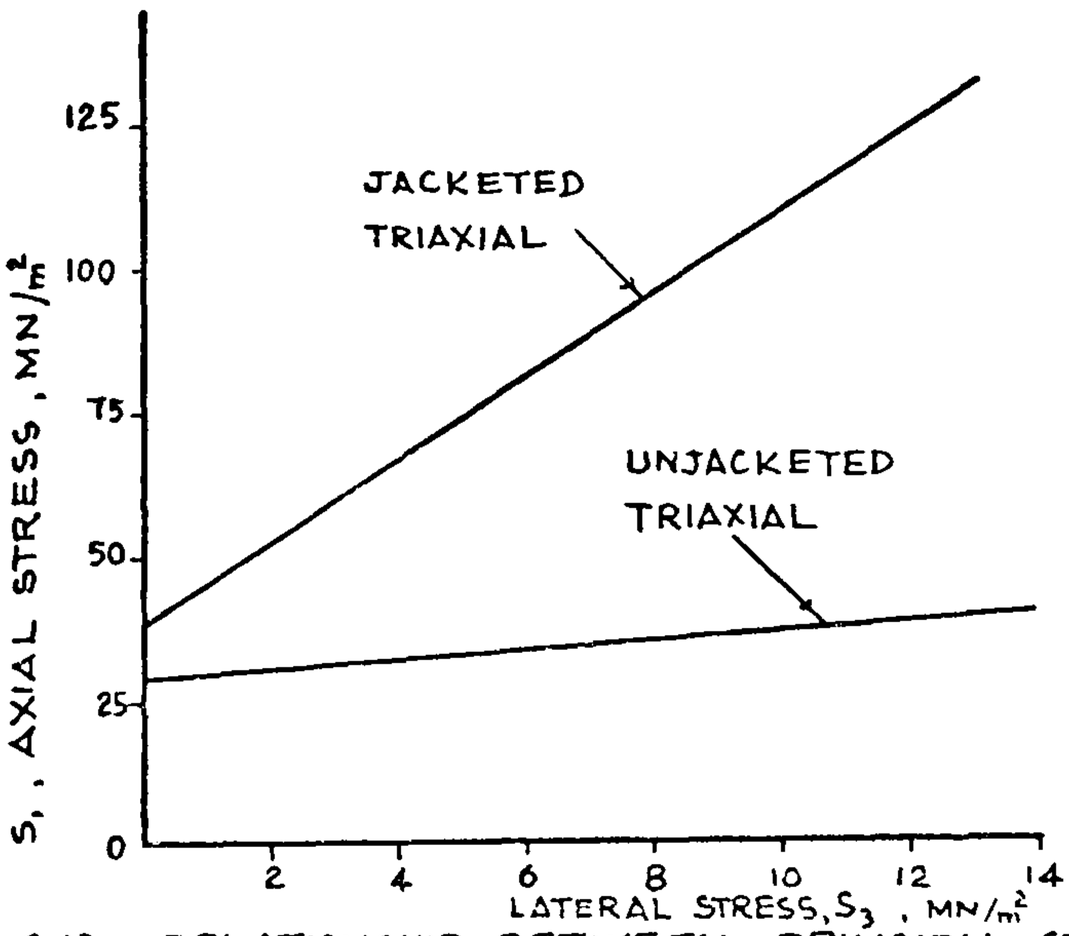

FIG. 3.10 RELATIONSHIP BETWEEN PRINCIPAL STRESSES AT FAILURE WITH OR WITHOUT PORE PRESSURE

[AFTER McHENRY (3.8)]

reduce peak values of the stress in X and Y directions, or, in other words, increase the apparent strength of the material, and also to steepen the descending branch of the stress-strain curve. The effective stress would also have a tensile component in the direction of heat transfer. (Fig.3.7)

The effective stress principle is implicitly used by Nekrasov et al. (3.5) (see Chapter 2) in the criterion,

$$(p+\sigma)\, K_1 \leqslant R_p^t \qquad (3.34)$$

where,

p = pressure of steam in concrete

σ = tensile temperature stress

K_1 = coefficent taking into account the approximation of the formula

R_p^t = tensile strength of the concrete at the temperature considered.

In other words, if σ is taken as the total stress in the concrete from all causes, the above equation follows from the principle of effective stress as used in soil mechanics.

The application of the effective stress principle to the concrete is not however new. First introduced by Therzaghi (3.6) the principle is applicable to unbonded granular material like sand. However, as reported by Leliavsky (3.7) tests have also been carried out on mortar specimens of cylindrical shape under triaxial loading. (Fig.3.8)

Therzaghi (3.6) tested some specimens under uniaxial loading only, and companion specimens under uniaxial loading with additional all around hydrostatic pressure.

These specimens were either protected by an all around membrane, thus preventing the fluid to penetrate in the material, or, unprotected, thus letting the fluid under pressure to fill the pore of the specimen.

The author noted that the hydrostatic force per unit area, 'p' on protected specimens, reduced to $p\ (1 - n_b)$, where n_b is the volume porosity, and used Mohr's criterion (see Fig.3.6) to obtain the following equation:

$$p(1-n_b) + \frac{T^2}{2a} - \frac{T}{2a}\sin\phi = \frac{T_2 - T}{2a} \qquad (3.35)$$

where, T_2 and T are experimental values for the failure load of unprotected and protected specimens respectively under hydrostatic pressure p, 'a' is the cross-sectional area, and ø is the angle of internal friction obtained from previous experiments carried out by other research workers.

Using this equation the volume porosity n_b, and the value of the uplift force due to pore pressure could be determined.

The average value of the volume porosity n_b, found this way was ranging from 0·97 to 0·998.

Although this seems to be too high a value for the porosity of the material, Terzaghi explained this apparently impossible figure, with the aid of the Fig.3.9

which shows that the points of contact in between the microsolids were of a still higher order of smallness than the microsolids themselves.

It is interesting to note that McHenry (3.8), using an indirect approach obtained the volume porosity approximately equal to unity, thus confirming Deliavsky's findings.

The implication of n_b being close to unity is that, p_b, which is equal to $p(1 - n_b)$ is approximately zero in these circumstances. This fact is also observed in Fig.3.10 where the effect of pore pressure on axial compressive strength is relatively small.

It should however be noted that the effect of the pore pressure seems to be negligible in these tests only because the specimens are enclosed in the test cell and therefore the lateral pressure is equal to pore pressure inside the specimen, thus cancelling each other. In other words all the solid particles are under all round hydrostatic pressure which is equivalent to no pressure at all. However, in a more general situation, the material would not be confined in such a cell, and, therefore, lateral pressure is atmospheric and pore pressure in the solid can be much higher than atmospheric.

The main conclusion from these tests is perhaps that the boundary porosity is approximately unity, that is, that the pore pressure is effective over approximately 100% of the potential surface of failure. The resulting force due to the pore pressure would therefore be

expected to have a substantial effect on the compressive strength of the material.

The tests carried out by Terzaghi (3.6) and by McHenry (3.8) were so designed that the failure was the result of a mechanical axial load, rather than being the result of internal pressure. In other words the failure was a compressive failure rather than a tensile one. However, in concrete exposed to high temperatures, the failure is assumed to be tensile in nature.

The importance of Terzaghi's and McHenry's tests is perhaps that they show that the principle of effective stress can be applied to concrete. However, in order to obtain precise information on the effect of internal pressure on concrete, tests must be planned to satisfy the following conditions:

a. The failure must be tensile
b. It's active agent must be the pore pressure, whereas the mechanical force must be an additional factor to counterbalance this destructive action.

It is interesting to note that if these conditions are fulfilled Mohr-Coulomb theory may not be applicable because, in tests in which mechanical axial load causes failure, the shape of the failure surface[x] is not

Footnote

x The angle α of the failure plane is the same no matter what the failure load is.

affected by the magnitude of the applied axial force, whereas with the pore pressure as agent of rupture, the surface of failure, although affected by many other physical factors, will also naturally tend to be of such a shape [x] as to produce a maximum breaking force, an effect which does not exist in the first case i.e. when the failure is the result of a mechanical load.

Tests somewhat related to the second case discussed above, where internal pressure is applied till the failure of concrete specimens under external loading are discussed in Chapter 5 of the present work.

A related failure mode quite different from the one suggested by Mohr-Coulomb theory is presented in Chapter 4.

3.3 Theories Based on the Calculation of Drag Forces

3.3.1 Meyer-Ottens' Theory

An alternative theory based on a model of behaviour very similar to Harmathy's (3.2) has been presented by Meyer-Ottens (3.9).

Like Waubke (3.10) he calculated the drag force exercised on the walls of the pores, due to escaping vapour, and, predicted failure if the stress due to this force exceeded the tensile strength of concrete.

Considering the water vapour to act as a Newtonian fluid, Meyer-Ottens assumed,

$$\tau_D = \eta_v \frac{dV}{dy} \qquad (3.36)$$

Footnote

x Parallel to the unloaded surface.

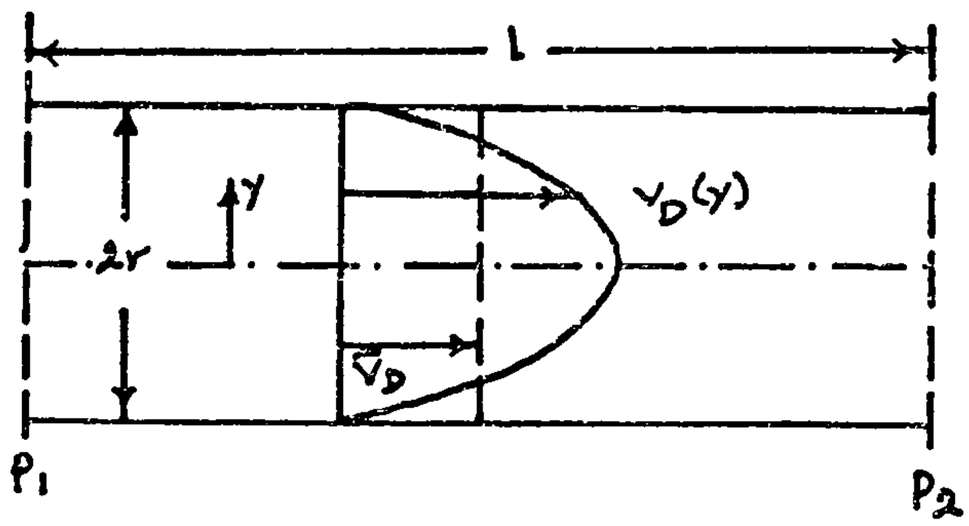

FIG. 3.11 VELOCITY DISTRIBUTION IN A PORE

[AFTER MEYER-OTTENS, (3.9)]

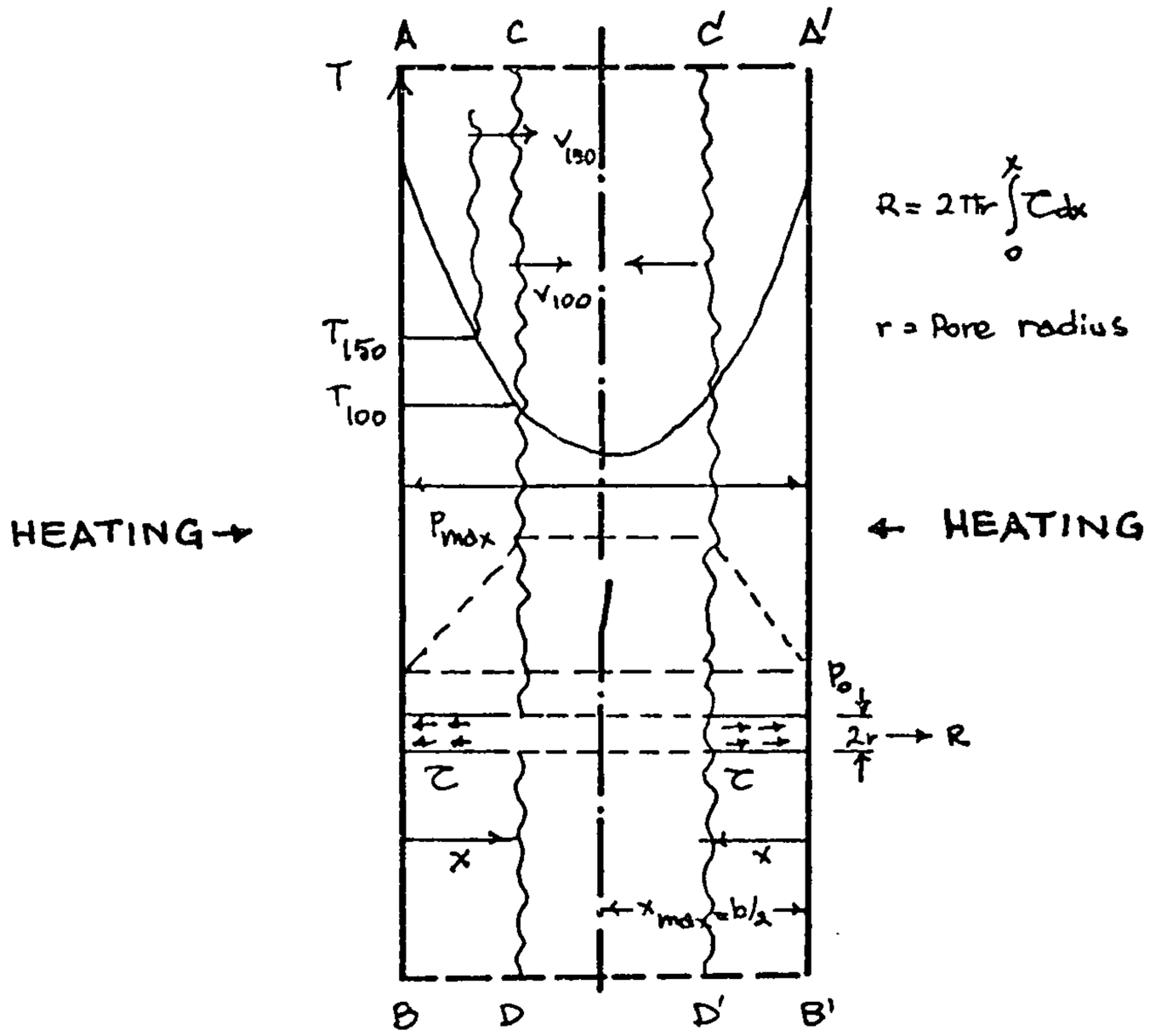

FIG. 3.12 DIAGRAM REPRESENTING CONCRETE WALL PANEL HEATED FROM BOTH SIDES

[AFTER MEYER-OTTENS, (3.9)]

where,

v_D = velocity of vapour flow (Fig.3.11)

η_v = dynamic viscosity of vapour

τ_b = shear stress on the walls

Meyer-Ottens assumed that, when concrete panels are exposed to heat a steep temperature gradient forms through the thickness of the material. Moreover, water in the region close to the surface, where corresponding temperature is above vaporization temperature of water, evaporates, thus forming a more or less distinct interface between the dry and wet regions (Fig.3.12). Obviously this vaporization process increases the pressure on the water in the central region and the excess pressure drives vapour through the capillaries to the atmosphere. However, quite differently from Harmathy who assumed the interface to be moving towards the cooler region under the effect of pressure, thus forming a saturated layer, Meyer-Ottens ignores the movement of the water particles due to pressure. Consequently, in this case, the interface seems to move towards the cooler region due only to vaporization, and, the wet layer is not saturated but keeps its original moisture content.

On this, Harmathy's view seems more likely to be correct. Movement of liquad water was observed in tests described in Chapter 8 of the present work which would support the idea of a saturated moisture clog.

For steady laminar flow in pipes the velocity distribution is parabolic. (Fig.3.11)

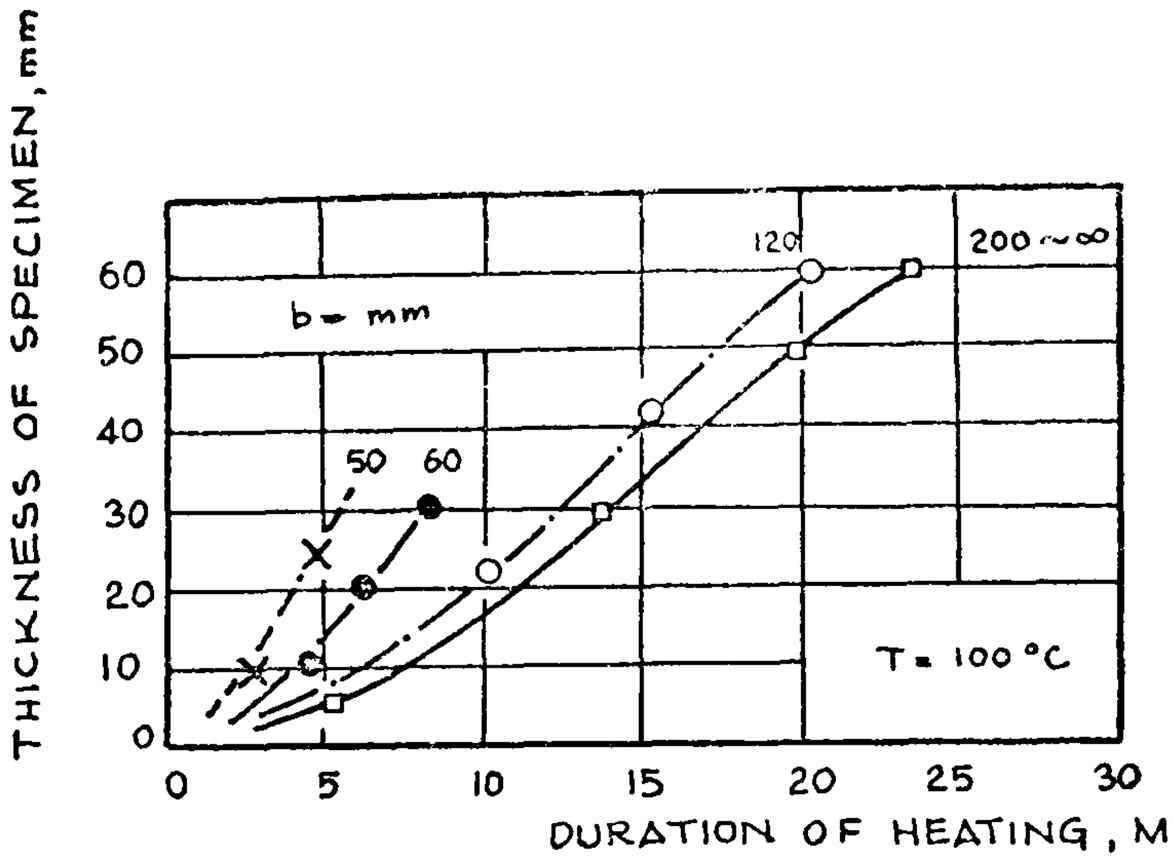

FIG. 3.13 POSITION OF EVAPORATION FRONT DURING EXPOSURE TO HEAT

[AFTER MEYER-OTTENS, (3.9)]

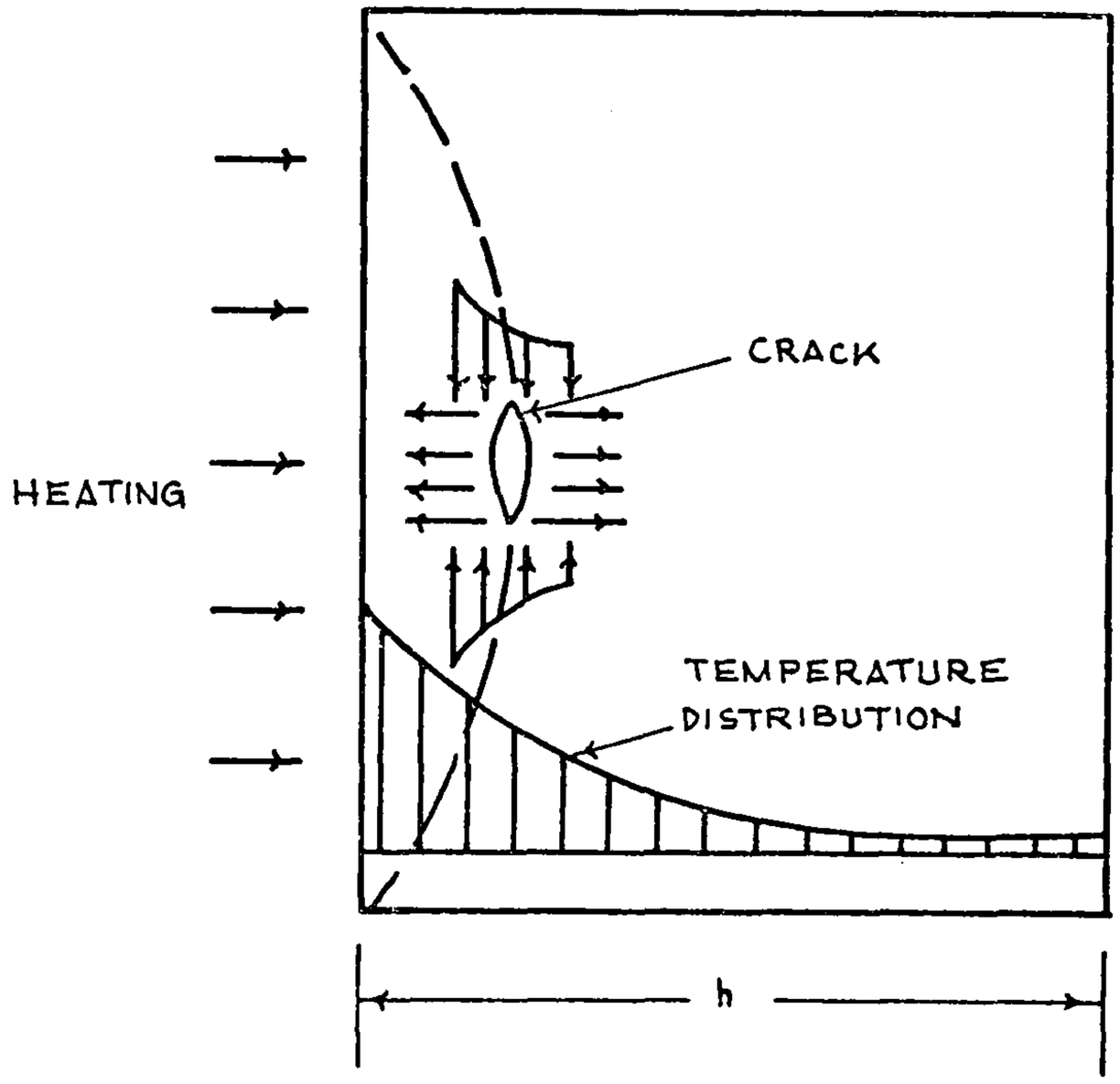

FIG. 3.14 STRESS DISTRIBUTION AROUND CRACKS AT THE MOMENT OF FAILURE

[AFTER ZHUKOV (3.13)]

Therefore, assuming the flow of vapour to be steady and laminar, Meyer-Ottens obtained,

$$v_D = 2 v_{av} \left(1 - \frac{y^2}{r^2}\right) \qquad (3.37)$$

Combining this with equation 3.36 we obtain,

$$\tau_D = \eta \left(-\frac{4 v_{av} y}{r^2}\right) \qquad (3.38)$$

so that, at $y = r$,

$$\tau_D = -\eta \frac{4 v_{av}}{r} \qquad (3.39)$$

Considering that,

$$V_{H_2O} = v_{100}\ \phi\ A \qquad (3.40)$$

where,

V_{H_2O} = volume of water evaporated per unit time

ϕ = moisture content

A = cross-sectional area

v_{100} = velocity of T = 100°C front [x]

Therefore, weight of water evaporated per unit area per unit time =

$$W_{H_2O} = V_{H_2O}\ \rho_{H_2O}\ \frac{1}{A} \qquad (3.41)$$

and, weight of vapour released per unit time per unit area =

$$W_v = W_{H_2O} \qquad (3.42)$$

Footnote

x T = 100°C front is, according to Meyer-Ottens the interface between the wet and dry regions assuming that evaporation occurs at 100°C. (Fig.3.13)

Meyer-Ottens then assumes that the volume of vapour released per unit time per unit area is,

$$V_V = \frac{W_V}{\rho_V} \tag{3.43}$$

where, ρ_V is the density of the vapour.

This assumption, however, implies that vapour is considered to be incompressible and that changes in its properties with temperature are ignored. In other words vapour, when travelling from the interface where the pressure is 'p' to the heated surface where the pressure is atmospheric, is assumed to undergo no volume change.

Meyer-Ottens noted that the volume of vapour released per unit time per unit area in equation 3.43 can also be expressed in the following way:

$$V_V = v_{av}\ A_P \tag{3.44}$$

where, A_P is the area of pores per unit area of concrete, V_V and v_{av} having their usual meaning.

Equating 3.43 and 3.44 we get,

$$v_{av} = \frac{v_{100}\ \phi\ \rho_{H_2O}}{A_P\ \rho_V} \tag{3.45}$$

and substituting 3.45 into 3.39 Meyer-Ottens obtained the equation for the shear stress on the walls of the capillary tube as,

$$\tau = -\frac{4\eta}{r}\ \frac{v_{100}\ \phi\ \rho_{H_2O}}{A_P\ \rho_V} \tag{3.46}$$

It should be noted that to obtain equation 3.45 it is necessary to assume that all pores are interconnected. This is another idealization. It is well known that

in concrete not all pores are connected (Neville 3.11) and that the continuously connected pores gradually become disconnected with age as hydration products block the pores. (Powers et al. 3.12)

However, on considering the pores as cylindrical tubes, the author obtained

$$R = \int_o^x 2\pi r \ \tau \ dx \qquad (3.47)$$

where, 'R' is the total drag force on a single tube, and 'r' is the radius of this tube.

Now, substituting the value of τ in this equation we obtain,

$$R = \int_o^x 2\pi r \ \frac{4\eta}{r} \ \frac{v_{100} \ \phi \ \rho_{H_2O}}{\Delta p \ \rho_{vap}} \qquad (3.48)$$

The total drag force on a unit area of the material is therefore found from,

$$\sigma_f = \sum_{r_n}^{r_m} A_l \ R \qquad (3.49)$$

where, A_1 is the number of pores per unit area of concrete.

Meyer-Ottens assumes spalling will occur when σ_f exceeds the tensile strength of concrete.

3.3.2 Zhukov's Theory

A major weakness in Meyer-Ottens' theory is the omission of the effect of compressive stresses on spalling. A step further would therefore be the calculation of stresses in concrete due to the pore pressure, compressive stresses due to the thermal gradient, and perhaps due to external loading. This

was in essence the approach adopted by Zhukov (3.13).

In this, he considered a panel of concrete infinitly large in Y and Z directions, and having a finite thickness in X direction (Fig.3.14), heated from face Y - Z.

Under three dimensional state of stresses we have,

$$\varepsilon_{xx} = \frac{1}{E}\left[\sigma_{xx} - \nu(\sigma_{yy} + \sigma_{zz}\right] \qquad (3.50)$$

where, ν is the Poisson's Ratio.

Assuming that the external load is in Y- direction only, while the thermal stresses are applied in Z and Y directions, we obtain,

$$\varepsilon_{xx} = \frac{1}{E}\left[\sigma_p + 2\nu(\sigma^c_{c_1}) + \nu\,\sigma^H_{c_1}\right] \qquad (3.51)$$

where,

σ_{c_1} is the stress due to the thermal gradient, and, $\sigma^c_{c_1}$ is the stress due to external loading, ν is the Poisson's Ratio.

According to Zhukov (3.13) the work done in X-direction is,

$$W_x = \frac{1}{2}\,\sigma_p\,\varepsilon_{xx} = \frac{1}{2}\,\sigma_p\left[\sigma_p + 2\nu(\sigma^c_{c_1}) + \nu\,c^H_1\right] \qquad (3.52)$$

where, σ_p = tensile stress due to the movement of the steam.

However, this expression gives the strain energy density and not work done and therefore should not be used.

On the other hand Zhukov obtains the expression for the work done to cause failure as,

$$W = \frac{1}{2} R_p \left(\frac{R_p}{E}\right) = \frac{1}{2} \frac{R_p^2}{E} \tag{3.53}$$

where R_p is the ultimate tensile strength of concrete.

Zhukov, taking equation 3.52 as expressing the work done and combining with equation 3.53 obtains

$$\sigma_p^2 + 2\nu C_{c_1}^c \sigma_p + \sigma_p \nu C_1^H = R_p^2 \tag{3.54}$$

It follows that the higher the compressive stresses due to the thermal gradient and external loading, the lower is the pore pressure necessary to cause failure.

In order to calculate the stresses due to pore pressure in concrete exposed to heat, Zhukov (3.13), similar to Meyer-Ottens, assumed that the tensile stresses are induced by the drag force exercised on the walls of the capillaries interconnected, thus forming tubes carrying the steam from the interface where vaporization occurs to the heated face.

Using equation 3.9 , and, assuming that,

$$v_a = \frac{v_d}{n_s} \tag{3.55}$$

where,

v_a = actual velocity

v_d = discharge velocity

n_s = surface porosity,

we have,

$$v_{cp} = \frac{K}{\eta} \frac{dP}{dx} \frac{1}{n_s} \tag{3.56}$$

where, K is the permeability, v_{cp} is the average

velocity, and, η is the dynamic viscosity.

Substituting equation 3.56 into 3.39,

$$\tau = \frac{4\eta}{r} \frac{K}{\eta} \frac{dP}{dx} \frac{1}{n_s} \qquad (3.57)$$

Total drag force in one capillary tube is therefore,

$$F = \int_0^x 2\pi r \ \tau \ dx \qquad (3.58)$$

or,

$$F = 8\pi \int_0^x \frac{K}{n_s} \ dP \qquad (3.59)$$

and,

$$\sigma_p = 8\pi N \int_0^x \frac{K}{n_s} \ dP \qquad (3.60)$$

where,

N = number of pores in unit area of concrete

σ_p = stress due to drag force in concrete.

However, ignoring the effect of compressive stresses due to thermal gradient and loading, Zhukov substituted plausible values in equation 3.60 and found that a pressure of 0·596 kg/cm^2 (59 KN/m^2) was sufficient to cause failure of an ordinary concrete.

Although Zhukov notes that this result is in line with his experimental findings, the tests described in Chapter 5 of the present work showed that much higher pressures can be generated in concrete without visible damage to the material.

Nevertheless, Zhukov concluded that the evaporation

process occurs without substantial increase in pressure, and, obtained a simpler expression for the tensile stresses due to drag force, in the following way:

The volume of the steam evaporated can be expressed as,

$$m = \frac{K_2 q}{\mathcal{L} \gamma_n} \tag{3.61}$$

where,

K_2 = a coefficient showing how much of the total heat supplied is actually used up by the water to evaporated,

q = heat flux

$\mathcal{L}$ = heat of vaporization

γ_n = specific mass of steam.

From the definition of K, Zhukov obtains the following relationship:

$$K_2 = \frac{c_w}{c_c} \frac{W_w}{(1-n_s)} \tag{3.62}$$

where,

c_w = specific heat capacity of water

c_c = specific heat capacity of concrete

W_w = weight of water in unit volume of concrete

However, equation 3.62 should read,

$$K_2 = \frac{c_w}{c_c} \frac{W_w}{(1-n_s)\rho_c} \tag{3.63}$$

with the inclusion of ρ_c, density of concrete, because, if K is the ratio of the heat consumed by the water in concrete to the total heat, we obtain,

$$K_2 = \frac{q_w}{q_{total}} = \frac{W_w\ c_w\ \Delta T}{W_c\ \ c_c\ \Delta T} \qquad (3.64)$$

where, W_w and W_c have their usual meaning.

Also, assuming all pores full of water,

$$n_s = \frac{V_w}{V_t} = \frac{V_t - V_s}{V_t} \qquad (3.65)$$

where,

V_w = volume of water in concrete of volume

Taking v_t = unit volume,

$$n_s = 1 - v_s \qquad (3.66)$$

or

$$v_s = 1 - n_s \qquad (3.67)$$

Also,

$$W_c = V_c\ \rho_c = V_s\ \rho_c = (1-n_s)\rho_c \qquad (3.68)$$

Therefore, substituting the value of W_c in equation 3.64, we obtain,

$$K_2 = \frac{c_w}{c_c}\ \frac{W_w}{(1-n_s)\rho_c} \qquad (3.69)$$

Remembering that $W_w = W_o$ = moisture content by volume, we get,

$$K_2 = \frac{c_w}{c_c}\ \frac{W_o}{(1-n_s)\rho_c} \qquad (3.70)$$

or, taking c_w = 1 cal [x]

and, c_c = 0·25 cal, as Zhukov did,

Footnote

x 1 cal in c.g.s. units

Table 3.I Properties of Concrete.(After Zhukov(3.I3))

Type of concrete	Porosity	r mm	Coef. of thermal conductivity $\lambda \times 10^{-12}$
Heavy	.03-.25	10^{-5}-10^{-3}	6.8-4.27
Light	.05- .4	10^{-5}-10^{-1}	2.2-0.9
Cellular	.05- .8	10^{-3}-10	.9 -0.39

Table 3.2 Results of calculations,(After Zhukov(3.I3))

Stress MN/m^2	Type of concrete		
	heavy	light	cellular
σ_p max	28.7	7	43×10^{-5}
σ_p min	2.4×10^{-3}	$1. \times 10^{-7}$	9×10^{-10}

we obtain,

$$K_2 = 4\frac{W_o}{(1-n_s)P_c} \tag{3.71}$$

However, Zhukov, taking the incomplete equation,

$$K_2 = 4\ \frac{W_o}{1-n_s} \tag{3.72}$$

and considering that,

$$v_{cp} = \frac{m}{n_s} \tag{3.73}$$

obtains,

$$v_{cp} = \frac{Kq}{\alpha \gamma_n n_s} \tag{3.74}$$

Also,

$$q = \lambda \left(\frac{dT}{dx}\right) \tag{3.75}$$

where, λ is the coefficient of thermal conductivity.

Substituting equation 3.74 into 3.39 we get the tensile force along one capillary,

$$Q = \int_o^x 2\pi r\, \tau\, dx = \int_o^x 2\pi r\ \frac{4\eta Kq}{r\, \alpha\, n_s \gamma_n}\, dx \tag{3.76}$$

Substituting the value of K from equation 3.72 into equation 3.76 we obtain,

$$\sigma_p = \int_o^x \frac{32\,\pi\,\eta\, W_o\, N\, \lambda}{\alpha\ n_s (1-n_s)\gamma_n}\, \Delta T \tag{3.77}$$

where,

σ_p = tensile stresses due to the drag force

N = number of pores per unit area of concrete

Substituting plausible values in equation 3.77 the author obtained Table 3.1 where results for tensile

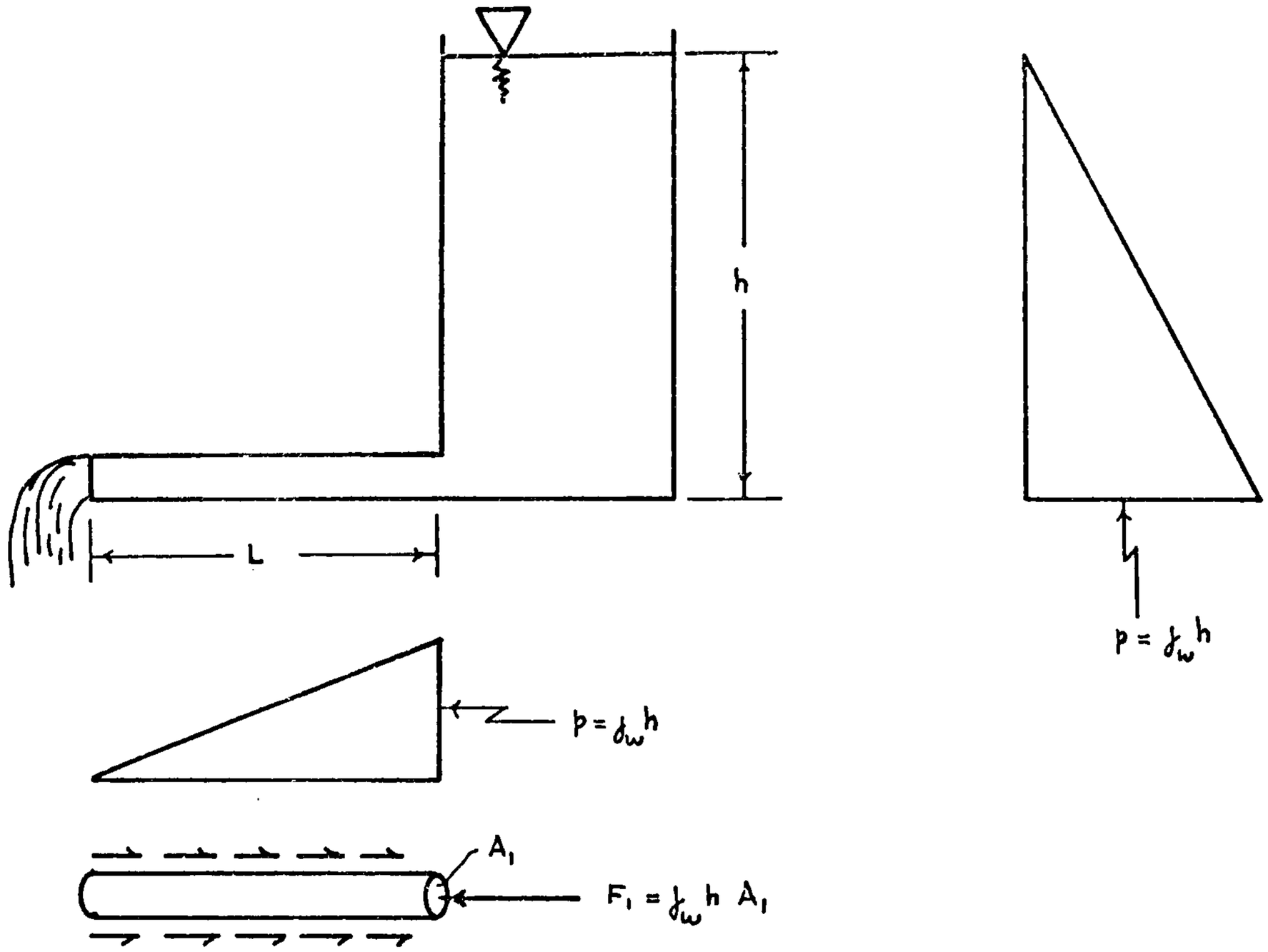

FIG. 3.15 WATER TANK ANALOGY

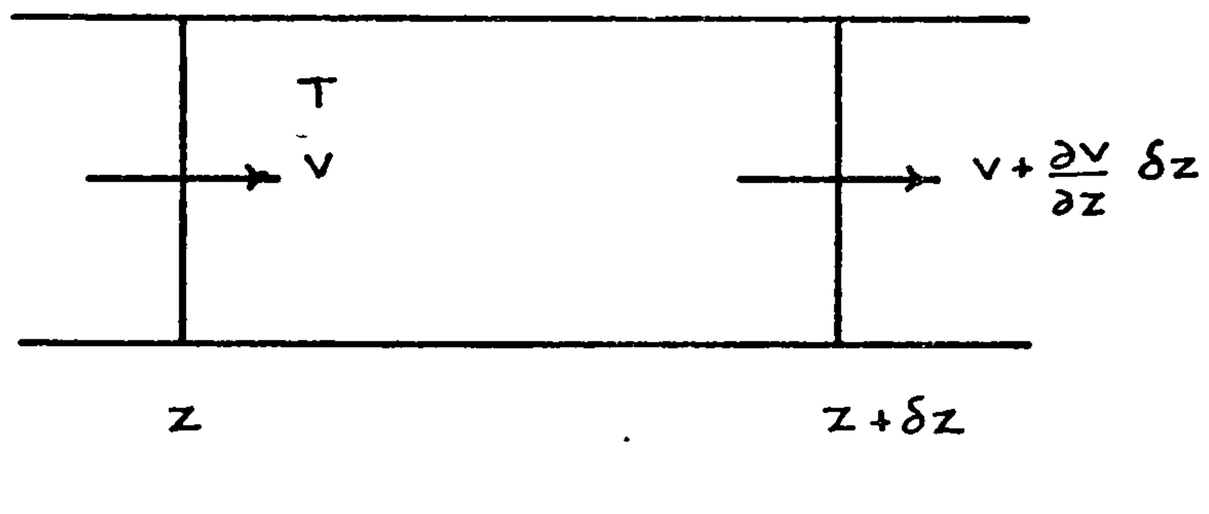

FIG. 3.17 VOLUME ELEMENT USED IN ESTABLISHING CONTINUITY

stresses due to drag forces are tabulated for heavy, light, and, cellular concrete.

Table 3.2 shows that tensile stresses up to 287 kg/cm^2 (28 MN/m^2) can be expected in dense concrete.

Although the correction of K with the introduction of ρ_c would reduce σ_p about 2·5 times, it is surprising that negligibly low pressures can produce such high drag forces.

In steady state conditions total drag force should be balanced by the force due to the pressure and therefore they should be equal.

After all, if no pressure difference exists between the ends of the capillary tubes no flow^x could be expected in these tubes. This point will be taken further in the following section.

Water Tank Analogy

Let us consider a tank full of water up to a height 'h', to which a pipe of cross-section A_1 is connected as shown in Fig.3.15. Assuming that the height 'h' is kept constant by a continuous supply of water to the tank.

Let us consider the water flowing in the pipe after steady state flow condition is reached. The forces on the cylinder of water is shown in Fig.3.15.

At steady state conditions we have,

Footnote

x Here the flow due to thermal expansion of the fluid is excluded.

$$v = \text{constant}$$

$$\tau = \text{constant}$$

and, $\sum F_x = 0$

Therefore,

$$\gamma_w h A_1 = 2\pi r \tau = 2\pi r 4\eta \frac{v_{cp}}{r} \tag{3.78}$$

or,

$$\gamma_w h A_1 = 8\pi\eta v_{cp} \tag{3.79}$$

Substituting the value of v_{cp} from equation 3.74 into equation 3.79 we get,

$$\gamma_w h A_1 = 8\pi\eta \frac{Kq}{\alpha \gamma_n n_s} \tag{3.80}$$

It is clear that the left handside of the equation 3.80 representing the force due to the pressure is dependent on the radius of the cylinder of water while the right handside is not. This implies that, if we increase the number of tubes, say from 1 to 2, while reducing the radius from r_1 to r_2 so that A_1 is kept at its original value for each cylinder of water, we obtain,

$$\gamma_w h \frac{A_1}{2} = 2\pi r_2 4\eta \frac{v_{cp}}{r_2} \tag{3.81}$$

or

$$\gamma_w h \frac{A_1}{2} = 8\pi\eta \frac{Kq}{\alpha \gamma_n n_s} \tag{3.82}$$

Obviously, the equality (equation 3.82) does not hold in this case, the right handside of the equation

being exactly the same as the previous case (equation 3.80) where there is only one pipe, the left handside is reduced by half.

In a similar fashion we increase the number of tubes per unit area from '1' to 'n', the area, and therefore the force due to pressure on one tube of water would increase 'n' times while the drag force on each tube remains constant.

This, however, is not logical, due to the fact that, at steady state conditions, the body is in equilibrium and the equation must hold no matter what the area of the tube is.

The conclusion is that equation

$$\tau = 4\eta \frac{4c_p}{r} \qquad (3.83)$$

where,

$$v_{cp} = \frac{K q}{\alpha \gamma_n n_s} \qquad (3.84)$$

is not realistic.

3.3.3 Comments on the Theories of Harmathy, Meyer-Ottens and Zhukov

The three theories that have been discussed are based on very similar physical models. In each there is a dry zone through which vapour is expelled to the heated surface and a distinct boundary between the dry and the wet zone. Both Meyer-Ottens and Zhukov concentrate their attention on behaviour in the nominally dry zone and deduce the pressure causing

spalling from the resistance to movement of the vapour . Obviously, the pressure at the interface calculated in this way should be equal to the pressure acting on the liquad at the boundary of the wet or saturated zone. Thus, there is no difference in principle when Harmathy calculates the pressure at the interface by considering the resistance to movement of the moisture plug. However, none of the authors uses the boundary conditions at the interface properly when calculating the pressure; and, each has to introduce arbitrary or experimental data in order to complete his theory. Thus Harmathy brings in his 'δ' factor, and Meyer-Ottens uses the observed velocity of the 100°C isothermal. Because of this, and a number of other approximations involved in the theories, there is no way of telling how consistant the various assumptions are or how useful the theories might be. The difficulty is made worse because the value of the theories can be tested only after inserting a large number of average or representative values for quantities that vary widely over the temperature range considered.

Because of these difficulties it seems worthwhile to formulate a theory based on the same physical model adopted by Harmathy, Meyer-Ottens and Zhukov in such a way that it is at least consistant in itself, even though the model provides only a somewhat idealised view of the real situation. This is done in the following section.

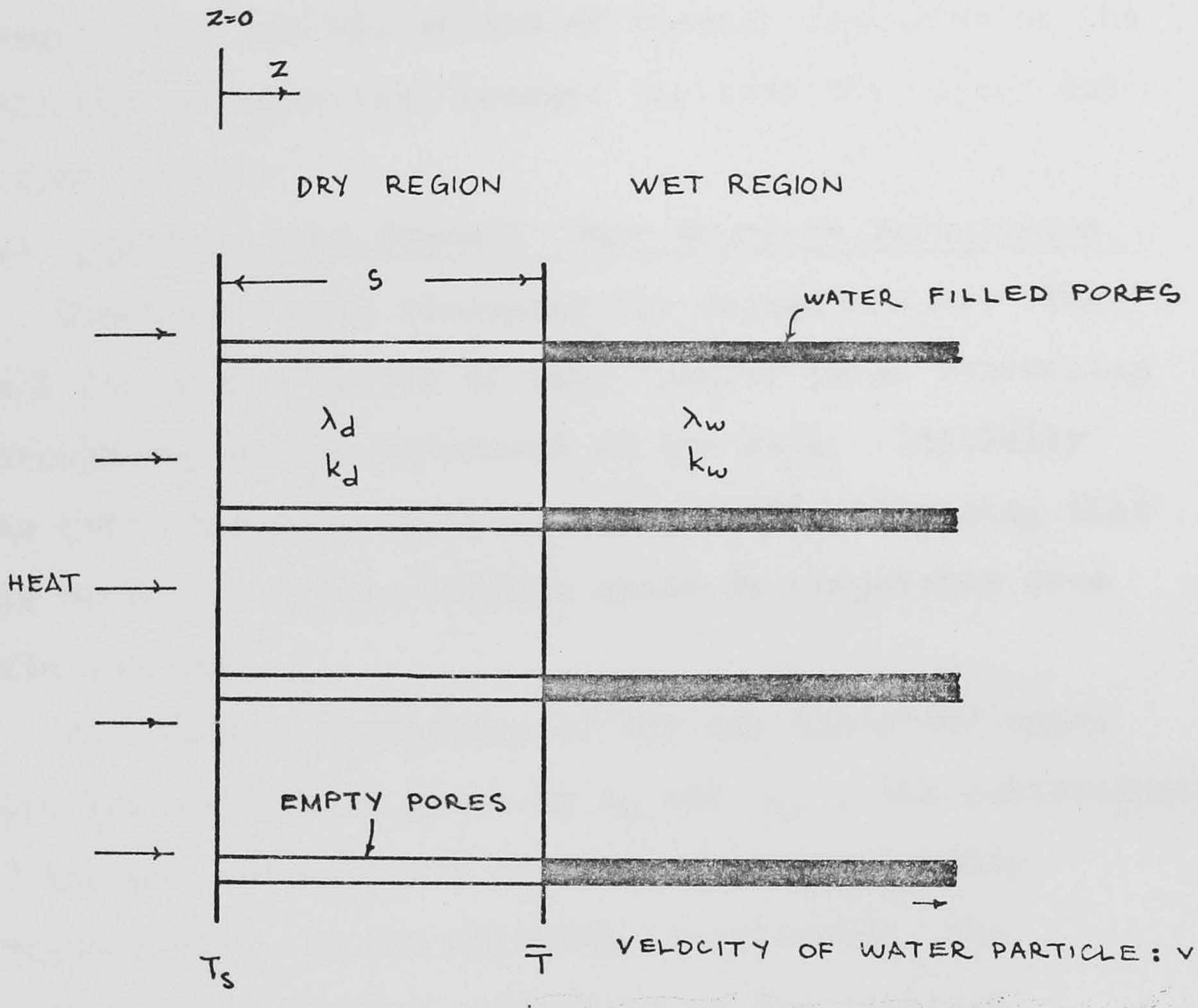

FIG. 3.16 ASSUMED POSITION OF THE INTERFACE SOMETIME AFTER THE START OF HEATING

The theory is based on the moisture clog concept but the boundary conditions at the interface are treated properly. In addition, the vapour is taken to be compressible and the effect of thermal expansion on the velocity is taken into account for both the vapour and liquad phases.

3.4 Moisture Clog Theory: More Complete Formulation

Consider a wall occupying the region $0 < z < \infty$. The wall contains a series of long tubular pores stretching through the entire thickness of the wall. Initially the pores are full of water. (Fig.3.16) Supposing that the surface z = 0 is heated, water is evaporated from this surface.

The thermal properties of the dry solid and empty pore system will be given by λ_d and k_d , the coefficients of thermal conductivity and thermal diffusibility respectively. If the material is saturated, the corresponding thermal properties of the combined material (solid + water) are λ_w and k_w .

Considering the situation when the surface Z = 0 has its temperature raised to T_s. Let us suppose that vaporization occurs at the interface between the wet and the dry region at a temperature $\bar{T}$ and let the depth of the dry region so formed be s.

Considering conduction of heat in the dry region,

$$k_d \frac{\partial^2 T}{\partial z^2} = \frac{\partial T}{\partial t} \qquad 0 \leqslant z \leqslant s \qquad (3.85)$$

with

$T = T_s$ at $z = 0$

and, $T = \bar{T}$ at $z = s$

In the wet region,

$$k_w \frac{\partial^2 T}{\partial z^2} = \frac{\partial T}{\partial t} \qquad z \geqslant s \tag{3.86}$$

with $T = \bar{T}$ at $z = s$

and, $T = T_a$ at $z \longrightarrow \infty$

At the interface, the heat absorbed must balance that required for vaporization.

The rate of movement of the interface is $\frac{ds}{dt}$, where,

$$\frac{ds}{dt} = \bar{v} + \frac{q}{m L \rho_w} \tag{3.87}$$

where,

$\bar{v}$ = the velocity of the water particles at $z = s$

q = the rate of heat absorbed per unit cross-section at $z = s$.

m = the proportion of evaporable water by weight in the total solid

and, L = the latent heat of vaporization of the liquad

But, from the definition of thermal conductivity,

$$q = -\lambda_d \left(\frac{\partial T_d}{\partial z}\right) + \lambda_w \left(\frac{\partial T_w}{\partial z}\right) \tag{3.88}$$

at $z = s$

So that the thermal conditions at the boundary are such that,

$$-\lambda_d \left(\frac{\partial T_d}{\partial z}\right)_{z^-} + \lambda_w \left(\frac{\partial T_w}{\partial z}\right)_{z^+} = m L \rho_w \left(\frac{ds}{dt} - \bar{v}\right) \tag{3.89}$$

3.4.2 Movement of the Liquid Plug

Continuity

Let us consider a section of a typical pore. (Fig.3.17)

The pore has a cross section 'A'. The velocity of the fluid particles is 'v' and the pressure is 'p'. The density of the fluid at temperature T is taken to be

$$\rho = \rho_o (1 - \alpha T) \tag{3.90}$$

where, α is the coefficient of volumetric expansion of the liquad and ρ_o is a datum value of density.

Consider the mass of liquid entering and leaving a volume element of cross section A and length dZ. The mass of liquid entering in unit time is,

$$A V \rho_o (1 - \alpha T) \tag{3.91}$$

where v is the fluid velocity.

Similarly the rate the liquid leaves is

$$A \rho_o \left(V + \frac{\partial V}{\partial z}\right)\left(1 - \alpha\left(T + \frac{\partial T}{\partial z}\,\delta z\right)\right) \tag{3.92}$$

so that, fluid is accumulated in the element at a rate of

$$\left[\alpha V \frac{\partial T}{\partial z}\,\delta z - \frac{\partial V}{\partial z}(1 - \alpha T)\delta z\right] A \rho_o \tag{3.93}$$

The volume element contains a mass of liquid,

$$A \rho_o (1 - \alpha T)\delta z \tag{3.94}$$

This changes due to change in temperature , the rate of increase in mass being,

$$-A \rho_o \alpha \frac{\partial T}{\partial t}\,\delta z \tag{3.95}$$

Thus, equating the rate of accumulation to the rate of increase in mass we obtain the equation of continuity,

$$(1 - \alpha T)\frac{\partial V}{\partial z} - \alpha V \frac{\partial T}{\partial z} = \alpha \frac{\partial T}{\partial t} \tag{3.96}$$

Then, if the thermal strain αT is small compared with unity, equation 3.96 becomes,

$$\frac{\partial V}{\partial z} - \alpha V \frac{\partial T}{\partial z} = \alpha \frac{\partial T}{\partial t} \qquad (3.97)$$

3.4.3 Pressure

Supposing that the pressure is related to the velocity by an equation of the form,

$$V = -\beta \frac{\partial p}{\partial z} \qquad (3.98)$$

where, β is related to the permeability of the material, the porosity, and the viscosity of the fluid. If β is constant equation 3.97 can be written as,

$$-\beta \frac{\partial^2 p}{\partial z^2} + \alpha\beta \frac{\partial p}{\partial z} \frac{\partial T}{\partial z} = \alpha \frac{\partial T}{\partial t} \qquad (3.99)$$

or

$$-\beta e^{\alpha T} \left(\frac{\partial e^{-\alpha T}}{\partial z} \frac{\partial P}{\partial z} \right) = \alpha \frac{\partial T}{\partial t} \qquad (3.100)$$

Thus the governing equation becomes[x],

$$\frac{\partial}{\partial z} \left(e^{-\alpha T} \frac{\partial P}{\partial z} \right) = - \frac{1}{\beta} e^{-\alpha T} \frac{\partial}{\partial t} (\alpha T) \qquad (3.101)$$

3.4.4 Expulsion of Vapour

Within the dry zone vapour is expelled under pressure. The vapour is taken to be an ideal gas so that the density is related to the absolute temperature

Footnote

If β is not constant we have,

$$\frac{\partial}{\partial z} \left(e^{-\alpha T} \left(\beta \frac{\partial P}{\partial z} + P \frac{\partial T}{\partial z} \frac{\partial \beta}{\partial T} \right) \right) = - e^{-\alpha T} \frac{\partial (\alpha T)}{\partial z}$$

and pressure in the following way,

$$\rho = \frac{P}{RT} \tag{3.102}$$

where, R is the specific gas constant.

Now, considering continuity we note that the mass of vapour entering the element in unit time is,

$$A \frac{P}{RT} V \tag{3.103}$$

and the quantity leaving is,

$$\frac{A}{R} \frac{\left(V + \frac{\partial V}{\partial z} \delta z\right)\left(P + \frac{\partial P}{\partial z} \delta z\right)}{\left(T + \frac{\partial T}{\partial z} \delta z\right)} \tag{3.104}$$

so that, after neglecting second order terms, the rate of accumulation of mass in the element is,

$$\frac{A}{RT}\left(\frac{VP}{T} \frac{\partial T}{\partial z} - V \frac{\partial P}{\partial z} - P \frac{\partial V}{\partial z}\right)\delta z \tag{3.105}$$

The mass of the element is,

$$A \frac{P}{RT} \delta z \tag{3.106}$$

The rate of increase of mass within the element is therefore,

$$\frac{A}{R}\left(-\frac{P}{T^2} \frac{\partial T}{\partial t} + \frac{1}{T} \frac{\partial P}{\partial t}\right)\delta z \tag{3.107}$$

Equating 3.105 and 3.107 we obtain the following equation of continuity:

$$\frac{VT}{P} \frac{\partial P}{\partial z} + T \frac{\partial V}{\partial z} - V \frac{\partial T}{\partial z} = \frac{\partial T}{\partial t} - \frac{T}{P} \frac{\partial P}{\partial t} \tag{3.108}$$

Assuming laminar flow and substituting for V from equation 3.98 in equation 3.108 we obtain,

$$-\frac{V^2 T}{P\beta} + T \frac{\partial V}{\partial z} - V \frac{\partial T}{\partial z} = \frac{\partial T}{\partial t} - \frac{T}{P} \frac{\partial P}{\partial t} \tag{3.109}$$

Chapter 4

OBJECTS OF THE RESEARCH UNDERTAKEN

4·1 Introduction

Tests described in Chapter 2 seemed to confirm that spalling is exacerbated by high moisture content and low permeability, thus suggesting pore pressure to be one cause for failure of the material.

These tests also indicated that the likelihood of spalling is increased by the presence of the compressive stresses. (See tests by Meyer-Ottens (4·1), in Chapter 2)

However, the theories considered in Chapter 3 do not seem to take this into account, and, do not, in fact, explain how failure occurs. To get over this difficulty, a possible mechanism of failure is proposed in this chapter, to take into account the simultaneous effects of the compressive stresses and the pore pressure induced in the heated material.

The development of the pore pressure in concrete exposed to heat has been discussed in the earlier chapters. Certain aspects of the development of compressive stresses will now be considered before the description of the proposed mechanism.

4·2 Thermal Stresses in Heated Concrete

The reason thermal stresses arise in a heated material is that thermal expansion or contraction is restricted in the body or in some of its parts. Free, homogeneous solids with a uniform or linear change in temperature throughout the solid, undergo free thermal expansion, which does not produce any macroscopic thermal stresses.

However, a freely expanding member is rarely encountered as a part of a structure, and, therefore,

when exposed to fire, members should be considered to be restrained to a certain degree, with its expansion depending on the properties of the member, its position within the entire structure, and the properties of the structure itself.

In some cases free expansion may even be restricted from within the body. Such a situation arises when a concrete wall panel is heated from both sides. As Dougill (4·15) suggested, in this case, shortly after the start of heating, the interior of the panel will be in tension and the heated surfaces in compression. Such compressive stresses may also be induced on the heated surface of a concrete panel heated from one side only, specially if the member is subjected to flexural restraint.

Clearly, such biaxial stresses may play an important role in the surface failure of concrete and therefore are worth considering.

4·3 Effects of Biaxial Compression

There is substantial evidence (Robinson,4·2) (Bresler and Pisler, 4·3), (McHenry and Karni, 4·4) that concrete specimens under mechanical biaxial loading fail in a plane parallel to the plane of the loading.

In fact Robinson (4·2) tested 254x254x102 mm mortar as well as concrete specimens of various mix ratios, at the age of 28 days, under biaxial loading using the machine described in Chapter 6 of the present work and

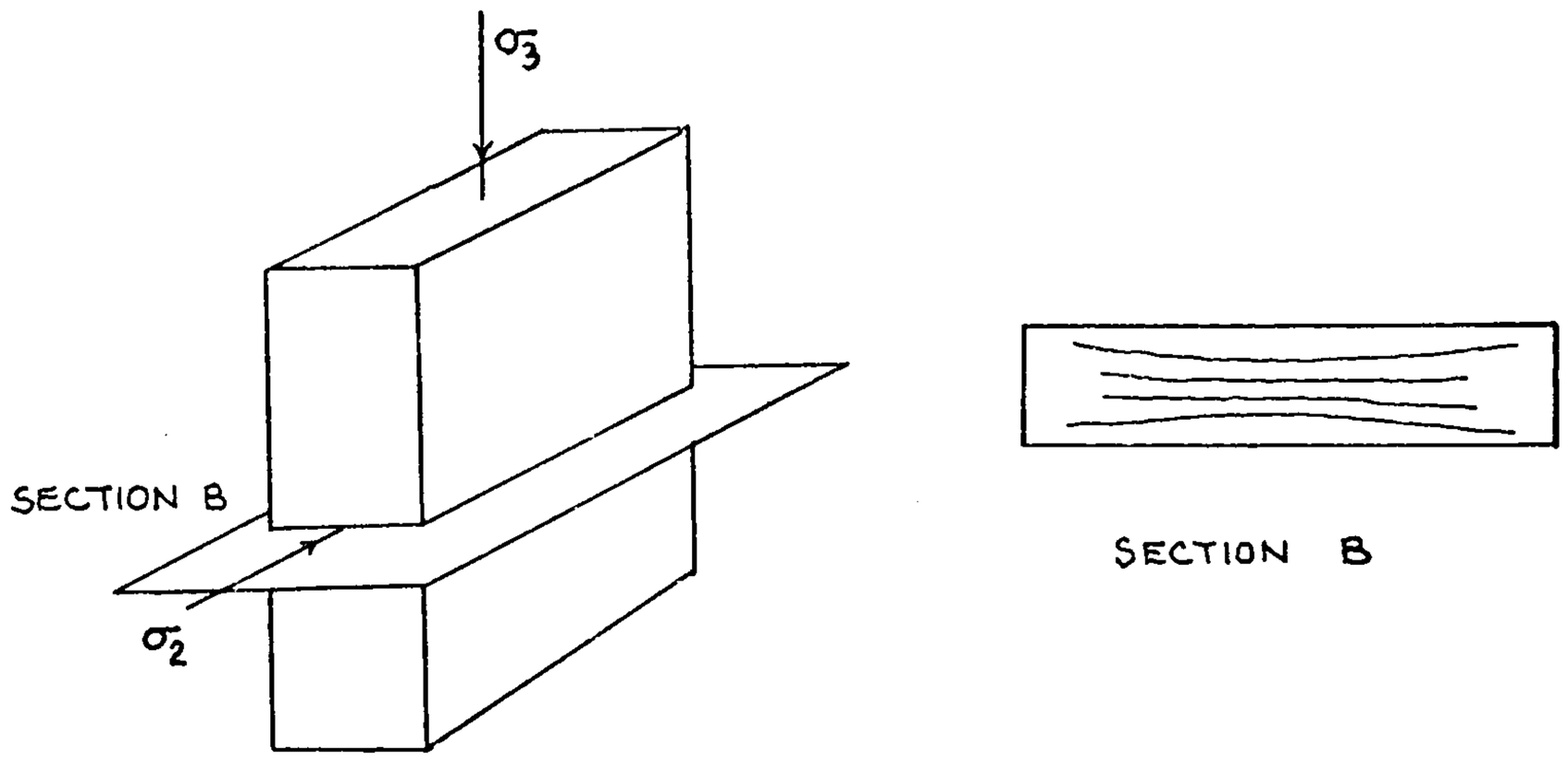

FIG. 4.1 MODE OF FAILURE OF CONCRETE UNDER BIAXIAL COMPRESSION

[AFTER ROBINSON, (4.2)]

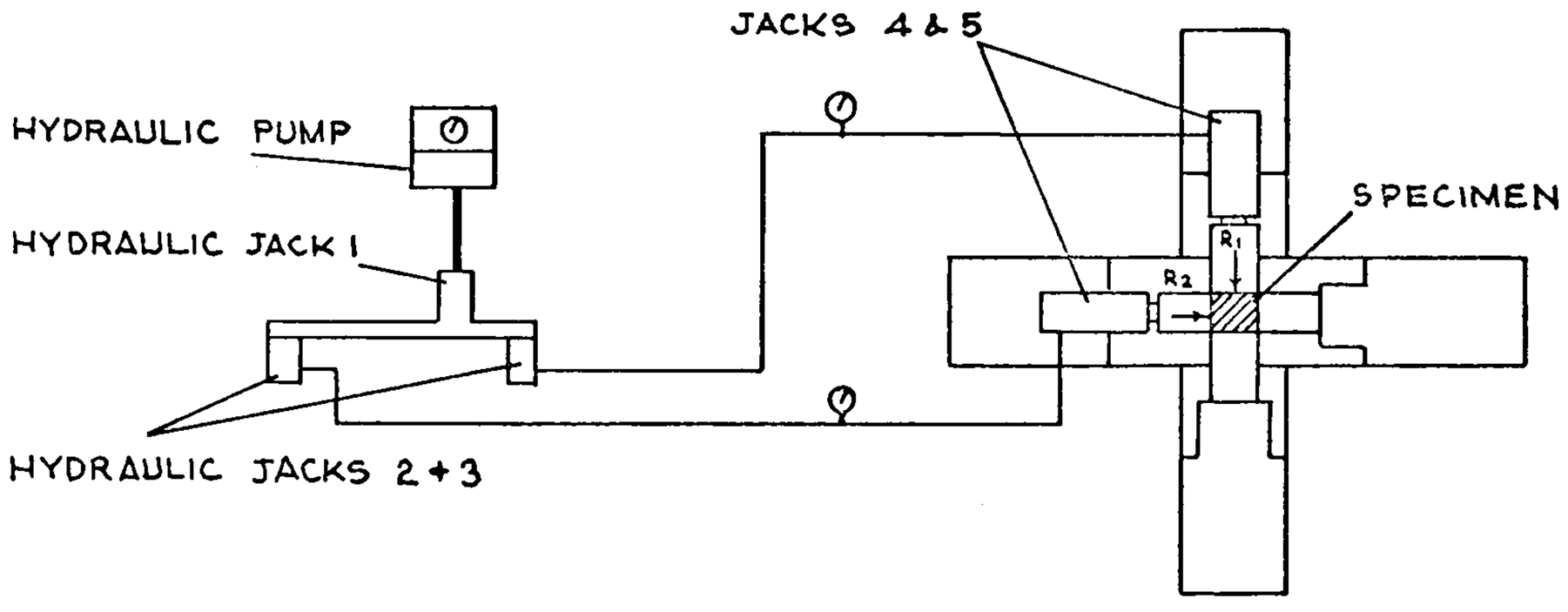

FIG. 4.2 HYDRAULIC SYSTEM USED BY KUPFER et AL. (4.6) TO APPLY BIAXIAL COMPRESSION

elsewhere (Robinson, 4·5) and observed a plate-like mode of failure. (Fig.4·1)

Tests basically similar to Robinson's have been performed by Kupfer et al. (4·6), where 28 days old concrete specimens, 200x200x50 mm,were subjected to biaxial stress combinations using the testing arrangement shown in Fig.4·2. A constant strain rate was maintained in loading the specimens, and the maximum load was reached after approximately 20 minutes. In agreement with Robinson (4·2), the authors observed microcracks parallel to the free surface of the specimens subjected to biaxial compression, and, at failure , a major crack, approximately parallel to the same free surface.

These cracks may not affect the biaxial compressive strength substantially, because, when they propagate, they tend to split the specimen into plates parallel to the unloaded face, thus the material is still capable of supporting the applied biaxial load. However, the tensile strength in the direction perpendicular to the applied biaxial loading is expected to be reduced substantially because the actual tensile stresses are increased as the uncracked surface upon which these stresses are applied decreases.

Alternatively, if the crack size is large enough as compared with the total dimensions of the member, buckling of the plate-like layer mentioned earlier on would occur much easier if a tensile stress acting in the direction perpendicular to the heated face existed.

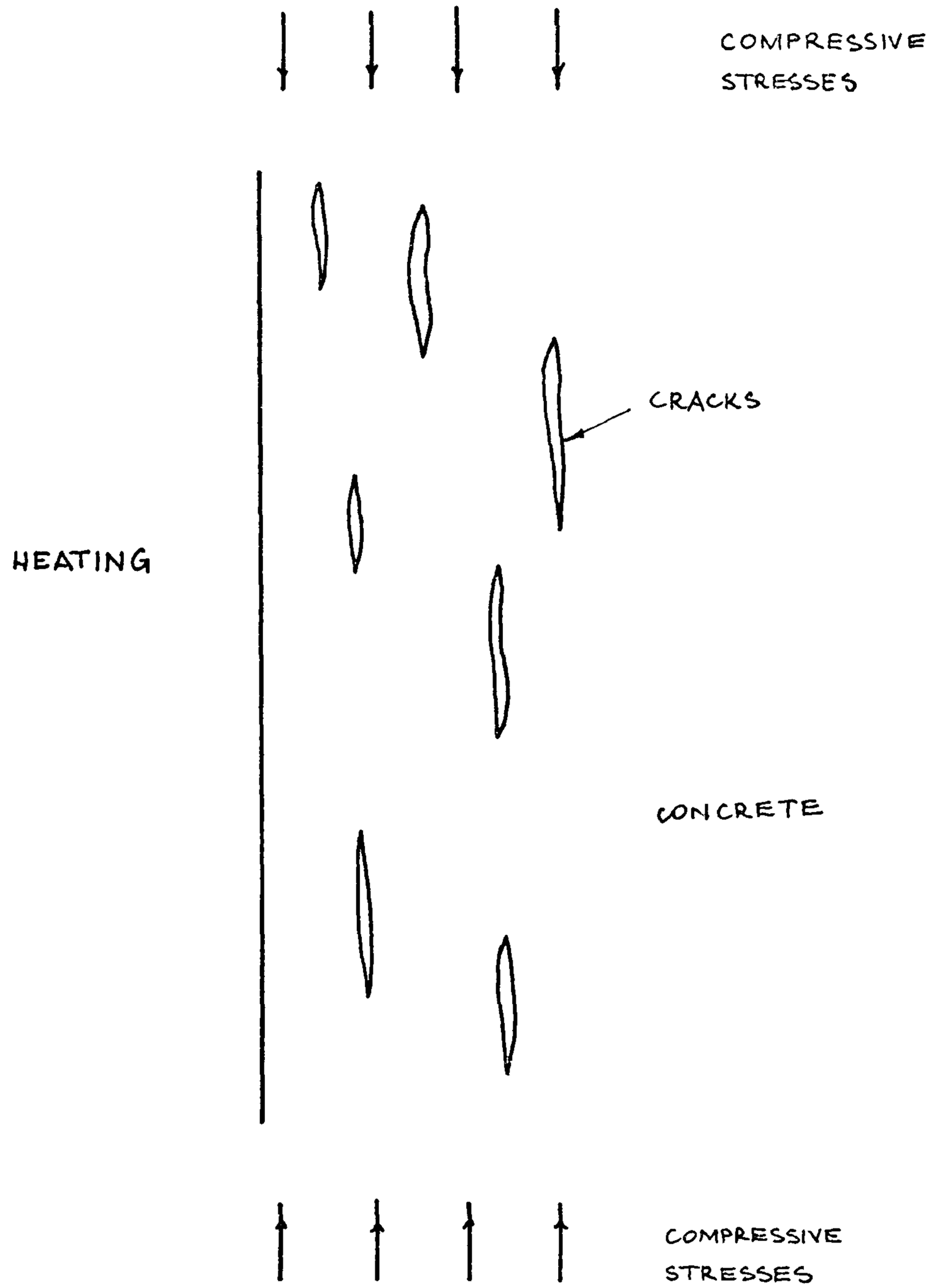

FIG. 4.2.a REPRESENTATION OF A CONCRETE WALL PANEL EXPOSED TO HEATING FROM ONE SIDE

This reduction in the tensile strength in the direction at right angles to the plane of biaxial loading has been observed by Hobbs (4·7) in a series of triaxial extension tests on solid cylindrical specimens, 140mm high and 54mm in diameter. It is entirely probable that biaxial compressive field induced by the cell pressure produced cracks parallel to the biaxial compression plane, so reducing the tensile strength in the axial direction.

4·4 The Suggested Mechanism

In the light of the previous discussion, let us now consider the model described in Chapter 1.

Shortly after the material is exposed to heat (Fig.4.2.a) compressive stresses are induced due to partially restrained thermal expansion. Consequently, small cracks parallel to the heated face would be expected to form and increase in number and size. In the meantime, as the temperature of the concrete reaches the temperature necessary for desorption of the water, vaporization would be expected to occur with an accompanying rise in pore pressure as described in Chapter 3. The cracks would therefore be filled with vapour under pressure. This would cause tensile stresses at right angles to the compressive stresses. As the heat exposure continues, the number and size of cracks would increase, and, when an unfavorable combination of high pressure applied on a comparatively large crack, situated relatively close to the heated surface, occurs, the material between the crack and the heated surface would be expelled.

The theory is particularly attractive because it accounts for the two important experimentally observed facts, namely, the increased likelihood of spalling with an increase in compressive stress, and, with an increase in pore pressure.

It could be argued that, as spalling has been observed to occur occasionally at the early stages of heating, the cracks may not exist in the material at this stage, and therefore, this condition might be out of the range of the application of the proposed mechanism. In reality, however, there is evidence that cracks may exist even before any compressive stresses are induced. In fact, Hsu et al. (4·8) removed thin slices of concrete, perpendicular to the direction of loading, from cylinders previously strained to various levels, and examined them microscopically. The authors concluded that microcracks exist at the coarse aggregate/mortar interface even before loading. Robinson (4·2), using an X-ray technique confirmed these results.

Soon after the application of loading on the material these cracks are expected to propagate and orient themselves mainly in the direction of the applied loading as observed by Spooner (4·9).

Newmann (4·10) claimed that the microcracks existing prior to loading do not become unstable and do not propagate before a certain level of loading, termed by the author the 'discontinuity level', is reached. However, Spooner and Dougill (4·11) did not

find any evidence to support the existence of 'critical' or 'discontinuity' stress levels. Consequently, the authors noted that the damage should be considered to be progressive in the manner proposed in earlier model studies by Dougill (4·12), (4·13), and observed in work on network structures (4·14).

Clearly, as soon as the pressure, the crack size and depth, reach certain critical value, spalling can be expected to occur. This critical level could be reached at an early stage of heating.

It is therefore worth carrying out experiments to see if the proposed mechanism of failure actually occurs.

However, before fixing on details of experimental procedure it is useful to discuss what parameters should be considered in such an experimental investigation. This is done in the next section.

Theoretical Investigation to Determine the Parameters Involved in the Proposed Mechanism

In the previous sections the overall behaviour of the material under the compressive stresses and pore pressures have been looked at. In this section, emphasis will be concentrated on an individual crack, parallel to the unloaded surface, filled with vapour under pressure.

Cases ranging from the simplest, where the effect of biaxial compression is ignored, to the more complicated ones where this effect is included, will be investigated in simple terms.

a) CASE I

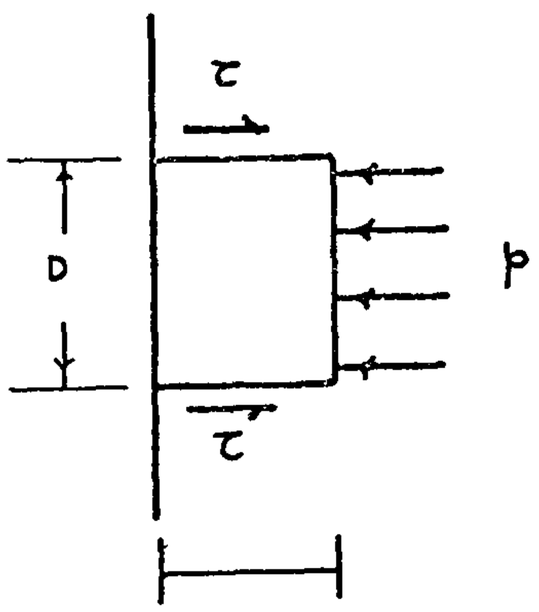

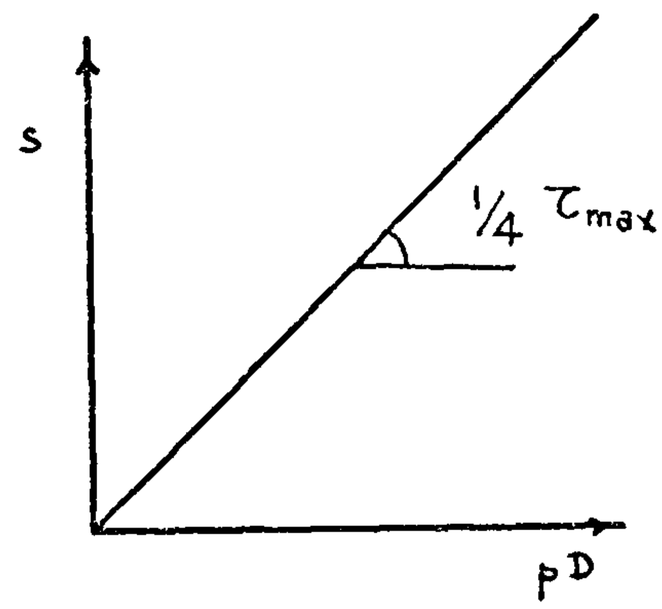

b) CASE II

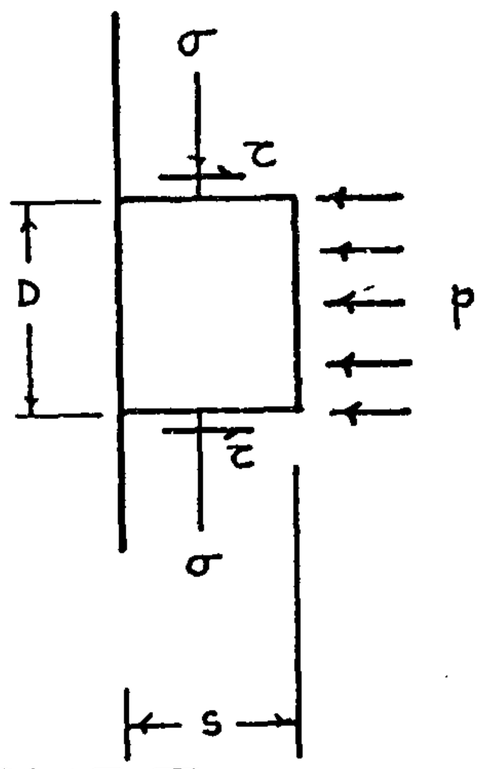

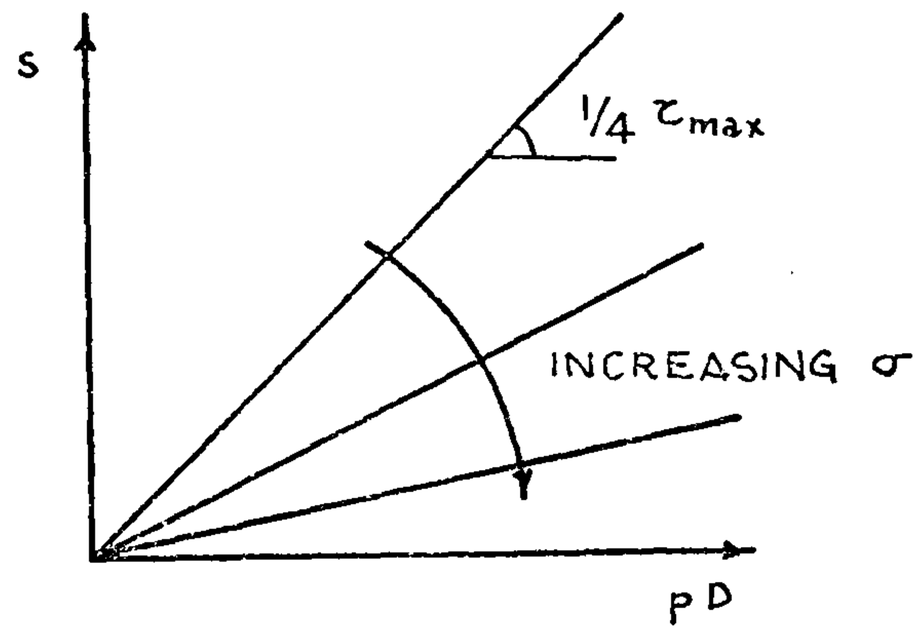

c) CASE III

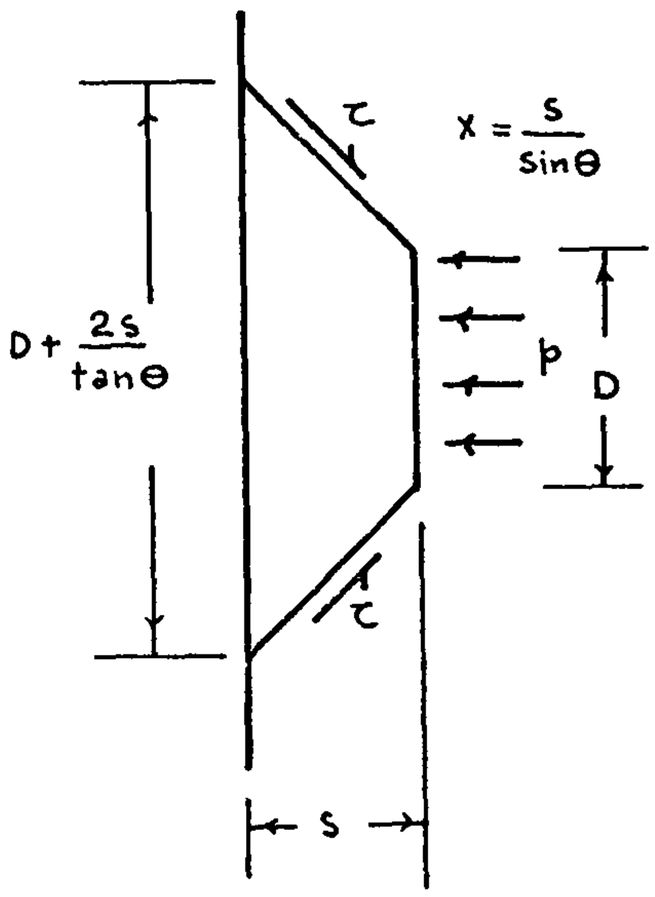

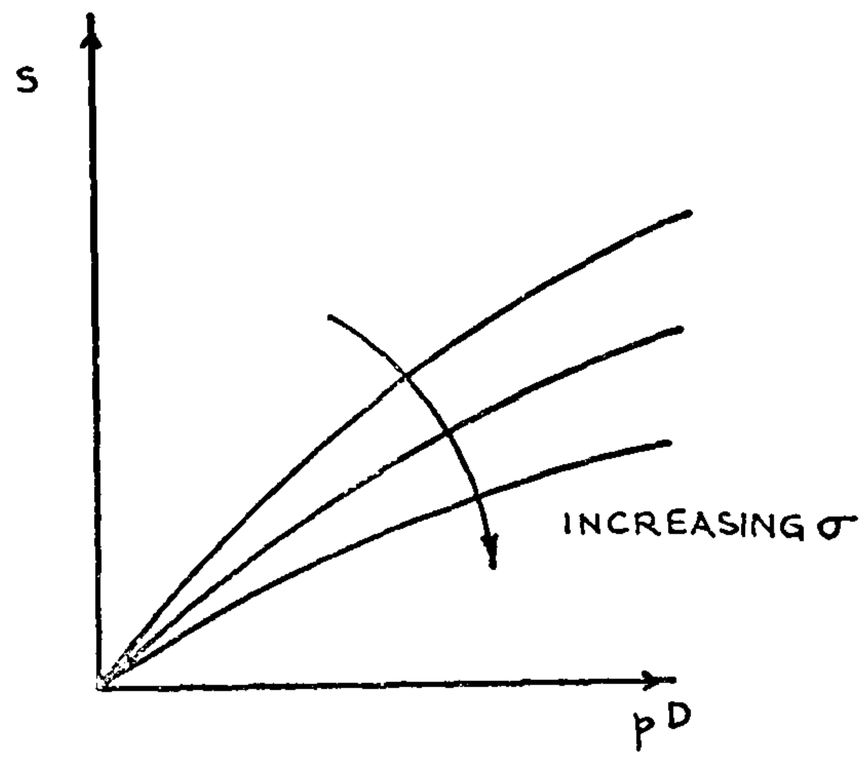

FIG. 4.3 SIMPLIFIED ASSUMED FORMS OF FAILURE USED TO DETERMINE THE PARAMETERS INVOLVED IN BREAK-OUT TESTS

Case I

Let us consider a crack of diameter 'D', parallel to the unloaded surface and at a depth 'S', at which depth an internal pressure 'p' is applied, as shown in Fig.4·3a.

Assuming that the failure surface is such that a cylindrical plug of material is expelled, we have,

$$\frac{\pi D^2}{4} p = \pi D \tau S \qquad (4\cdot1)$$

where τ is the shear stress, so that at failure,

$$p D = 4 \tau_{max} S \qquad (4\cdot2)$$

where, τ_{max} is the shear strength of the material along the failure plane, and 'p' is now the pressure to cause failure.

The form of the equation suggests the linear relationship shown in Fig.4·3a.

Substituting in equation (4·2) the plausible values, $p=2MN/m^2$, S=0·02m, D=0·1m, we obtain,

$$\tau_{max} = \frac{PD}{4S} = \frac{(1)\ (2)\ (0\cdot1)}{(4)\ (0\cdot02)} = 2\cdot5MN/m^2 \qquad (4\cdot3)$$

Although this analysis is based on a crude simplification, the value obtained for τ_{max} is of the same order of magnitude as the average shearing strength of concrete ($\tau_o = 2MN/m^2$) quoted by McHenry and Karni (4·4). This suggests that the approach is worth further consideration.

Case II

Let us now consider the same situation as in Case I but with the introduction of compressive stresses. (Fig.4·3b) Assuming that the shear stress at failure is related to the compressive stresses in the following way:

$$\tau = \lambda\sigma + c \qquad (4.4)$$

where, λ and c are constants depending on the material, we obtain,

$$p \frac{\pi D^2}{4} = \pi D S (\lambda\sigma + c) \qquad (4.5)$$

leading to the result in Fig.4·3b.

Case III

Spalled pieces actually have a shape closer to a cone than a cylinder. Accordingly we now take the failure surface to be conical, instead of cylindrical, and obtain,

$$p \frac{\pi D^2}{4} = \tau \sin\theta \frac{S}{\sin\theta} \pi \left(D + \frac{S}{\tan\theta}\right) \qquad (4.6)$$

or,

$$pD = 4S(\lambda\sigma + c) \left(1 + \frac{S}{D \tan\theta}\right) \qquad (4·7)$$

Equation 4.7 and Fig.4.3c imply that main parameters are depth of crack, S, pressure, p, and crack diameter, D.

It has already been pointed out that the presence of these cracks parallel to the surface increases substantially the total force causing failure which is represented by the left hand side of equation 4·1,

because this force is proportional to the square of the crack diameter D, while the resisting force is only linearly proportional to D.

Alternatively, it has also been pointed out that cracks perpendicular to the direction of tensile forces decrease the area over which these forces are applied, and therefore increases the actual tensile stresses on this area. Consequently, the tensile strength would be expected to reduce in a manner discussed earlier on in this chapter. Therefore, if the mechanism suggested in this chapter is correct, pressures less than the ones necessary to cause the failure of an uncracked concrete, might be high enough to cause failure of concrete containing cracks parallel to the surface.

It therefore seems important to find out experimentally what pressures applied at a crack parallel to the surface are required to cause failure of the material. These tests, termed 'Break-out' tests are described in detail in Chapters 6 and 8 of the present work.

As a natural follow up to the 'Break-out' tests are ones to find out whether such pressures can be generated in heated concrete. These tests, termed 'Pore Pressure' tests, are described in Chapter 5.

Chapter 5

PORE PRESSURE TESTS

5.1 Introduction

5.1.1 Object

Fire tests on reinforced concrete slabs and walls are generally carried out by applying heat from one side only. However tests on I-beams with thin web heated from both sides which are to a certain extent comparable to a wall heated from both sides, exhibit more frequent explosive spalling when compared with the ones heated from one side only (Meyer-Ottens, 5.2) This behaviour suggests that concrete walls and slabs too, if exposed to fire from both faces, may present a more dangerous situation. It is the object of this chapter to investigate experimentally the pore pressures generated in wall panels in such circumstances.

5.1.2 Relation to Panel Situation

If a concrete wall is exposed to heat on both sides, some time after the start, dry layers form next to both surfaces and a saturated layer is expected to form in the central region in a manner described by Harmathy (5.1) (See Chapter 2). At this stage, vapour generated at the interface can only escape through the dry layer. Due to the limited permeability in this layer, the pressure at the interface will increase and failure can be expected to occur.

There is, however, no clear indication whether this pressure is, by itself, capable of causing spalling following the manner described by Harmathy (5.1), Meyer-Ottens (5.2), Zhukov (5.3), or, whether it may

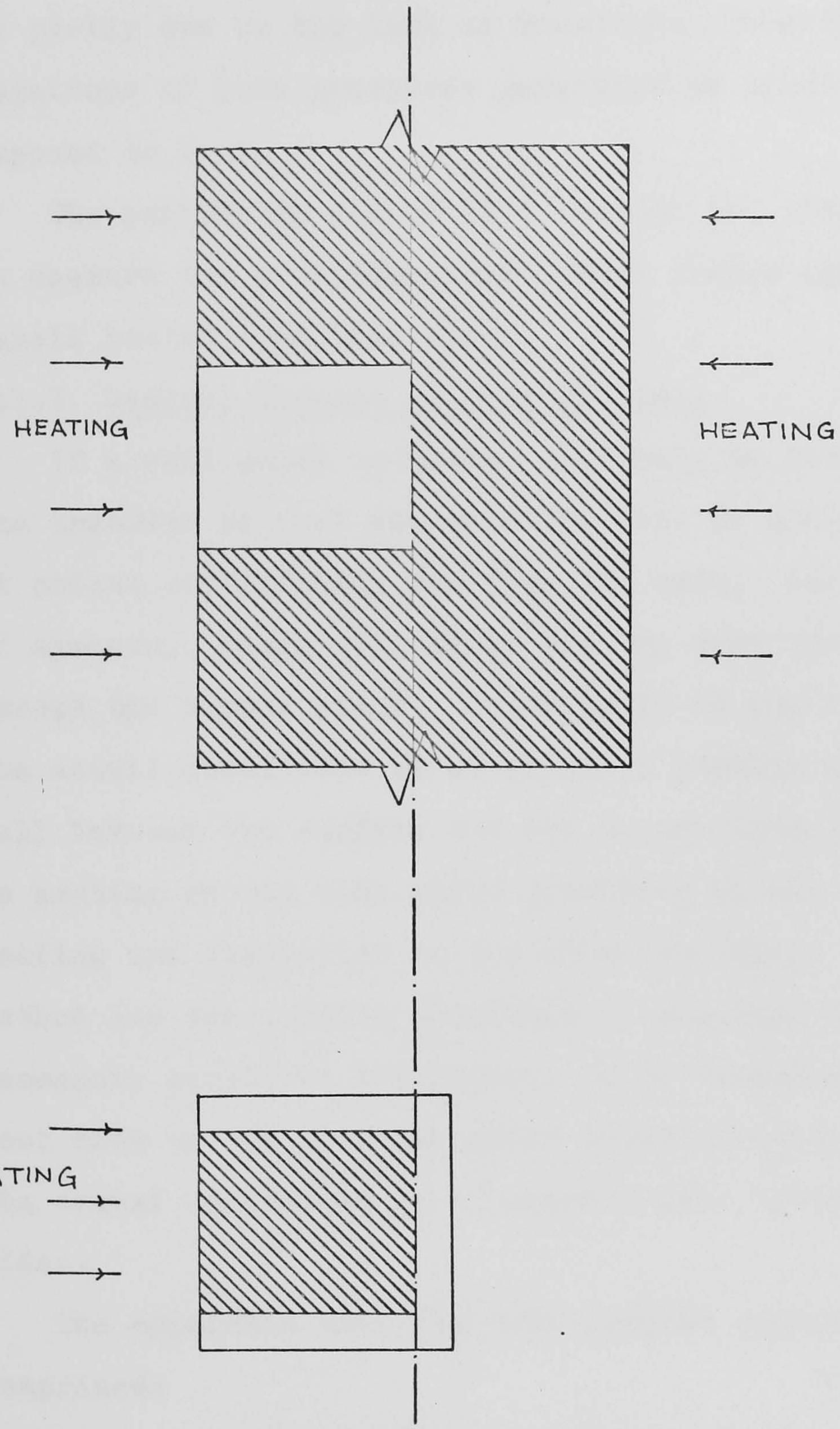

FIG. 5.1 WALL PANEL HEATED FROM BOTH SIDES

cause failure only if coupled with compressive stresses in the manner proposed in Chapter 4. This uncertainly is partly due to the lack of knowledge concerning the magnitude of pore pressures generated in concrete exposed to heat.

The particular aim of this chapter is, therefore, to measure the pore pressures formed inside concrete panels heated from both sides.

5.1.3 General Concept of Pressure Cell

If a wall panel is heated uniformly on both faces the transfer of heat and moisture will be unidirectional at points sufficiently far from the ends. Also, because of symmetry, there will be no heat or mass transfer across the middle plane. Accordingly we can represent the actual conditions if we expose a portion of the wall between the surface and the centre line (Fig.5.1) to heating on one side while providing an all round sealing and insulation at the other surfaces. This method has the obvious advantage of allowing the necessary sensitive instruments to be connected to the cool side of the specimen while satisfactorily representing the actual conditions in a concrete wall heated from both sides.

The apparatus used for this purpose basically comprised:

a) A steel cylinder around the specimen referred to as the barrel, and a stiff end closure called the diaphragm, to provide pressure sealing.

b) Insulating material to provide insulation of all but the heated face,

c) the heating system,

and, d) the necessary instruments to measure the pressure and the temperature during heating.

For convenience this chapter is devided into two parts: Part I dealing with equipment and test procedure, and, Part II, with the tests and the results.

5.2 Part I: Equipment and Procedure

5.2.1 The Pressure Cell: Barrel, diaphragm and Gasket

5.2.1.1 Original Design

The design criteria were such that, the cell should, firstly, be strong enough to stand the pressures likely to be generated[x], secondly be used as a mould when casting, because, a good bond between the specimen and the cell was necessary to prevent any leak to the atmosphere, thirdly, possess a coefficient of thermal expansion close to the one of concrete (or mortar) to prevent leakage, or additional compressive stresses as the case may be, and, finally, possess an end plate which should be fixed on to the body (the barrel) in such a way that, while providing complete sealing during the test, should be easily removed after test so that the tested specimen could be extracted and

Footnote

At first, pressures above 700 KN/m^2 were not expected, and therefore, the design was made accordingly.

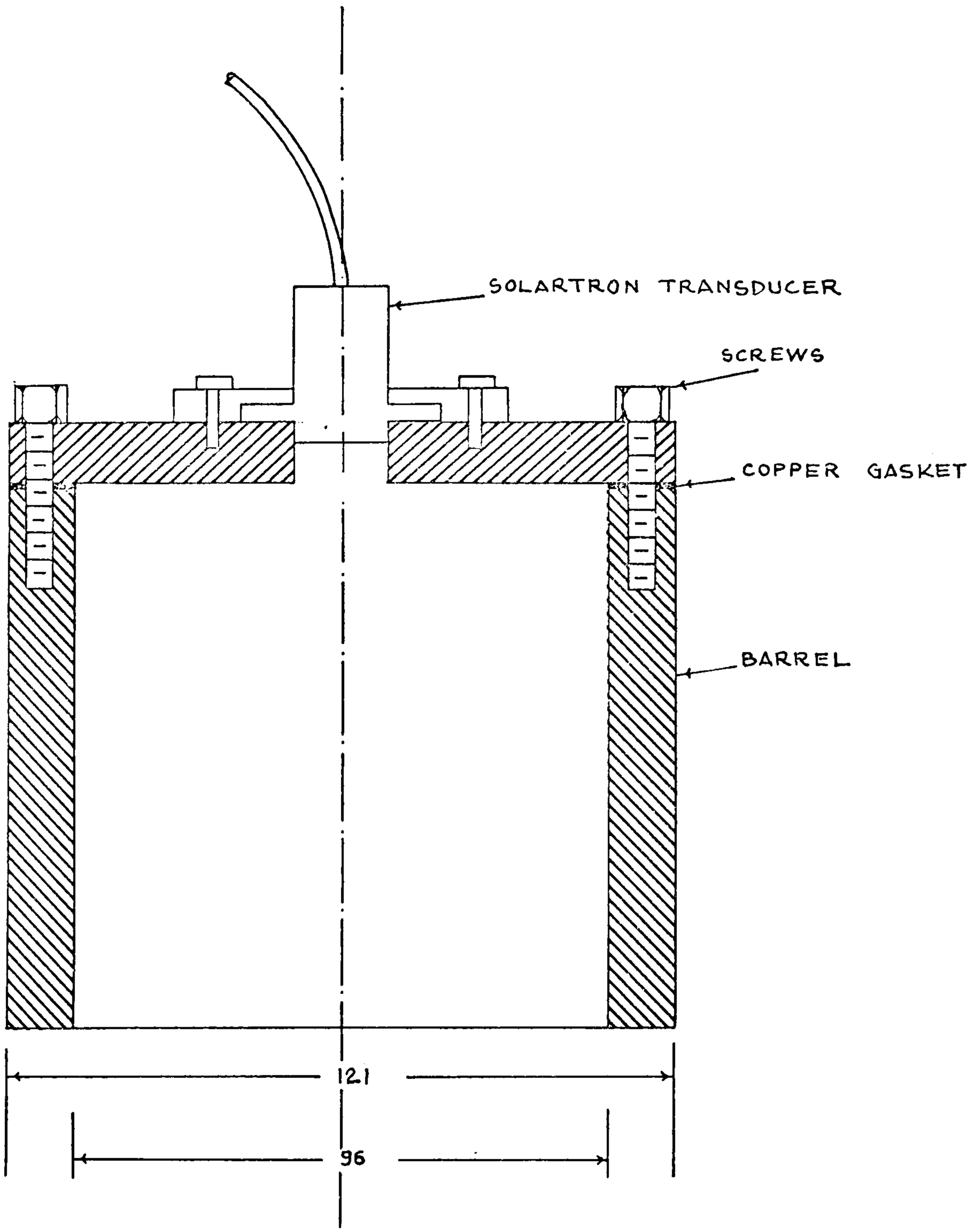

FIG. 5.2 CROSS-SECTION OF THE ORIGINAL PRESSURE CELL

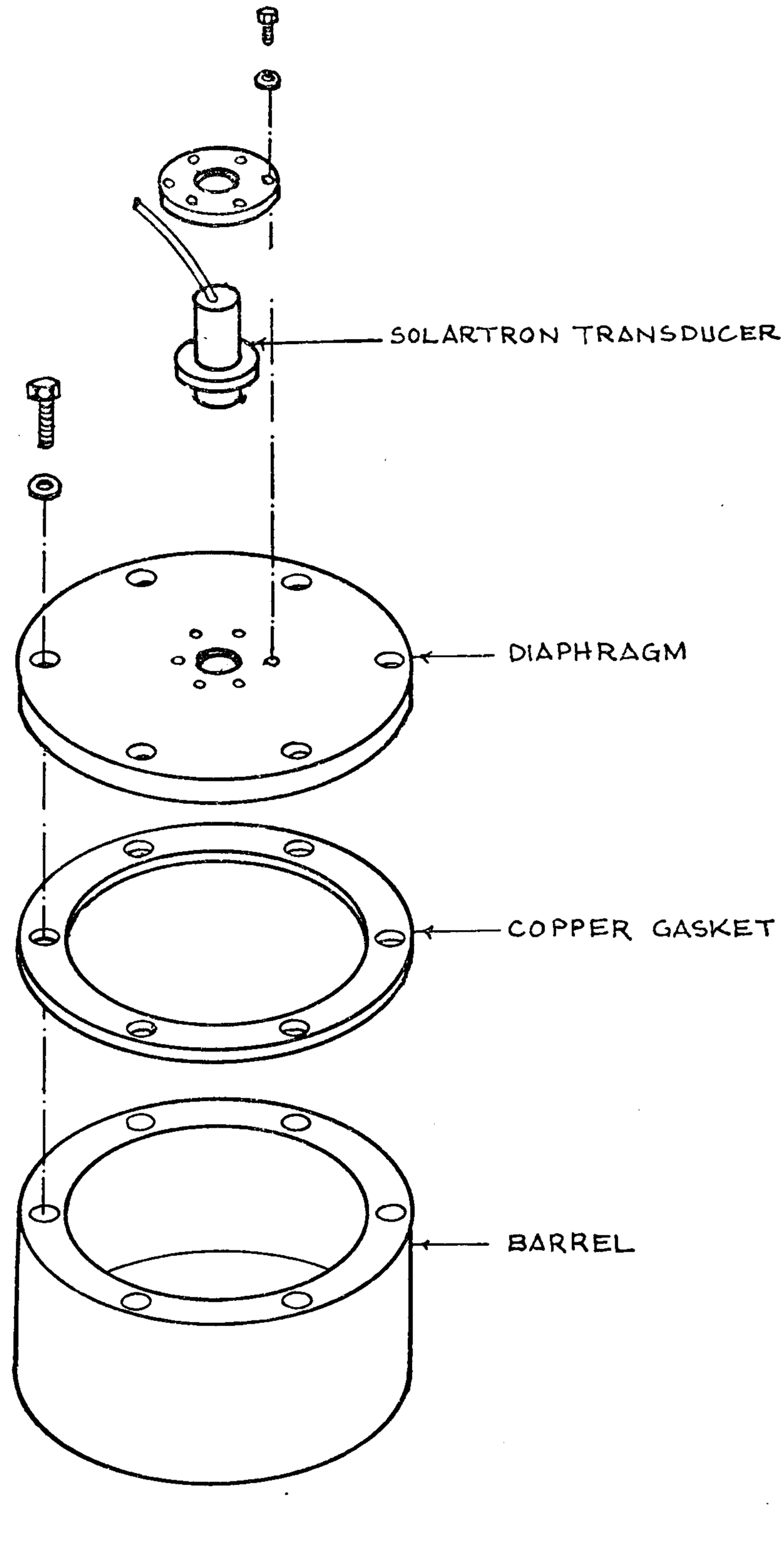

FIG. 5.3 EXPLODED VIEW OF THE ORIGINAL PRESSURE CELL

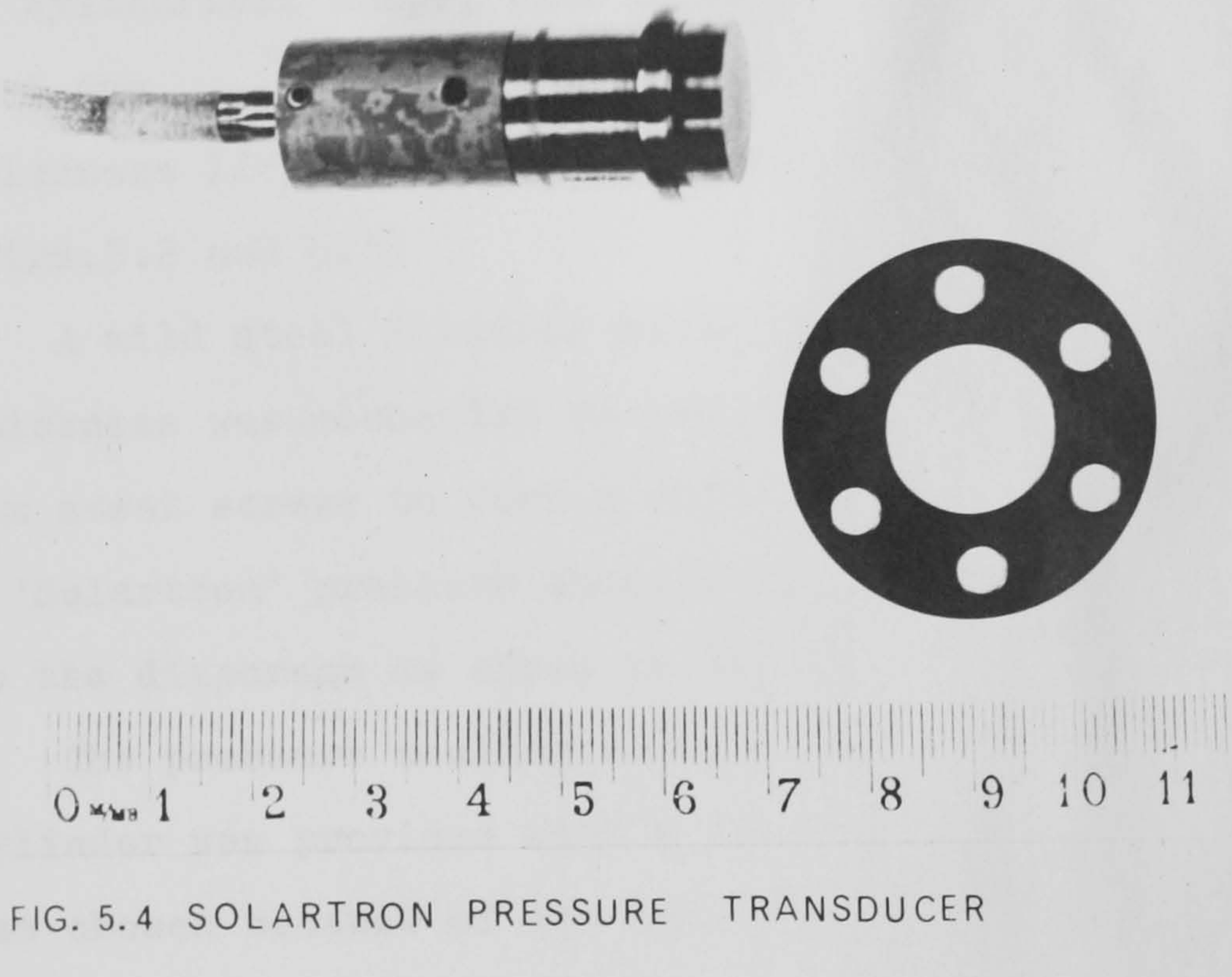

FIG. 5.4 SOLARTRON PRESSURE TRANSDUCER

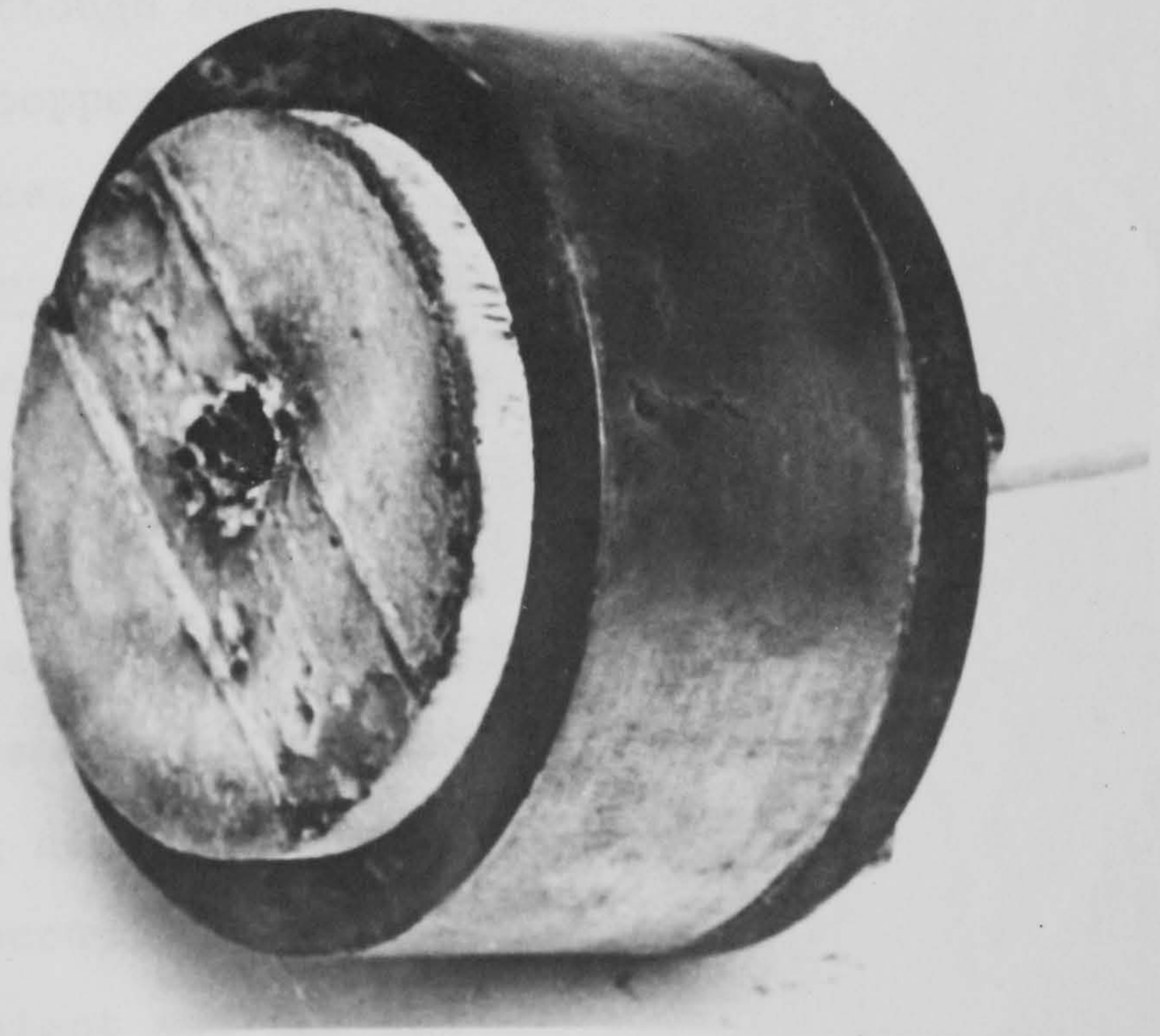

FIG.5.5 SPECIMEN PARTLY FORCED OUT AFTER THE FIRST PRESSURE TEST

replaced.

Conforming to these criteria, six mild steel cells of cylindrical shape, with heights ranging from 25mm to 6 4mm , with internal diameter 96mm, and wall thickness 12·5mm were designed and made in the workshop. (Figs.5.2 and 5.3)

A mild steel circular plate (diaphragm) of 12·5mm thickness was connected to one end of the barrel with six steel screws to form a stiff end closure. (Fig.5.3) A 'Solartron' pressure transducer (Fig.5.4) was fixed to the diaphragm as shown in Fig.5.2 and Fig.5.3.

The pressure sealing between the diaphragm and the cylinder was provided with a plain copper gasket. Copper was chosen because of its inherent ductility leading to a good sealing capacity.

Although corrugated copper gaskets were available, plain copper was used as gasket material in the first instance.

The First Pressure Test

The object of the first pressure test was to measure the pore pressures generated at the cool side of the specimen enclosed in the cell, when the free side was exposed to heat. No attempt had been made to measure the temperature distribution inside the specimen during heating because the problem of introducing the thermocouple wires through the pressure cell with sufficient sealing had not been solved at the time.

The results of the first test were interesting in

FIG. 5.6 BARREL

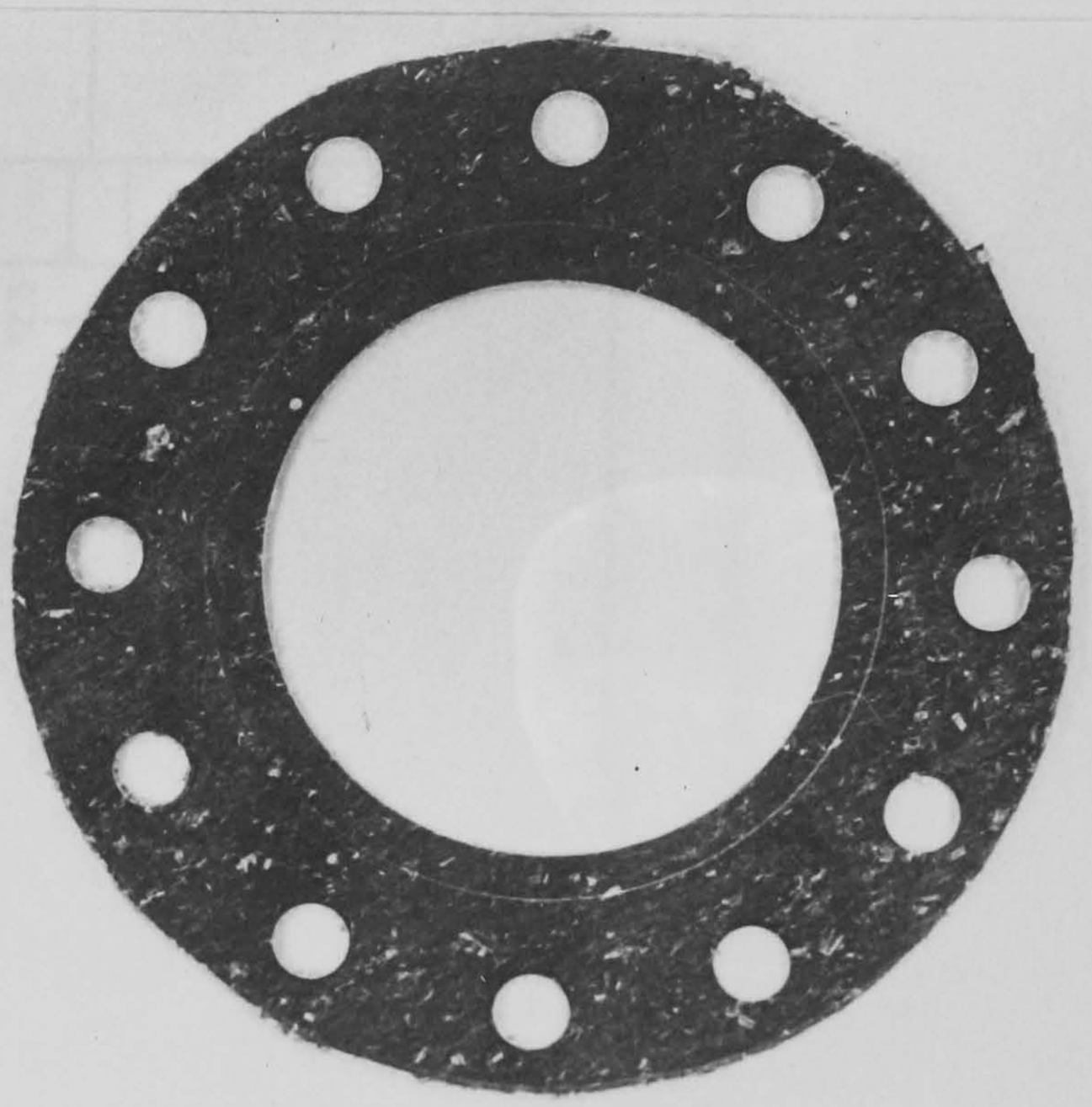

FIG. 5.9 ASBESTOS JOINTING

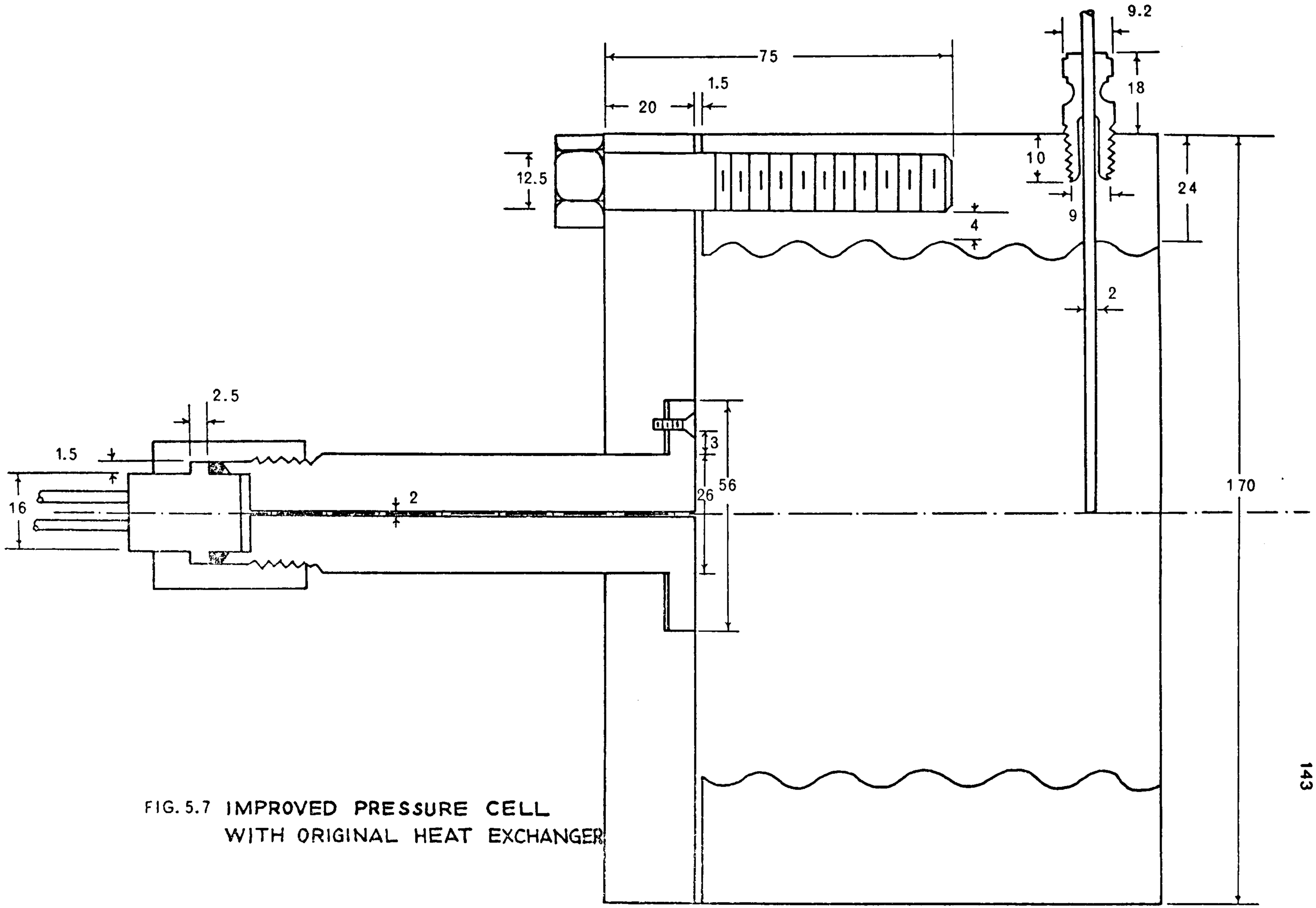

FIG. 5.7 IMPROVED PRESSURE CELL
WITH ORIGINAL HEAT EXCHANGER

the sense that the test had to be stopped 9 minutes after the start when the pressure reached 552 KN/m^2 (80 psi), in order not to cause damage to the pressure transducer, because, the maximum working pressure of the pressure transducer was 689 KN/m^2 (100 psi). Furthermore the specimen was nearly forced out of the cell, travelling a distance of 40mm under the effect of vapour pressure (Fig.5.5).

The results of this first pore pressure test suggested that: a) A pressure transducer with a higher range was needed, b) the pressure cell should be replaced with a stronger one to stand the higher pressures, and c) the expulsion of the specimen under vapour pressure during the test should be prevented.

5.2.1.2 The Improved Design

Consequently, another set of cylindrical pressure cells with 25, 40, 55, 70 and 85mm heights, 170mm outside diameter and 26mm wall thickness were designed. (Fig. 5.6 and 5.7) T 152 hot rolled thick wall seamless steel tube, supplied by 'Le Bas Steel Co.', was cut to the required sizes, and 4mm depth of thread, 4mm pitch corrugation was provided to the internal wall to prevent the movement of the specimen under the pressure. (Fig.5.6)

To provide the required gasket [x] area even after the drilling of 12·7mm diameter screw holes and the 4mm deep

Footnote

x
See 'Gasket Design' (Appendix III)

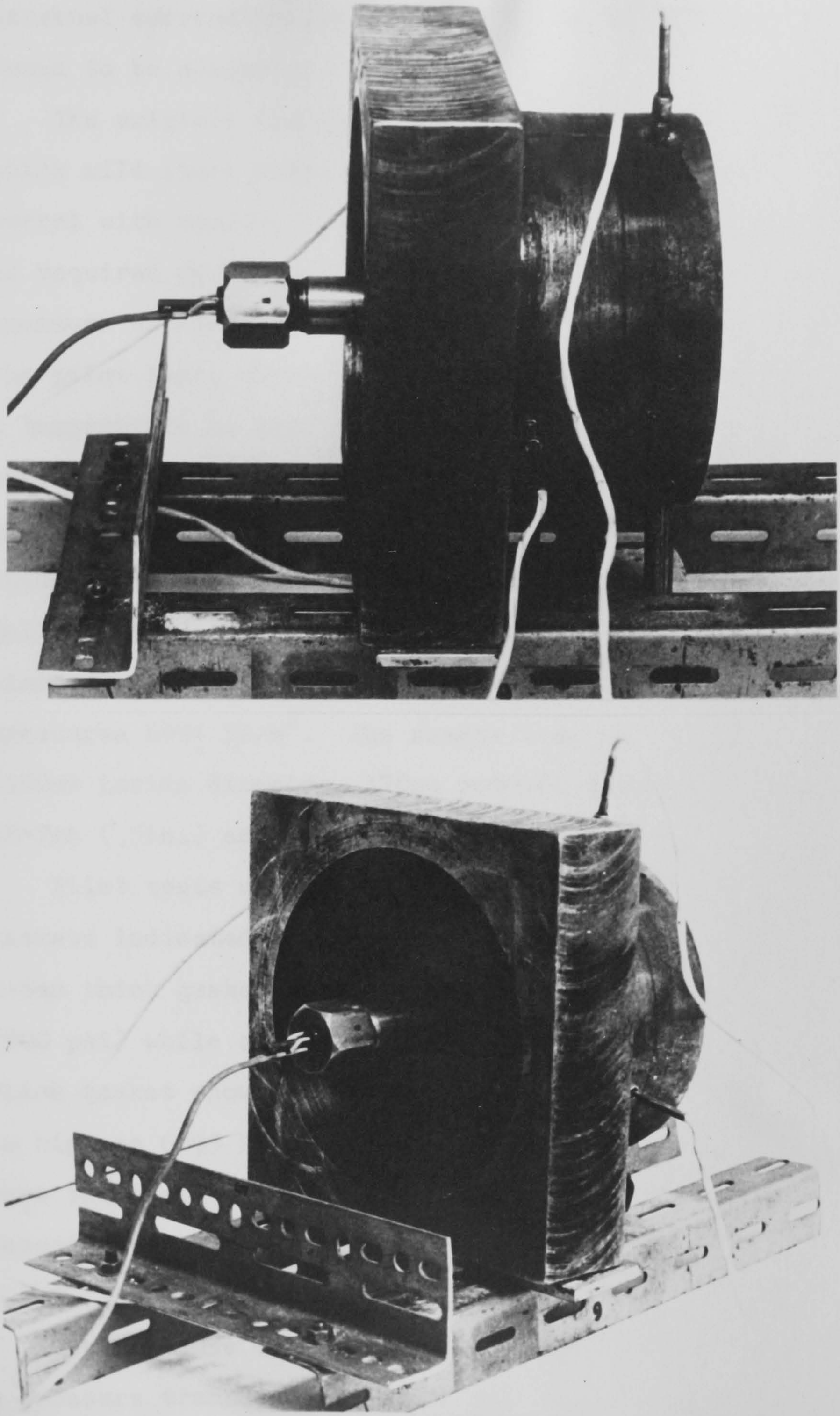

FIG. 5.8 PRESSURE CELL WITH THE ORIGINAL HEAT EXCHANGER

internal corrugation, a wall thickness of 26mm was found to be adequate.

The original diaphragm was also replaced by a 20mm thick mild steel plate (Fig.5.8), fixed on to the barrel with twelve, 12·7mm high tensile steel screws as required by the calculations for an internal pressure of about 6·8 MN/m^2. Also, after carrying out the pilot test, which showed that, at a depth of 25mm a temperature as high as 600°C could be obtained, copper seemed unsuitable as a gasket material. Accordingly, it was decided to use 0·8mm and 1·6mm thick asbestos jointing grade J 80 sheets supplied by Bell's Ltd. as gasket material because the manufacturers claimed satisfactory performance up to 540°C and pressures 6894 KN/m^2. The sheets were cut to size (100mm inside diameter, 170mm outside diameter) and 12·7mm (.5in.) screw holes punched (Fig.5.9).

Pilot tests using 0·8mm and 1·6mm thick asbestos gaskets indicated that two out of three cells using 0·8mm thick gasket showed signs of leakage at 3448 KN/m^2 (500 psi) while all the 3 cells tested using 1·6mm thick gasket showed no sign of leakage even at pressures as high as 6895 KN/m^2 (1000 psi). 1·6mm thick gaskets were therefore used successfully throughout the tests described in this chapter.

5.2.2 Pressure Measuring System

The pressure measuring system comprised basically a pressure transducer to sense the vapour pressure in

the specimen and to convert it into electrical output, a constant voltage supply, and a readout unit to record the output of the transducer.

5.2.2.1 Pressure Transducer

In the first instance a 'Solartron' (Fig.5.4) unbonded resistance strain gauges forming a Wheatstone Bridge, type NT 4-313, supplied by 'Solartron' Ltd., having a pressure range of 690 KN/m^2 was used. The reason for this selection was mainly the corosion resistance, the satisfactory temperature compensated range (0 - 121°C) safe operating range (148°C), quick delivery and relatively low cost.

The excitation and the output could be supplied through four numbered pin-type connectors. The body and sensing diaphragm were made in one piece, with no seals or joints in contact with the pressurized medium, thus allowing vapour pressure measurement without damage to the transducer.

However, following the first pore pressure test described in section 5.2.1.1 it was realised that 0 - 690 KN/m^2 (0 - 100 psi) pressure range of these transducers was not adequate.

Consequently, a 'Solartron' strain gauge pressure transducer type NT4-313,of similar characteristics as the previous ones but of a pressure range 0 - 10343 KN/m^2 (0 - 1500 psi) was obtained. However, although this transducer was substantially cheaper than the previous one, it was from a discontinued range and therefore

with a limited guarantee. It was therefore decided that a transducer of a more reliable character should also be ordered in case this one would fail to work satisfactorily.

Bell and Howell strain gauge pressure transducer, type 4 - 366, of 0 - 6895 KN/m^2 (0 - 1000 psi) range was chosen for this purpose.(Fig.5.10) Although the operating temperature range (-54°C - 120°C) compared unfavourably with high temperature resistance types in the market, 4 - 366 seemed to have the best combination of high pressure range, moisture and shock resistance and reasonably high operating temperatures. Type 4 - 366 was therefore purchased bearing in mind that a cooling system would be required in conjunction with these transducers. The cooling system is described in the following section.

5.2.2.2 Heat Exchanger

5.2.2.2.1 Original Design

The heat exchanger was devised as a metal rod linking the pressure transducer to the pressure cell. The main purpose of this part was to keep the transducer away from excessive heat while transferring the cell pressure to the transducer. Initially the heat exchanger was so designed that the pressure would be transferred by the water in the central 2mm diameter tube while allowing air cooling through the skin. The inside diameter was kept to minimum to introduce as little extra water as possible to the system. The exchanger was made out of brass and connected to the

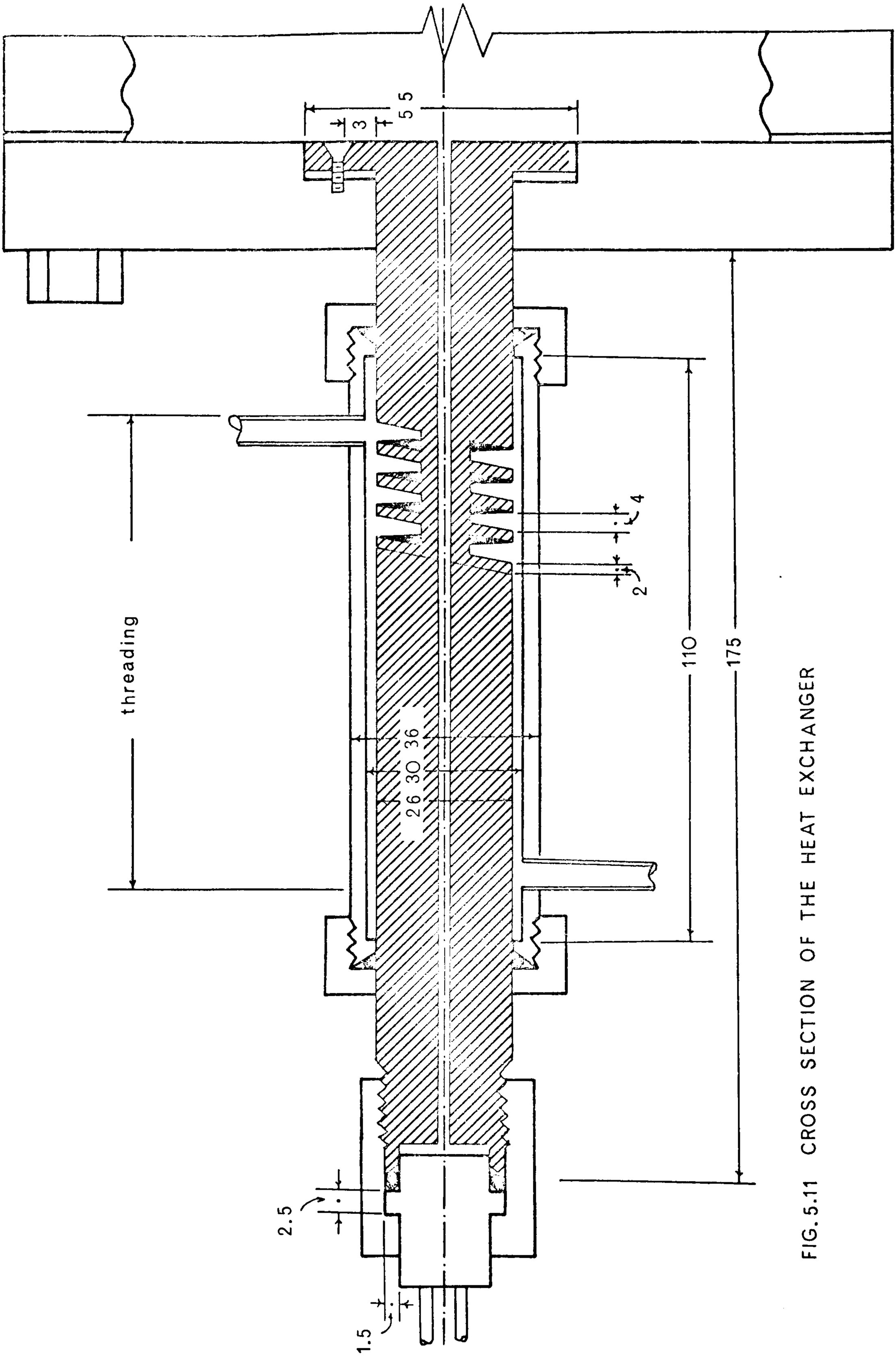

FIG. 5.11 CROSS SECTION OF THE HEAT EXCHANGER

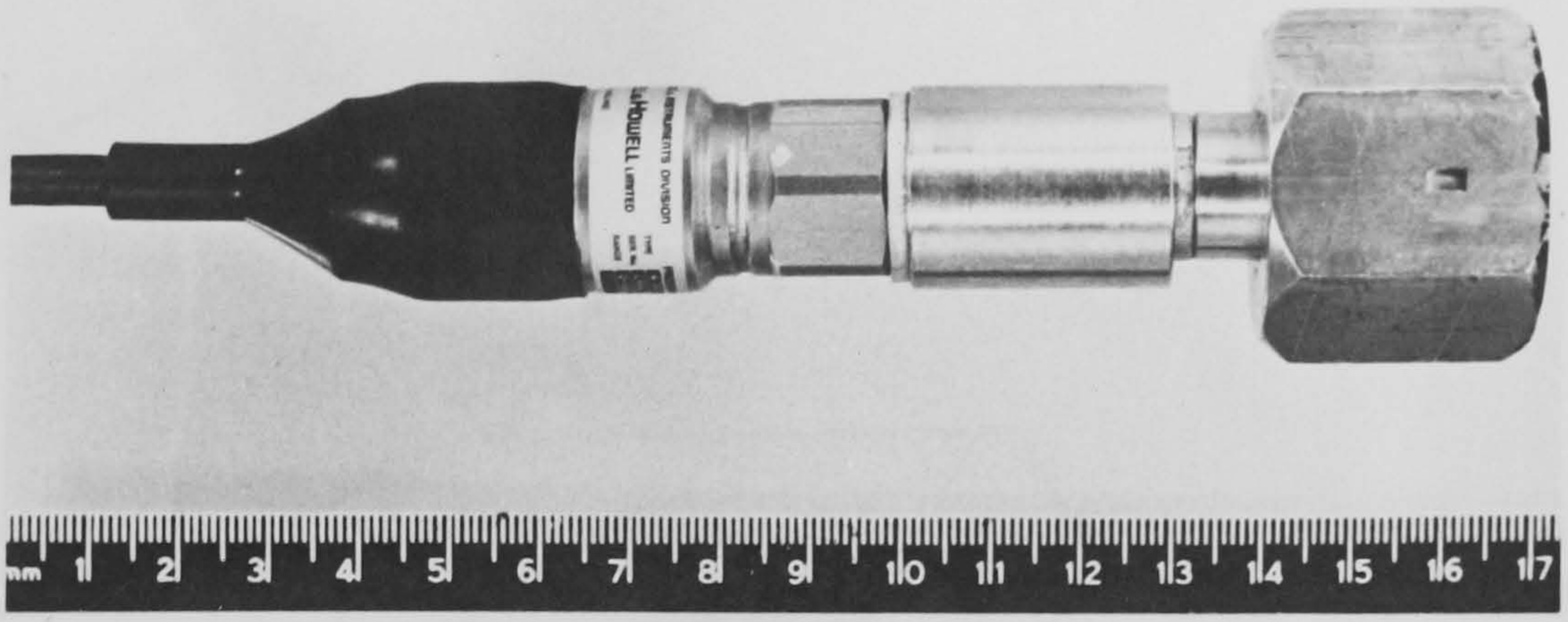

FIG. 5.10 BELL & HOWELL PRESSURE TRANSDUCER AND ATTACHMENTS

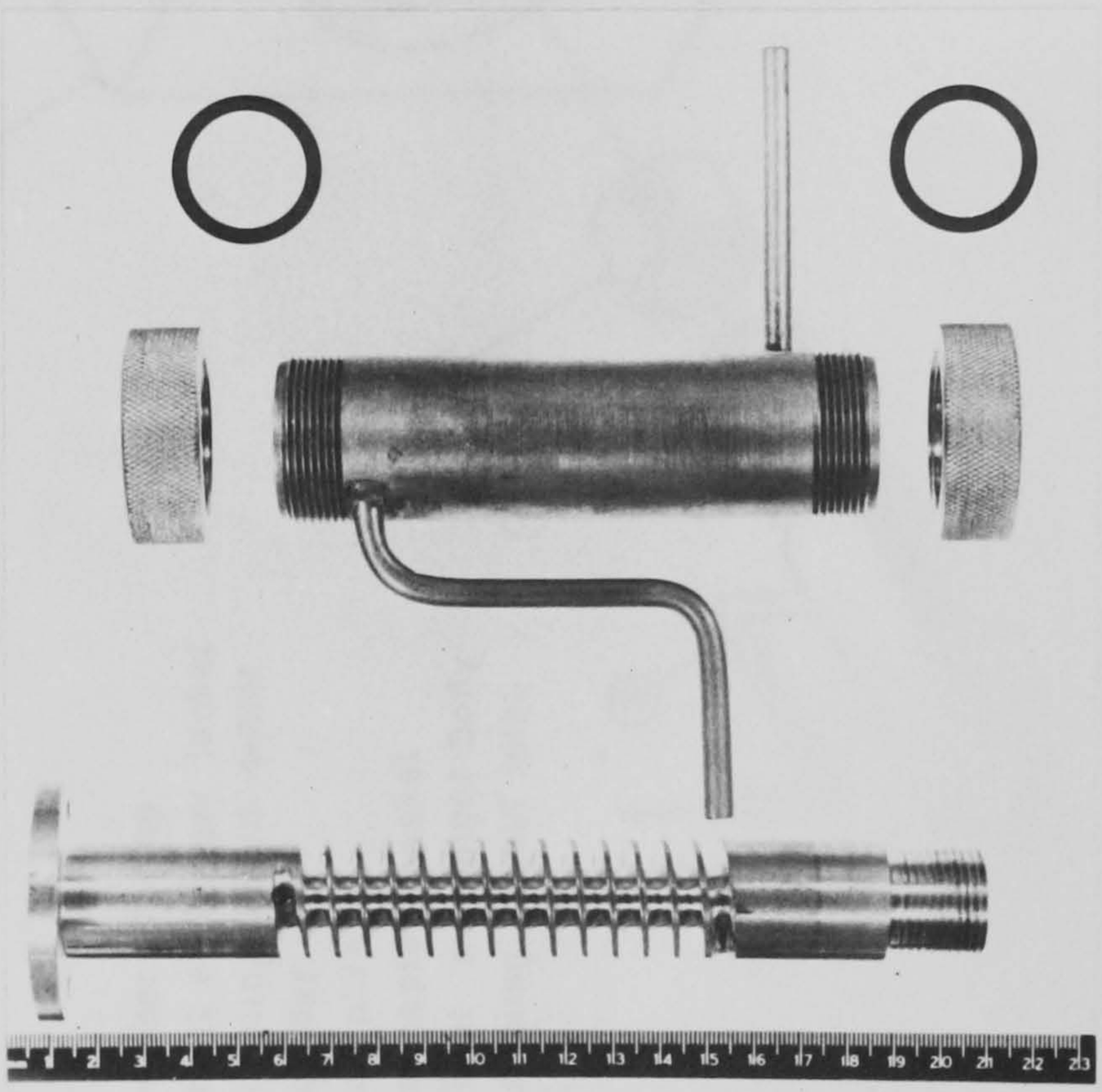

FIG. 5.12 'IMPROVED HEAT EXCHANGER' PARTS

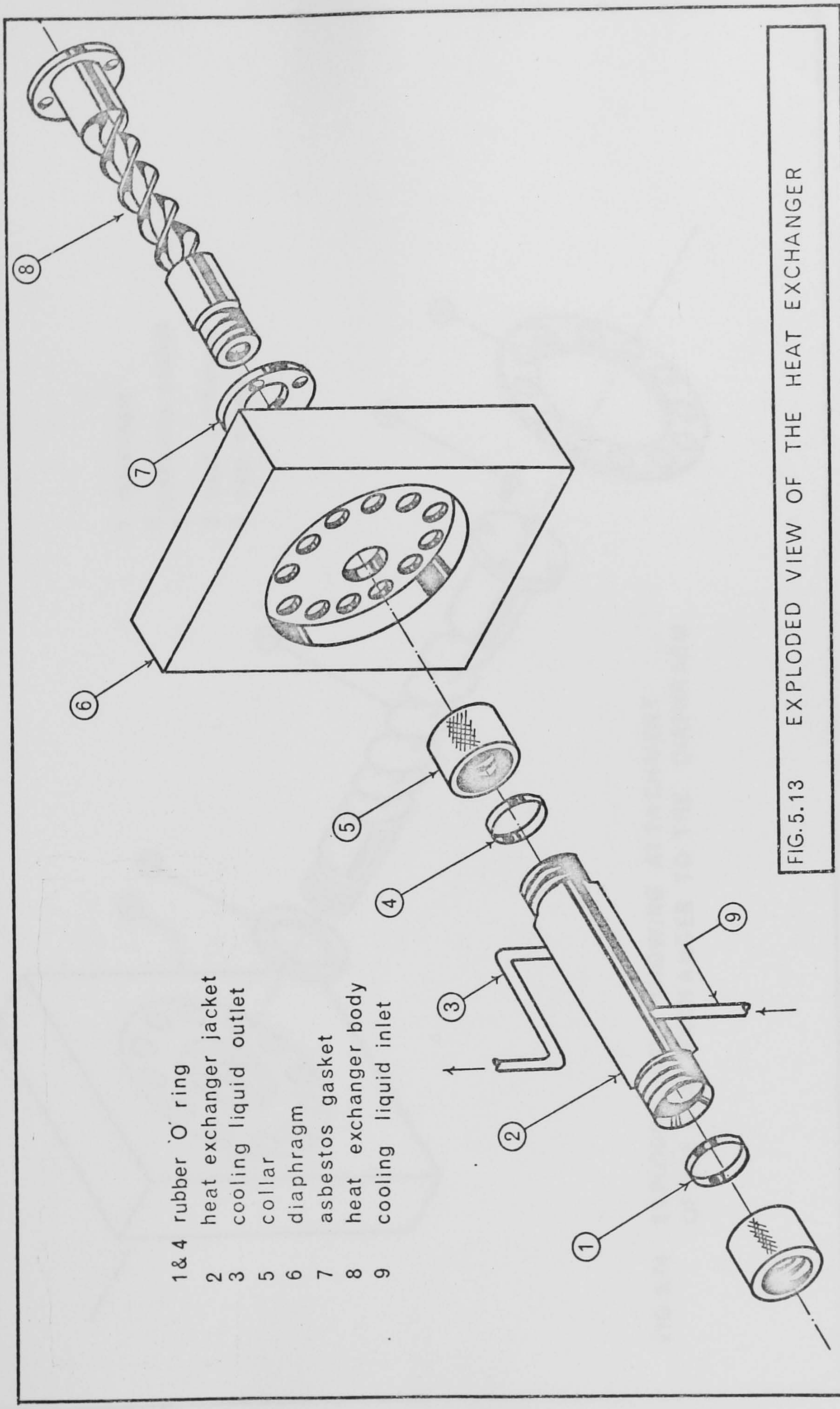

FIG. 5.13 EXPLODED VIEW OF THE HEAT EXCHANGER

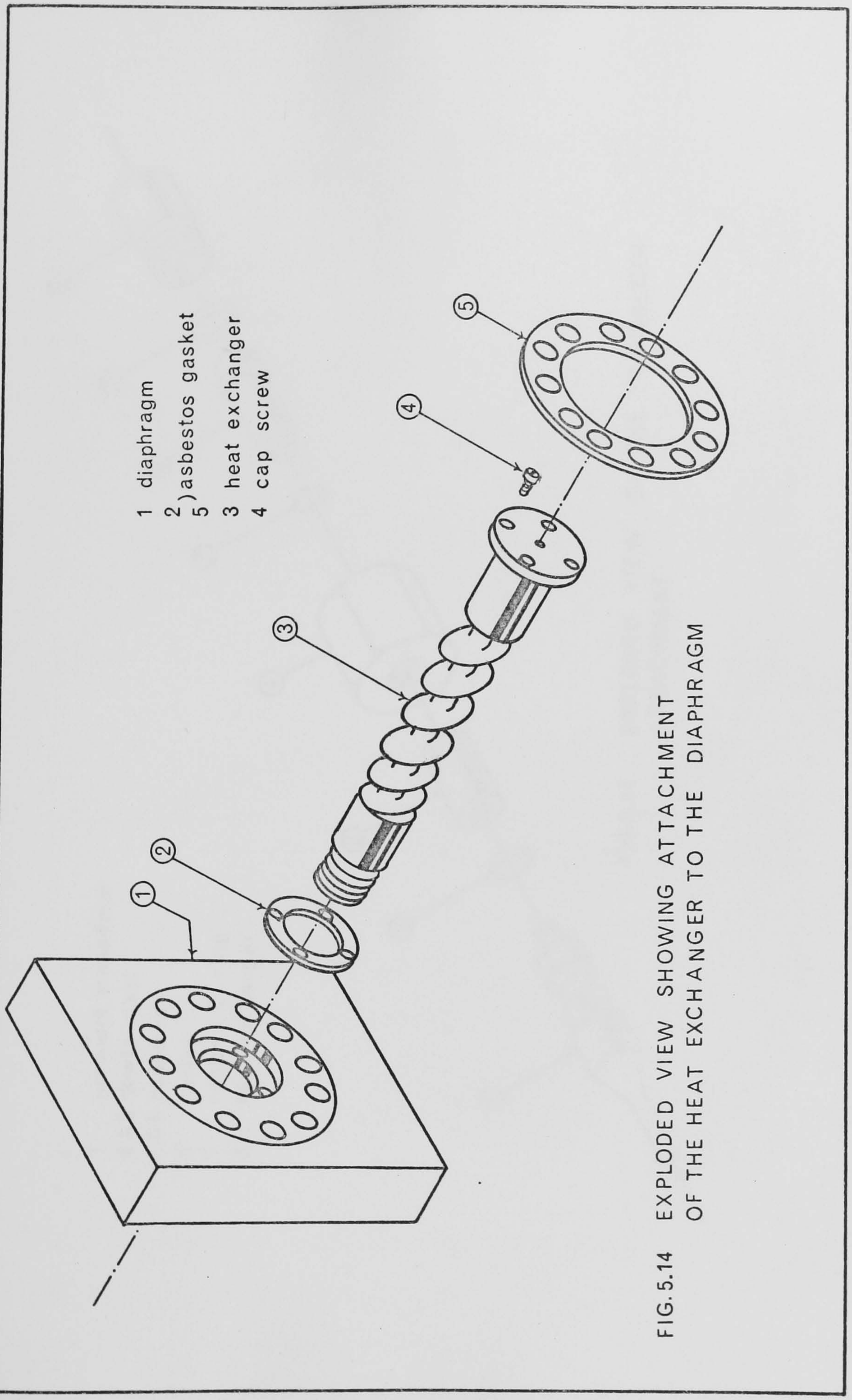

FIG. 5.14 EXPLODED VIEW SHOWING ATTACHMENT OF THE HEAT EXCHANGER TO THE DIAPHRAGM

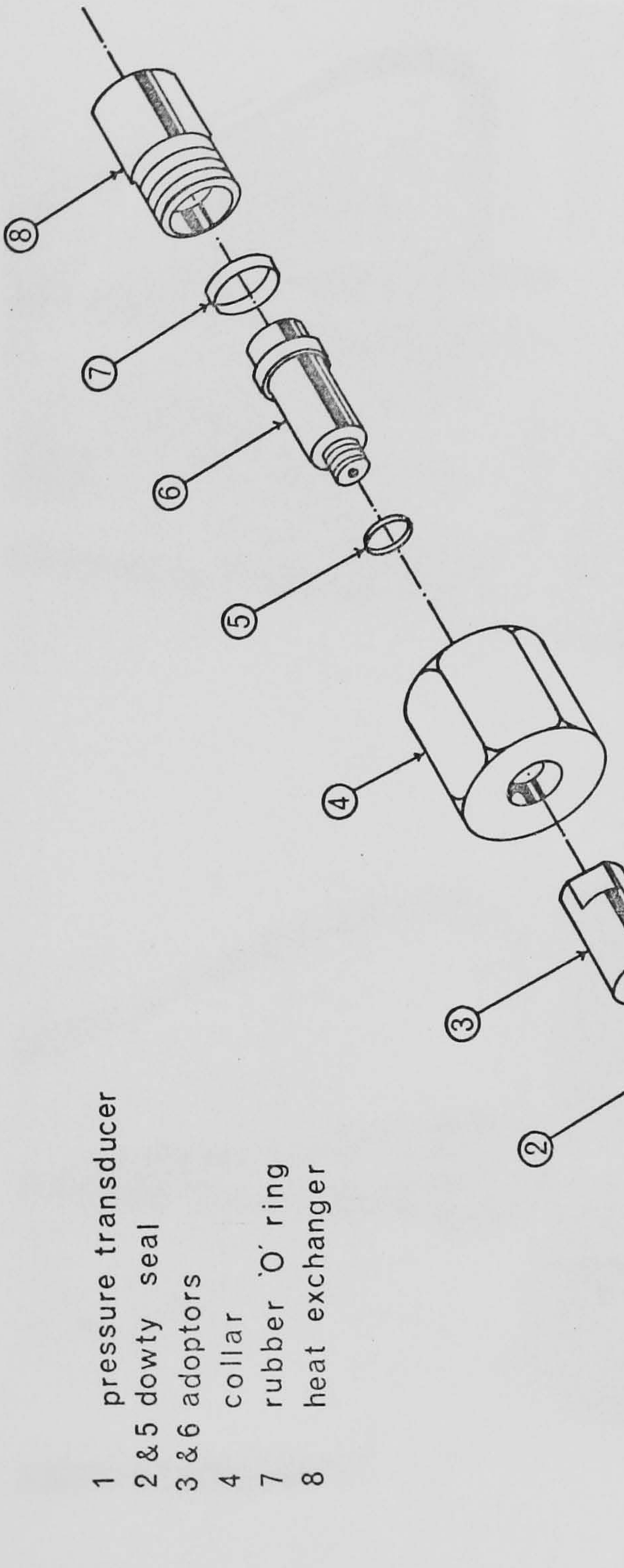

1 pressure transducer
2 & 5 dowty seal
3 & 6 adoptors
4 collar
7 rubber 'O' ring
8 heat exchanger

FIG.5.15 EXPLODED VIEW OF THE TRANSDUCER ATTACHMENT

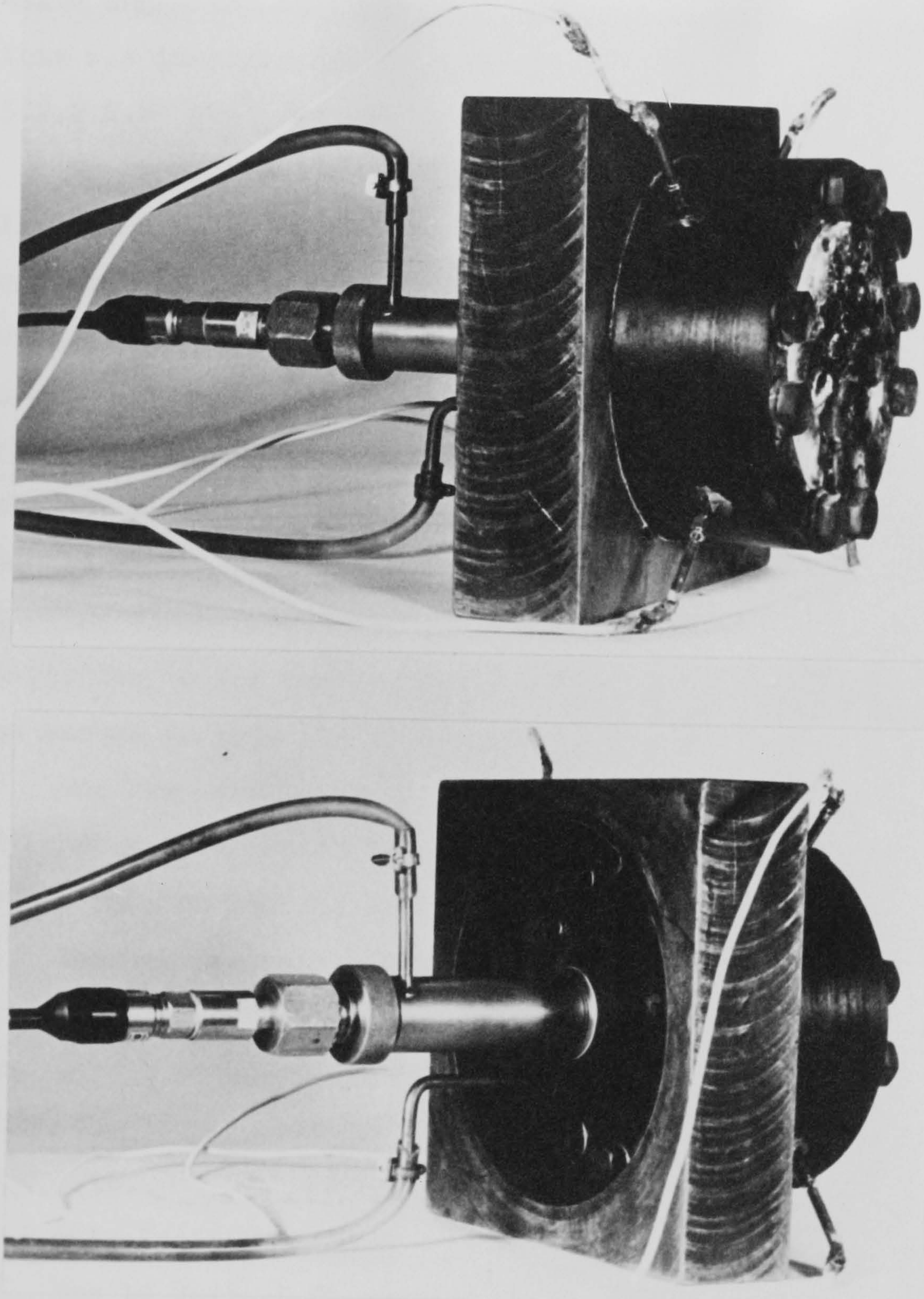

FIG. 5.16 PRESSURE CELL IN ITS FINAL FORM

diaphragm as shown in Fig.5.7 and Fig.5.8. Subsequent tests suggested additional cooling was required and this was incorporated in a later design.

5.2.2.2.2 Improved Design

An improved water-cooled heat exchanger, 215mm long, having 2mm and 25·5mm inside and outside diameters respectively, enclosed in a jacket with a 2mm clearance was produced as shown in Fig.5.11 and Fig.5.12. The body of the exchanger was threaded (single thread having 5mm axial pitch and 9mm thread depth) to increase the surface area. Approximate calculations showed that a continuous 0·5 l/min supply of water flowing through the body and the jacket, in the opposite direction to the heat transfer from the test cell would be enough to keep the transducer below 120°C.

The heat exchanger was connected at one end to the diaphragm as shown in Fig.5.13 and Fig.5.14 and at the other end, to the 'Solartron' transducer. Fig.5.15

The heat exchanger was fitted with the adapters shown in Fig.5.10 and Fig.5.15 to make use of the Bell and Howell pressure transducer possible. In its final form the 'pore pressure' test apparatus was as shown in Fig.5.16.

5.2.2.3 Instrumentation

The 10 Volts D.C. excitation required by the transducers was supplied by the 'Stabilized Power Supplier' made by 'Farnell Instruments'. The power supplier was connected to the two input terminals of

the transducer, and the two wires representing the output terminal was connected to a Bryans X-Y-Y plotter with a chart drive unit for continuous recording.

5.2.3 Temperature Measuring System

5.2.3.1 Introduction

Although the main purpose of the pore pressure tests was to measure the vapour pressure generated in the specimen exposed to heat, it was necessary to know the temperatures reached in the specimen in order to assess: a) the effect of heating regime on the maximum pressures generated, and, b) the variation in heating pattern between different tests.

Temperature measurement was by means of thermocouples.

5.2.3.2 Thermocouples and Connections

The thermocouple wires which were needed to be embedded in the specimen could either enter or leave the specimen through the heated face or through the pressure cell. The introduction of the wires through the heated face could cause the escape of internal pressure, and, therefore, it was better to introduce them through the walls of the pressure cell. However, keeping the pressure cell sealed while having the thermocouple wires through the walls created some problems.

5.2.3.2.1 Initial Method

Glass/Metal seals

The requirements for measuring the temperature

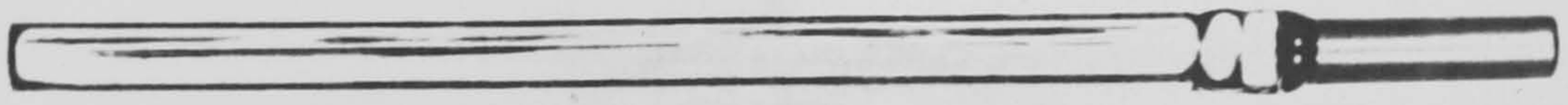

FIG. 5.17 GLASS TO METAL SEAL

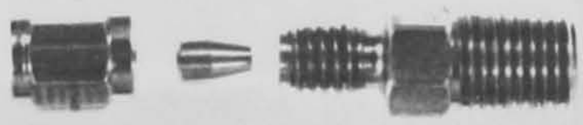

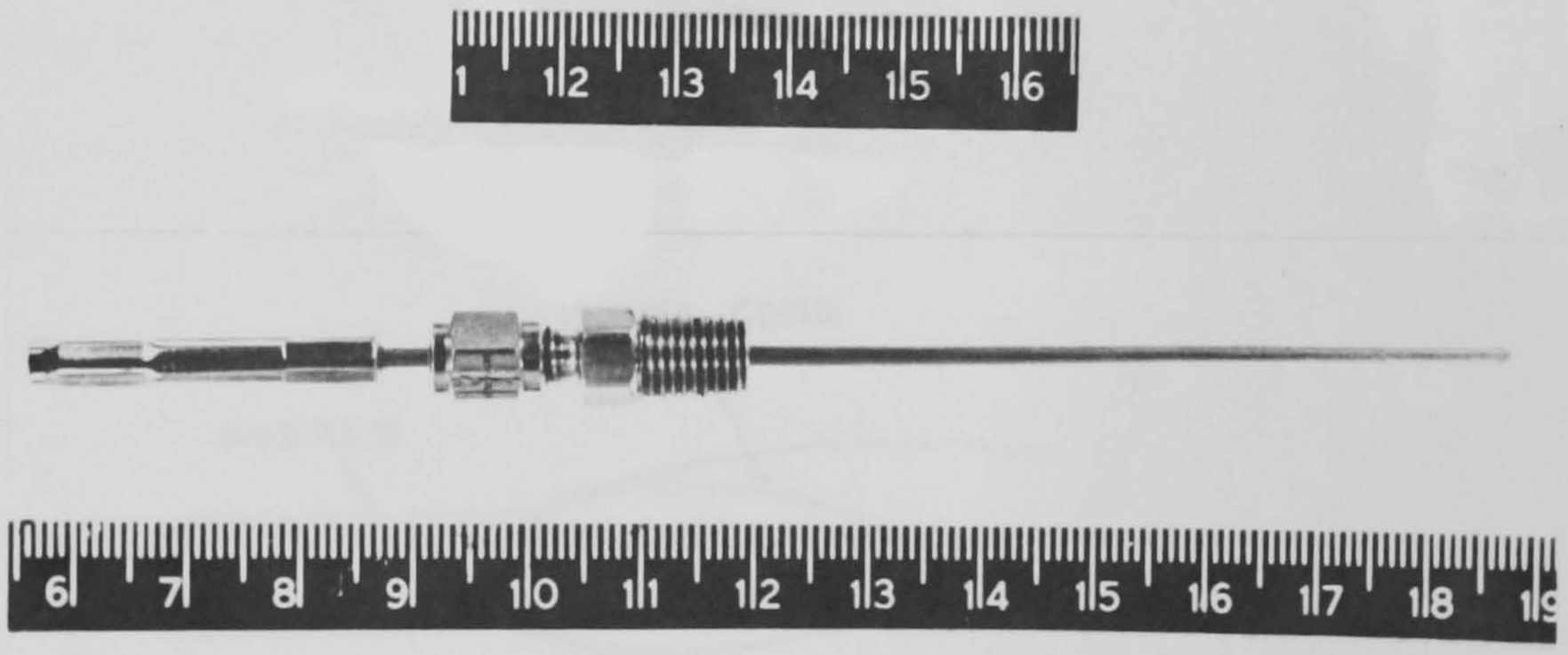

FIG. 5.19 THERMOCOAX THERMOCOUPLE PROBE WITH THERMOLOK GLAND

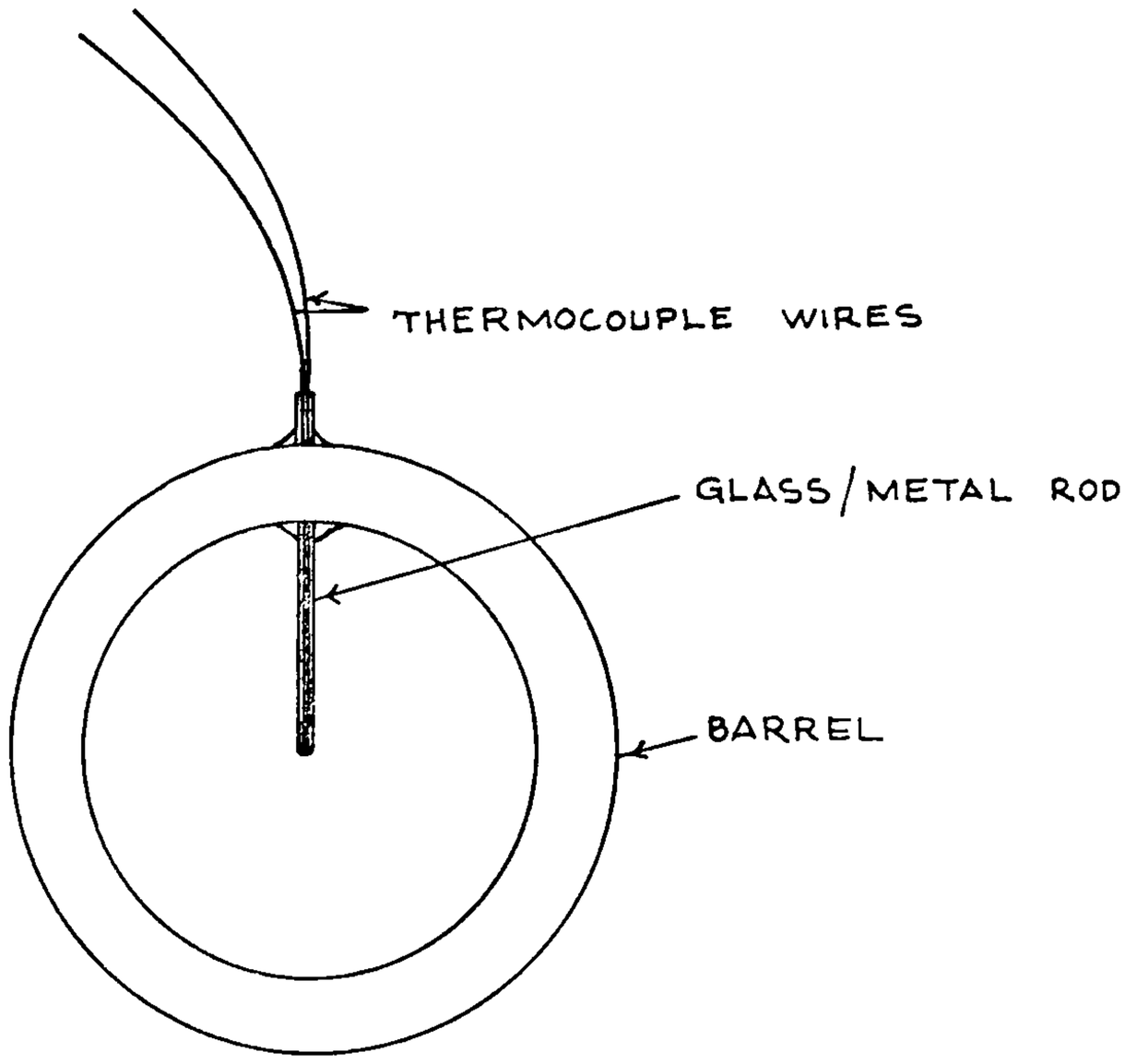

FIG. 5.18 INTRODUCTION OF THERMOCOUPLE WIRES INTO THE CELL THROUGH GLASS/METAL ROD

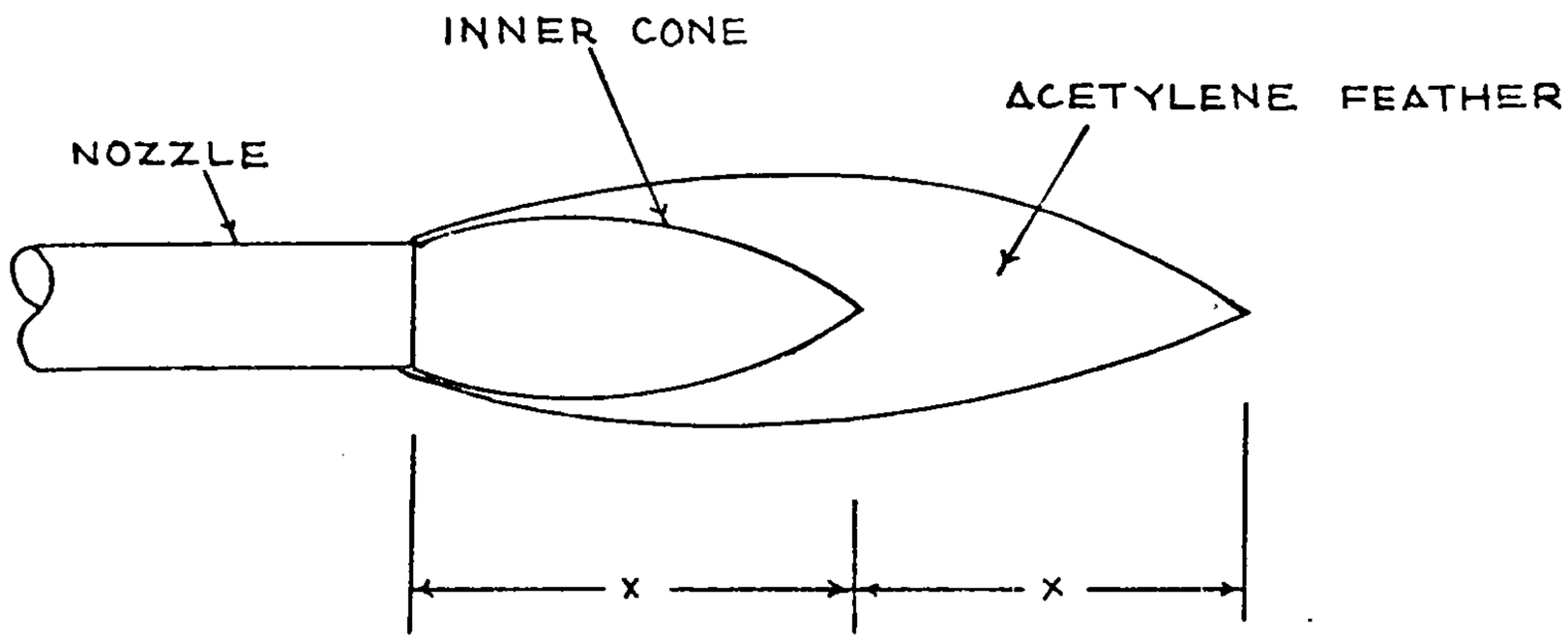

FIG. 5.21 CARBURISING FLAME CHARACTERISTICS

were such that the thermocouple wires should be introduced in the specimen through an insulating material which a) would not absorb moisture so that the amount of water available for evaporation would not be altered, b) would not give in under pressure so as not to alter the level of pressure, c) should be easily fixed on to the walls of the pressure cell in order to preserve the pressure tightness of the system, d) should resist shocks and elevated temperatures and e) should be recoverable after each test or at least should be cheap enough to replace after each test.

Glass to metal seals, supplied by 'Jencons Ltd.' seemed to be suitable and four were purchased for trial tests. These were made of 25mm 'Kovar' tubes connected by a special sealing to 120mm long 6mm outside diameter pyrex tubes (Fig.5.17). In a preliminary test to check the effectiveness of the glass to metal seal, the metal part of the glass to metal tubing was soft soldered on to the wall of the barrel as shown in Fig.5.18. Chromel/alumel thermocouple wires supplied by 'Saxonia Ltd.' were then prepared and fixed at the end of the pyrex tubing by melting down the tip of the latter using a Bunsen burner.

Using the barrel as a mould, a mortar specimen was cast and tested after 7 days by applying oxyacetylene heating to one face for a period of 30 minutes. During the first 15 minutes, vapour was observed to escape through the exposed face and during the last 15 minutes through the cool face which was open to the atmosphere.

No vapour was observed to leave through the tubing, and, therefore, it was assumed that the glass/metal seal was not damaged during the test. Although the glass/metal tubing seemed to work satisfactorily in the conditions of the trial test, it was obviously impossible to recover it after the test, so this method was abandoned as being too expensive.

5.2.3.2.2 Improved Design: Thermocoax Thermocouples and Glands

A less expensive method was subsequently introduced by the use of ready made thermocouples (Fig.5.19) supplied by 'Pye Unicam Ltd.' under the trade name 'Thermocoax Thermocouples'. Each thermocouple comprised chromel and alumel conductors protected by a 2mm outside diameter metallic sheath, the insulation between the conductors and between the conductors and sheath being compacted magnesium oxide powder. The probe was extended by a flexible extension cable having chromel and alumel conductors and a copper shielding braid insulated and protected by an outer plastic cover.

Besides being shock resistant, watertight and high pressure resistant, the most important advantage claimed for these thermocouples was that they could be fitted with 'thermolok glands'. These glands were specially designed to allow thermocouples to be introduced into a pressure vessel without loss of pressure.

The thermolok glands consisted of three stainless steel parts: a body, a ferrule, and a gland nut.

1 gland nut
2 ferrule
3 barrel
4 body
5 thermocouple probe

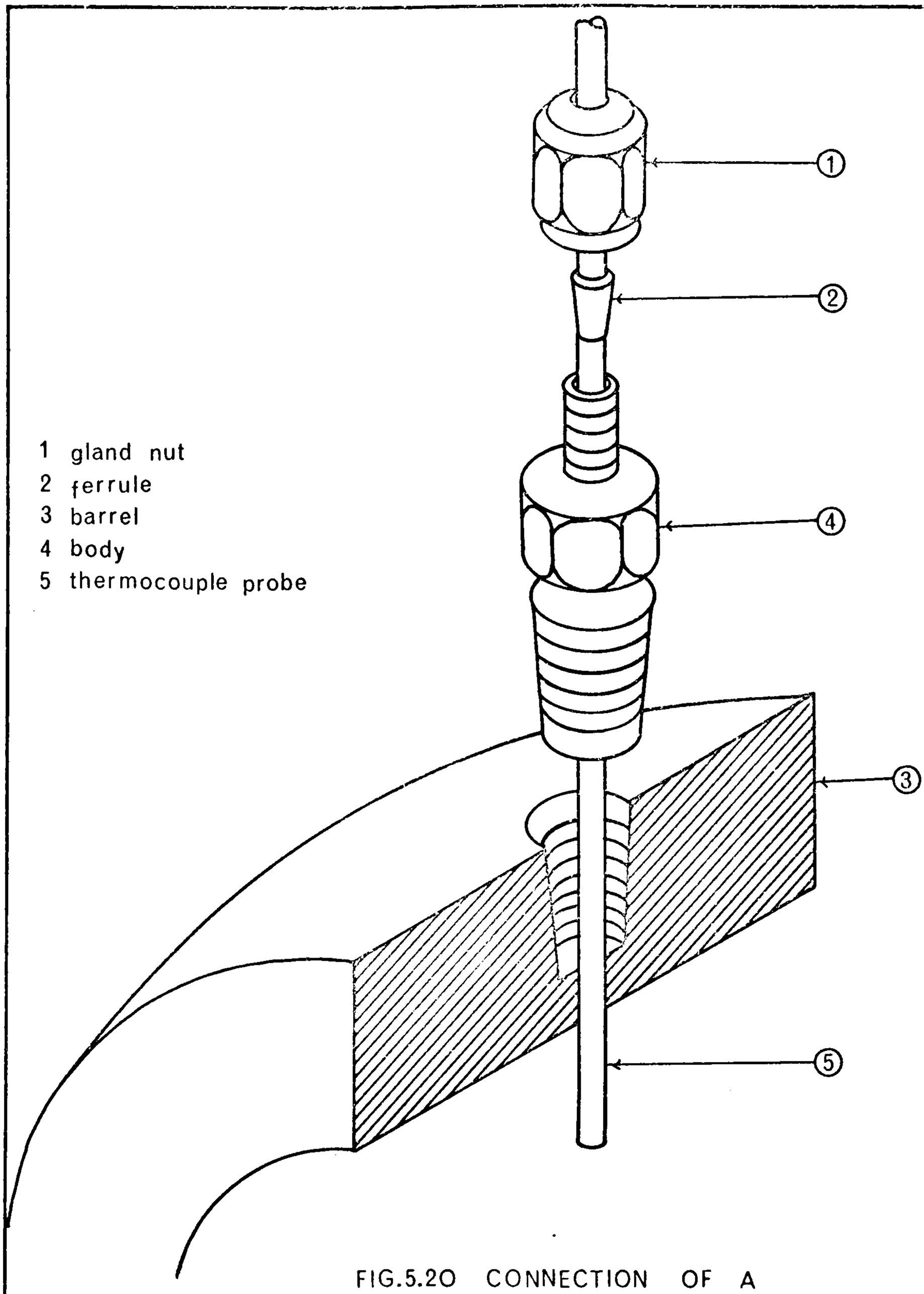

FIG.5.20 CONNECTION OF A THERMOCOUPLE TO THE PRESSURE CELL

(Fig.5.19). The body was screwed into the previously drilled and tapped (1·58mm (1/16 in) N.P.T.F., National (USA) Pipe Taper Fuel) hole in the wall of the barrel. (Fig.5.20) The probe of the thermocouple was then lead through the gland nut and the ferrule,as shown in Fig.5.20,and the gland nut tightened, applying a torque of 3 Nm as suggested by the manufacturers. These glands could be removed and refitted without any alteration and an extra 1/8 turn every time the gland was refitted was claimed to provide pressure sealing.

However, several tests on various glands to measure sealing capacity (See section 5.3.1.2 for sealing tests) showed signs of leakage around the thermolok glands at pressures as low as 345 KN/m^2 (50 psi). This unsatisfactory performance was subsequently attributed by the manufacturer to faulty workmanship exercised when tapering the holes in which the glands were fitted. This may or may not have been the answer. Clearly though,the system depended very much on the quality of the workmanship and the assembly procedure. The sealing problem was subseqently solved by silversoldering the thermolok glands to the wall of the pressure cell. The silver soldering operation, however, required care to be exercised as a number of trials ended up unsuccessfully due to inherent difficulty in soldering stainless steel,and to difficulty in bringing both materials to the same temperature, a condition required for a satisfactory soldering, because

the sizes and surface areas of the two parts differed considerably.

The soldered thermolok glands and companion thermocouples were then used throughout the pore pressure tests, and exhibited good pressure tightness at pressures as high as 4137 KN/m^2 (600 psi). (See section 5.3.1.2 for sealing tests)

5.2.3.3 Instrumentation

The temperature was recorded by 'Speedomax G' temperature recorder made by 'Leeds and Northrup Ltd. ' The thermocouples were directly connected to the recorder without the need of a cold junction as the recorder was fitted with an automatic cold junction compansating device.

5.2.4 Heating Arrangement

Due to absence of a specially designed furnace, the heat supplied had to be local in character and powerful enough to overcome the heat loss to the atmosphere. It was therefore decided to use an oxyacetylene flame to heat the specimens.

Acetylene and oxygen were supplied from pressure cylinders. They were burned at the tip of a blowpipe with nozzle size 25. The two gases were led to the torch through pressure reducing valves on each gas tank, and connecting hose. The pressure regulators on the tanks were necessary to maintain the desired lower pressure at a uniform value throughout the test.

The recommended gas pressure corresponding to nozzle No. 25 was 41 KN/m^2 (6psi) for both gases.

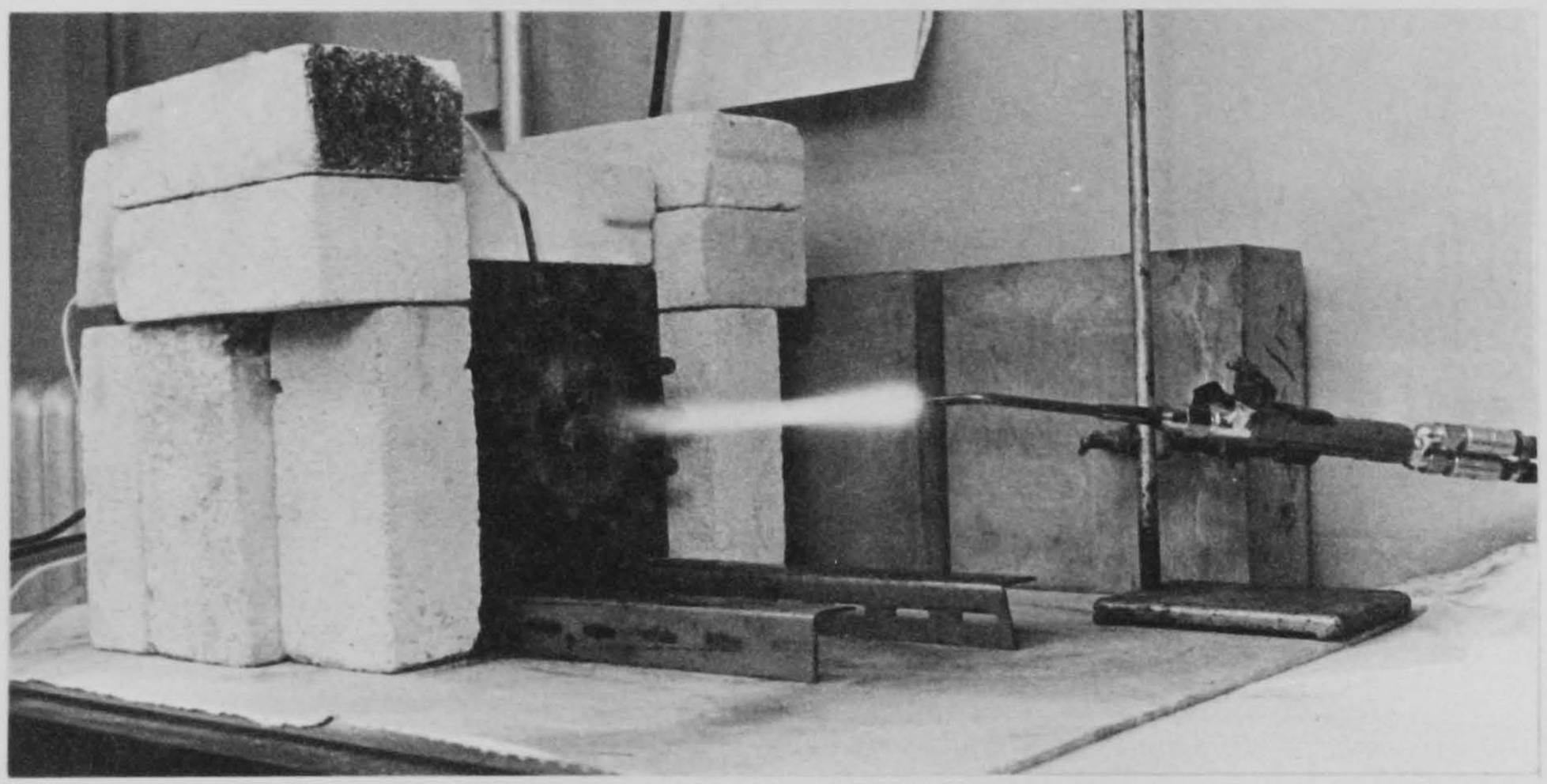

FIG. 5.22 APPLICATION OF HEAT TO THE SPECIMEN

However, preliminary tests showed that occasional explosion due to the accumulation of solid material (probably carbon) at the tip of the nozzle could occur. After trying various combinations of gas pressures, best results were obtained when oxygen and acetylene pressures were kept at 28 KN/m^2 (4 psi) and 14 KN/m^2 (2 psi) respectively.

A carburizing flame (Fig.5.21) obtained by the right combination of the two gases was used throughout the tests. This was obtained by visual inspection and by playing with the two nobs on the blowpipe, thus increasing or decreasing individually the discharge of the two gases.

Before the start of heating, the blowpipe was clamped on a stand as shown in Fig.5.22. After heating started, the blowpipe and the stand fixed to it was moved nearer to the specimen in such a way that the tip of the acetylene feather (Fig.5.21) touched the surface of the specimen. The expected highest temperature at the tip of the inner cone was about 3500°C and the recorded temperature at the tip of the acetylene feather was 1200°C.

With this heating arrangement the temperature distribution in the specimen depended very much on the amount of insulation provided as well as on the thickness of the specimen. Test with a 64mm deep specimen showed that, in the absence of insulation, a point 5mm away from the heated surface reached a

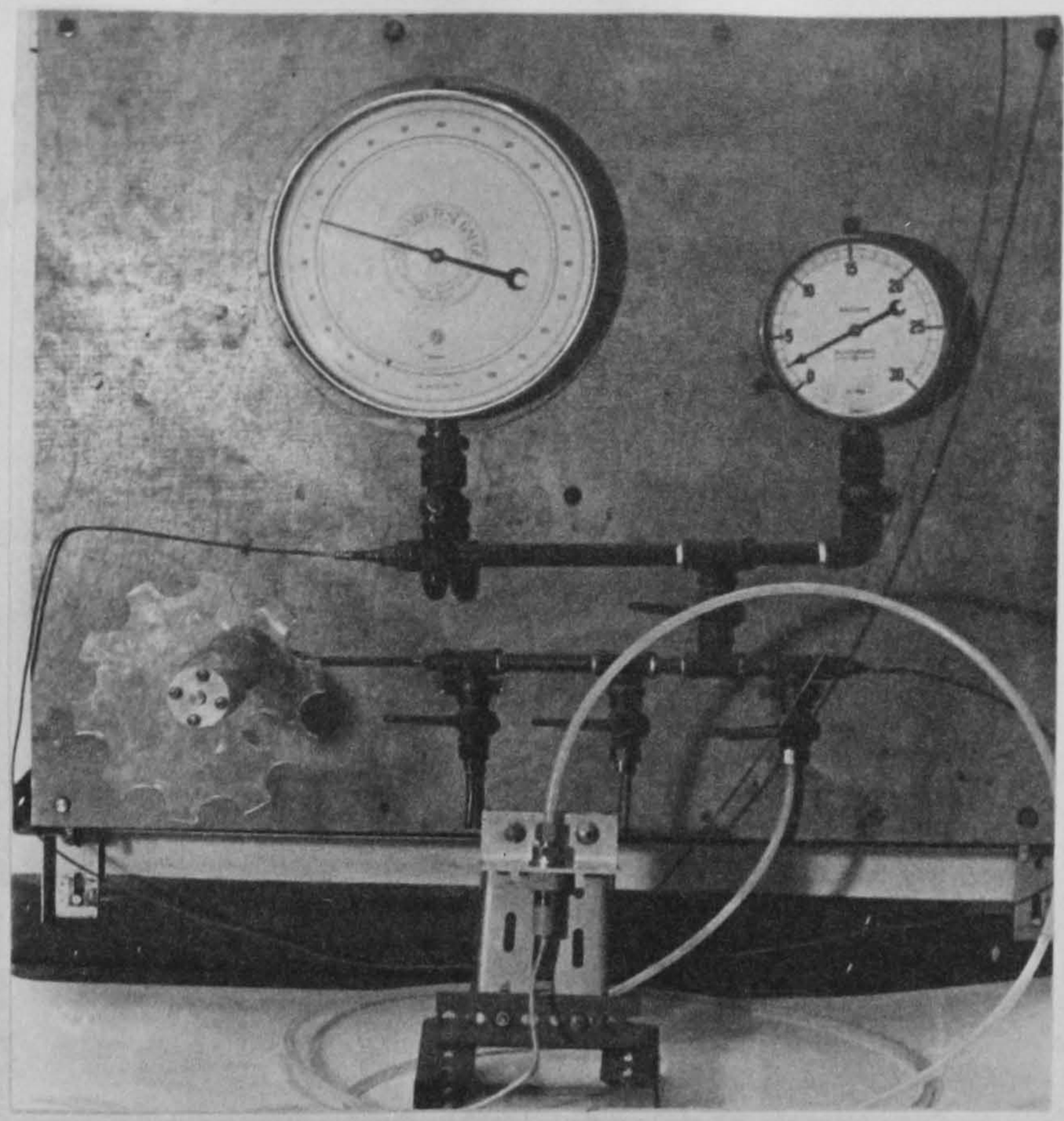

FIG. 5.23 PRESSURE TRANSDUCER CALIBRATION DEVICE

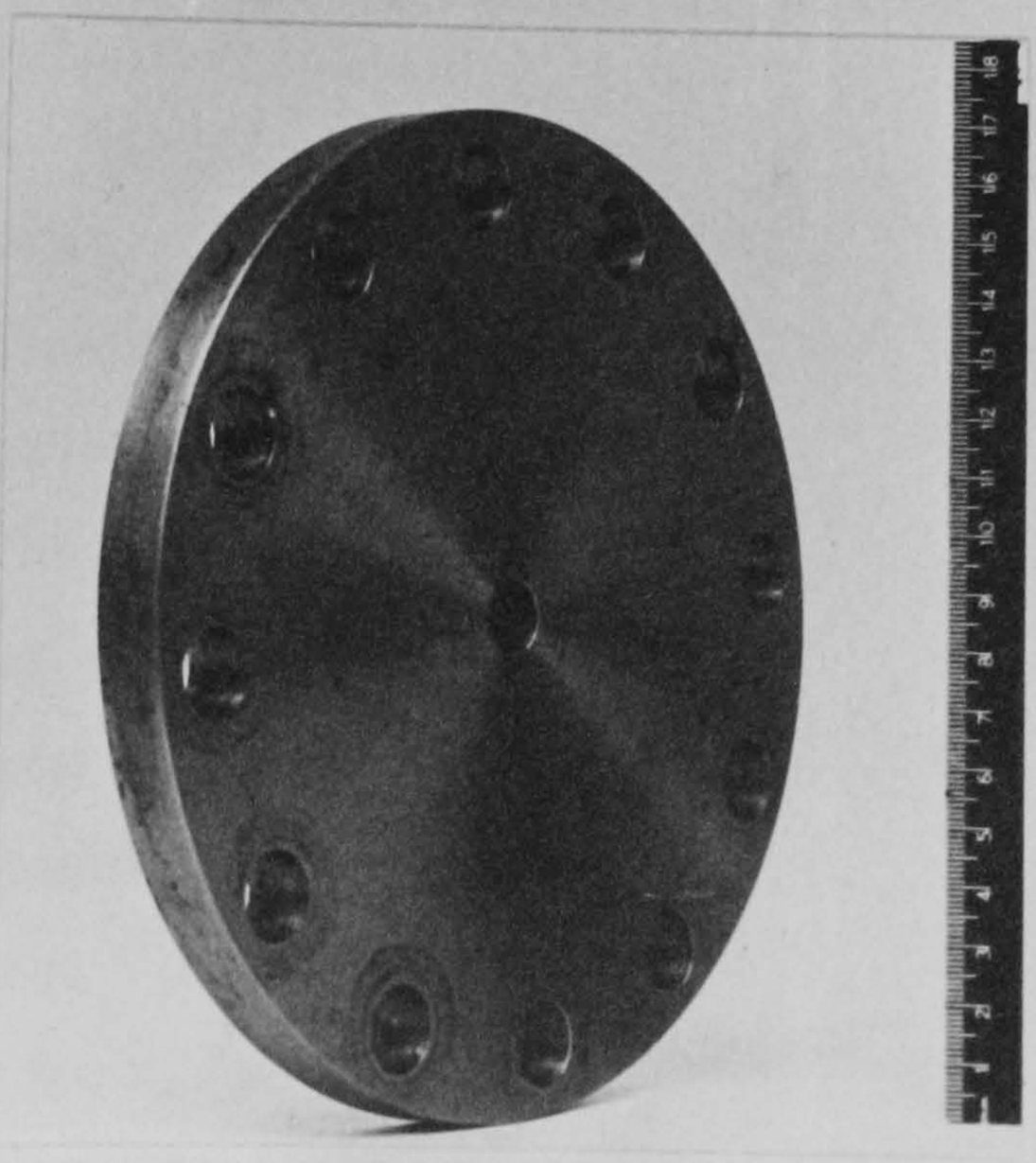

FIG. 5.26 BLANK END PLATE USED FOR CALIBRATION AND SEALING TESTS

maximum of 415°C after 60 minutes of heating, while in another test, in a specimen of the same depth as the previous one but provided with all round insulation, a maximum temperature of 920°C was recorded at a depth of 10mm, after the same duration of heating as the previous one.

Therefore besides paying attention to provide the same heating regime by applying the same type of flame at the right distance from the surface, special emphasis was also placed on keeping the same thickness of insulation around the pressure cells throughout the tests.

5.3 Procedure

5.3.1 Pressure Transducer Calibration and Tests on Sealing Arrangement

5.3.1.1 Calibration

5.3.1.1.1 Method

Although the performance of all the transducers referred to in this chapter were tested by the manufacturer, and a calibration certificate supplied with each of them, it was considered necessary to recalibrate them. For this, the inlet of a hydraulic pressure application device shown in Fig.5.23 was connected to an oil reservoir, and the outlet pipe to the pressure transducer. The input terminals of the transducer were, in turn, connected to the constant volt supplier, and the output terminals to the digital voltmeter. The calibration was then accomplished by applying

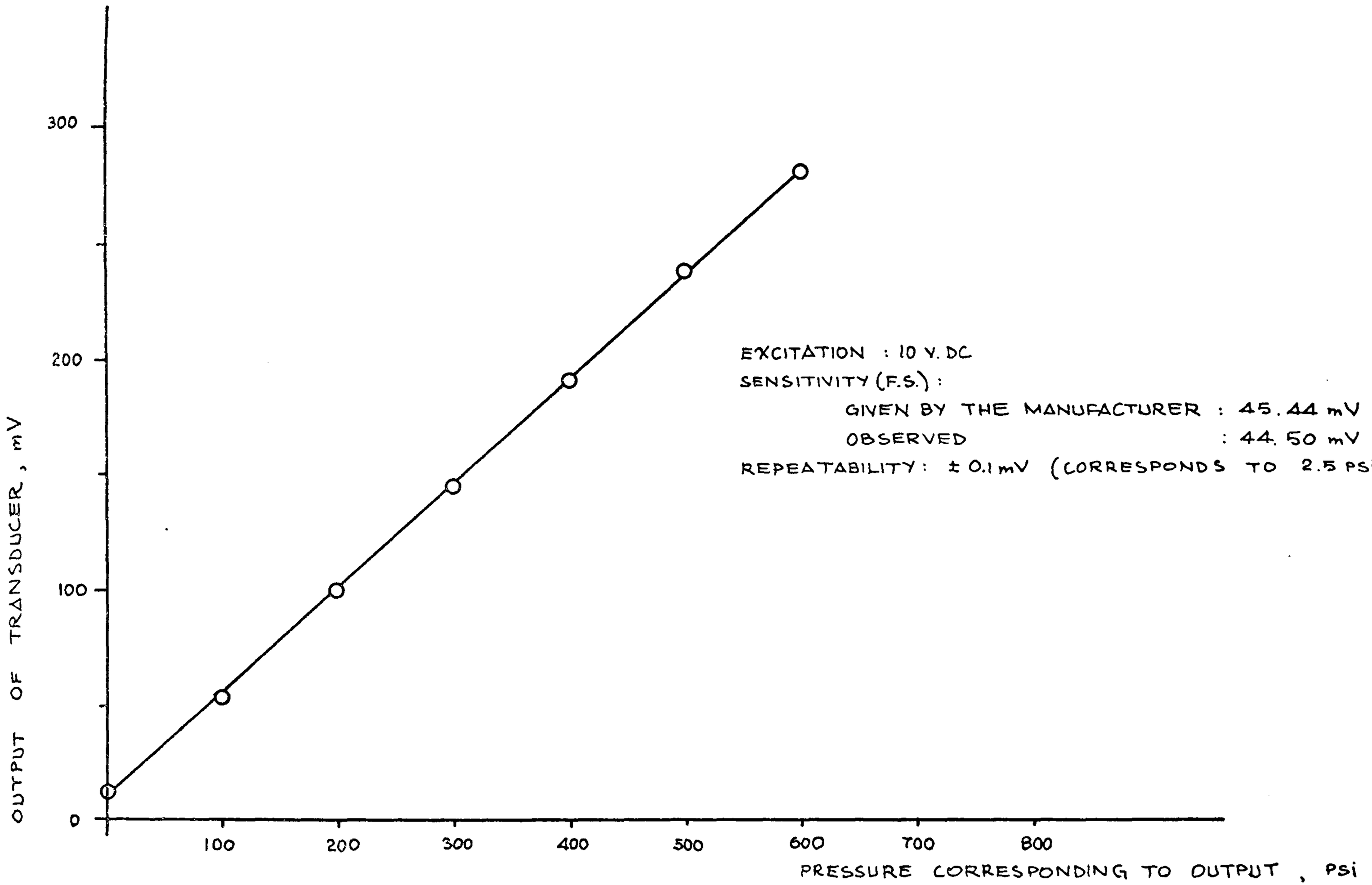

EXCITATION : 10 V. DC
SENSITIVITY (F.S.) :
GIVEN BY THE MANUFACTURER : 45.44 mV
OBSERVED : 44.50 mV
REPEATABILITY : ± 0.1 mV (CORRESPONDS TO 2.5 PSi)

FIG. 5.24 PRESSURE TRANSDUCER CALIBRATION CURVE

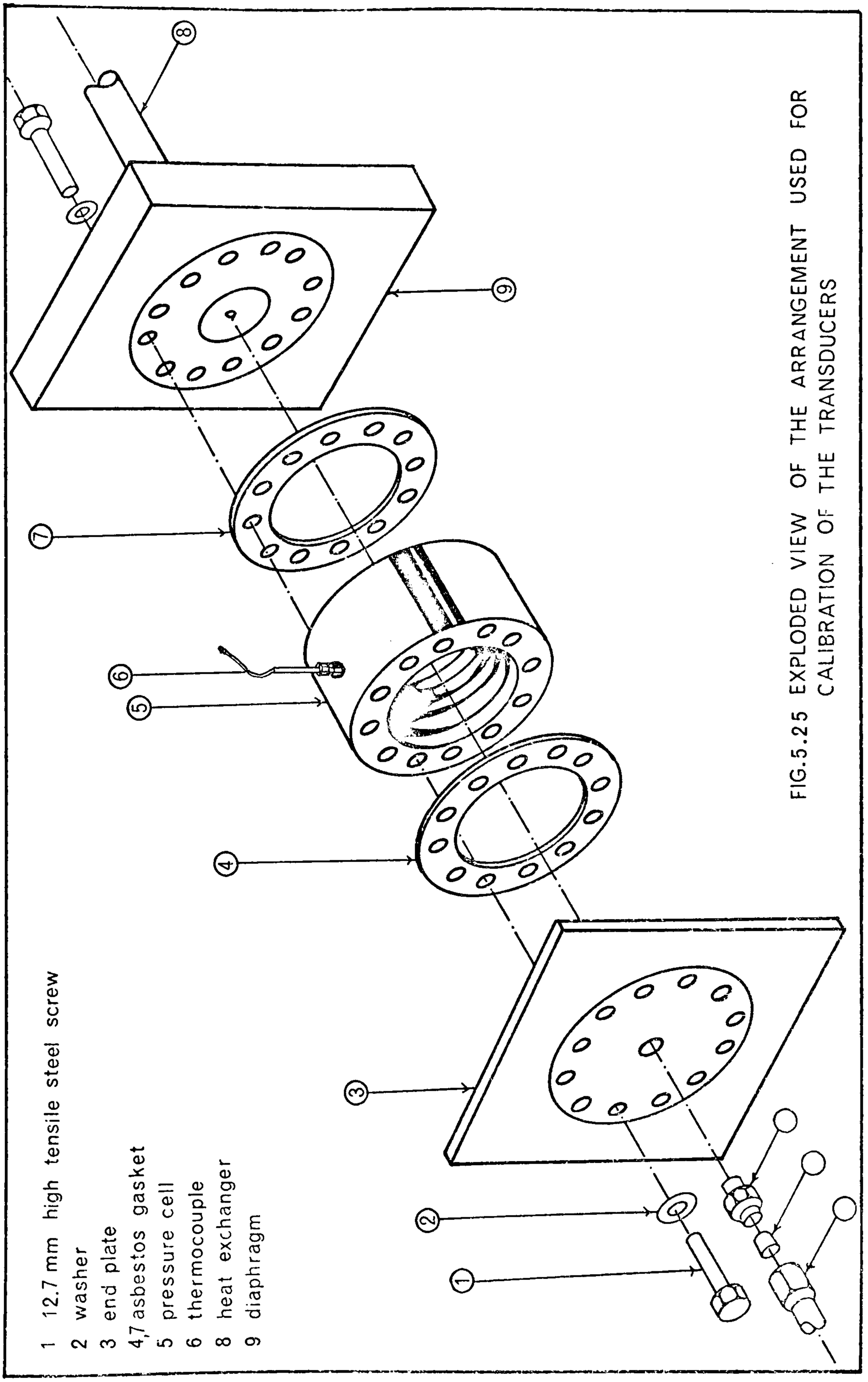

FIG.5.25 EXPLODED VIEW OF THE ARRANGEMENT USED FOR CALIBRATION OF THE TRANSDUCERS

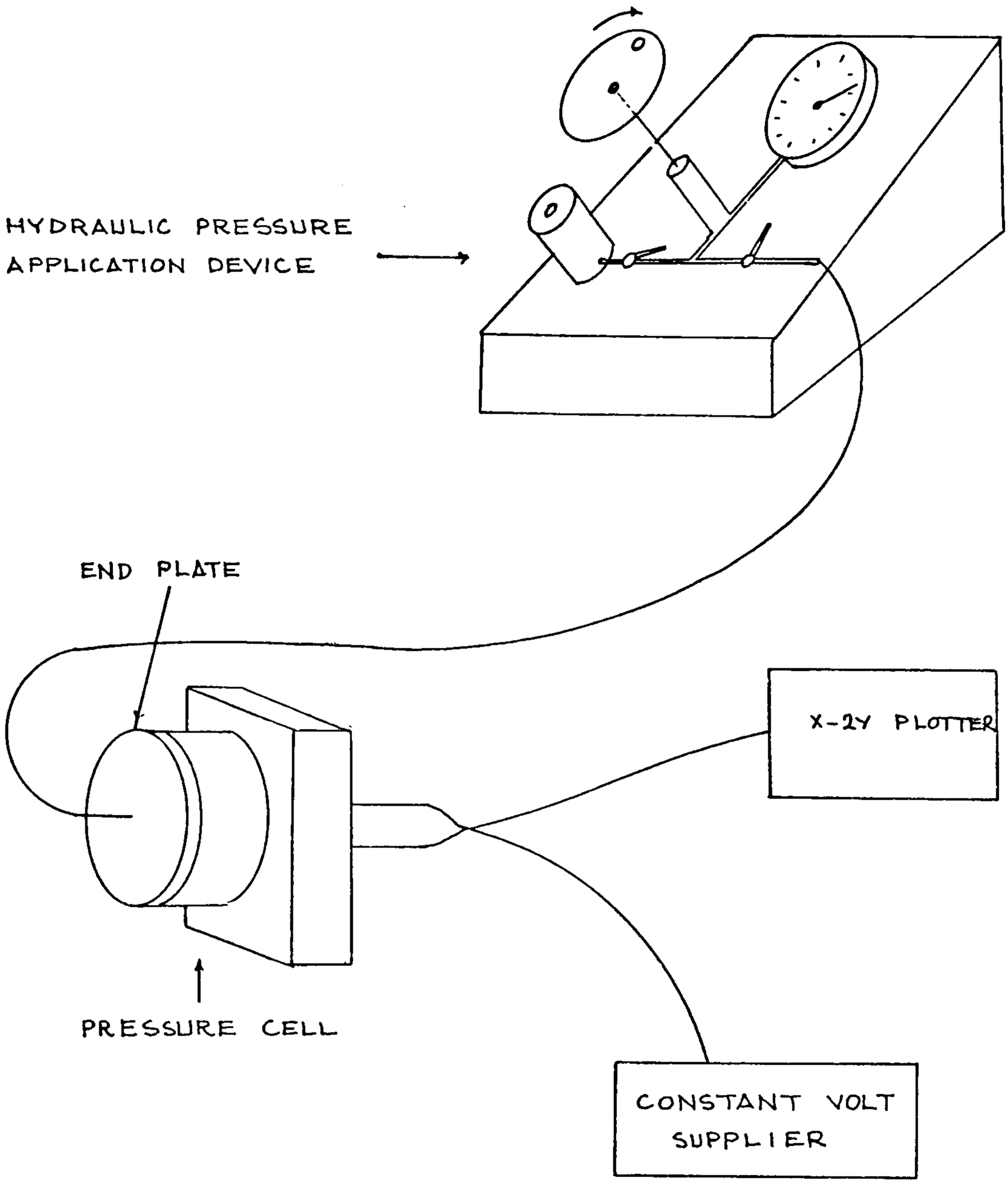

FIG. 5.27 DIAGRAMMATIC VIEW OF PRESSURE TRANSDUCER CALIBRATION

hydraulic oil pressure to the transducer in steps of 10%, from 0 to 100% of the range, and then reducing the pressure using the same steps in reverse order.

The transducer's output at each level was recorded on the calibration record. Two additional tests were subsequently performed to verify the transducer's repeatability and absence of short term drift.

5.3.1.1.2 Calibration Results

The results of the calibration tests (Fig.5.24) showed that the full scale sensitivity of the Bell and Howell transducer was with repeatability better than $\pm$ 0·1 mv corresponding to approximately $\pm$ 17·24 KN/m^2 (2·5 psi).

5.3.1.2 Tests on Sealing Arrangement

To make sure that all pressure cells were leakproof, after the soldering operation described in section 5.2.3.2.2 , all cells were tested under hydraulic pressure up to 4137 KN/m^2 (600 psi). In this, one end of the cell was connected to the diaphragm (Fig.5.25) and the other end to a 12mm thick plate (Fig.5.26) to which the 'pressure application device' was connected, as shown in Fig.5.27. Sealing between the plate, the barrel and the diaphragm was provided with asbestos jointing and the thermocouples were connected and tightened as required for perfect pressure tightness. The pressure was then increased in a similar way as in calibration tests, up to 4137 KN/m^2 (600 psi). Longer term pressure tightness was also checked by leaving the pressure on for 24 hrs.

These tests were carried out on each cell, once

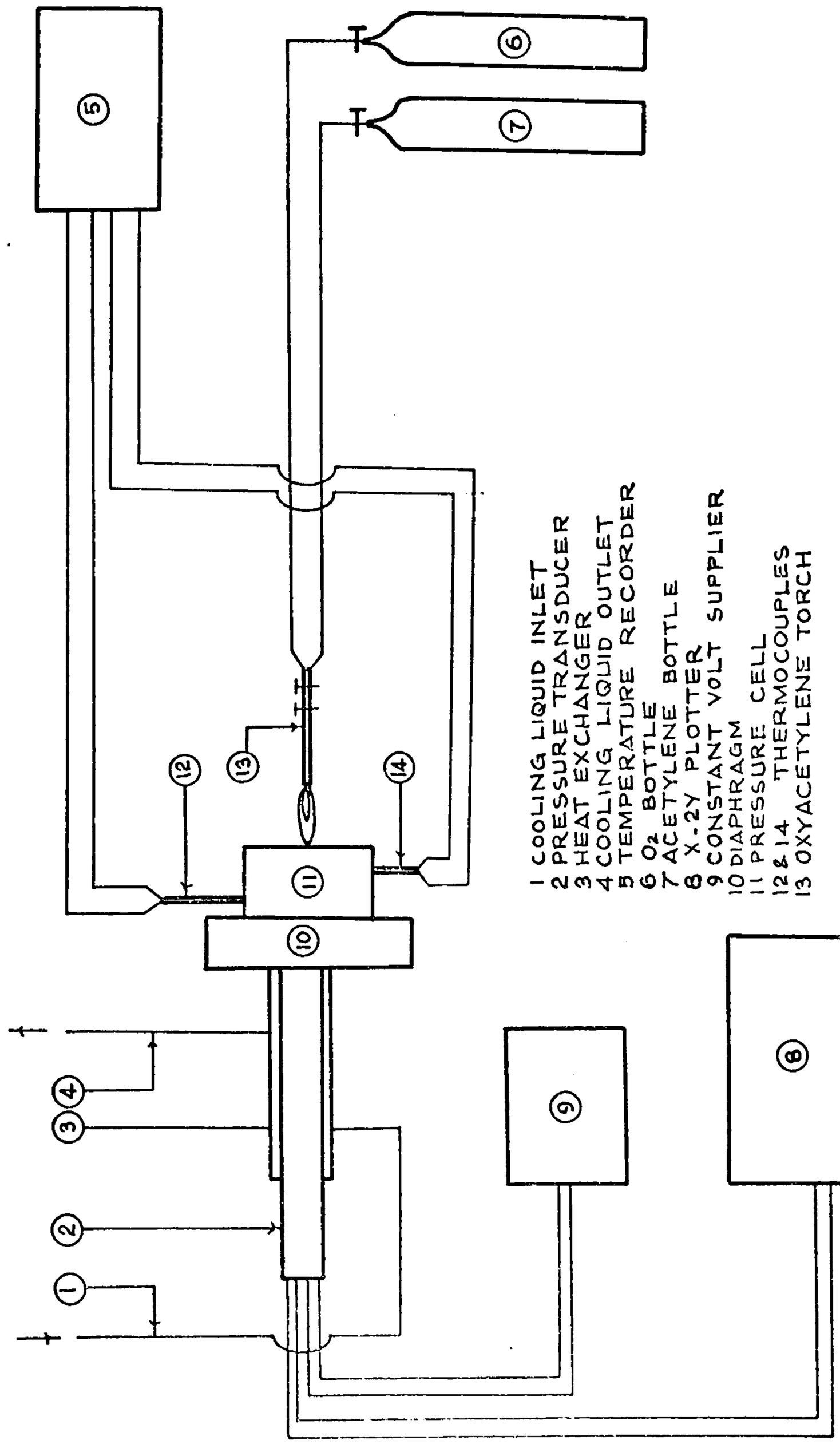

FIG. 5.28 SCHEMATIC VIEW SHOWING PORE PRESSURE TEST SET-UP

FIG. 5.29 OVERALL VIEW OF THE PORE PRESSURE TEST SET-UP

before the start of the Pore Pressure test series, and a second time, halfway during the test series. Initial tests revealed unsatisfactory soldering of some of the thermolok glands and some leaks around asbestos jointings. The glands failing the test had to be resoldered and tested until satisfactory. The leak around the abestos jointing was believed to be due to either too much or not enough tightening of the high tensile steel screws. In fact, after tightening the screws to the required torque of 54 N-m (40 ft-lb) (See Appendix V) no leakage was observed.

After alterations following the preliminary tests described earlier in this chapter, the pressure cell looked as shown in Fig.5.16. The overall view of the apparatus is shown in Figs.5.28 and 5.29.

5.3.2 Casting and Test Procedure

5.3.2.1 Preparation of Barrel of Pressure Cell

After each test the specimen was forced out of the barrel using mechanical loading in a compression testing machine.

A jet of water was then applied to the interior of the barrel which was subsequently cleaned with a wire brush.

The interior and exterior surfaces were then greased to prevent corrosion.

The day before casting, the grease was removed using carbon tetrachloride, and a 12mm thick steel plate, referred to as the blank end plate, was

FIG. 5.30 SPECIMEN AFTER CASTING

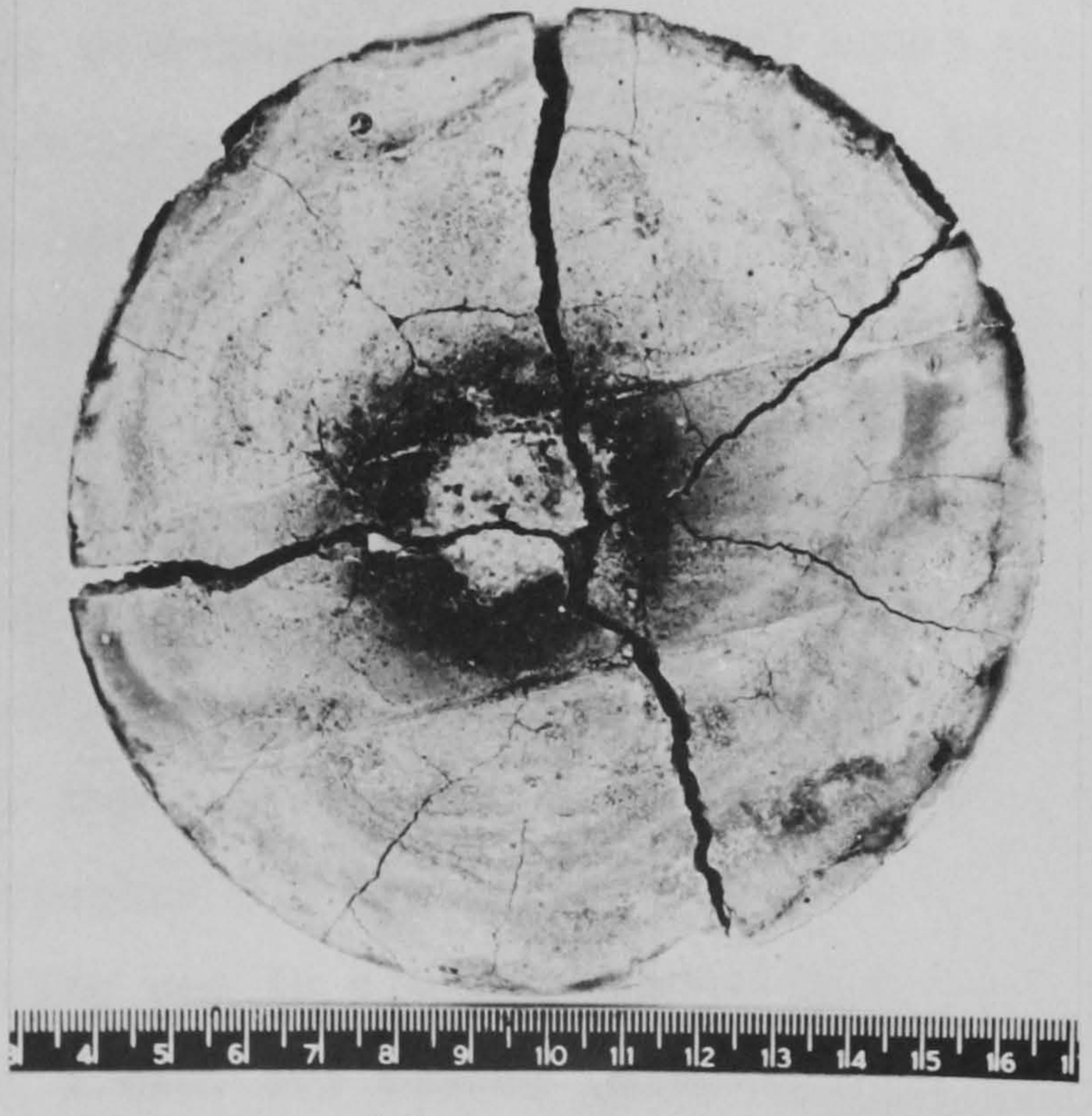

FIG. 5. 33 25mm SPECIMEN AFTER TEST

connected to the barrel using 12·7mm (1/2in) steel screws, to provide a base during casting. The interior surface of the blank end plate was then greased to prevent a bond forming between the specimen and the plate. The thermocouples were fixed in position and wrapped by a thin aluminium foil to prevent bonding to the specimen. Wrapping up the thermocouples was necessary because initial tests showed that it was impossible to extract the thermocouples after the completion of the test if the bond of the thermocouples to the specimen was allowed to develop.

5.3.2.2 Casting

On the day of casting, the barrel with the end plate (Fig.5.30) was clamped to a vibrating table, together with three, 101·6mm (4in) cubes and six 11·2mm diameter, 30·5mm high cylinders for use as control specimens.

Mortar with a mix ratio of 1 cement + 1·5 sand + 0·45 water (or 0·40) was used throughout.

The aggregate was bin dried 4·76mm (3/16 in) down to 0·5mm (2/100 in) sand passing number 7 sieve but retained at number 100 sieve. (See Appendix VI)

All the cement used was from a single batch. (See Appendix VII for properties of the cement)

Mixing was in a 0·14m^3 capacity double rotating mixer; 1 min. dry mixing followed by 5 min. wet mixing during which water was added gradually.

1 BARREL
2 WATER
3 POLYETYLENE SHEET
4 METAL BRACELET
5 THERMOCOUPLE PROBE
6 BLANK END PLATE

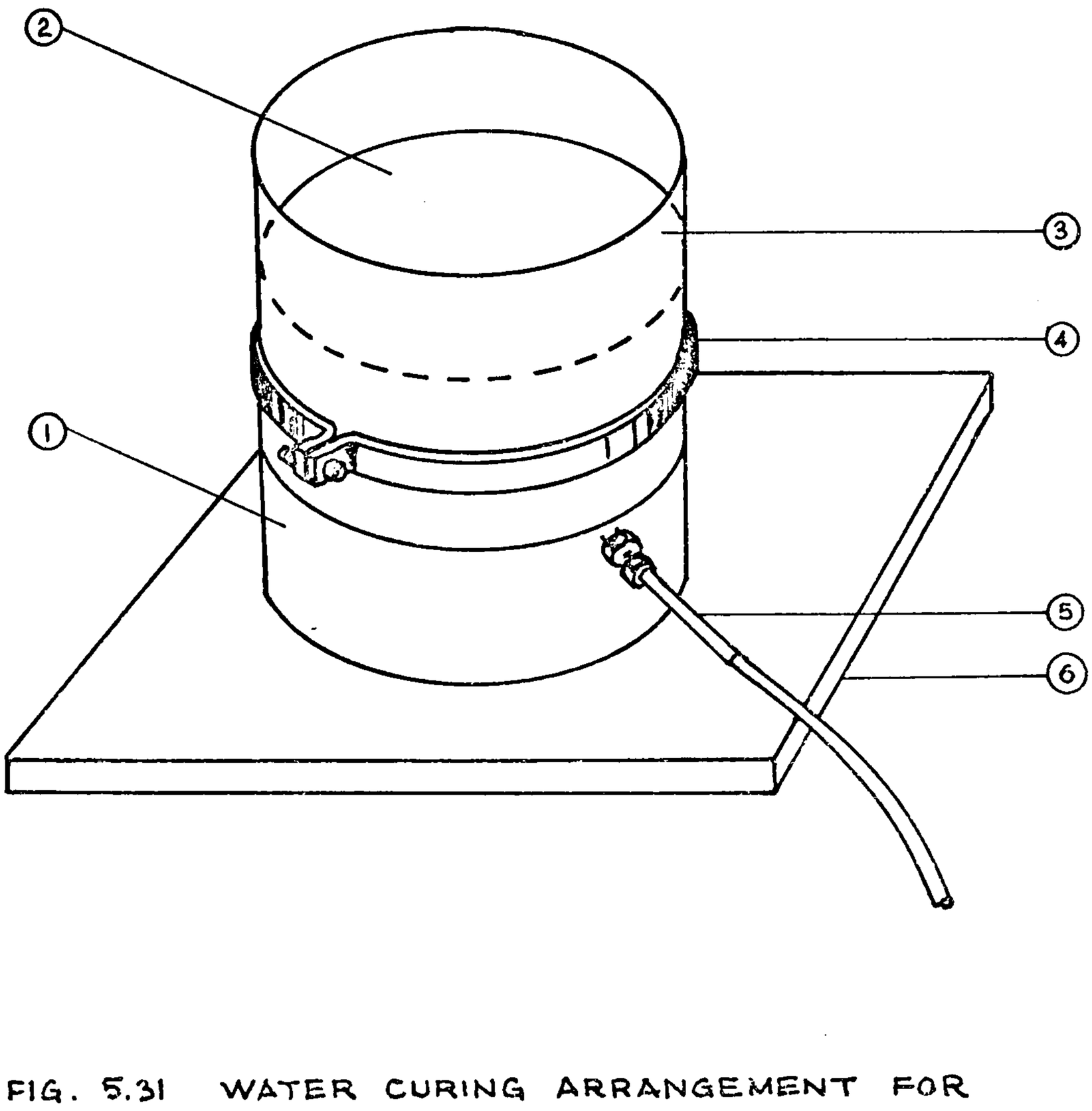

FIG. 5.31 WATER CURING ARRANGEMENT FOR PORE PRESSURE TEST SPECIMEN

The mix was placed in 3 layers with one minute vibration after each layer. After the top layer had been compacted, the surface was finished level to the top of the barrel by means of a trowel.

5.3.2.3 Curing

Three hours after casting, the test and control specimens were taken to the curing room kept at approximately 21°C and at 94% relative humidity. The control specimens were, demoulded 24 hrs. after casting. The test specimen itself was either left for moist curing or water curing using the arrangement shown in Fig.5.31.

This consisted of a thick polyethylene sheet fixed around the barrel using a metal bracelet. Water was then poured in this basin to completely cover the specimen up to about 20mm depth. Waterproofing was provided with plasticene strip placed between the barrel and the cylindrical polyet ylene sheat, directly under the bracelet.

Pore Pressure Tests

Pore pressure tests consisted of exposing one face of the specimen to heating while measuring the increase in pressure and temperature at some distance from the surface, inside the specimen.

The test procedure was as follows:

1. The central hole of the heat exchanger was filled with water in order to prevent the loss of water from the specimen to the heat

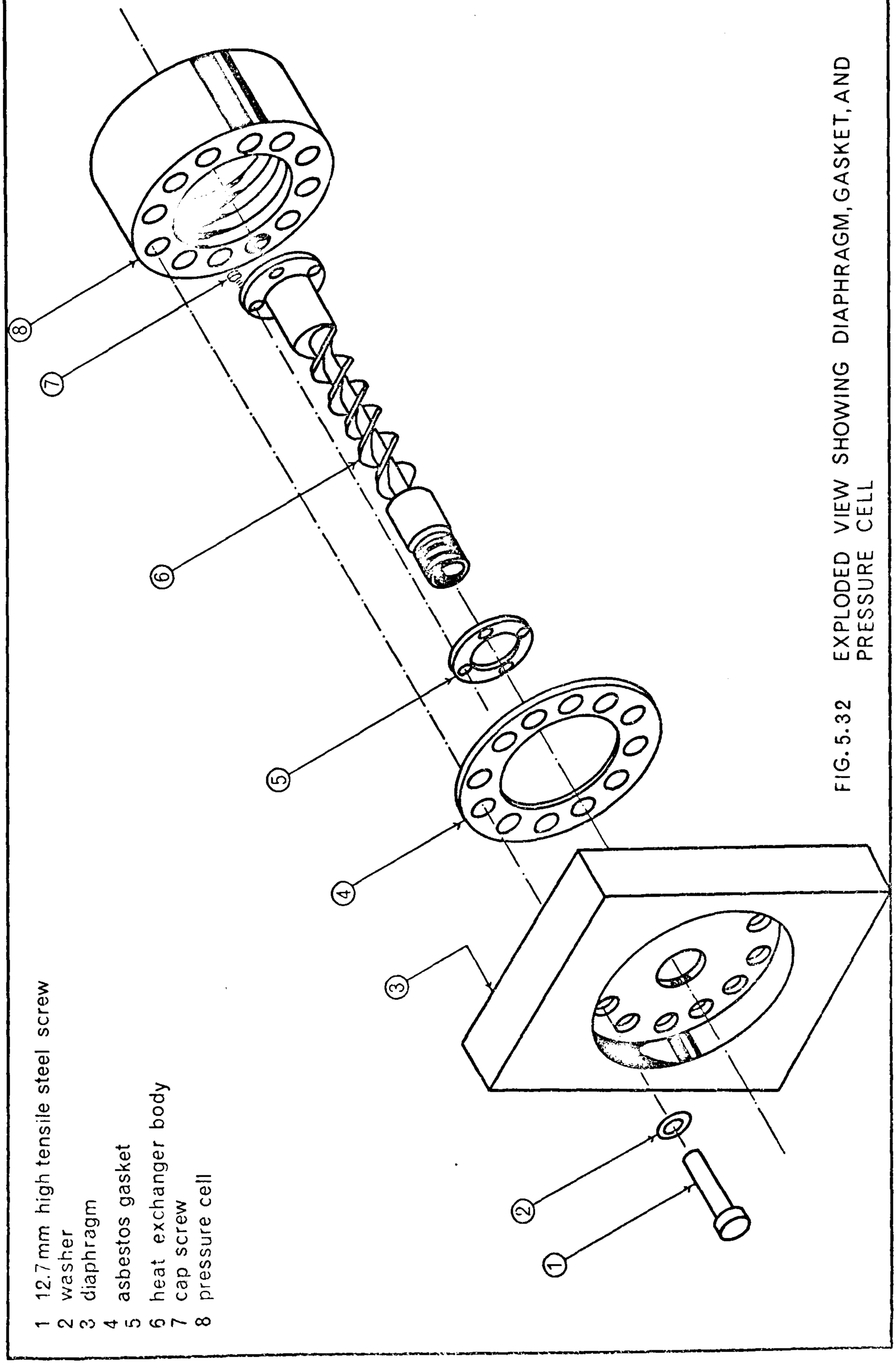

FIG. 5.32 EXPLODED VIEW SHOWING DIAPHRAGM, GASKET, AND PRESSURE CELL

exchanger.

2. The end plate was disconnected from the barrel and replaced with the diaphragm. (Fig.5.32) Sealing between the two parts was provided by an asbestos gasket. (Figs. 5.9 and 5.11)

3. The twelve high tensile screws were tightened by applying a torque of 54 N-m to each one of them.

4. The thermocouples were connected to the temperature recorder.

5. The input of the pressure transducer was connected to the 'constant volt supplier' and the output to the X-2Y plotter.

6. The inlet to the cooling jacket was connected to the water supply source and a continuous flow of 0·5 l/min was allowed to circulate through the heat exchanger.

7. Insulation all round except for the face to be heated was arranged using refractory bricks. (Fig.5.22)

8. Heating system was started, oxyacethylene torch fixed to a stand, and heat was applied to the face of the specimen as shown in Fig.5.22.

Part II: Tests and Results

In order to avoid confusion each test has been given an individual reference number preceded by either

Table 5.2 Pore pressure test results. Series BI.

Ref. no.	Age days	Curing type	Compressive strength MN/m^2	Tensile strength MN/m^2	W/C	Depth of specimen mm	Period of heat application min.	Max. recorded pressure KN/m^2	Time to max. pressure min.	Remarks
B_{I2I}	28	2	38.80	2.80	.45	40	I00	40	I63	no spalling
B_{I3I}	28	I	4I.66	3.93	.45	55	I20	43	345	no spalling
B_{I4I}	28	4	37.I0	2.85	.45	70	I33	I33	2I00	no spalling
B_{I5I}	28	3	4I.00	3.95	.45	85	-	-	-	spalling

Table 5.3 Pore pressure test results. Series B2.

Reference no	B_{2II}	B_{22I}	B_{23I}	B_{24I}
Age, days	I4	90	42	90
Curing type	I	I	2	2
Compressive strength $MN/_m^2$	39.0	44.36	38.8I	42.62
Tensile strength $MN/_m^2$	2.95	3.33	3.75	2.89
W/C	.45	.45	.45	.45
Depth of specimen mm	25	25	25	25
Period of heating min.	50	60	40	46
Time to max. pressure min.	42	50	22	34
Max. recorded pressure $KN/_m^2$	200	260	675	739
Remarks	no spalling	"	"	"

Table 5.4 Pore pressure test results. Series B3.

Reference no	B_{33I}	B_{34I}
Age, days	88	28
Curing type	I	5
Compressive strength $MN/_m^2$	46.0I	44.20
Tensile strength $MN/_m^2$	3.62	3.45
W/C	.45	.45
Depth of specimen mm	70	55
Period of heating min.	I20	90
Time to max. pressure min.	II5	70
Max. recorded pressure $KN/_m^2$	92	4I5
Remarks	no spalling	"

Table 5.I Various Curing Types Used in Pore Pressure and Break-Out Tests

Type I	Moist curing in curing room (R.H.95%)
Type 2	Water curing for 7 days followed by moist curing. Specimens kept in the lab for the last two days before testting.
Type 3	Water curing for 7 days followed by moist curing for 7 days. Specimens kept in the lab for the last I4 days before test.
Type 4,5	Same as 3, except the surface of the specimen is occasionally wetted to prevent sudden drying.

'A' or 'B' corresponding to break-out or pore pressure tests respectively.

In this chapter the tests were devided into B and BB series according to the water/cement ratios of the specimens.

In B series water/cement ratio was kept at 0·45 and the specimens were more permeable than the ones in BB series where the water/cement ratio was 0·40.

Each of the B and BB series were furthermore devided in 3 subseries, namely: B_1, B_2, B_3 and BB_1, BB_2, BB_3.

Series B_1 was initially planned to investigate the effect of depth of specimen on the maximum pressure obtained. The age of the specimens tested were therefore kept at 28 days.

Different types of curing as summarized in Table 5.I were also investigated. The results of this series of tests are presented in Table 5.2.

In Chapter 3 it is pointed out that permeability of concrete is perhaps much more important than the moisture content in causing spalling of concrete. Permeability, however, is very much affected by the age of the specimen and the curing method.

It was therefore decided that the effect of age and curing method on the generation of pore pressures would also be investigated, and, as a result, test series $B_2$and B_3 were planned. The results of these tests are tabulated in Tables 5.3 and 5.4.

Table 5.5 Pore pressure test results. Series BBI,BB2,and BB3.

Reference no.	Age days	Curing type	Compressive strength MN/m^2	Tensile strength MN/m^2	W/C	Depth of specimen mm	Period of heat min.	Time to max. pressure min.	Max. recorded pressure KN/m^2	Remarks
BB_{III}	56	2	46.20	3.90	.40	25	-	-	-	spalling
BB_{I2I}	56	2	43.60	3.3I	.40	40	-	-	I05	spalling
BB_{I3I}	56	2	44.90	3.85	.40	85	-	-	-	spalling
BB_{I4I}	56	2	47.75	3.II	.40	55	-	-	-	spalling
BB_{23I}	90	2	47.70	3.99	.40	25	-	-	-	spalling
BB_{32I}	66	2	48.88	2.50	.40	70	60	56	770	no spalling
BB_{3II}	56	2	46.70	2.90	.40	85	-	-	-	spalling

As seen in Tables 5.3 and 5.4, the effect of age and curing type seemed to affect the generation of pore pressures substantially. This gave incentive to investigate further the effect of permeability on the pore pressures. Accordingly the series BB was designed, where the specimens had a lower water/cement ratio, higher age at the time of the test, and were all water cured for 7 days, then moist cured, followed by a period of a few days in the laboratory to encourage carbonation. All these factors were believed to reduce the permeability of the specimen and so contribute to higher pore pressures. However, the specimens in this series spalled in the early stages of testing and, as seen in Table 5.5 no appreciable pressures could be recorded.

Discussion and Conclusions

The maximum pressures in most tests lay in the range 350 - 800 KN/m^2, although in one particular case a pressure as high as 2100 KN/m^2 was recorded.

Considering that the measured average tensile strength of the material at room temperature was about 3200 KN/m^2, even the highest pressure recorded in these tests does not seem to be enough to cause failure.

It may be argued that, as the tensile strength of the concrete would be expected to drop with increase in temperature, the maximum pressure recorded could be enough to cause spalling at high temperatures.

In the actual fact,at the point where a pressure of 2.I $MN/_m2$ was obtained,a maximum temperature of approximately 250°C was recorded.However,as pointed out by Saemann and Washa (9.2),at this temperature the tensile strength is reduced only by 25% of the strength at 20°C.

This suggests that the pressures possibly generated in ordinary concrete are, even at high temperatures, not enough, by themselves, to cause failure of the material.

This, however, applies to concrete kept in normal conditions, because, in unusual circumstances such as

the ones in test series BB, failure may occur mainly due to higher pressures developed.

Series B

The qualitative results of the series I tests could be summarized as follows:

1. The maximum pressure obtained seems to be proportional to the depth of the specimen.
2. The deeper the specimen the higher is the pressure.

The first of these two results could in some way be predicted by the theories presented in Chapter 2. In fact, Harmathy's theory (Chapter 3) assumes that the larger is the distance from the interface to the heated surface the larger is the amount of water available for evaporation. Thus, the maximum pressure would be expected to be proportional to the depth of the material.

On the other hand, although adopting a different approach, Meyer-Ottens (5.2) and Zhukov (5.3) predicted that the larger the distance from the interface to the heated surface the larger are the drag forces. If the total drag force directly corresponds to the static pressure as shown in Appendix II then higher pressures could consequently be expected when heating thicker specimens.

Series B2

Summary of Results (Also see Table 5.3)

1. For the same thickness, the older the

specimen the higher is the maximum pressure obtained.

Series BB

Summary of Qualitative Results

1. Spalling was always obtained in specimens cured in water during the first seven days following the casting.

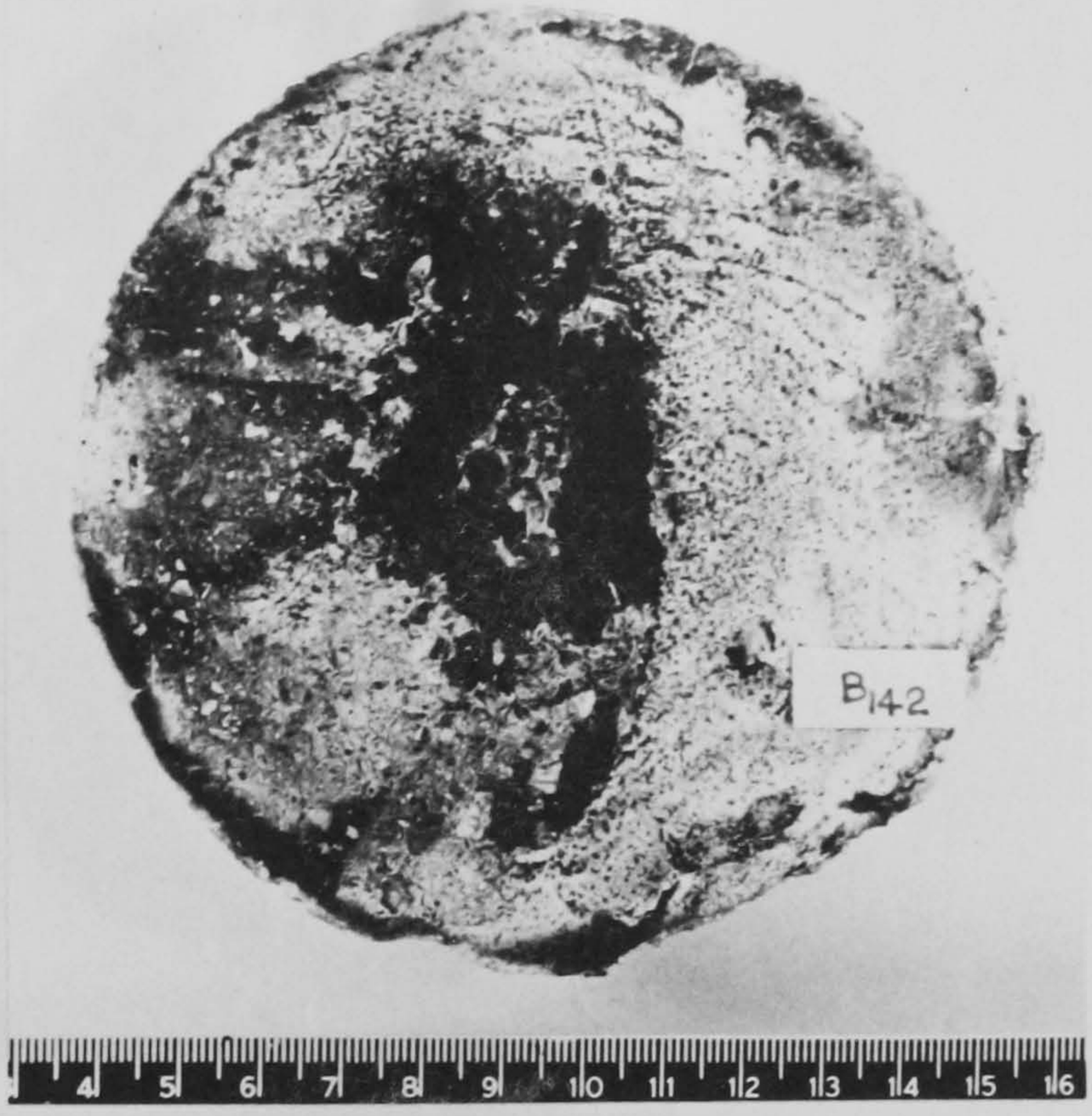

FIG. 5.34 70mm SPECIMEN AFTER TEST

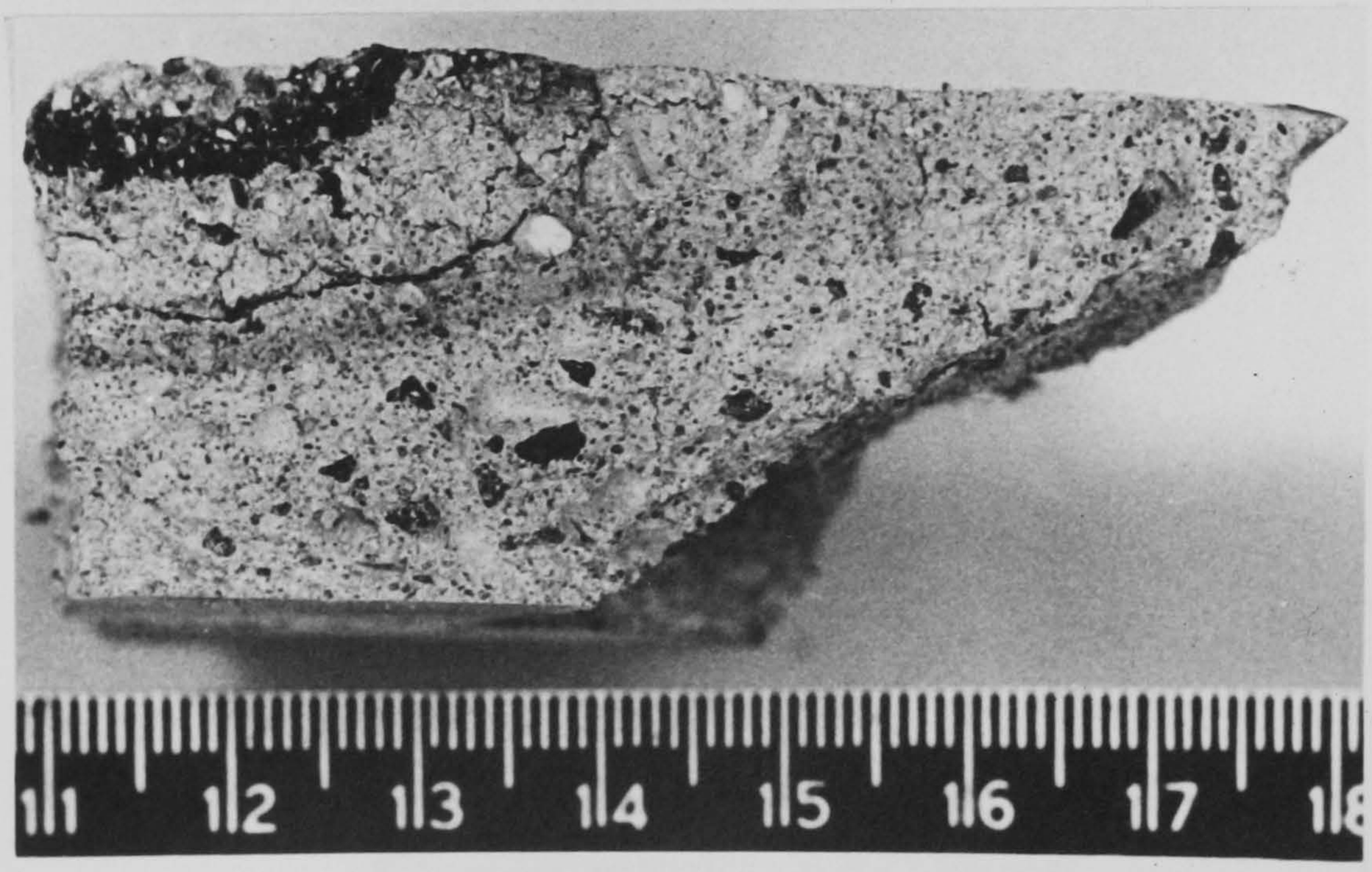

FIG. 5.35 CROSS SECTION OF A 25mm SPECIMEN AFTER TEST

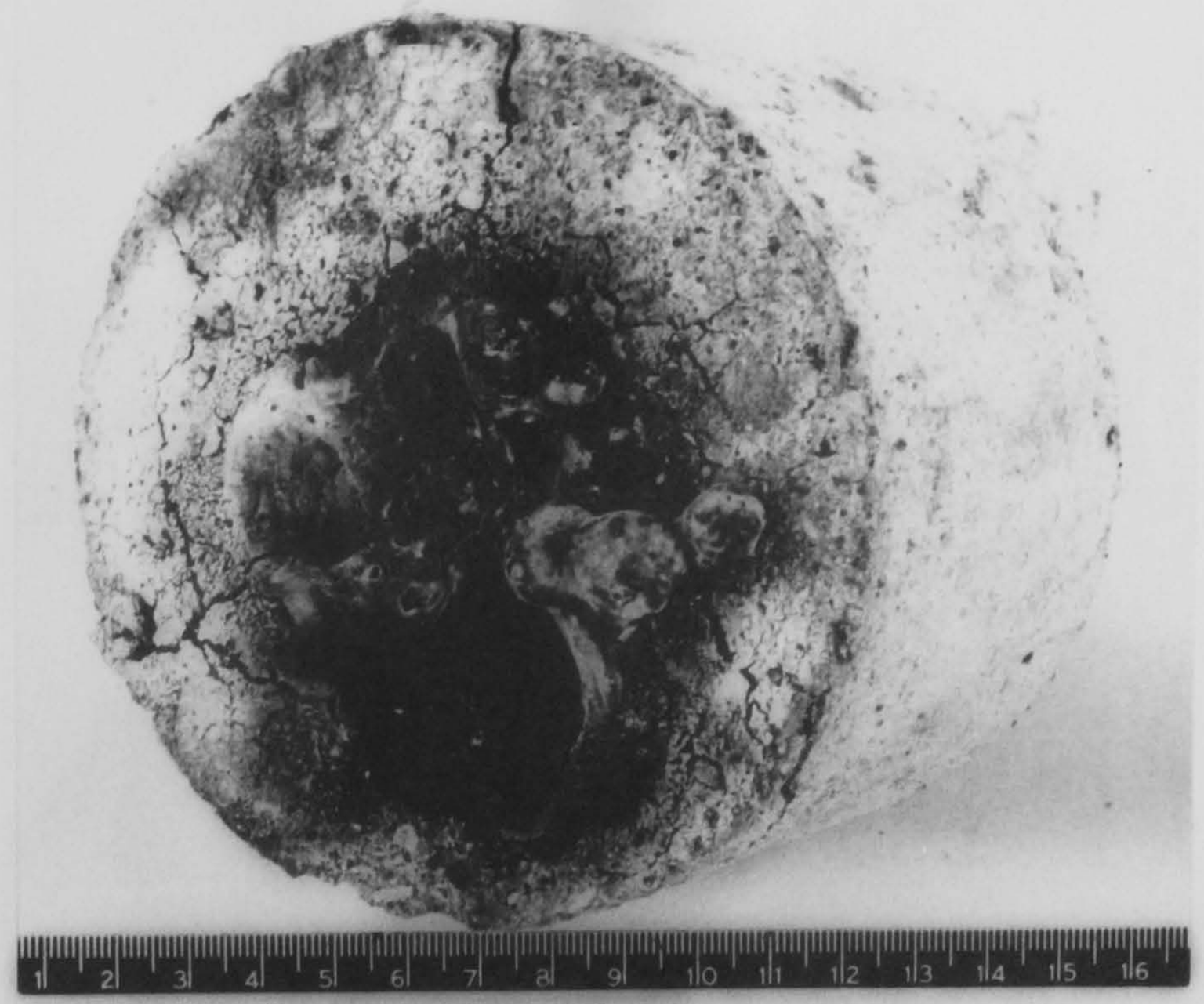

FIGS. 5.36 & 5.37 85mm SPECIMEN AFTER TEST

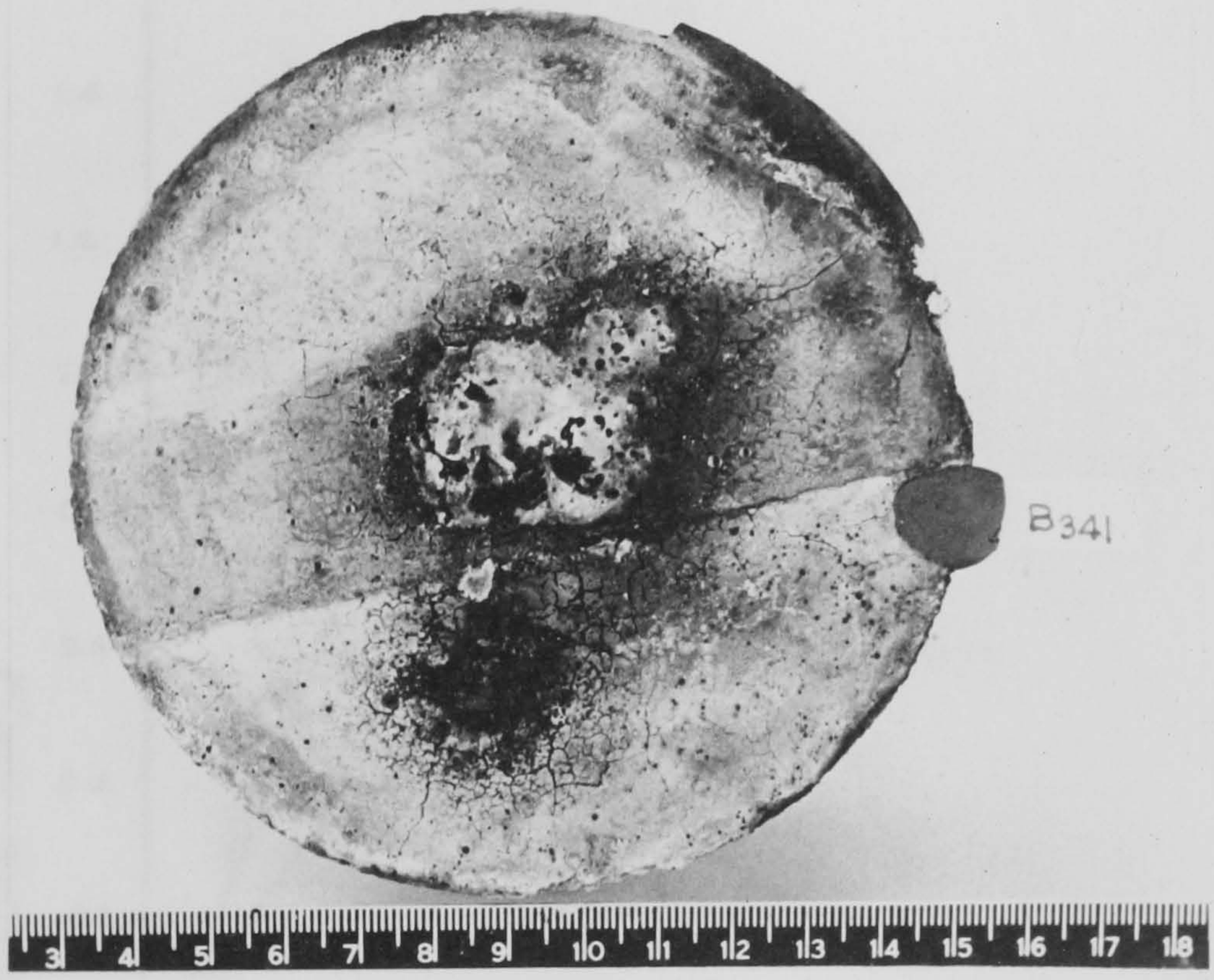

FIG. 5.38 55 mm SPECIMEN AFTER TEST

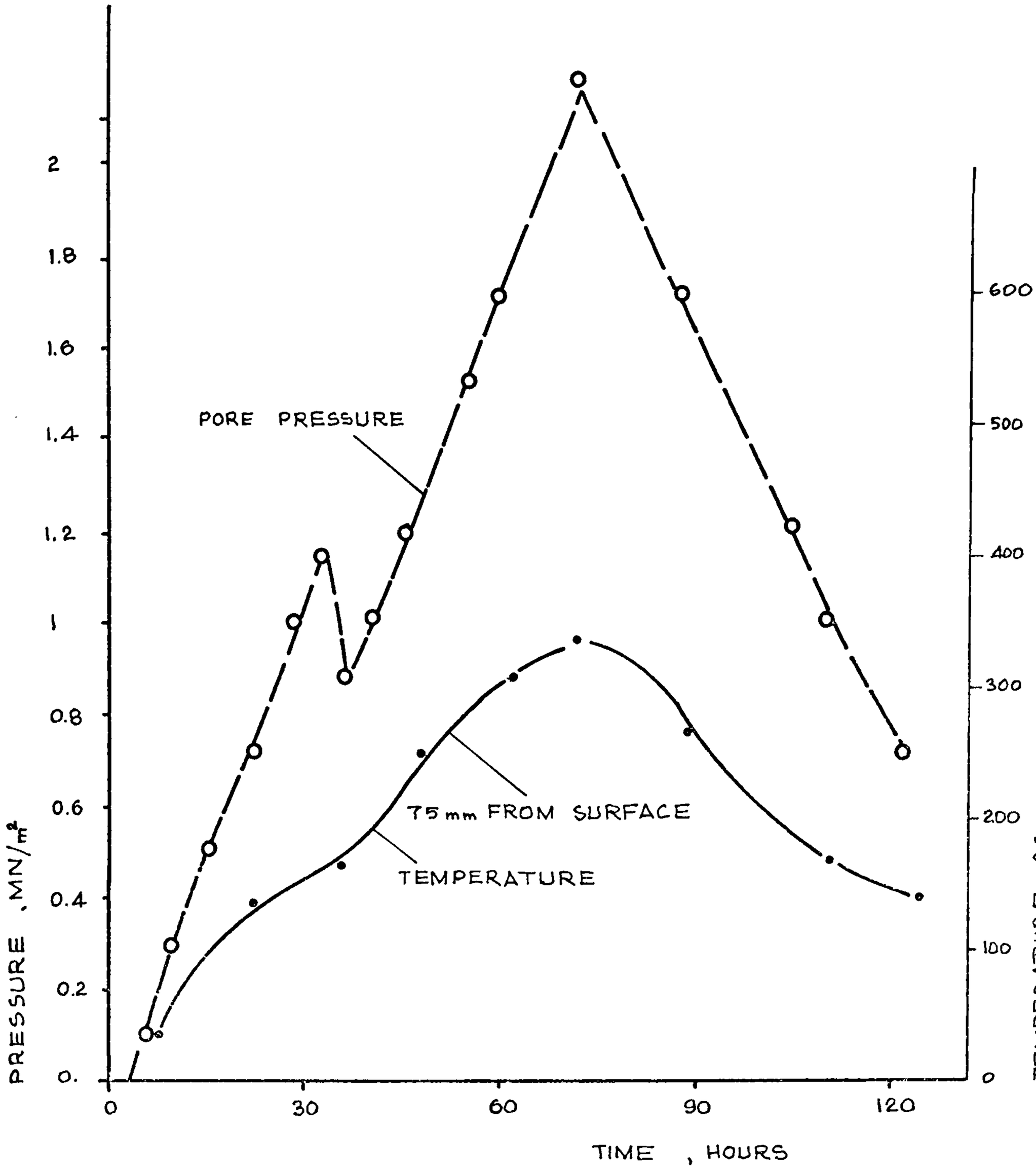

FIG. 5.33 PORE PRESSURE TEST RESULT (B_{141})
DEPTH OF SPECIMEN 85mm.

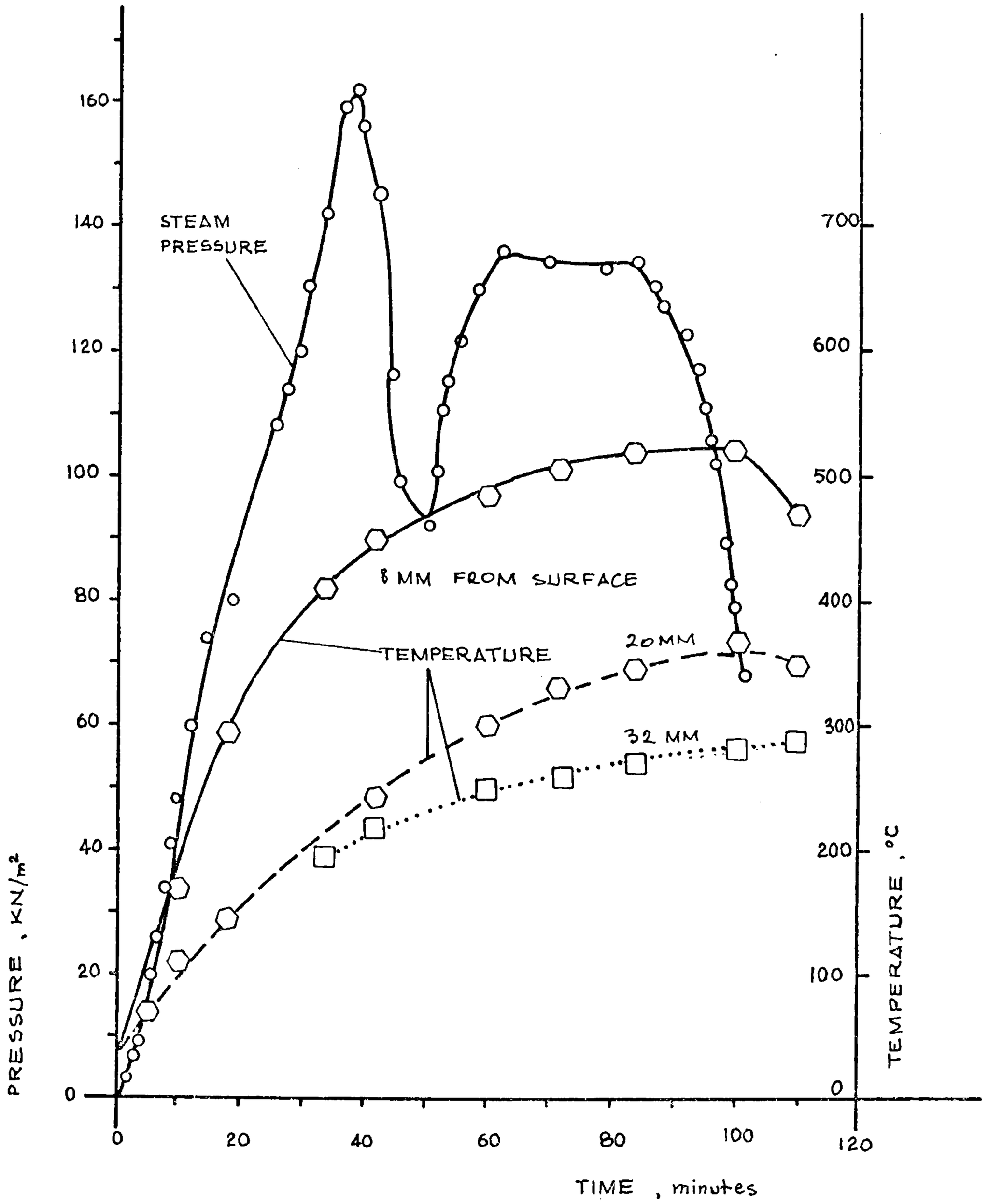

FIG. 5.4.0 PORE PRESSURE TEST RESULT (B_{12I})

DEPTH OF SPECIMEN : 40 MM

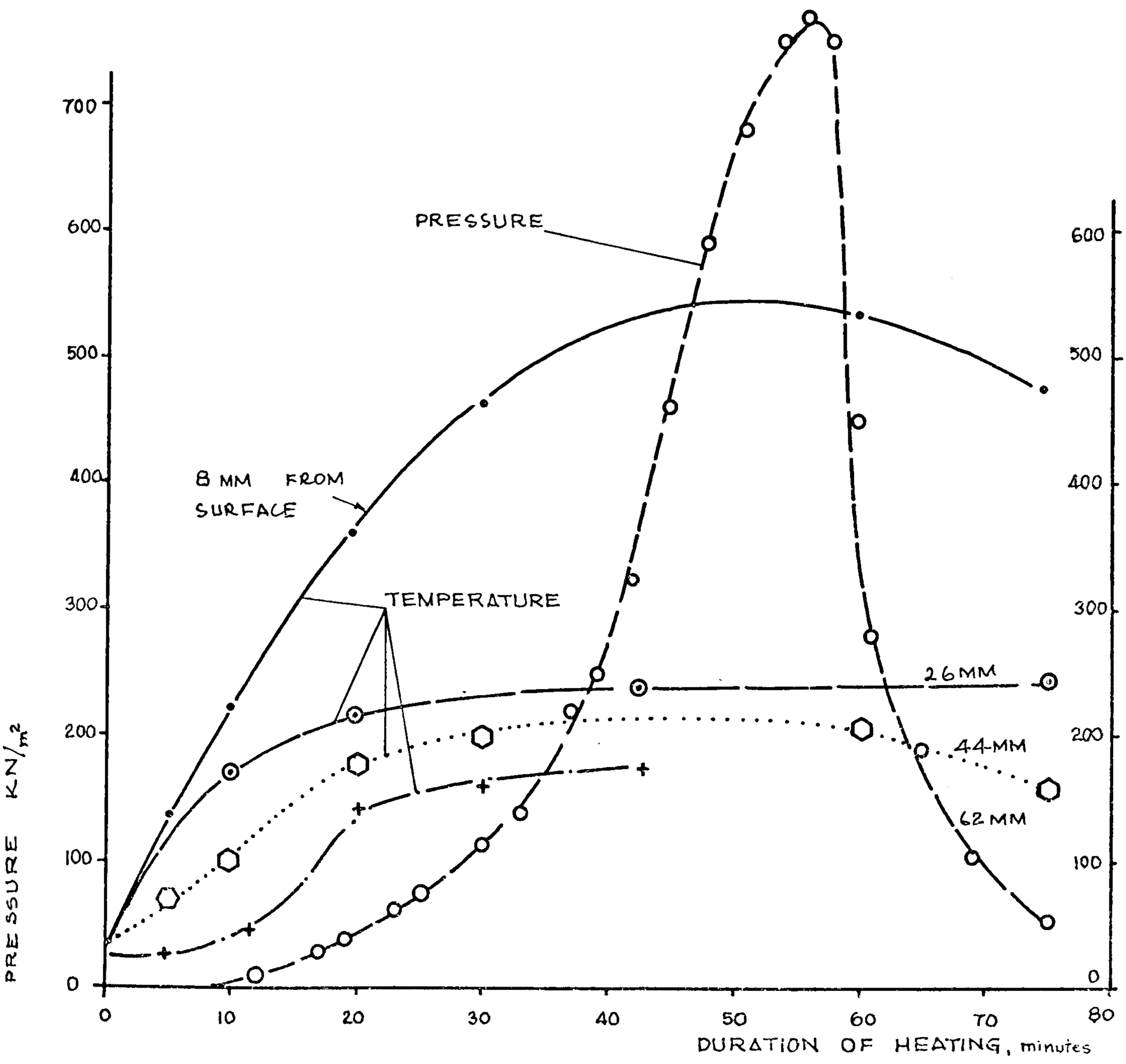

5.41 PORE PRESSURE TEST RESULT (BB_{321})

DEPTH OF SPECIMEN : 70mm

NUMBER OF THERMOCOUPLES : 4

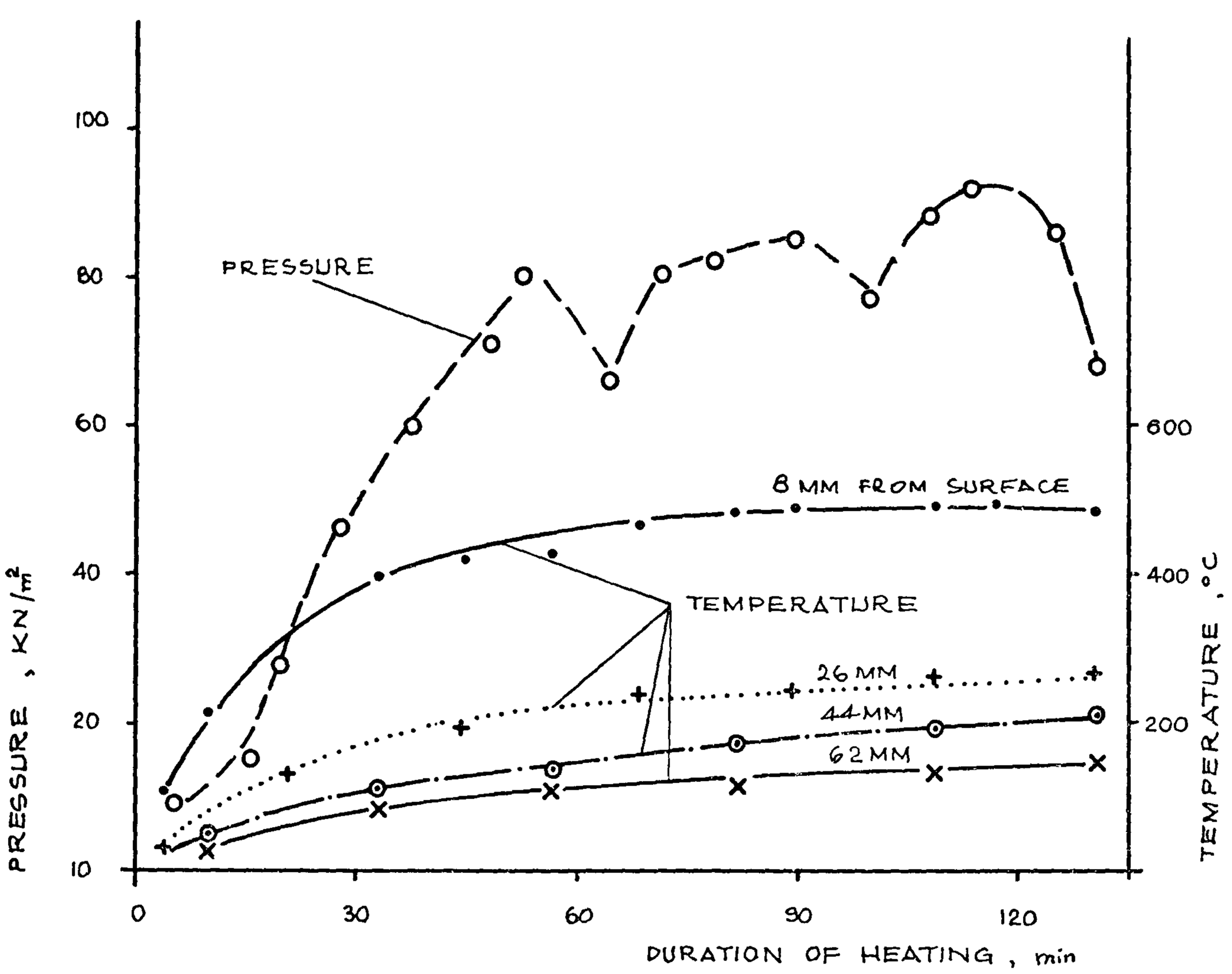

FIG. 5.4-2 PORE PRESSURE TEST RESULT (B_{331})

DEPTH OF SPECIMEN : 70 mm

NUMBER OF THERMOCOUPLES : 4

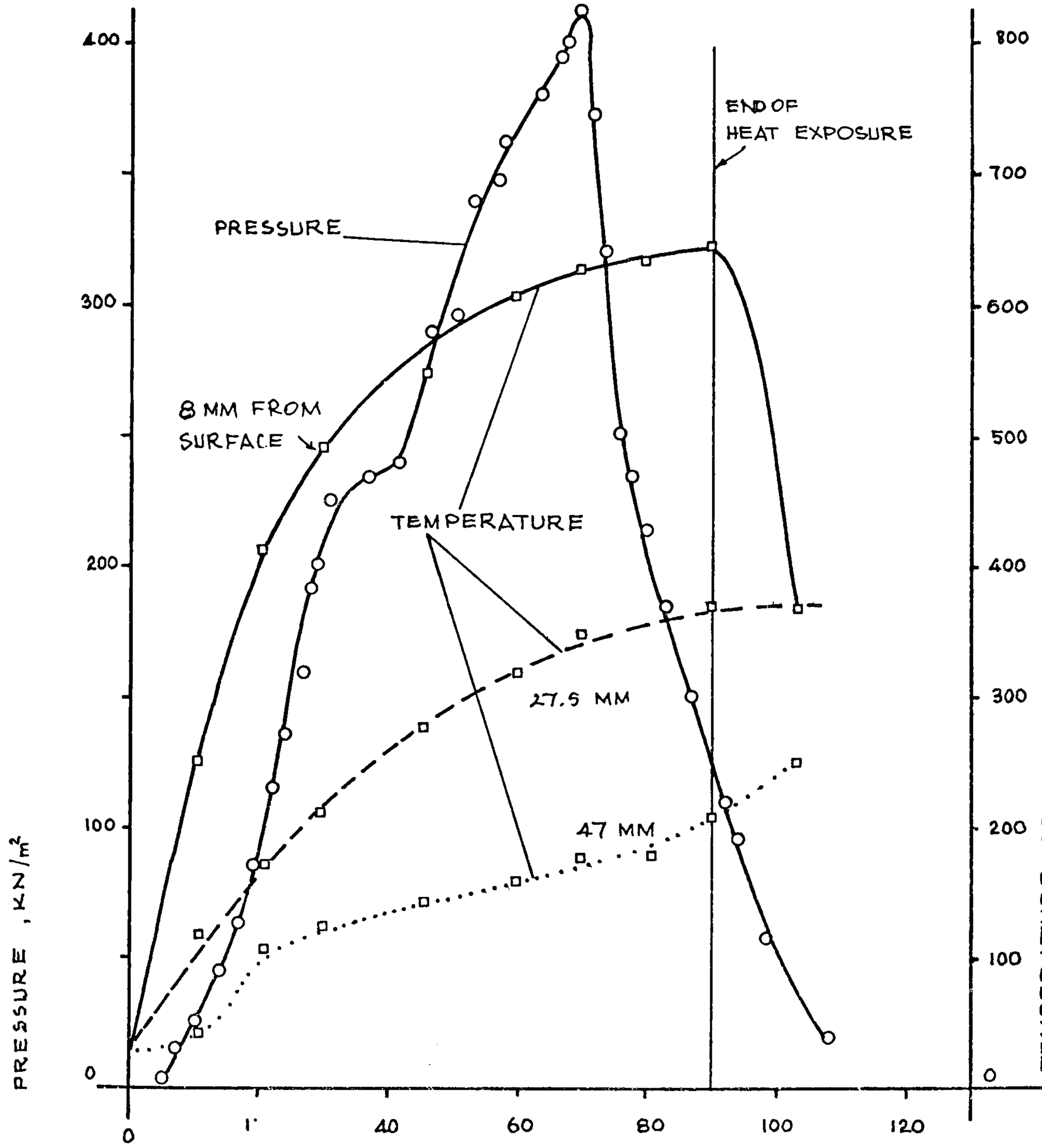

FIG. 5.43 PORE PRESSURE TEST RESULT (B_{341})
DEPTH OF SPECIMEN : 55 mm
NUMBER OF THERMOCOUPLES : 3

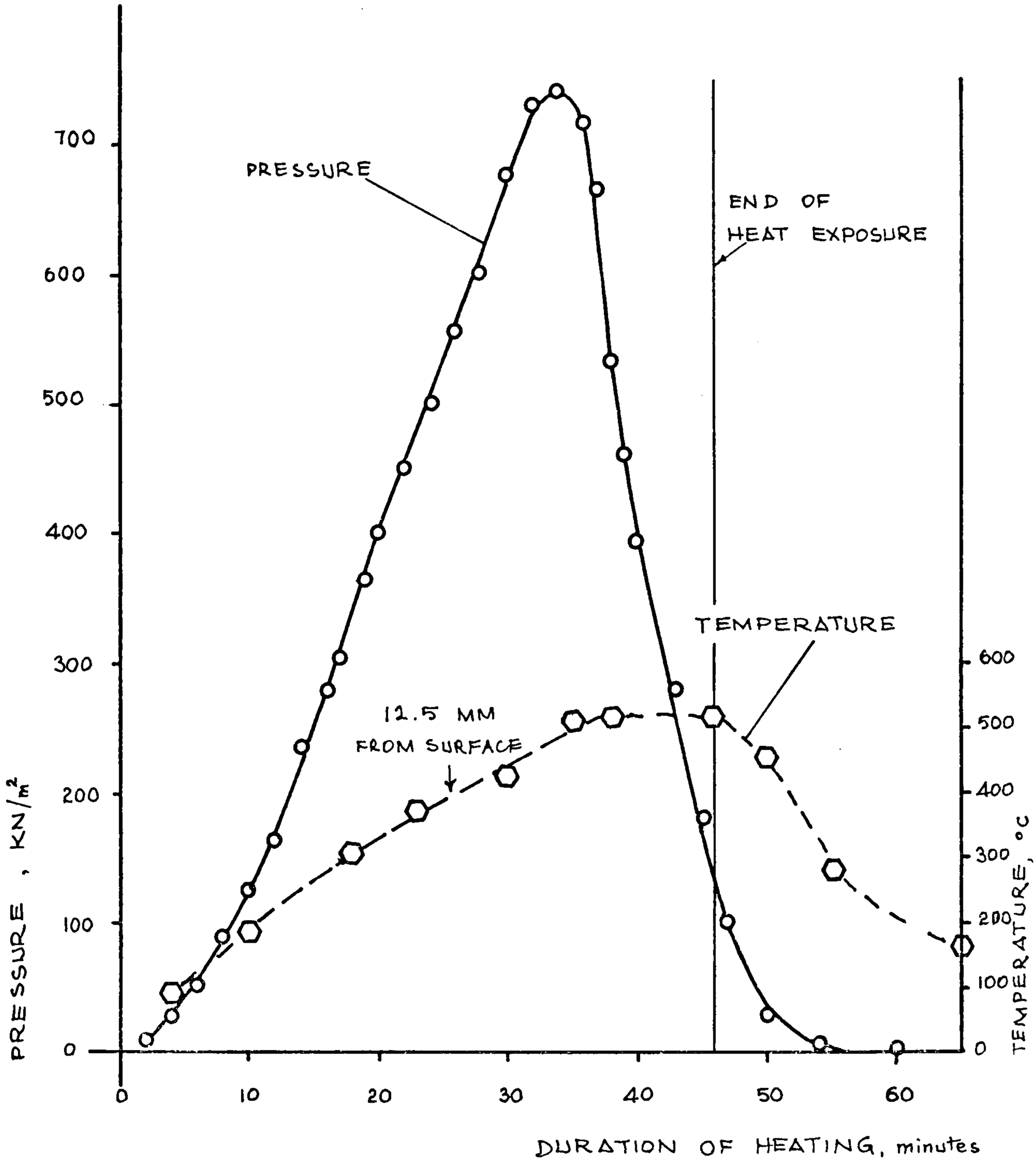

FIG. 5.44 PORE PRESSURE TEST RESULT (B_{241})

DEPTH OF SPECIMEN : 25 MM

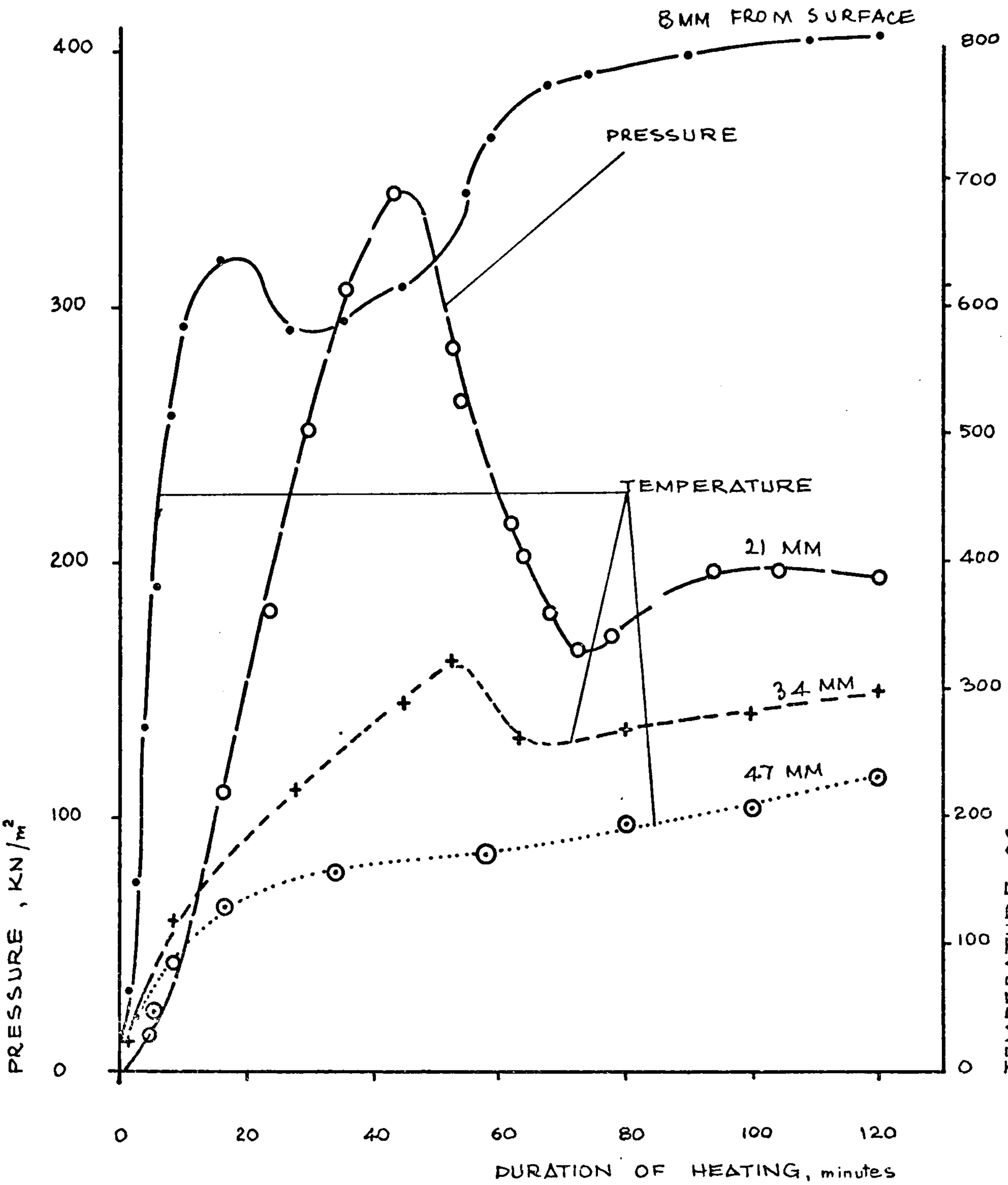

FIG. 5.45 PORE PRESSURE TEST RESULT (B_{131})
DEPTH OF SPECIMEN 55 MM

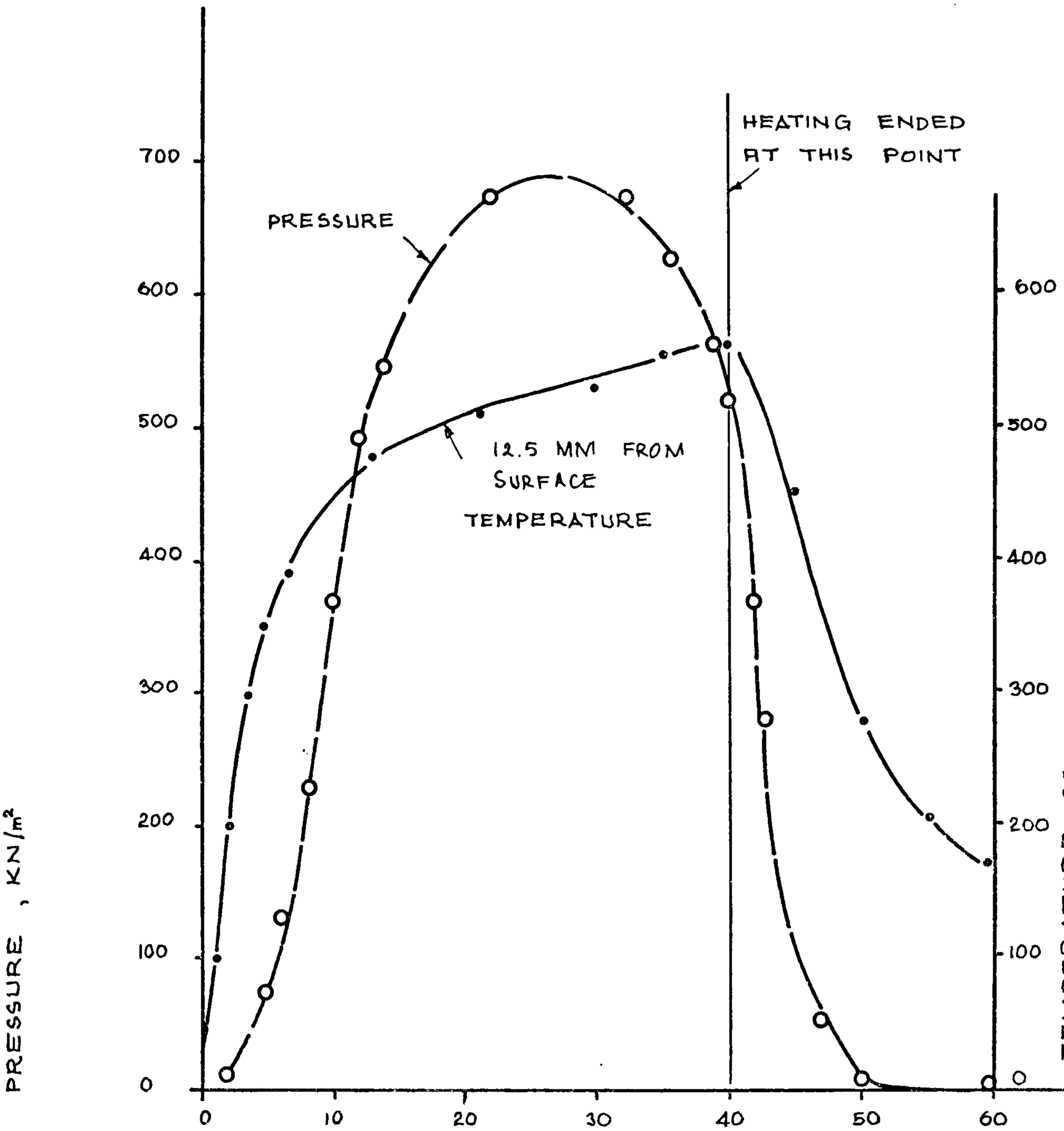

FIG. 5.46 PORE PRESSURE TEST RESULT (B_{231})

DEPTH OF SPECIMEN : 25mm

NUMBER OF THERMOCOUPLES : 1

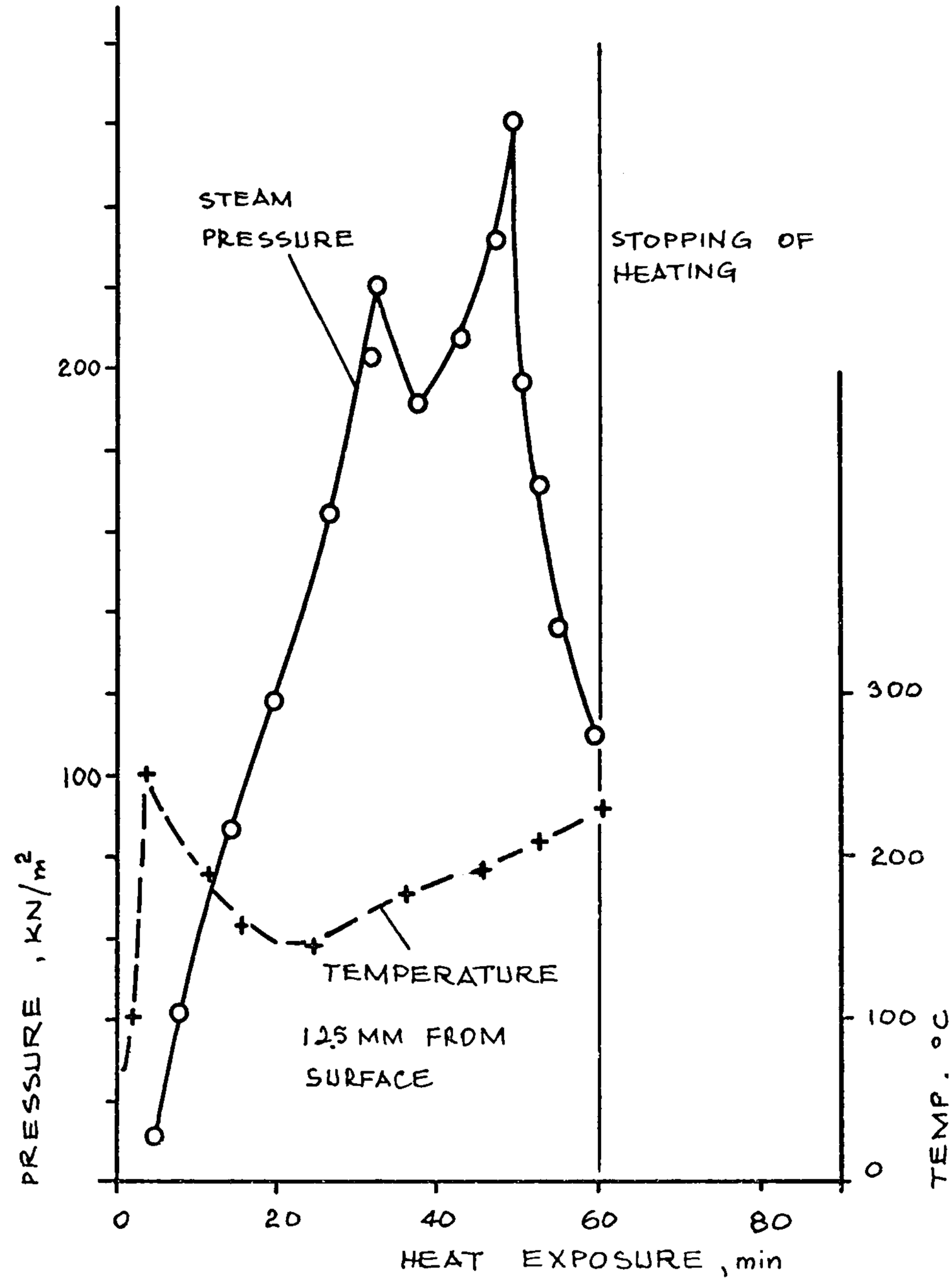

FIG. 5.47 PORE PRESSURE TEST RESULT (B 221)
DEPTH OF SPECIMEN: 25mm
NUMBER OF THERMOCOUPLES: 1

Chapter 6

BREAK-OUT TESTS AT ROOM TEMPERATURE

6.1 Introduction

The mechanism of spalling proposed in Chapter 4 is based on the assumption that, if cracks parallel to the heated face are present, relatively small pressures applied at these cracks are capable of causing failure of the material between the crack and the surface.

In order to assess the validity of this assumption it is necessary to find the pressures necessary to cause failure outside cracks of various sizes, at various distances from the heated surface, and also to measure the pressures actually generated in heated concrete.

The second investigation has been carried out under the name of 'Pore Pressure' tests described in the previous chapter. The first of these investigations will be described in this chapter under the name of 'Break-Out' tests.

These tests basically involved an artificially created crack in a mortar specimen, pressurized internally from an external source.

The theory explained in Chapter 4 assumes that the cracks parallel to the surface are caused by loading in the direction parallel to the surface. However, in the presence of biaxial loading the pressures necessary to cause failure of the material may be substantially different from the pressures necessary to cause failure of the material in the absence of compressive loading. Therefore the failure pressures for each

FIG. 6.1 CYLINDRICAL SPECIMENS AFTER TEST

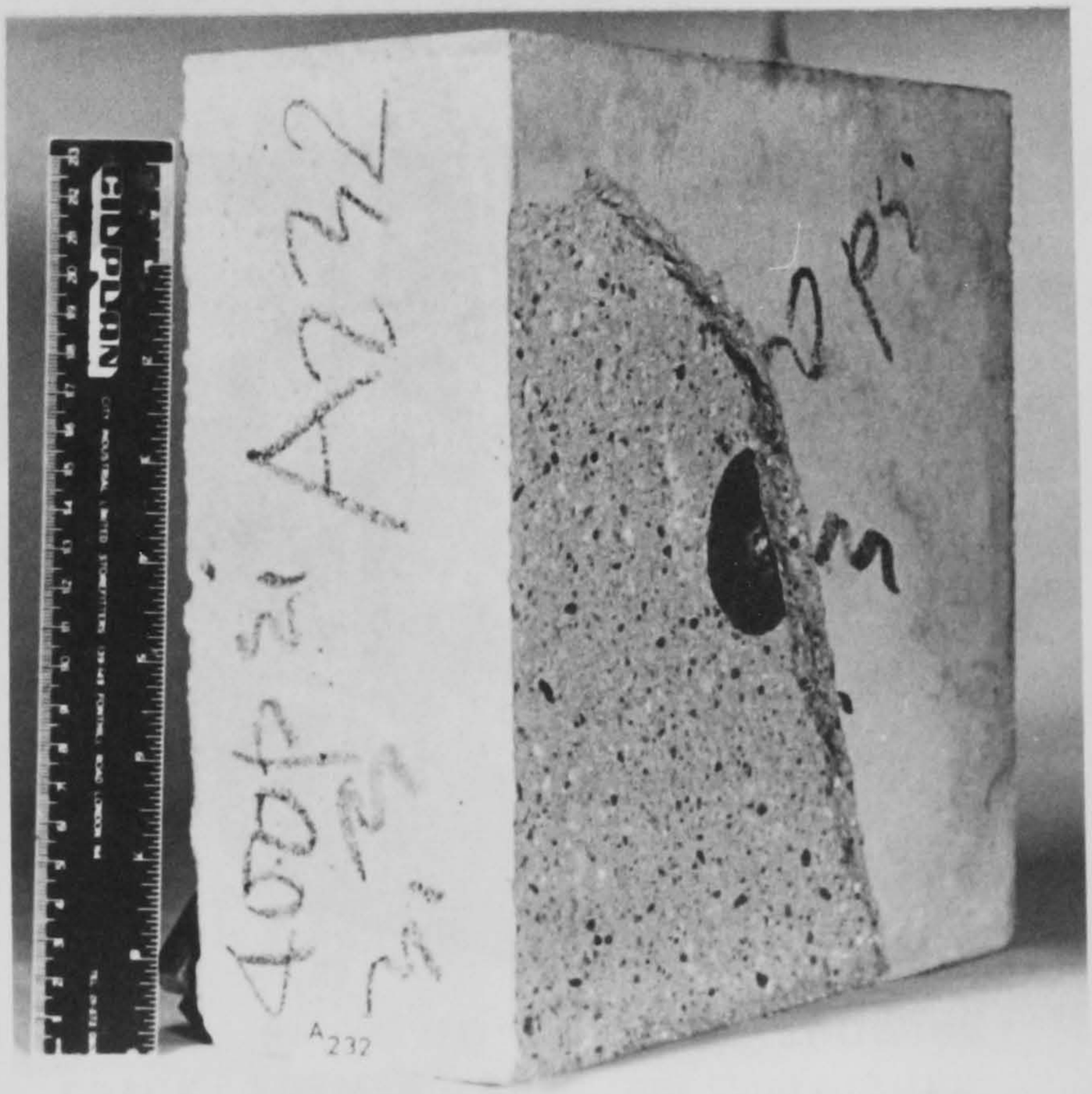

FIG. 6.2 PRISMATIC SPECIMEN AFTER TEST

FIG. 6.3 ARTIFICIAL CRACK FORMER

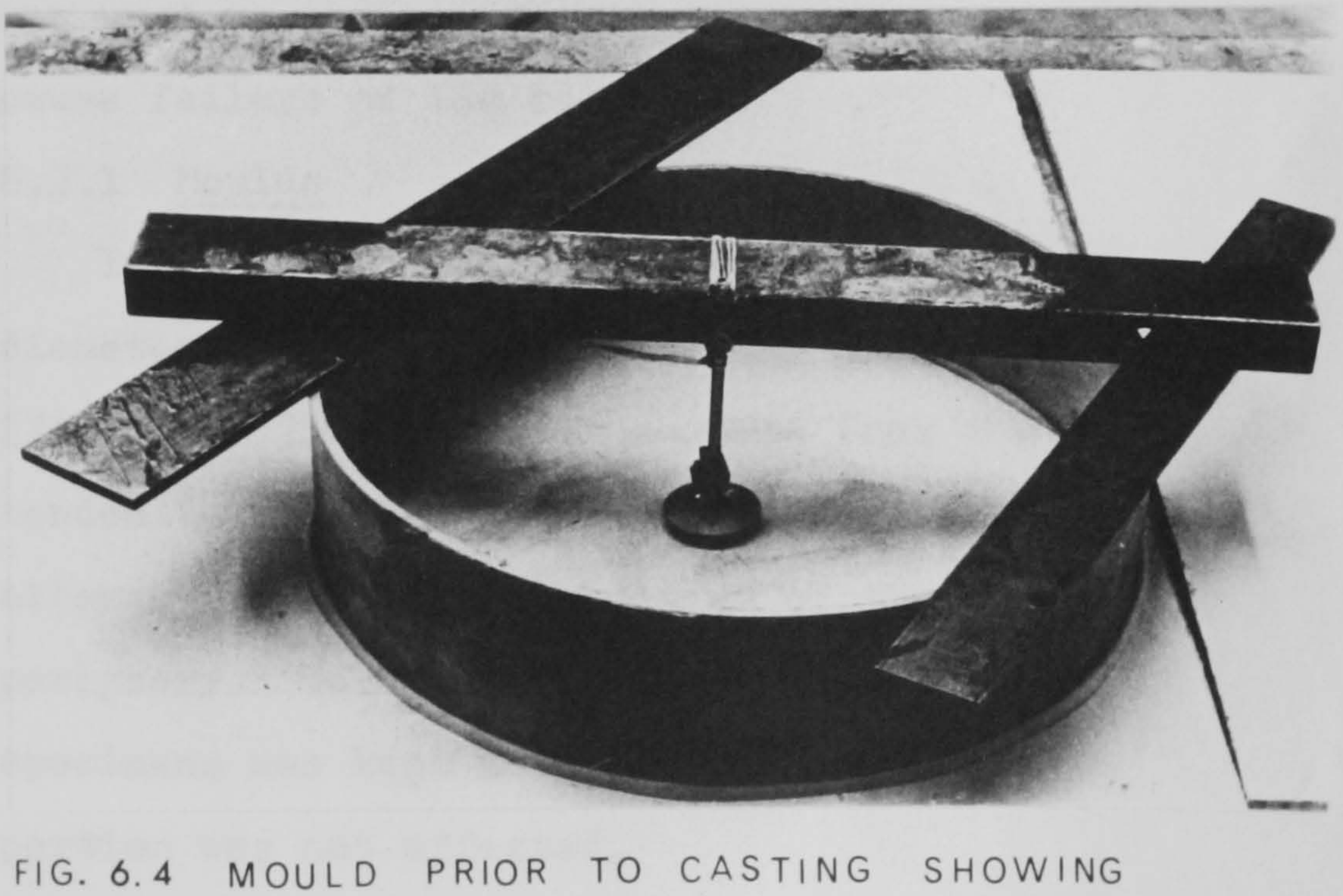

FIG. 6.4 MOULD PRIOR TO CASTING SHOWING CRACK FORMER AND PRESSURE TUBE

crack depth and size should be determined for biaxially loaded specimens as well as specimens without any applied load. Each of these tests will be described in detail in sections 6.5.2 and 6.5.3.

6.2 Specimens

Specimens for the 'Break-Out' test were initially 101·6mm high 419mm diameter mortar cylinders (Fig.6.1) subsequently replaced by 254x254x101·6mm prisms. (Fig.6.2)

In either form they contained a centrally located metal disc (See section 6.2.2) and a copper tubing permanently fixed to it. (Fig.6.3) The disc formed an artificial crack in the specimen and, the tubing was used to apply external pressure to the crack to cause failure of the material.

6.2.1 Moulds

Initially mortar was cast in 101·6mm high 419mm diameter and 10mm wall thickness cardboard rings. (Fig.6.4) They were not removed from the specimen and tended to absorb moisture from the mortar and thus altered the moisture condition of the specimen at the periphery. To minimize this effect the size of the specimens was kept large enough so that the central portion was not affected.

At a later stage specimens to be tested under biaxial compression [+] were cast in, 254x254x102mm mild

Footnote

These tests were done using the biaxial compression machine at Imperial College. (See section 6.5.3)

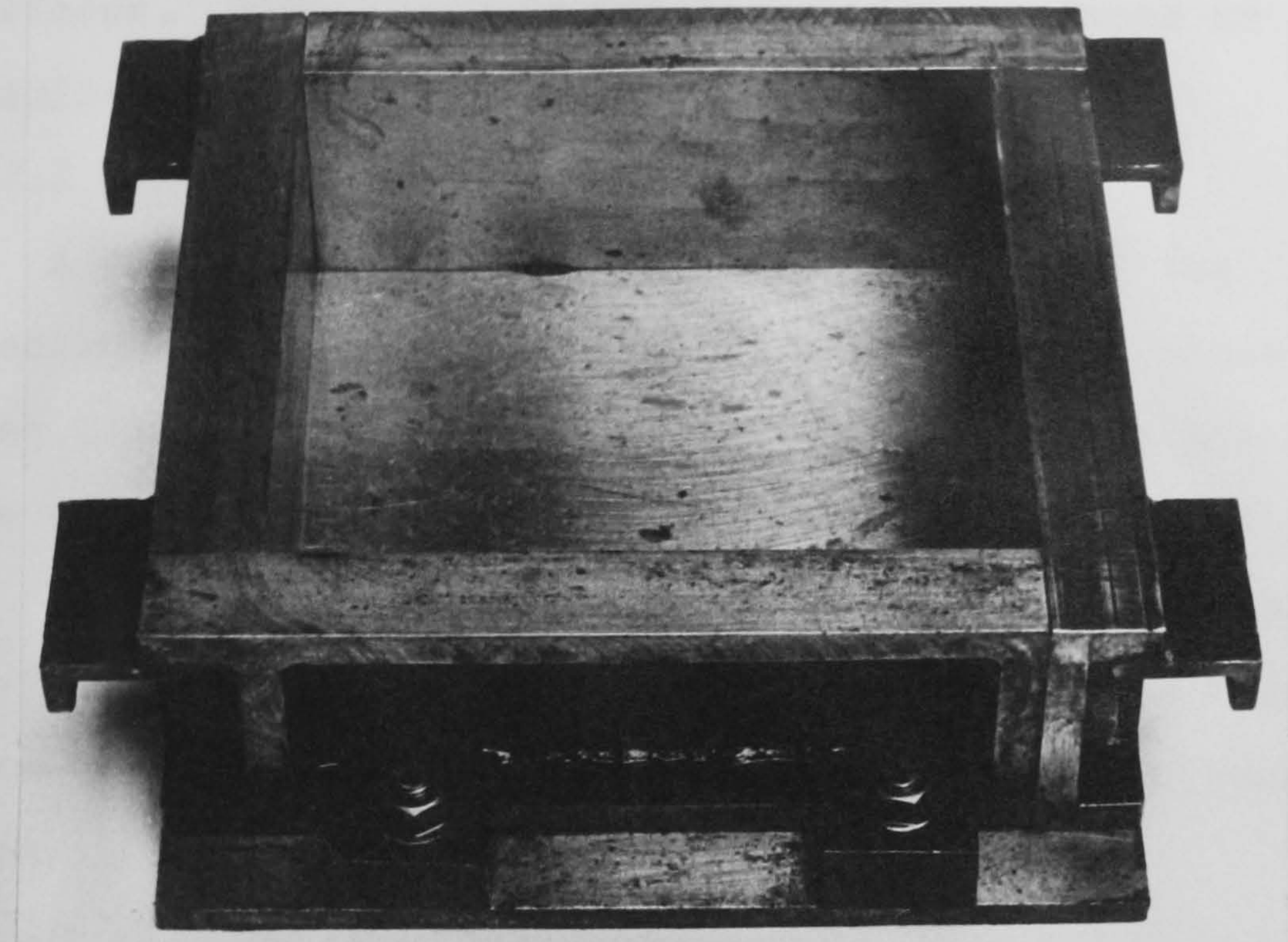

FIG. 6.5 STEEL MOULD

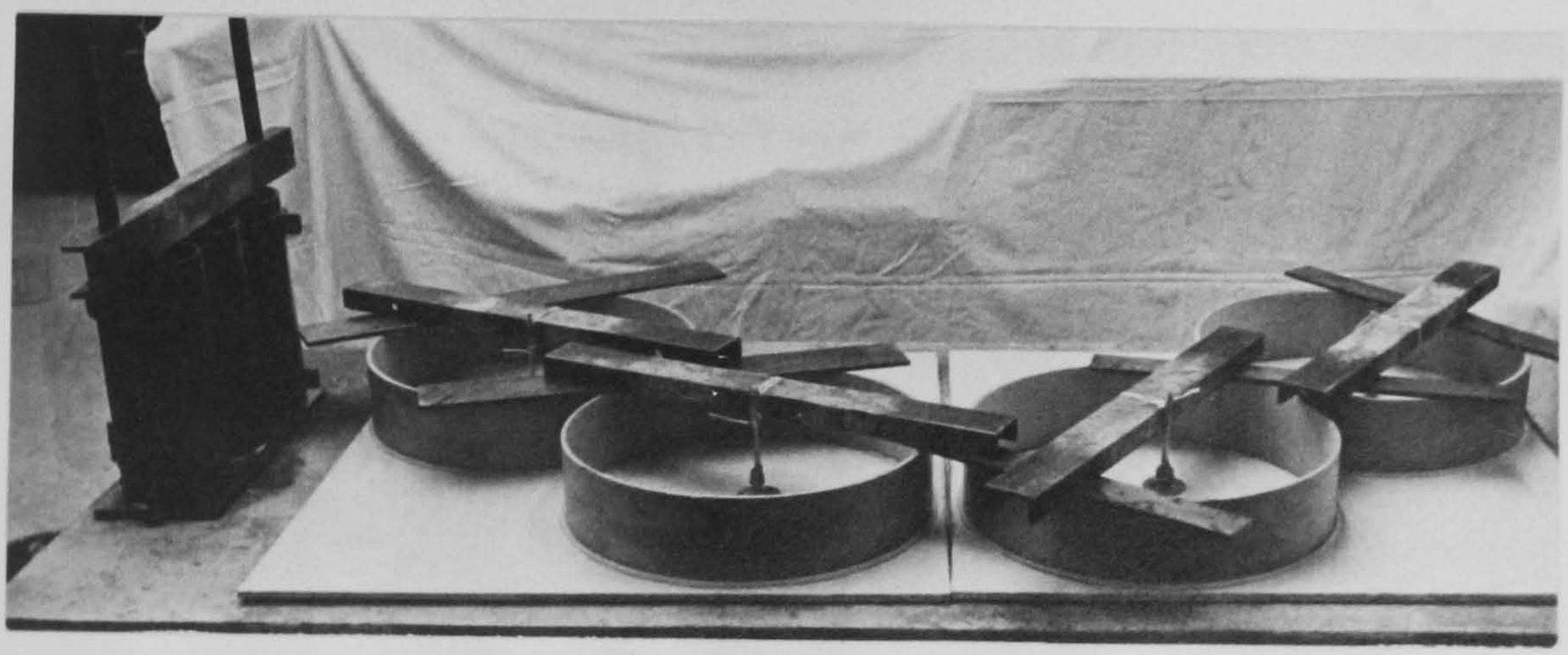

FIG. 6.6 CARDBOARD MOULDS ON VIBRATING TABLE

steel moulds (Fig.6.5) with smoothly polished interior surfaces. This produced specimens with surfaces as required for the biaxial compression tests.

6.2.2 Artificial Cracks

A crack parallel to the largest surface of the specimen was produced by casting a 1·5mm thick brass disc containing a 6·35mm (1/4") central hole to which the end of a copper tube was soldered as shown in Fig.6.3.

Three different sizes of discs, namely: 19·05mm, 31·75mm, and 50·8mm, were used at various depths ranging from 5mm to 25mm. In no test was more than one crack cast in a single specimen.

6.2.3 Casting procedure

In the previous section it was pointed out that, initially, cardboard rings were used as moulds. 12mm thick plywood bases were also provided to form a base for the rings as shown in Fig.6.6. These were previously painted to minimise absorption of moisture and to provide a smooth surface.

The day before casting took place, 4 cardboard rings and their plywood bases were placed on the vibrating table. (Fig.6.6)

The copper tube and brass disc described in the previous section was then fixed on to a metal bar using plastic padding in such a way that the disc stood at the required distance from the base. The bar and the copper tube connected to it were then placed on the cardboard ring as shown in Fig.6.4 and the interior wall and the base was carefully greased.

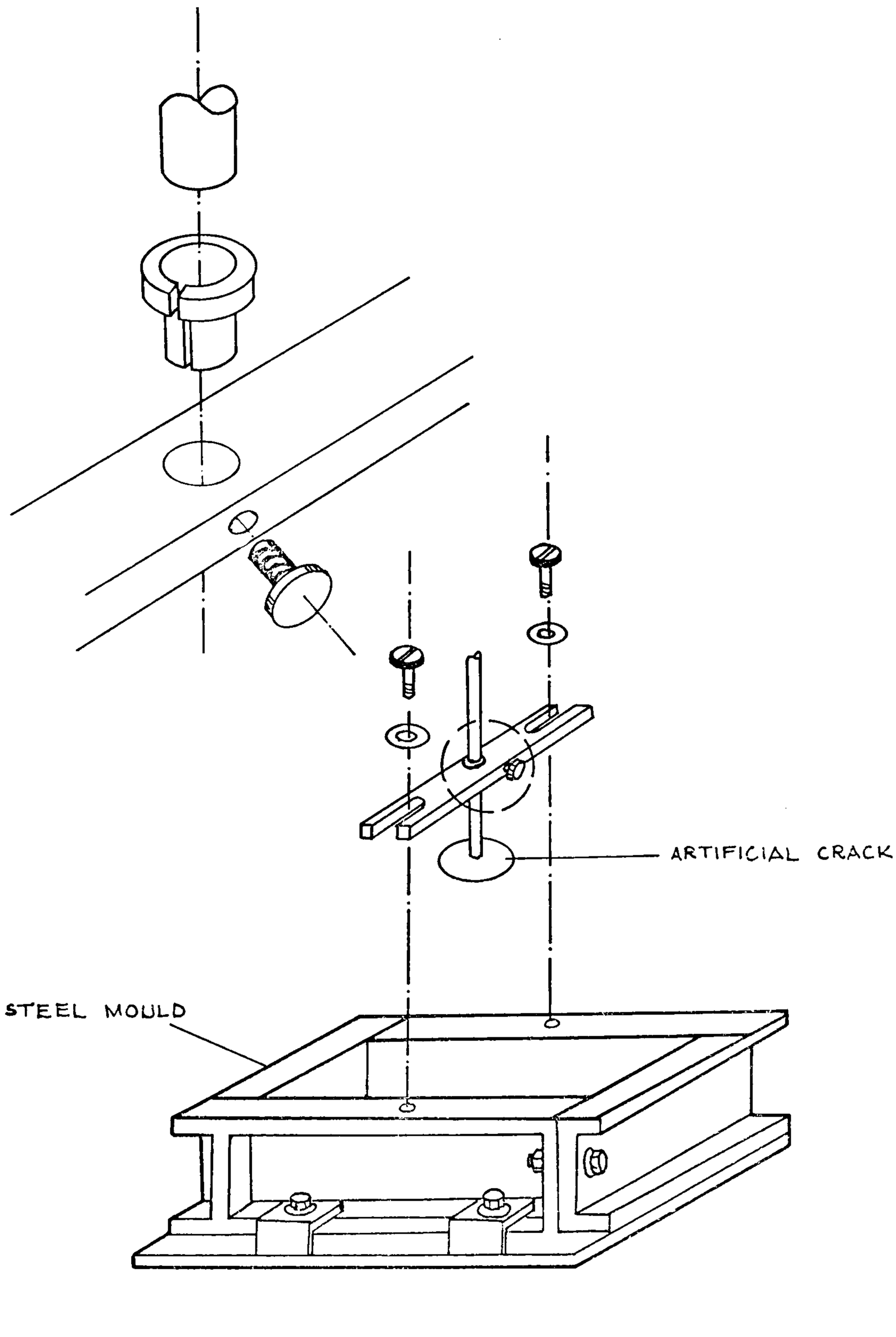

FIG. 6.7 STEEL MOULD AND THE FIXATION OF ARTIFICIAL CRACK

The process of preparation of steel moulds was similar but with a different method for fixing the copper tube. For this, a removable steel cross bar was made and the tube connected to it as shown in Fig.6.7. The bar itself was fixed on the mould as shown in Fig.6.7.

Mortar was used throughout, with a mix ratio of 1 cement + 1·5 sand + 0·45 (or 0·40 later) water.

Bin dried 4.76mm down to 0·5mm sand passing No.7 sieve but retained at No.1CO sieve was used as aggregate.

All the cement used was from a single batch. (See Appendix VII)

Mixing was done by a 0·14m^3 capacity double rotating mixer,1min. dry mixing followed by 5min. wet mixing.

Before the start of mixing, the moulds were fixed on the vibrating table, properly oiled to prevent bonding. The brass disc soldered on to the copper tube, was completely covered with an elastic membrane to ensure uniform application of pressure. The copper tube was subsequently fixed on to the cross-bar across the top centre of the mould. The depth was then adjusted and the copper tube was fixed more permanently on the cross-bar using a cap screw.

The mortar was placed in the moulds in three layers with 1min. vibration after each layer. Three 101·6mm (4") cubes and six 11·2mm diameter, 30·5mm high cylinders were also cast as control specimens.

6.2.4 Curing

Three hours after casting the specimens in moulds

were taken to the curing room kept at 21°C and at 94% relative humidity. Demoulding of the steel moulds took place after 24hrs. of casting. After proper labelling the specimens were taken back to the curing room to be moist cured or kept underwater depending on the case.

In some moist cured specimens the weight loss was recorde during the curing period to determine the period necessary for moisture equilibrium with the surroundings. (See Appendix IV)

Specimens to be tested in biaxial compression were transported to Imperial College and placed in the curing room at least one week before the date of the test.

6.3 Pressure Set

A pressure set was designed to apply static pressure to the crack in the specimen. It comprised a pressure source and a pressure regulating device.

When a concrete wall is heated, there is no clear evidence whether the maximum pressure occurs in the dry region due to water vapour pressure, or in the wet region due to water under pressure. Obviously there is a possibility that the mode of failure and the amount of pressure required for failure could be different depending on the type of pressure applied. In fact, water vapour being compressible, energy is accumulated during compression which, at sudden failure, is released in a catastrophic fashion. On the other hand, water, being incompressible, undergoes no energy accumulation in compression and therefore the mode of

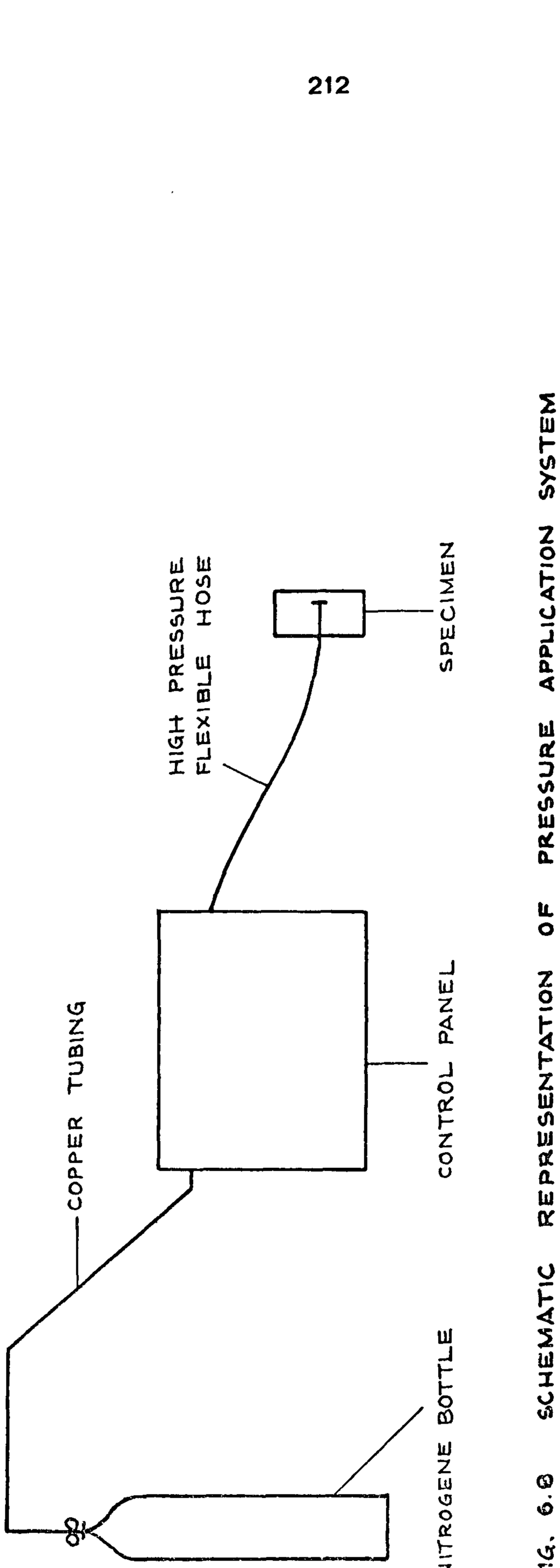

FIG. 6.8 SCHEMATIC REPRESENTATION OF PRESSURE APPLICATION SYSTEM

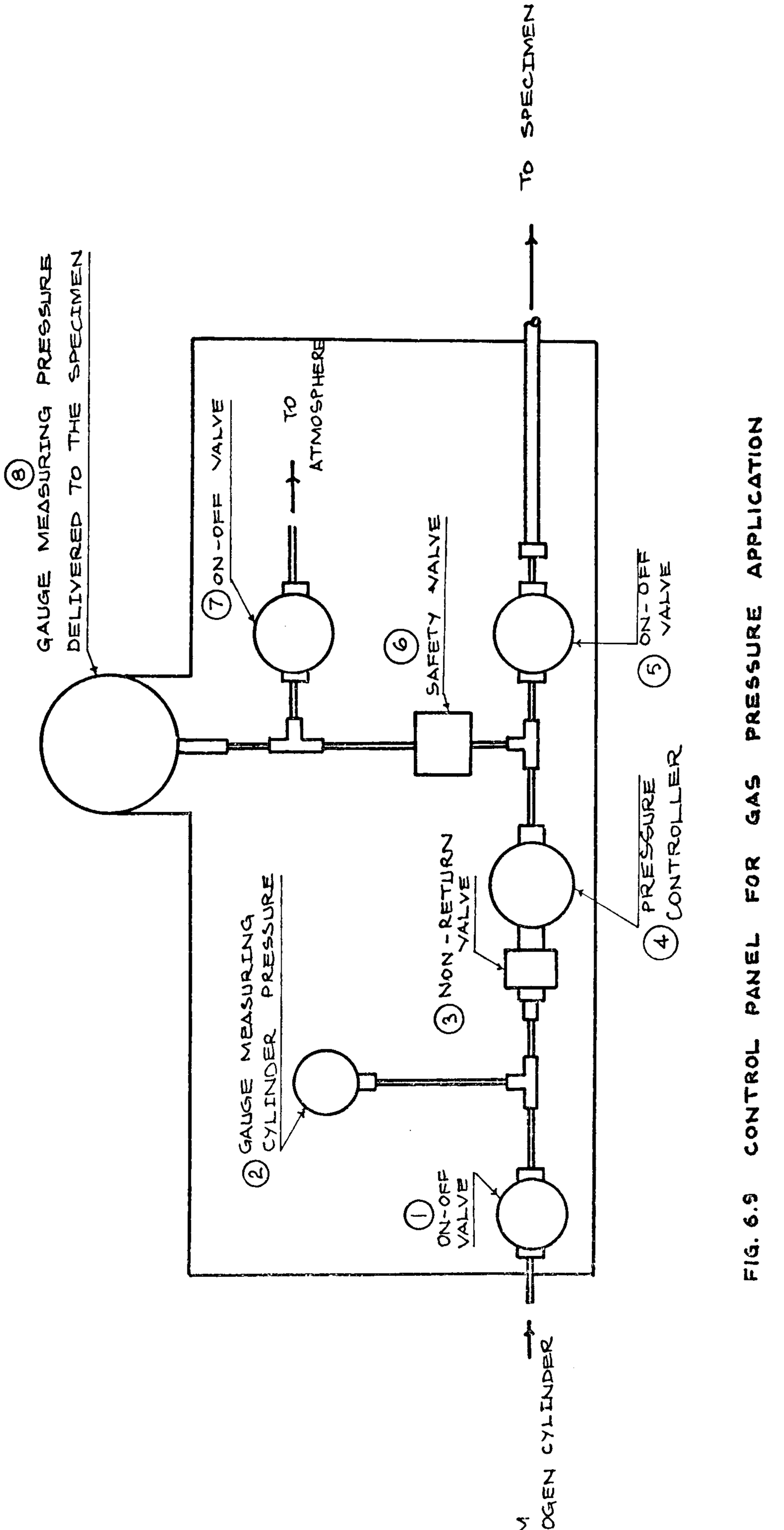

FIG. 6.9 CONTROL PANEL FOR GAS PRESSURE APPLICATION

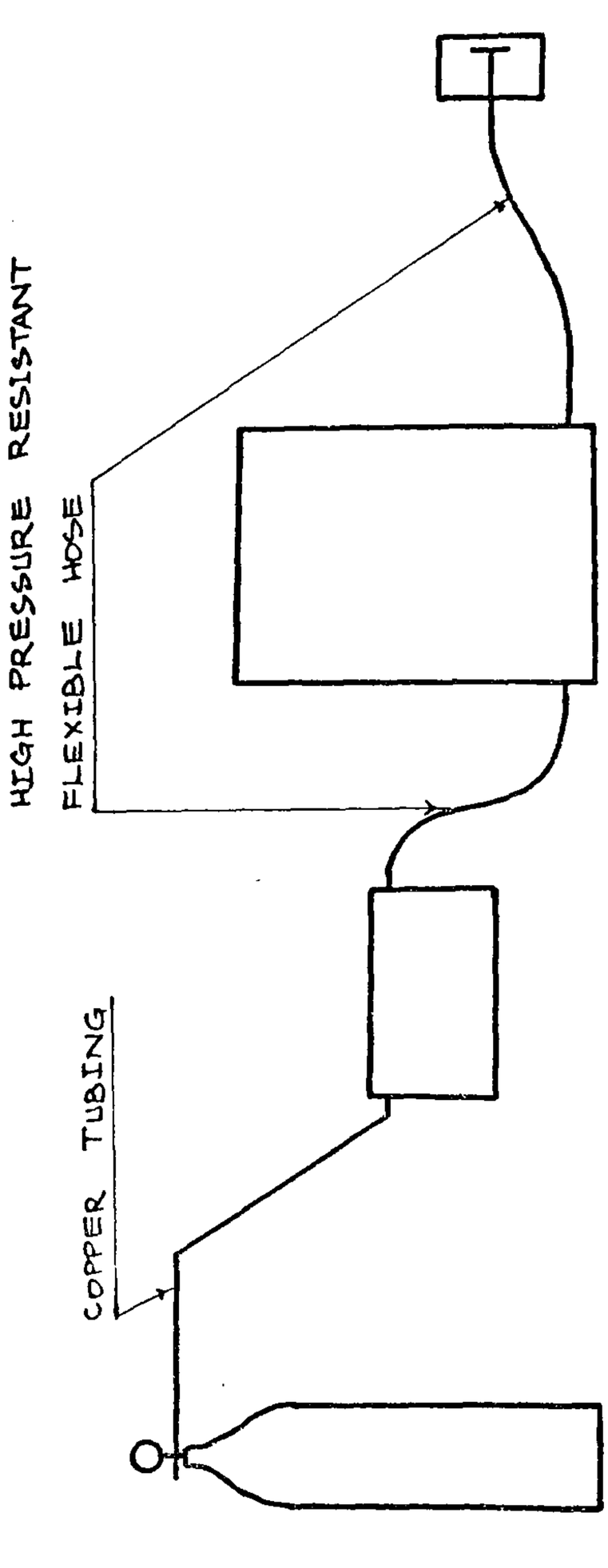

FIG. 6.10 SCHEMATIC REPRESENTATION OF WATER PRESSURE APPLICATION SYSTEM

failure of a material under water pressure may be substantially different from the mode of failure of the same material under gas pressure.

To study both cases, tests using gas pressure and water pressure were performed separately using different pressure sets.

6.3.1 Set Using Gas Pressure

The system comprised a high pressure source, 13 MN/m^2 nitrogen cylinder, a control panel and high pressure flexible hose connecting the panel to the specimen. (Fig.6.8)

The control panel (Fig.6.9) contained a control valve for gradual application of pressure, two pressure gauges with a range of 14 MN/m^2, one before and one after the control valve to indicate the input and output pressures, a non-return valve, and three on-and-off valves one of which used to release the pressure to the atmosphere after the test.

6.3.2 Set Using Water Pressure

The system for water pressure application comprised a high pressure source, 13 MN/m^2 nitrogen cylinder, a hydraulic pressure unit to convert the gas pressure to water pressure, a pressure control panel, and high pressure resistant hose. (Fig.6.10)

The hydraulic pressure unit made to order by 'Olin Ltd.' was a 'Haskel' miniaturized air driven hydraulic pump capable of boosting a gas pressure of 620 KN/m^2 (90 psi) up to 20·68 MN/m^2 (3000 psi) oil pressure. An air filter, a pressure regulator, two

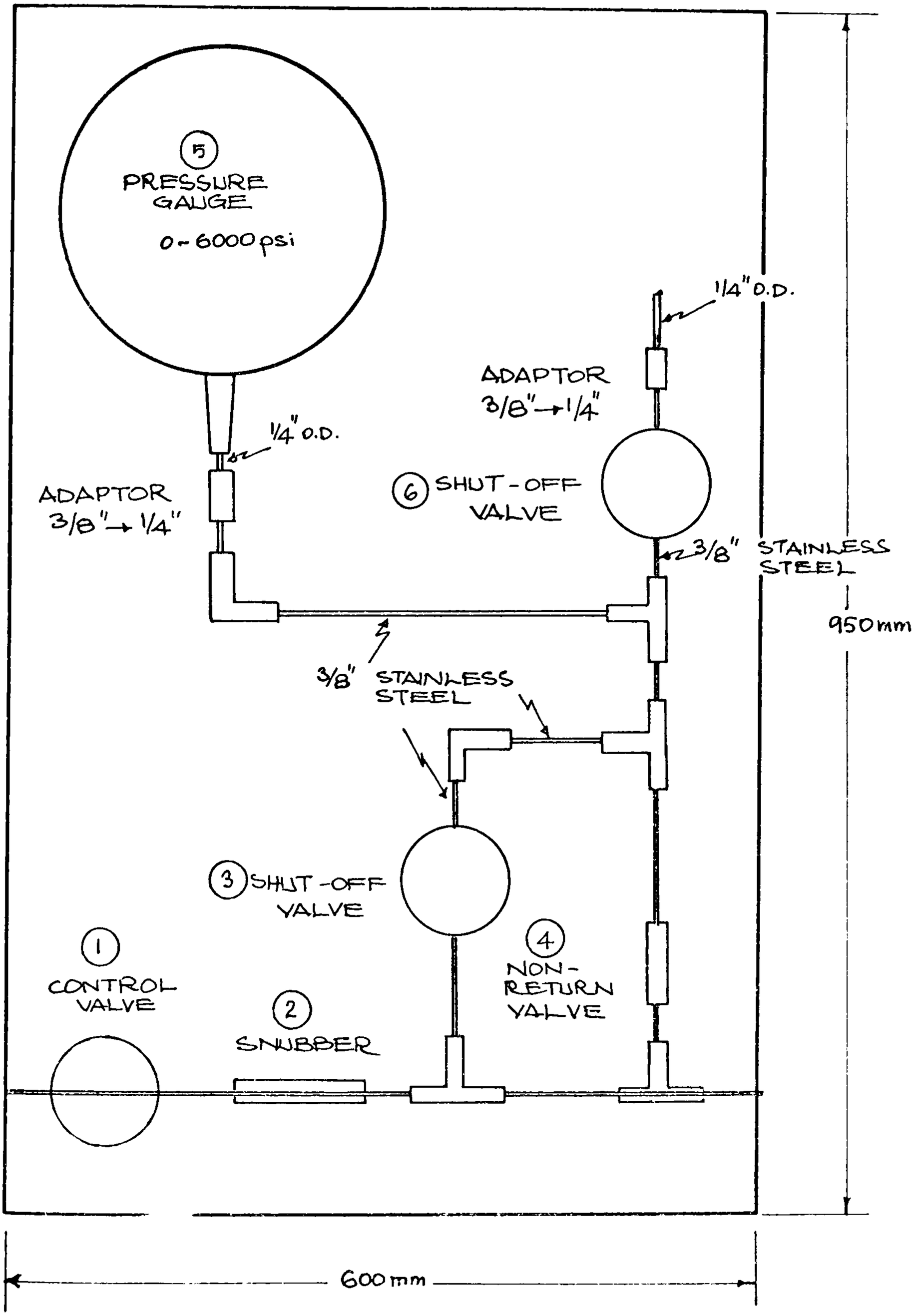

FIG. 6.12 CONTROL PANEL FOR WATER PRESSURE APPLICATION

separate inlet and outlet pressure gauges and an hydraulic oil reservoir completed the hydraulic pressure unit.

The pressure panel (Fig.6.12) was made up of a control valve (See Fig. 6.I2) in order to regulate the gradual increase of pressure during the test, a non-return valve to prevent any pressure drop after the failure of the specimen so that the pressure indicated by the gauge could be recorded, a shut-off valve to release pressure after the completion of the test, and, a pressure gauge to indicate the pressure applied to the crack. All tubing and connecting parts were 9·5mm (3/8'') stainless steel to minimise corrosion.

Some of the tests were planned to be carried out at Imperial College and Fire Research Station and therefore special emphasis was placed on making the set portable. Consequently, 'Ermeto' high pressure double braid flexible hose (10mm bore), capable of standing pressures up to 27·56 MN/m^2 (4000 psi) was chosen to connect the hydraulic pressure unit to the panel and the panel to the specimens, the connections provided by 'Ermeto' being re-usable couplings specially designed for the pressure hose in question.

6.4 Preliminary Tests and Modification to the Test Procedure

The preliminary tests involved the application of gas pressure in cylindrical specimens, each containing 6·35mm (1/4'') crack. The depth of these artificially

formed cracks varied between 6mm and 2 2mm among specimens.

These specimens were of mortar, with 1 cement + 1·5 sand + 0·5 water mix ratio and were tested at the age of 14 days.

The result of these tests was that no spalling was obtained in any of the specimens although in some cases pressures up to 9·65 MN/m^2 (1400 psi) were applied. In most cases the gas started leaking at pressures between 345 KN/m^2 (50 psi) and 5·52 MN/m^2 (800 psi) and this was related to the bonding of the mortars to the metal disc. No artificial crack was therefore formed and the pressure was applied only at a much smaller surface than the one predicted. Clearly, much higher pressures would then be required to cause failure and therefore, leaking would start as soon as the pressure reached a favourable level[x].

In order to prevent the bonding of the mortar to the metal disc the latter was covered with a rubber membrane as shown in Fig.6.4. Subsequent tests using this method proved completely satisfactory.

6.5 Test Programme

6.5.1 General Description of the Test Programme

Although the objective of all the tests was the

Footnote

Incidentally this level of pressure need not be high, because, specimens, being only 14 days old, were highly permeable.

Table 6.I Various forms of Break-out tests carried out.		
Pressure medium		Additional loading
I.	gas	none
2.	gas	biaxial
3.	water	none
4.	water	varied but mainly biaxial

measurement of the applied pressure at the failure of the crack, the individual tests were somewhat varied in their details. They could however be grouped under 4 major headings as shown in Table 6.1.

6.5.2 Tests Without Additional Loading

These tests, carried out at King's College, involved the application of gas or water pressure without additional loading . The procedure followed will be explained in the following section.

6.5.2.1 Test Involving the Application of Gas Pressure

Procedure

1. The specimens were taken from the curing room.
2. The nitrogen gas cylinder was connected to the pressure board (Fig.6.9) through 6.35mm (1/4") outside diameter copper tubing, using 6·35mm (1/4") 'Ermeto' fitting.
3. The copper tubing protruding from the specimen was connected to the flexible hose, using 6.35mm (1/4") Ermeto nuts.
4. The On-Off valves (Part No.I and 5 in Fig.6.9) were kept open while the On-Off valve (Part No. 7 in Fig 6.9) was kept shut. After releasing the gas under pressure from the bottle, the pressure controller (Part No. 4 in Fig.6.9) was gradually turned clockwise to increase the gas pressure on the specimen.
5. The pressure level shown by the pressure gauge (Part No. 8 in Fig.6.9) was continuously

observed and the level corresponding to the failure of the specimen was recorded. The failure was accompanied with a sudden drop of pressure shown on the pressure gauge and with an audible explosion occurring simultaneously.

6.5.2.2 Tests Involving the Application of Water Pressure

Procedure

1. The nitrogen cylinder was connected to the hydraulic pressure unit through 6·35mm (1/4") outside diameter copper tubing, using a 6·35mm (1/4") 'Ermeto' nut. The unit in turn was connected to the pressure control panel (Fig.6.11) through the high pressure flexible hose. Finally the specimen was connected to the pressure board as shown in Fig.6.10.
2. The gas under pressure was then released and the inlet pressure was increased using the control (Part No. I in Fig.6.12) on the hydraulic pressure unit. At this stage the pump started operating and the water was delivered under pressure to the flexihle hose connecting the unit to the pressure board.
3. The shut-off valves (Part No 3 and 6 in Fig.6.12) being kept shut, the pressure of the water in the system was then increased by turning the control valve (Part No. I in Fig.6.12) in the clockwise direction till

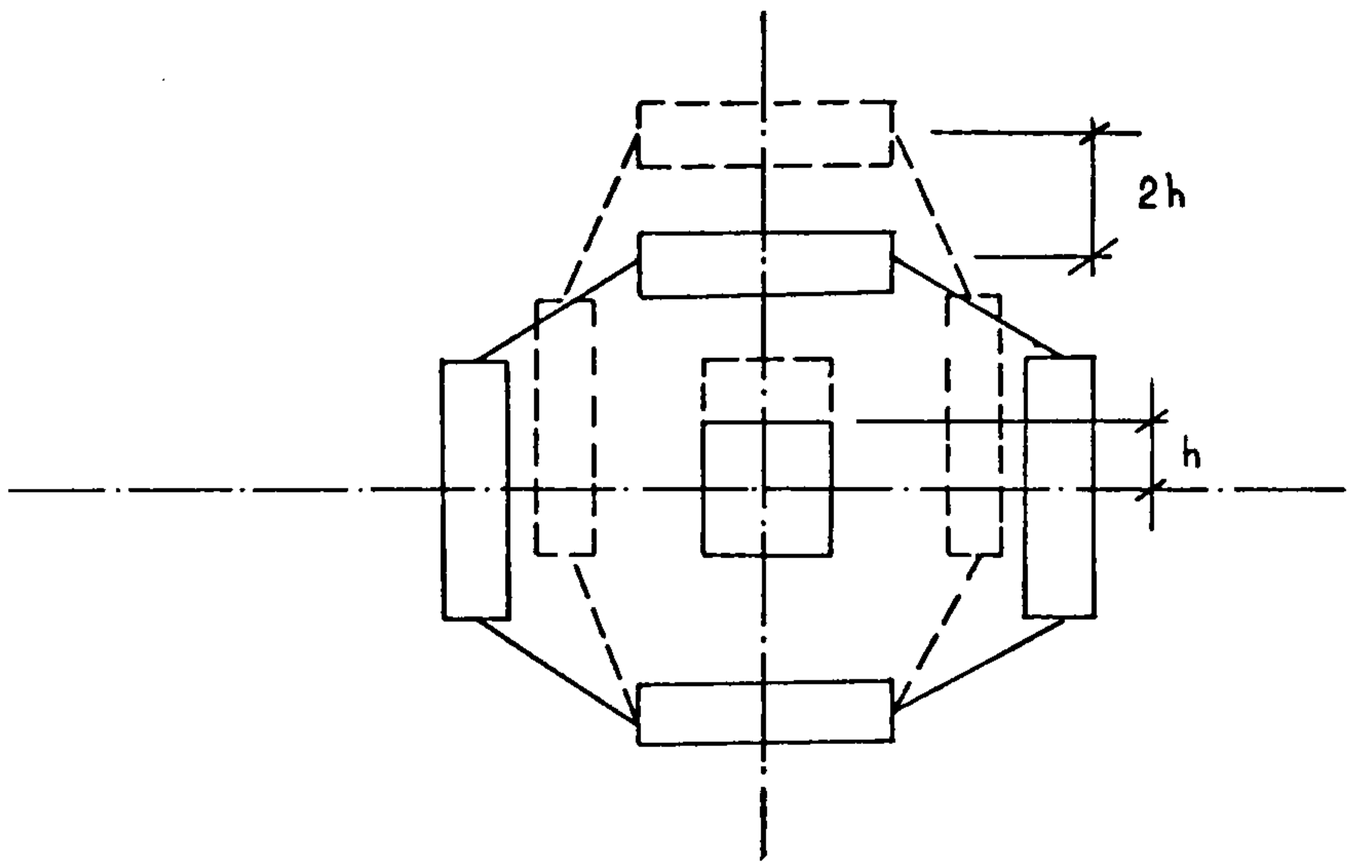

FIG. 6.13 SELF-LEVELING SYSTEM OF BIAXIAL COMPRESSION MACHINE

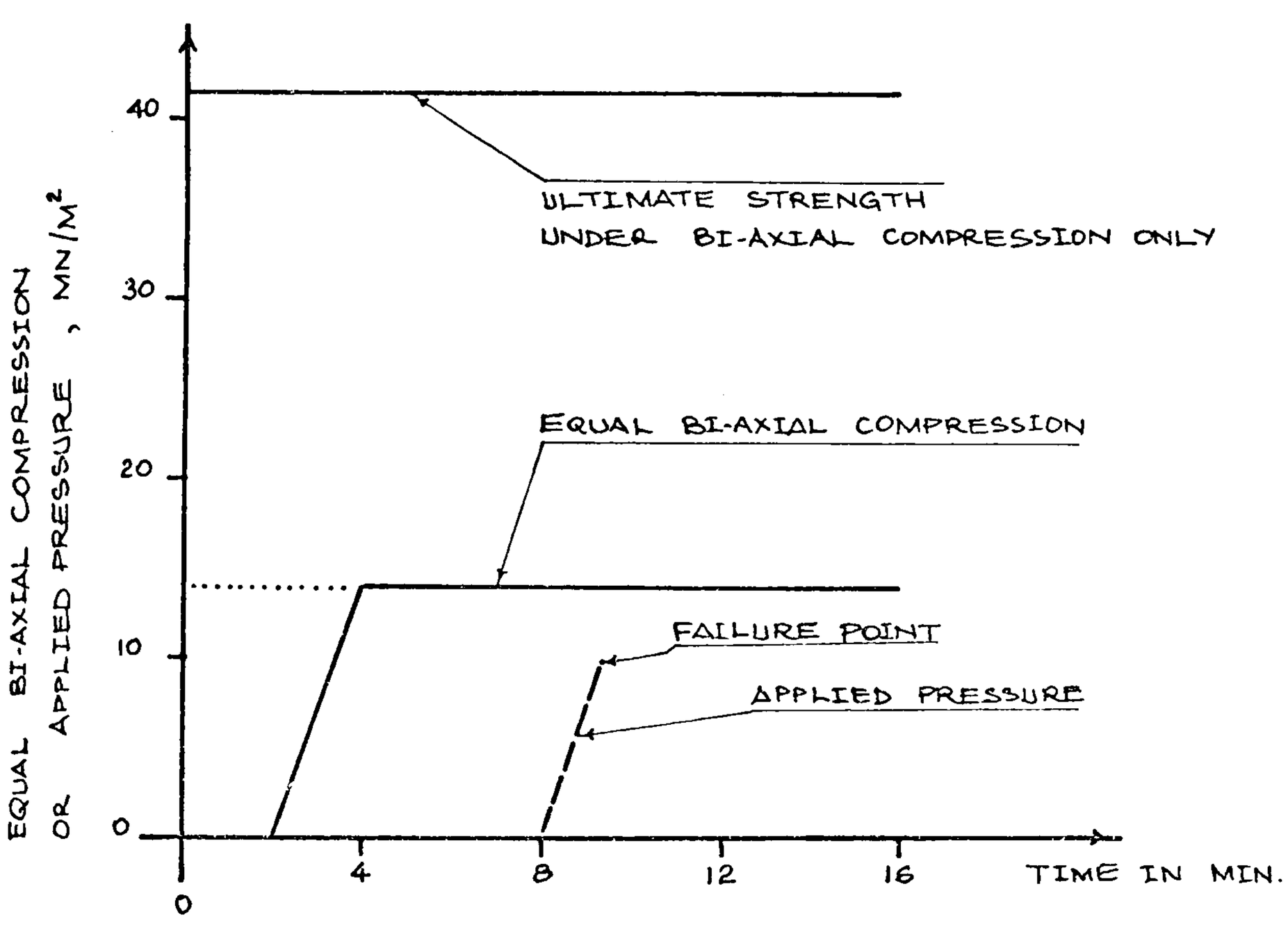

FIG. 6.14 SCHEMATIC REPRESENTATION OF BREAK-OUT TEST PROCEDURE

failure of the specimen occurred. The maximum pressure shown on the gauge (Part No. 5) was then recorded and the pressure in the system released by operating the shut-off valve. (Part No. 3 in Fig.6.12)

6.5.3 Tests Involving Biaxial and Uniaxial Loading

These tests performed at Imperial College involved the loading of the specimens and pressurizing the crack internally from an external gas or water pressure source while keeping the loading on.

The biaxial compression machine consisted of two four-column testing frames supported at right angles and containing opposed pairs of 200 ton hydraulic compression jacks. (Fig.6.13) The vertical frame was fixed on the machine skeleton but the horizontal frame was supported on rollers and was free to move horizontally.

The specimens cast at King's College were carefully transported to Imperial College and placed in the curing room at least one week before the test date.

6.5.3.1 Tests Involving the Application of Gas Pressure.

These tests were carried out according to the following procedure:

1. The specimen was placed between the platens of the biaxial compression machine.
2. The nitrogen bottle, the gas pressure board, and the specimen were connected as shown in Fig.6.8.
3. The biaxial loading was then increased to

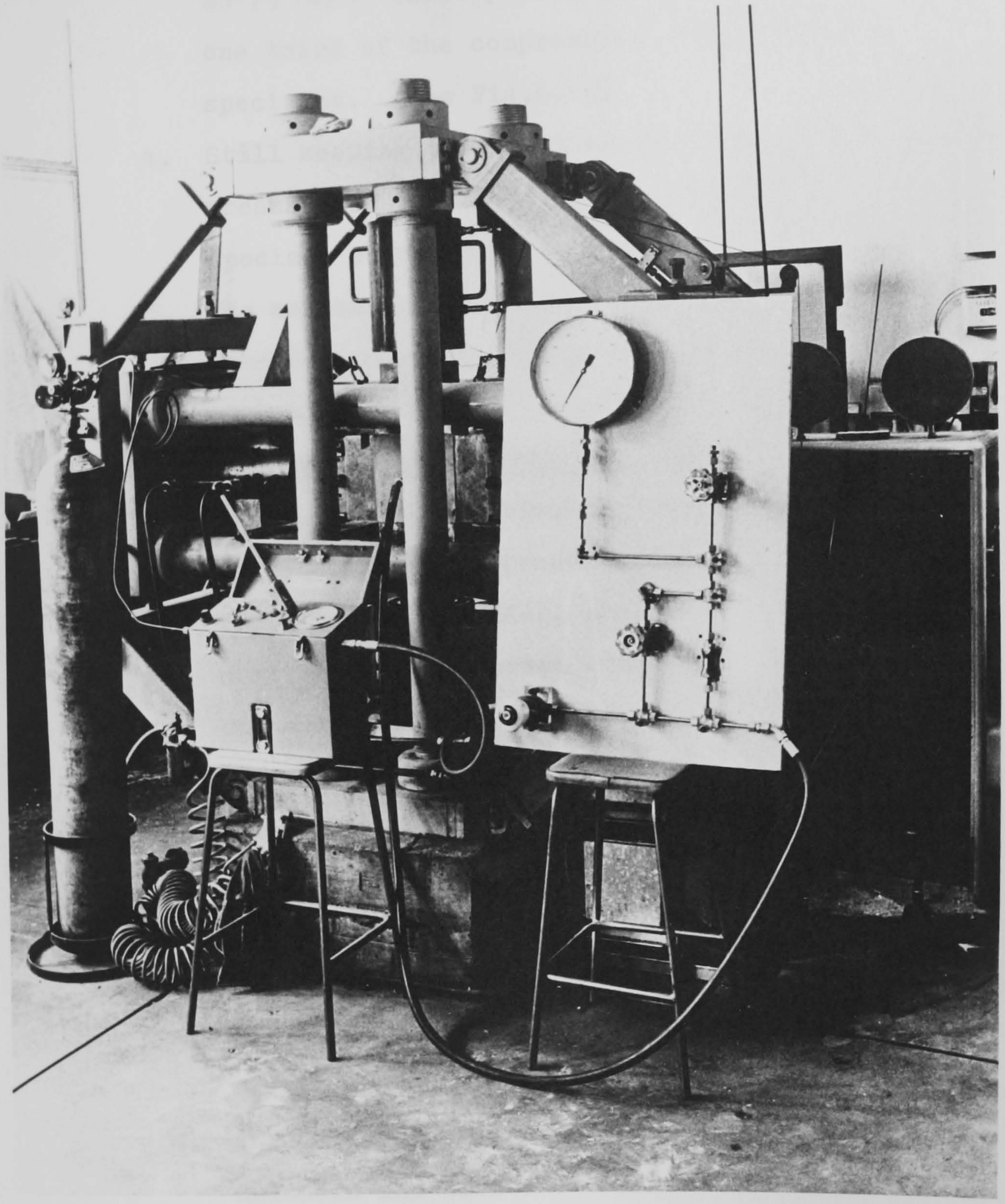

FIG.6.15 OVERALL VIEW OF "BREAK OUT" TEST SET-UP

13·79 MN/m^2 (2000 psi) which was approximately one third of the compressive strength of the specimens. (See Fig.6.14)

4. Still keeping this loading on, the gas pressure was applied until failure of the specimen occurred.

5. The maximum pressure was then recorded, the specimen unloaded, disconnected, and replaced with another one.

6.5.3.2 Procedure for Specimens Subjected to Water Pressure

1. The specimen was placed between the platens of the biaxial compression machine.

2. The nitrogen cylinder, the hydraulic pressure unit, and the pressure board were then connected as described in section 6.3.2 and shown in Fig.6.15.

3. The biaxial loading was then gradually applied, and kept constant at 13·79 MN/m^2 (2000 psi).

4. The water pressure was then increased in a manner described in section 6.5.2.2 until failure of the specimen occurred.

5. The failure pressure was recorded, specimen unloaded and disconnected and replaced with another one.

6.7 Discussion of Results and Conclusion

6.7.1 General Discussion

The main objective of the 'Break-Out' tests was to determine the magnitude of pressures necessary to cause

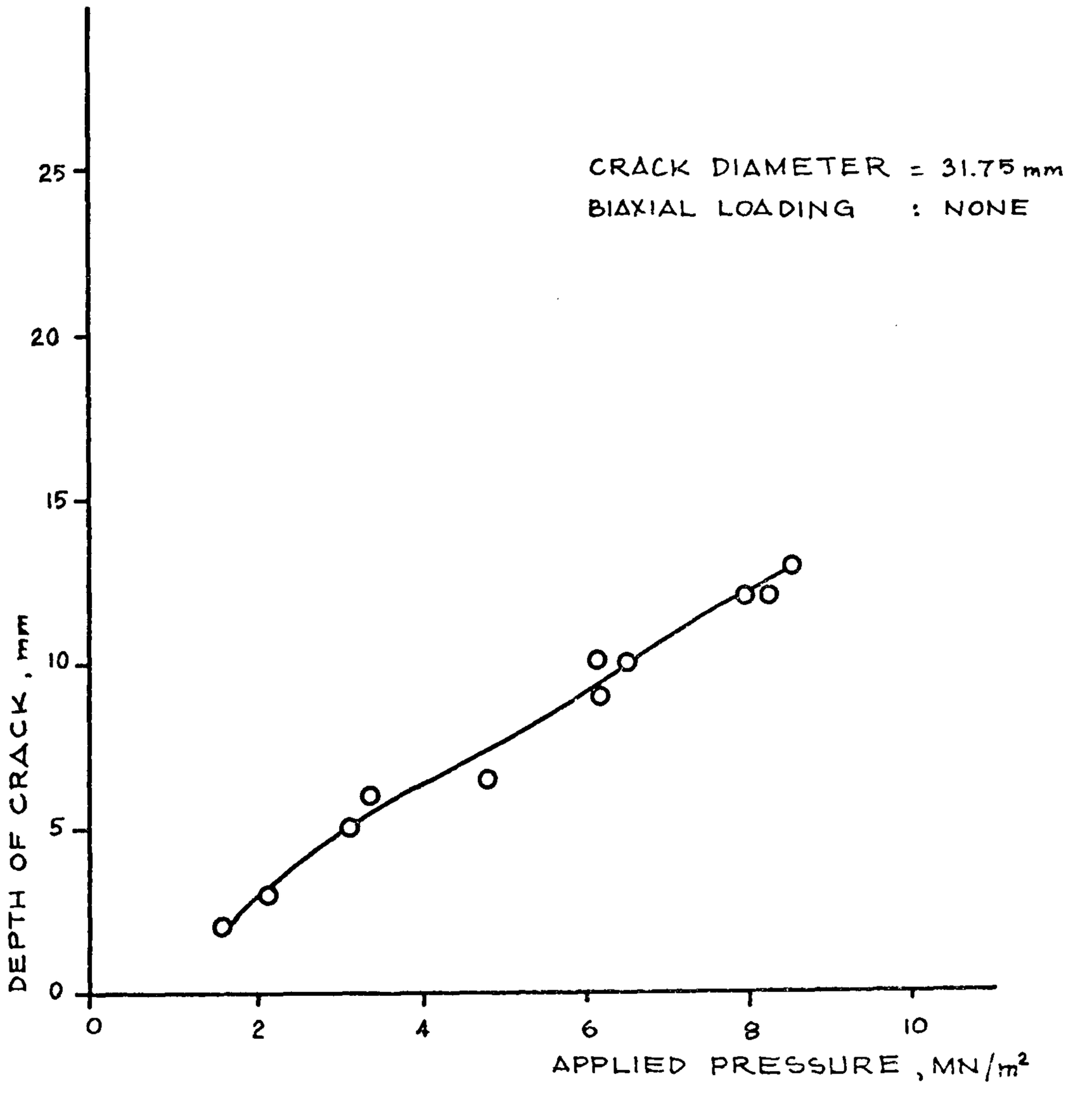

FIG. 6.16 VARIATION OF APPLIED PRESSURE WITH CRACK DEPTH

CRACK DIAMETER : 50.8 mm
BIAXIAL LOADING : NONE

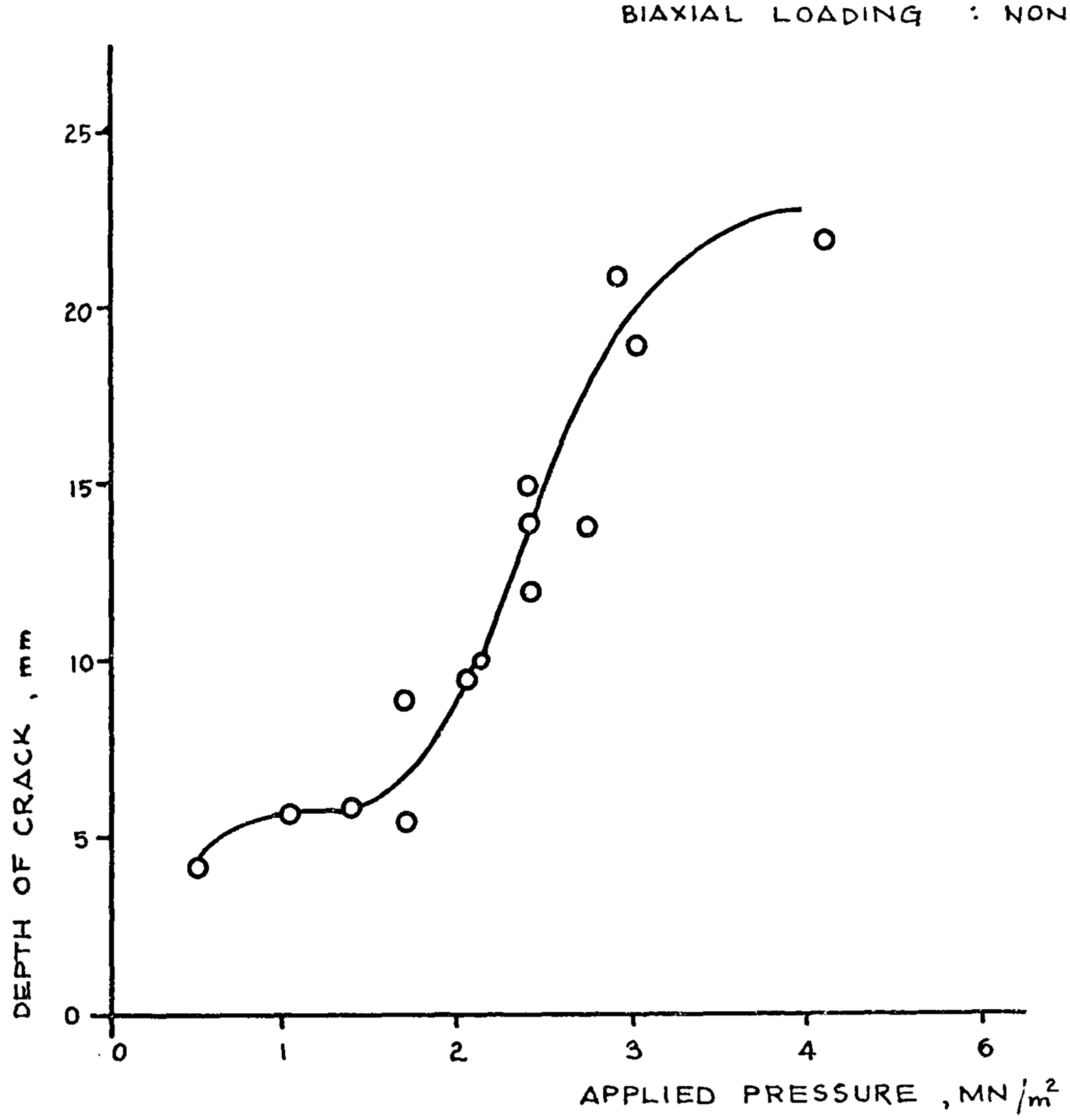

FIG. 6.17 VARIATION OF APPLIED PRESSURE WITH CRACK DEPTH

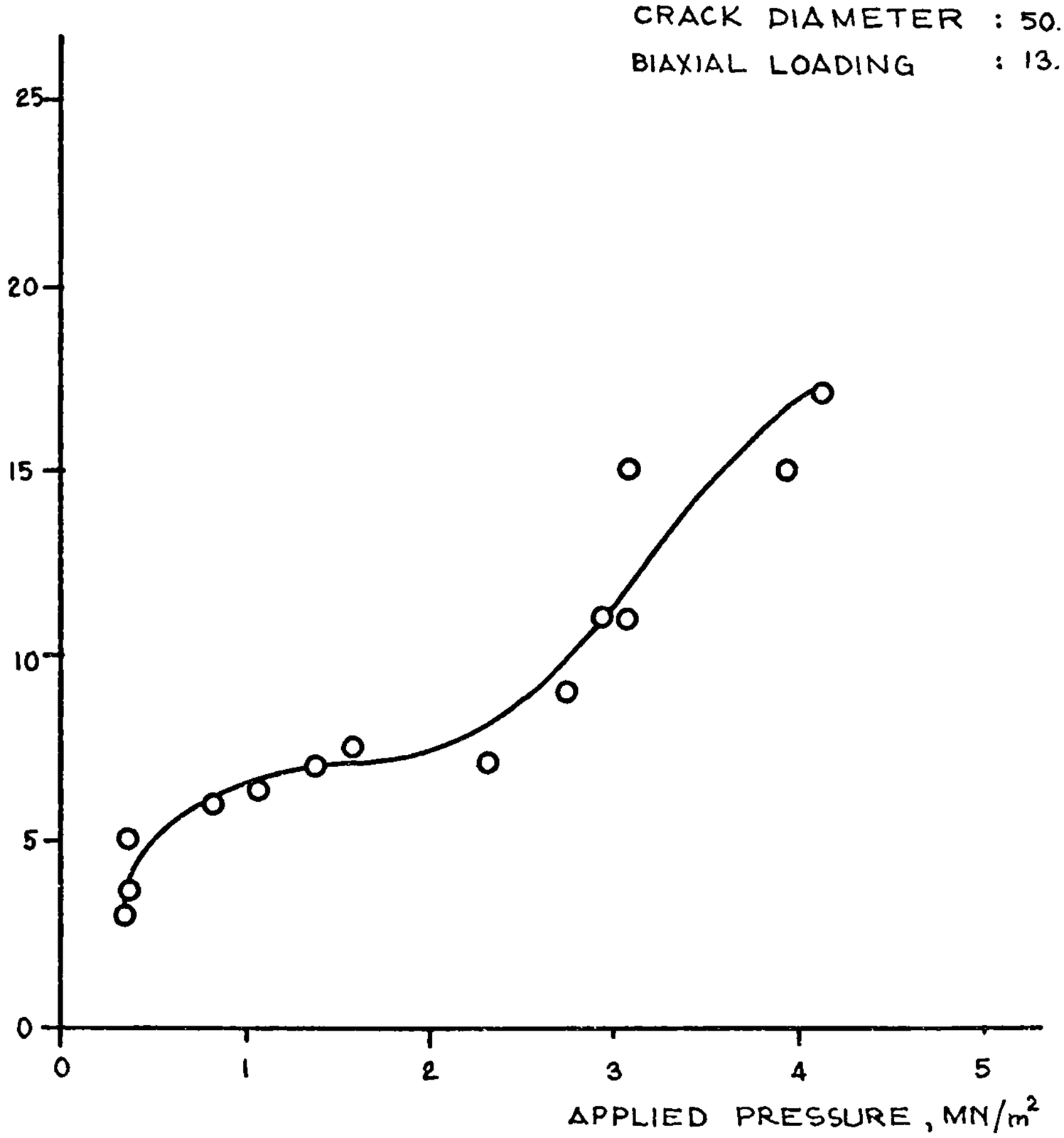

FIG. 6.18 VARIATION OF APPLIED PRESSURE WITH CRACK DEPTH

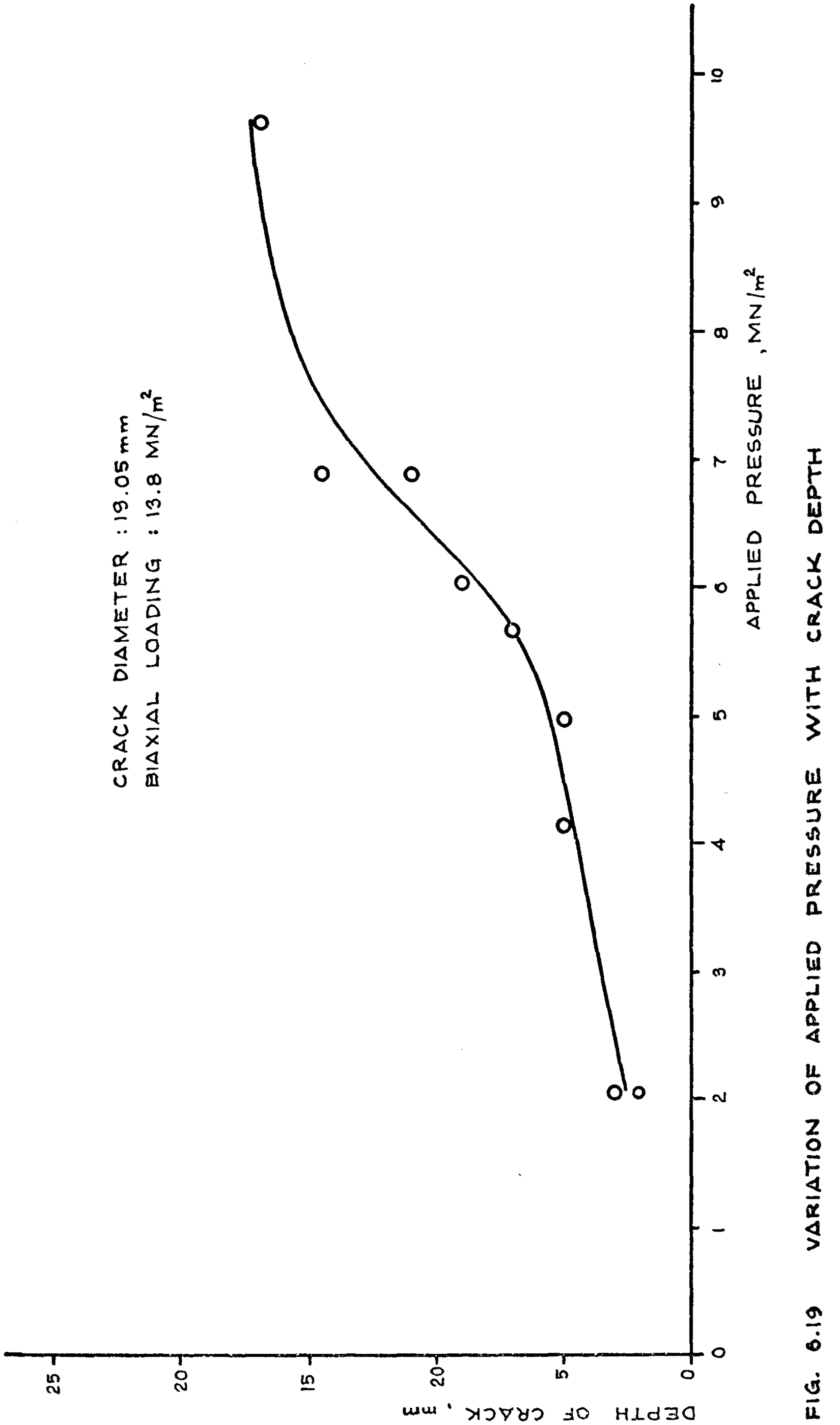
CRACK DIAMETER : 19.05 mm
BIAXIAL LOADING : 13.8 MN/m²
VARIATION OF APPLIED PRESSURE WITH CRACK DEPTH
APPLIED PRESSURE , MN/m²
DEPTH OF CRACK , mm
0
5
6
7
8
10
1
2
3
4
0
5
20
15
20
25

FIG. 6.19

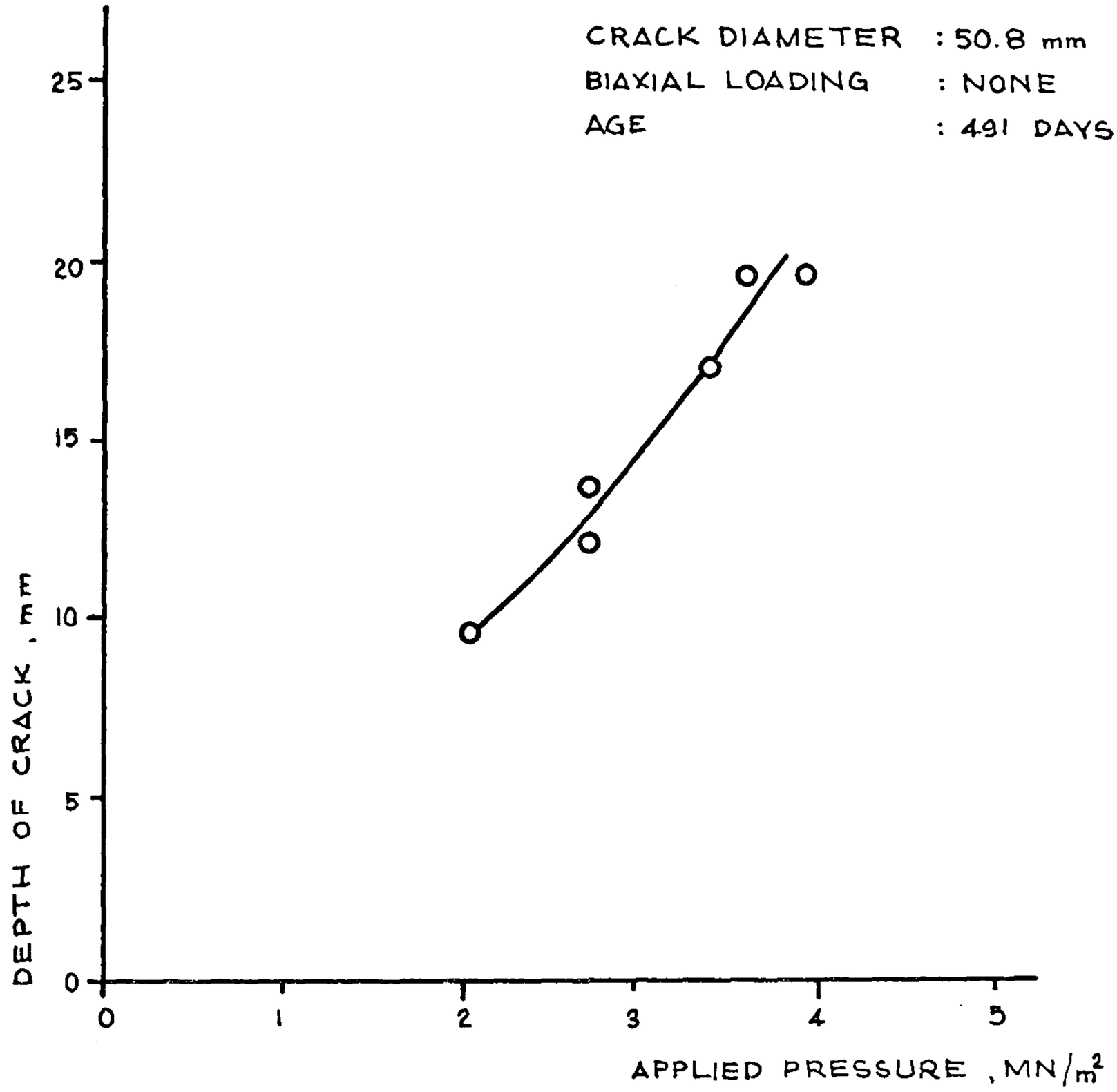

FIG. 6.20 VARIATION OF APPLIED PRESSURE WITH CRACK DEPTH

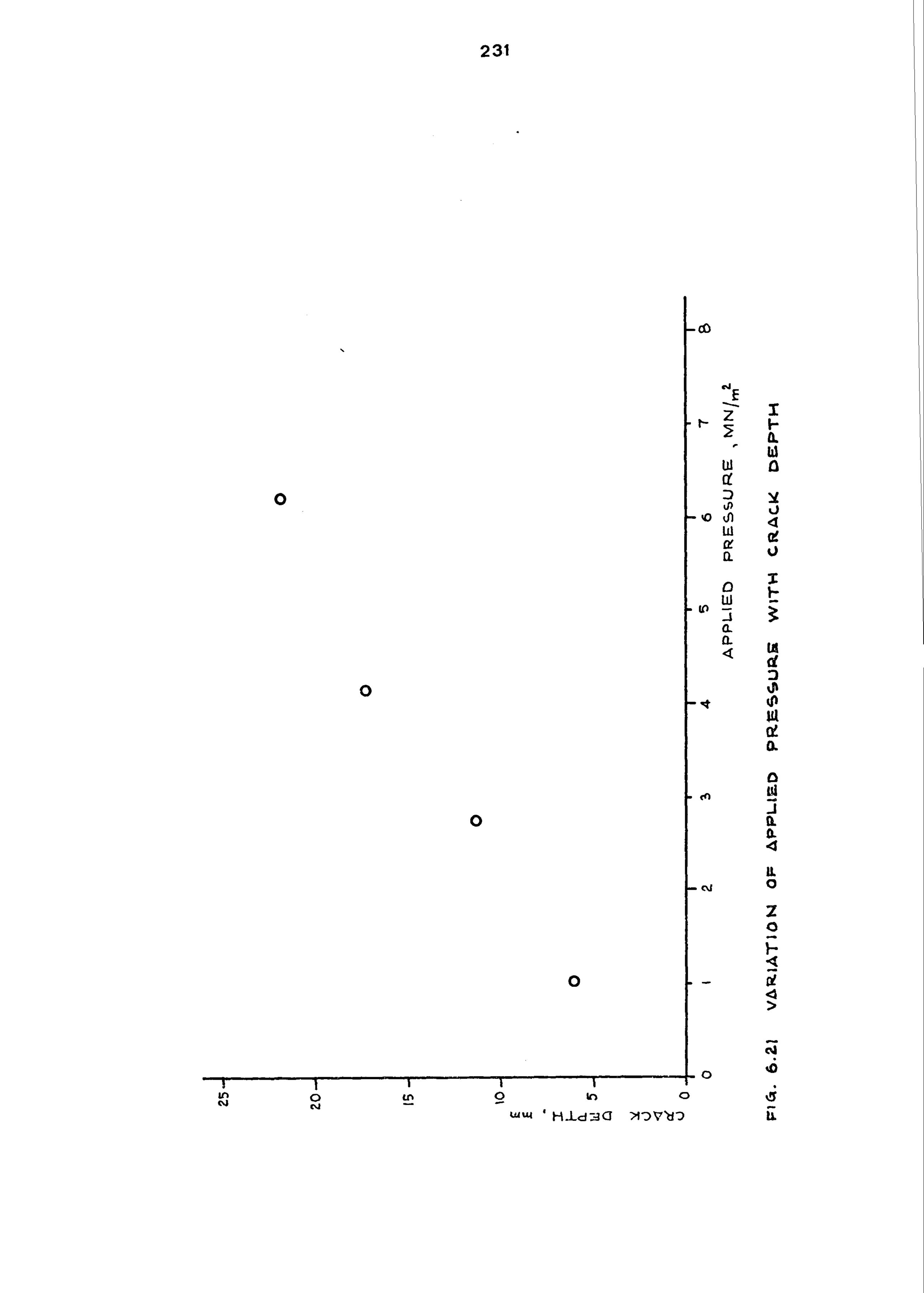
VARIATION OF APPLIED PRESSURE WITH CRACK DEPTH
APPLIED PRESSURE, MN/m²
CRACK DEPTH, mm
0
1
2
3
4
5
6
7
8
0
5
10
15
20
25

FIG. 6.21

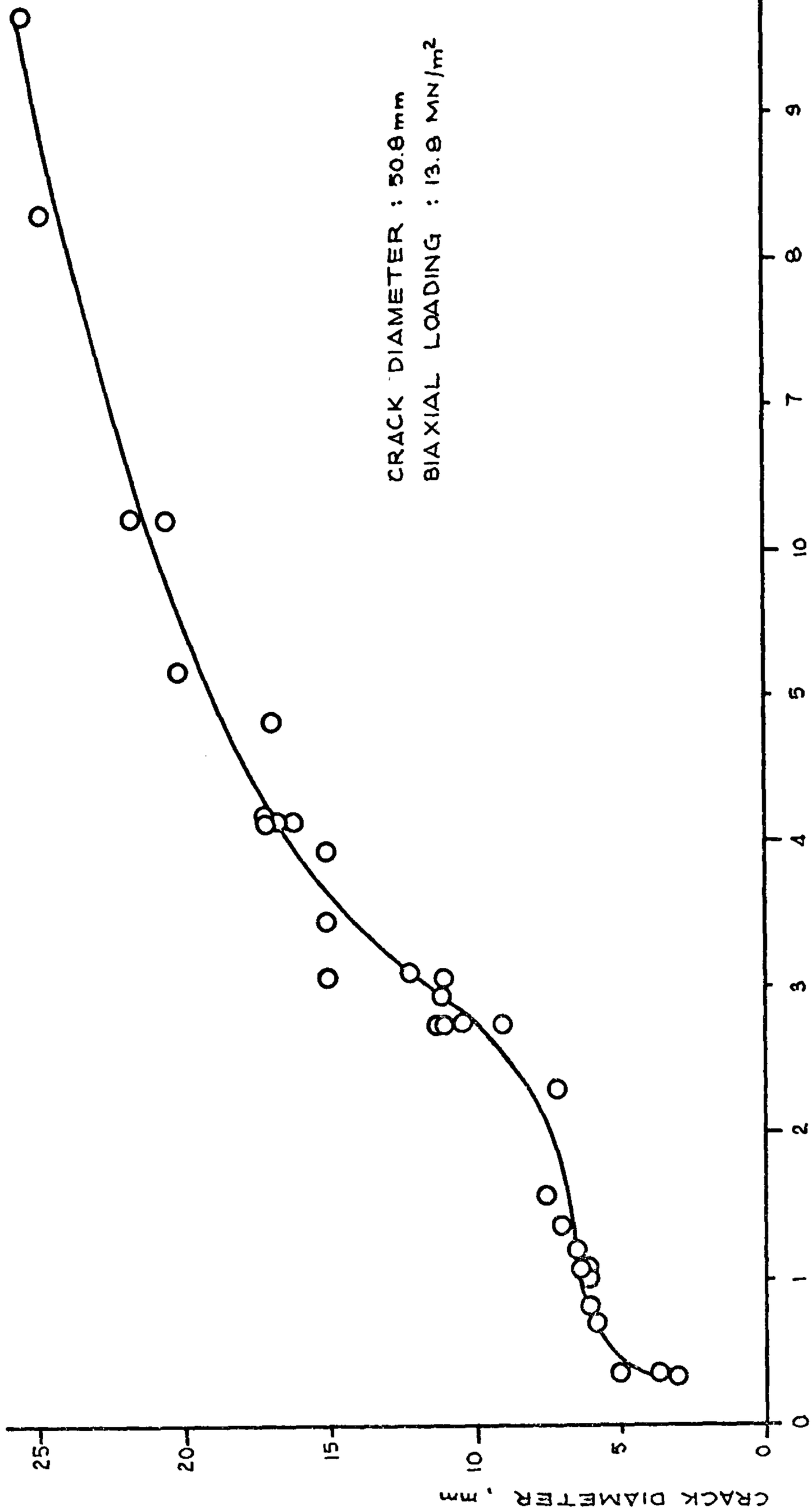

FIG. 6.22 VARIATION OF APPLIED PRESSURE WITH CRACK DEPTH

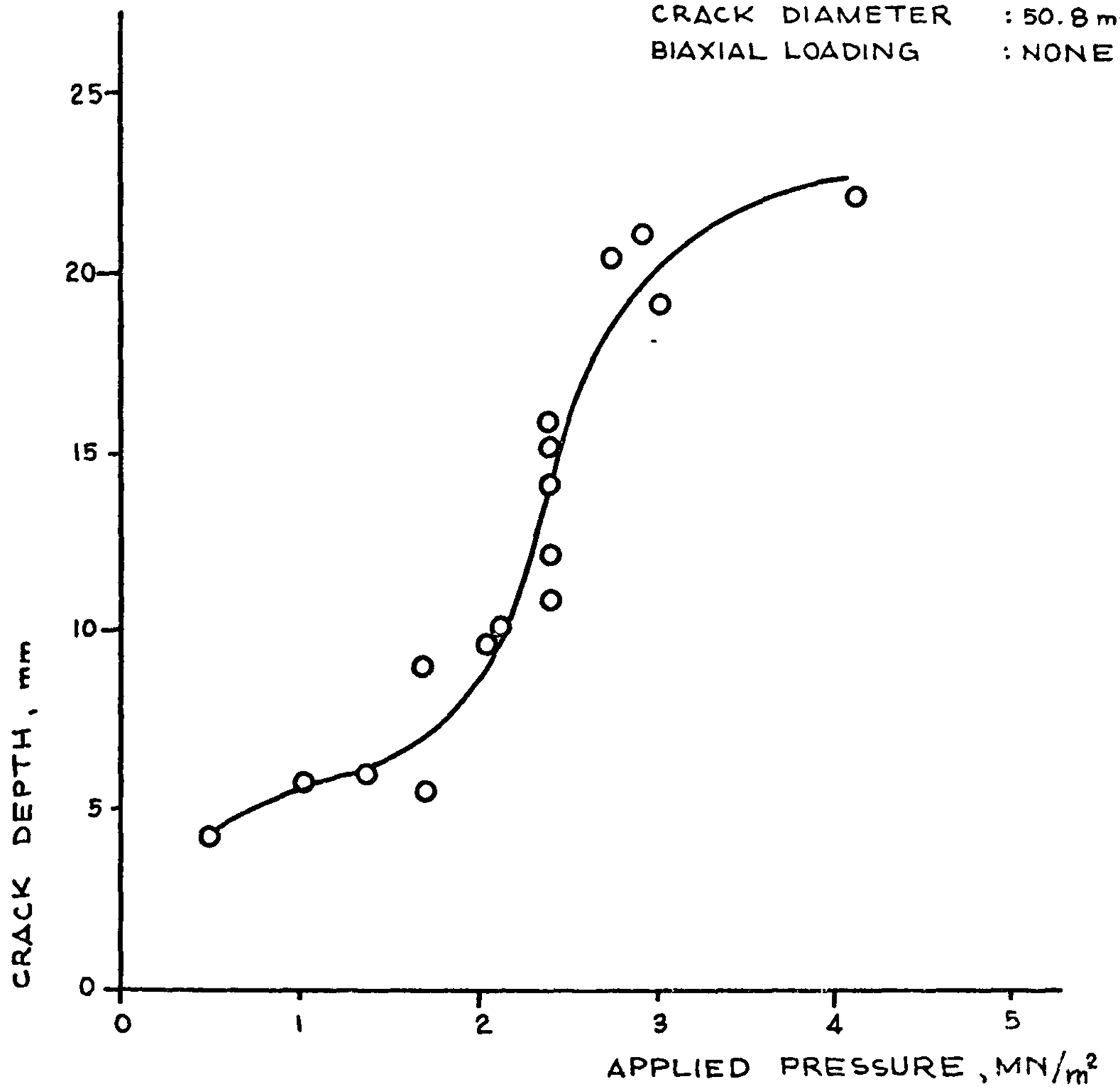

FIG. 6.23 VARIATION OF APPLIED PRESSURE WITH CRACK DEPTH

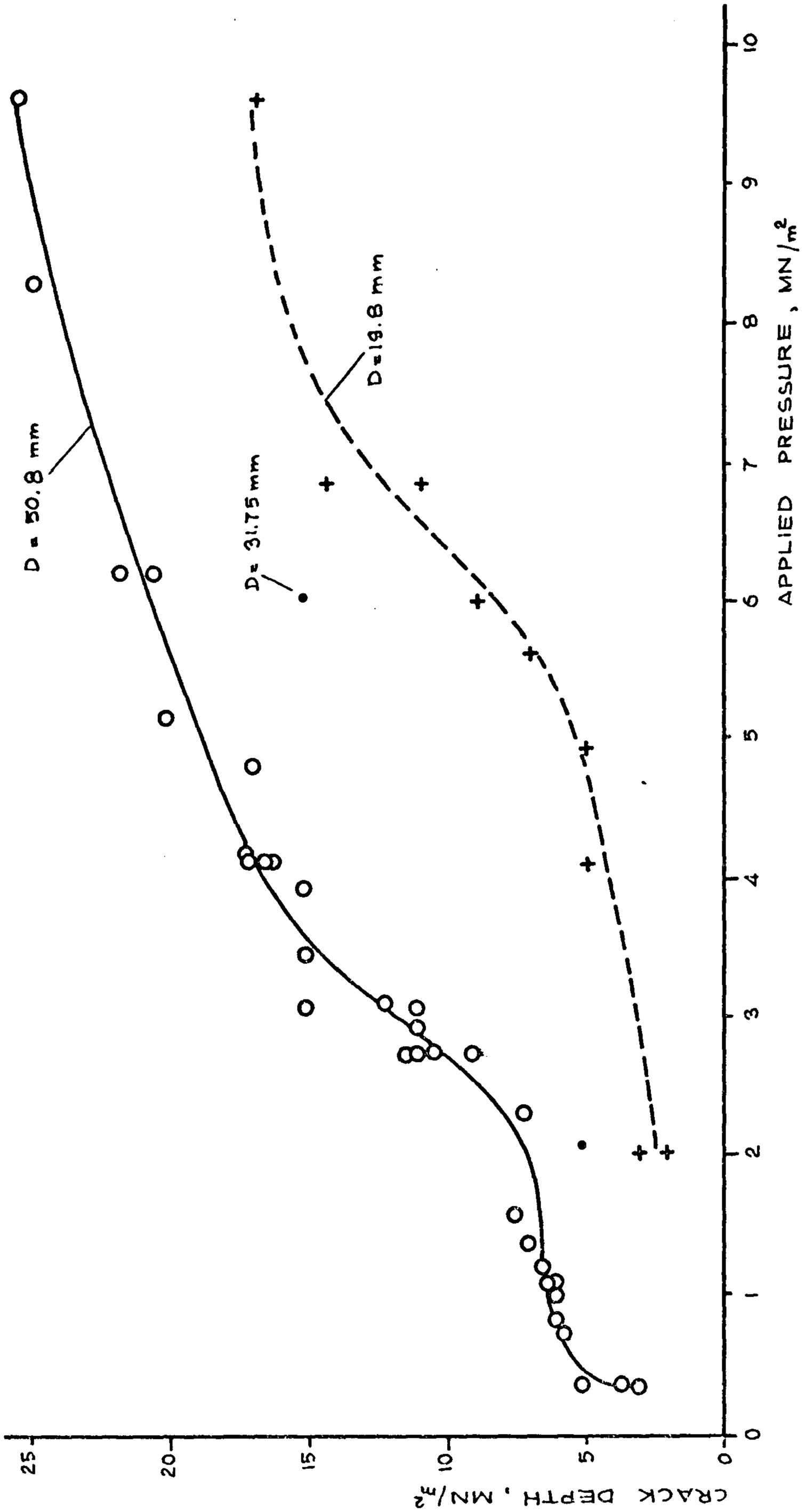
BIAXIAL LOADING : 13.8 MN/m²
D = 50.8 mm
D = 31.75 mm
D=19.8 mm
APPLIED PRESSURE, MN/m²
CRACK DEPTH, MN/m²
EFFECT OF CRACK SIZE

FIG. 6.24

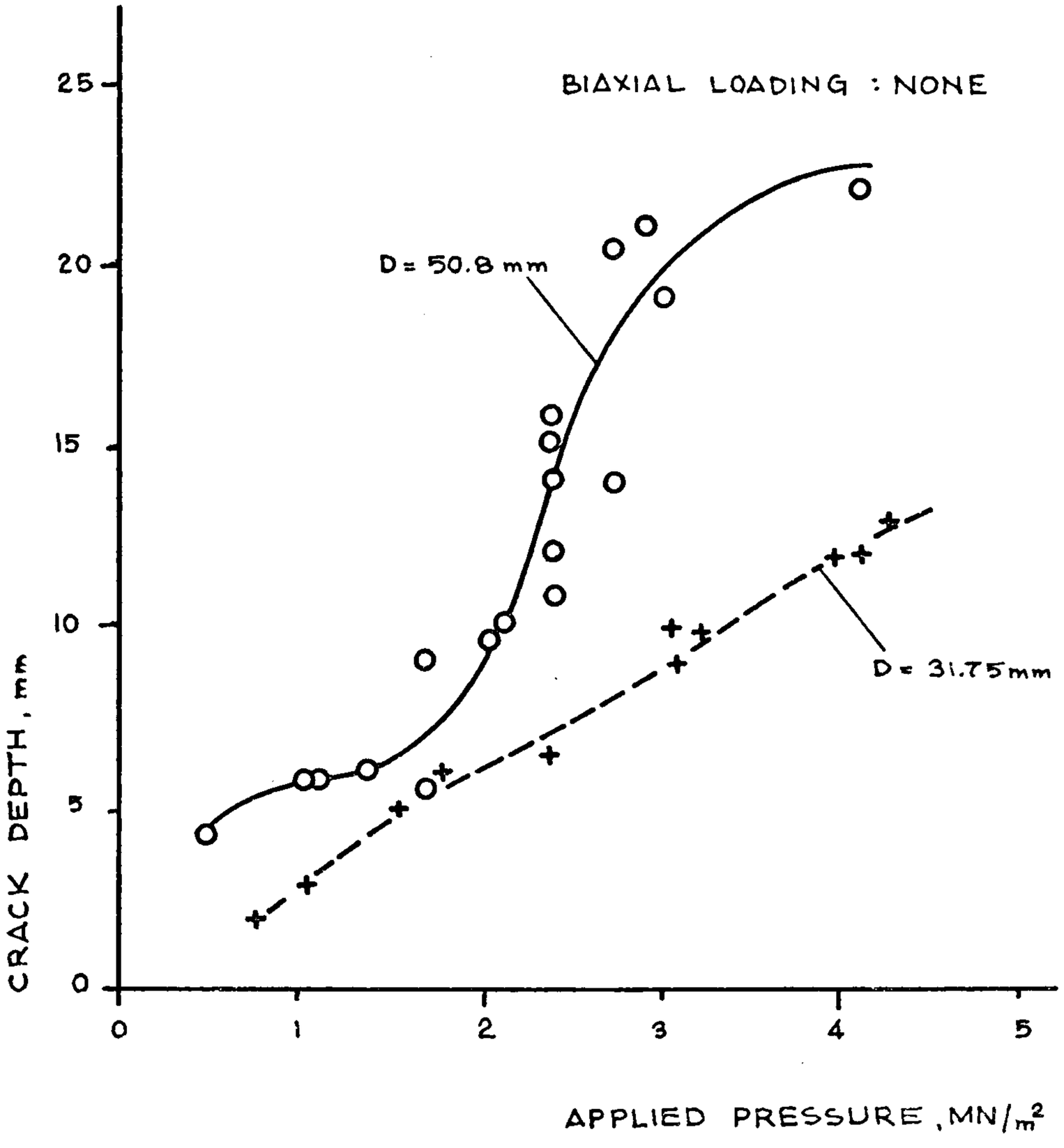

FIG. 6.25 EFFECT OF CRACK SIZE

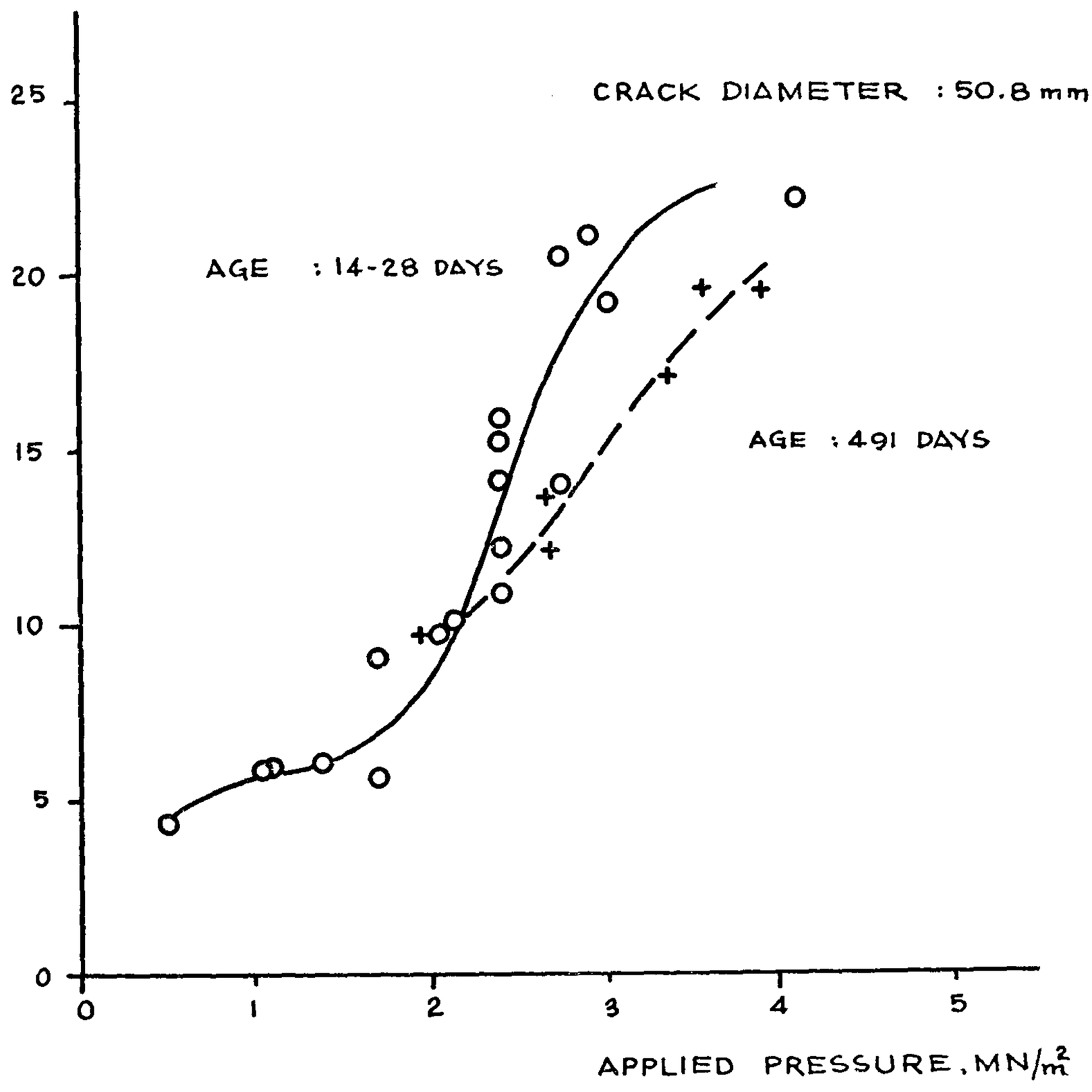

FIG. 6.26 EFFECT OF AGE

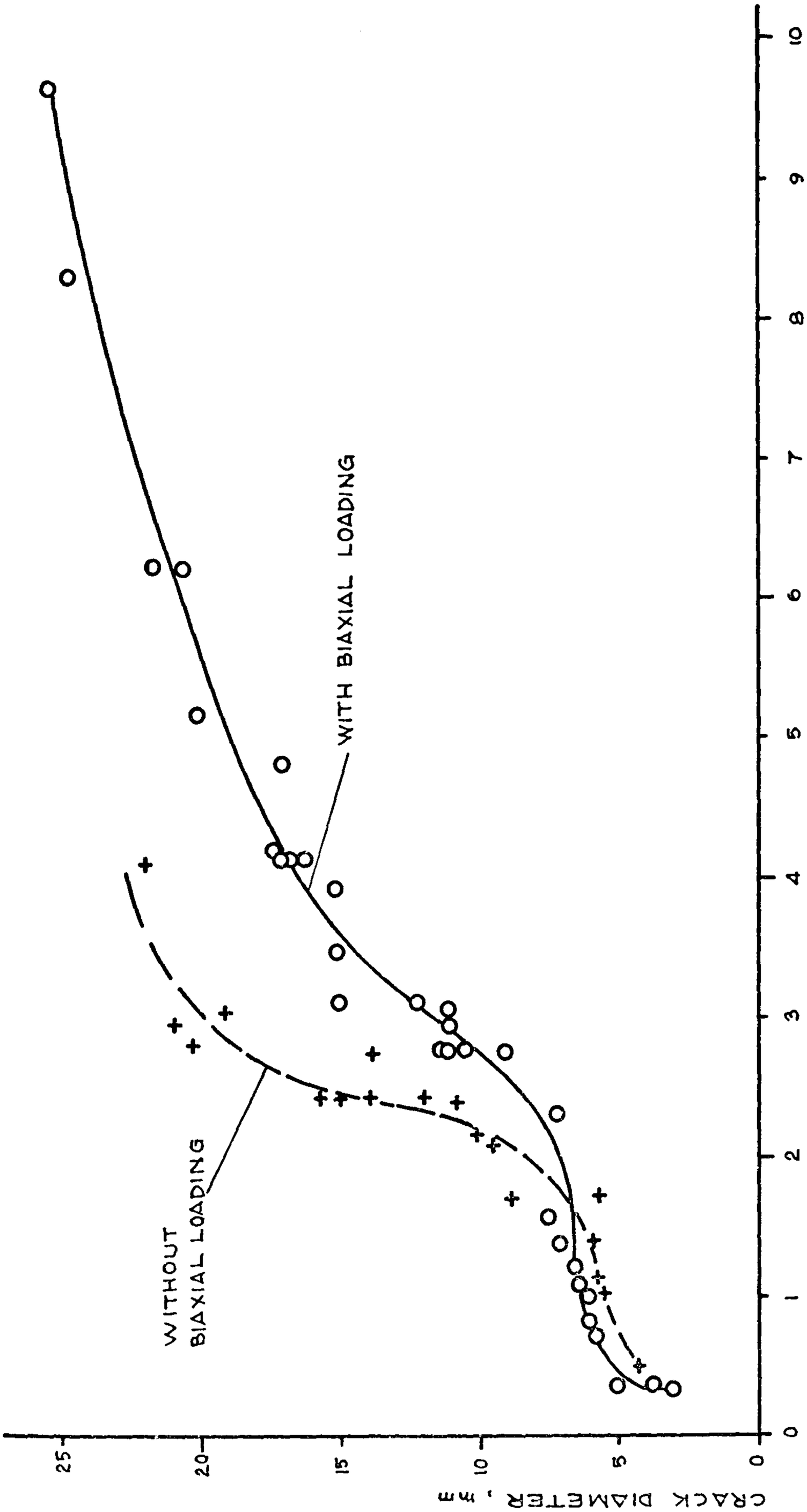

FIG. 6.27 EFFECT OF LOADING

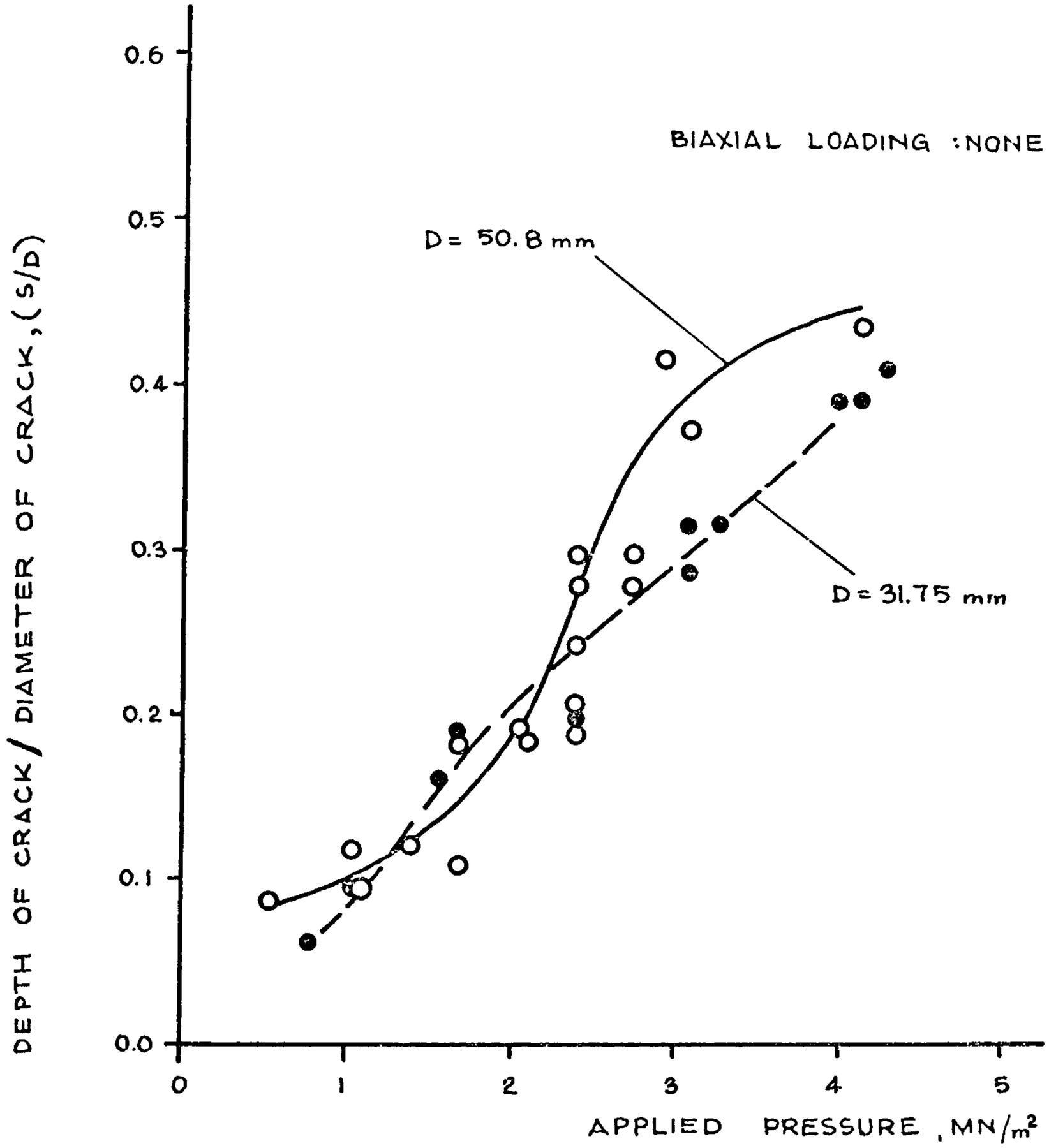

FIG. 6.28 S/D VS. PRESSURE CURVES FOR VARIOUS CRACK DEPTHS

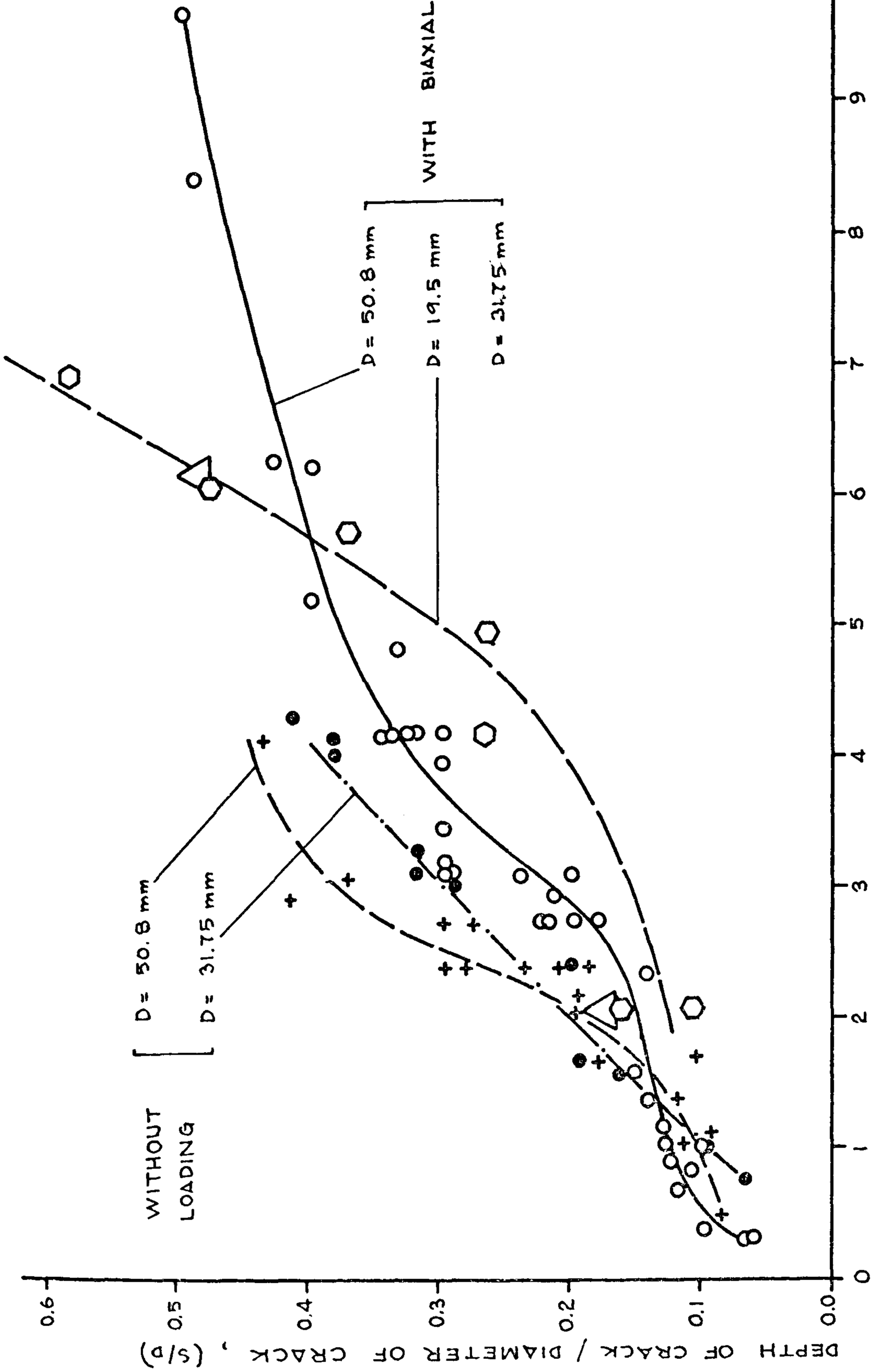

FIG. 6.23 s/D VS. PRESSURE CURVES FOR VARIOUS CRACK SIZES

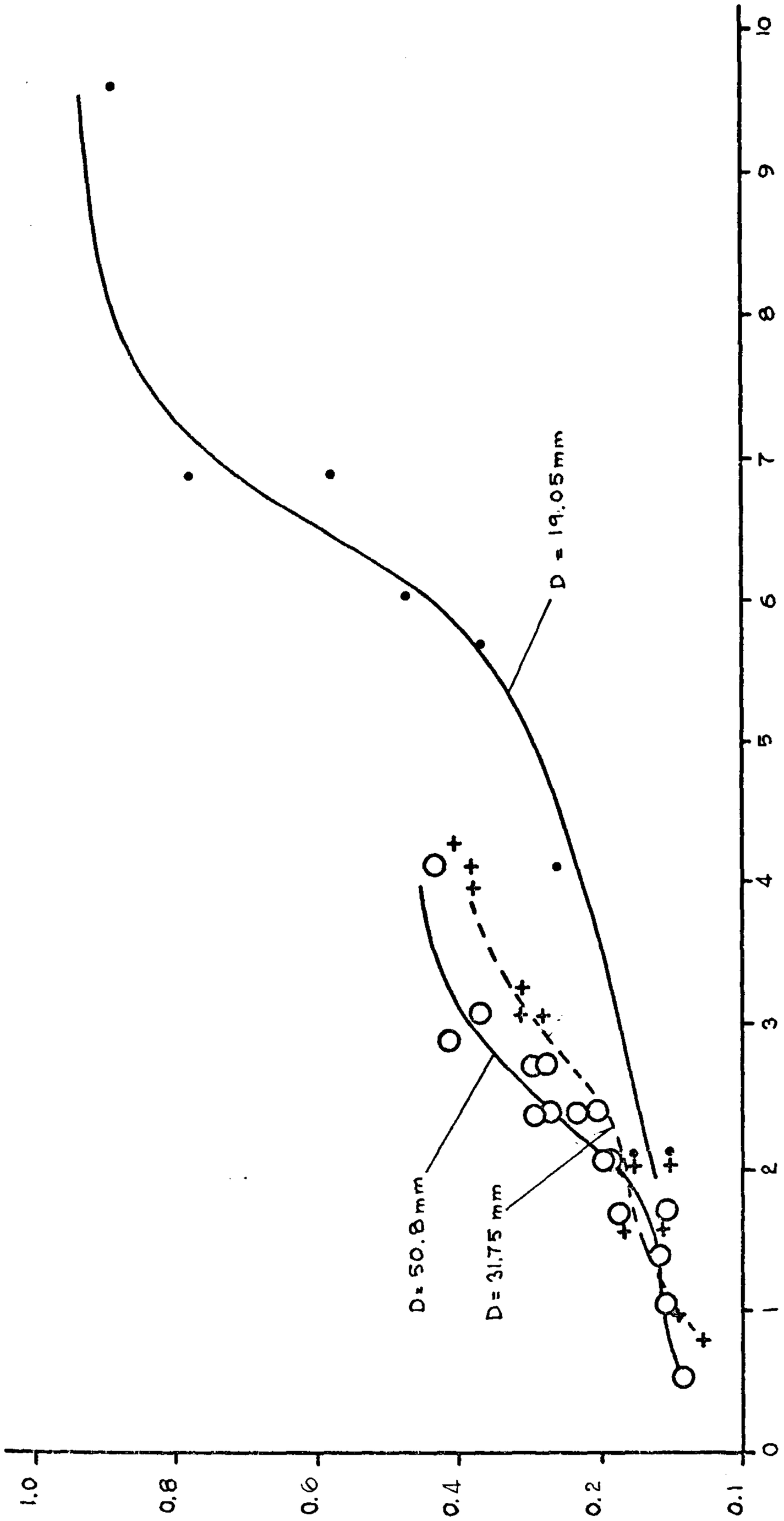

FIG. 6.30 S/D VS. PRESSURE CURVES FOR VARIOUS CRACK SIZES

failure of the material between cracks at various depths and the surface.

For this, pressure was applied in cracks of different sizes, and located at various depths, and, the pressures causing failure were recorded (Fig.6.16 to 6.30)

Fig.6.23 shows that the larger is the distance from the crack to the surface, the larger are the pressures necessary to cause failure.

It is well known that most surface spalling observed in actual fires occur in the 25mm thick layer next to the surface of concrete. Fig. 6.23 shows that, in order to cause failure of a crack of 50·8mm diameter located at a distance 25mm from the surface a pressure of 4·3 MN/m^2 is necessary. However the highest pressure recorded in pore pressure tests was 2·1 MN/m^2, and, therefore, according to Fig.6.23, was only capable to cause failure down to a depth of 10mm. It should however be remembered that Fig.6.23 is the result of tests carried out at room temperature and, at higher temperatures a pressure of 2·1 MN/m^2 may be capable of causing failure of deeper cracks. (See Chapter 8)

It can therefore be concluded that pressures recorded in 'Pore Pressure' tests are capable to cause failure outside cracks mentioned in this chapter, down to 25mm depth.

It should also be noted that Fig.6.23 is based on tests on cracks of 50·8mm diameter and, therefore, cracks of different sizes can lead to different quantitative results.

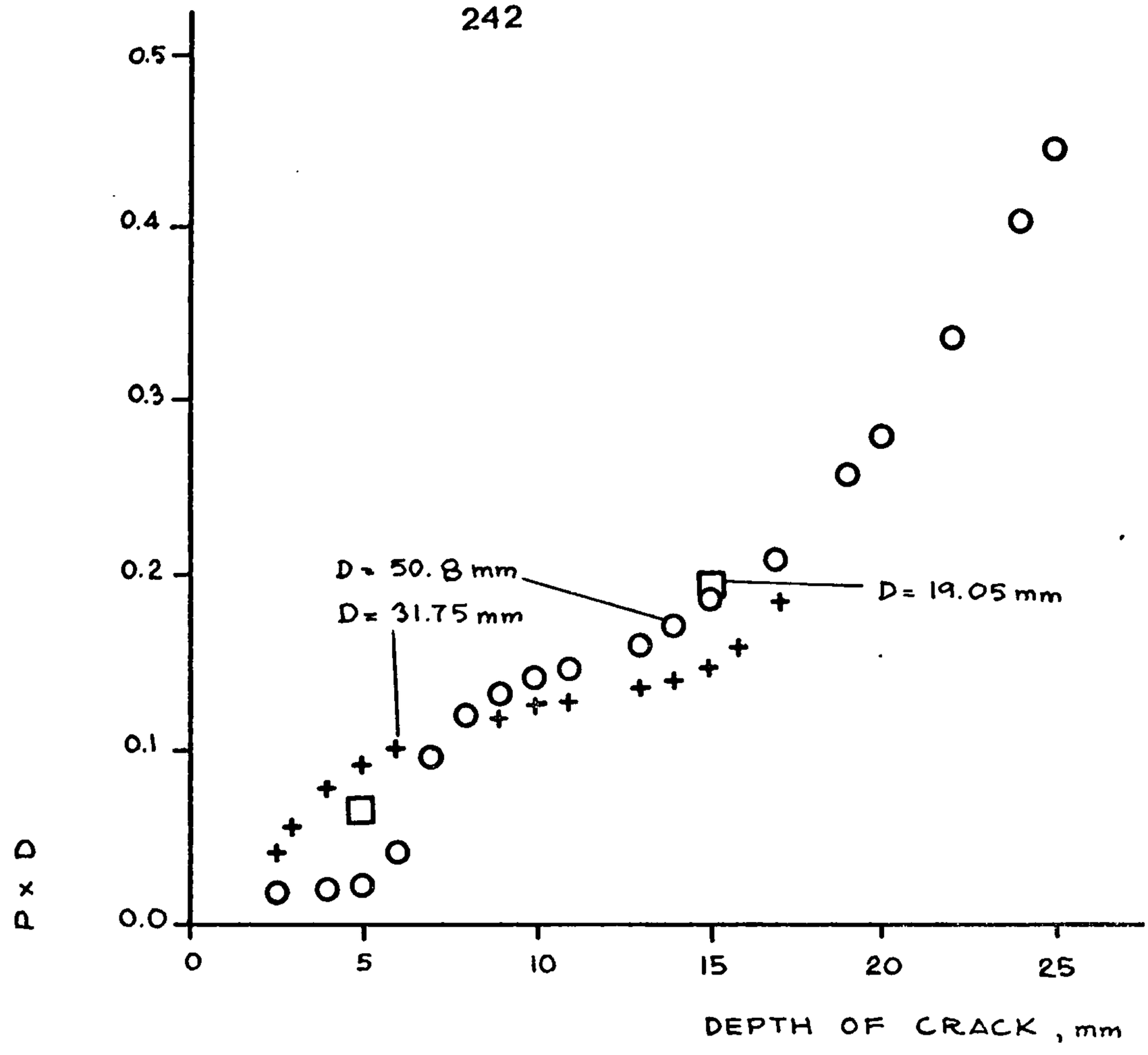

FIG. 6.32 P×D vs. CRACK DEPTH
BIAXIAL LOADING : 13.8 MN/m^2

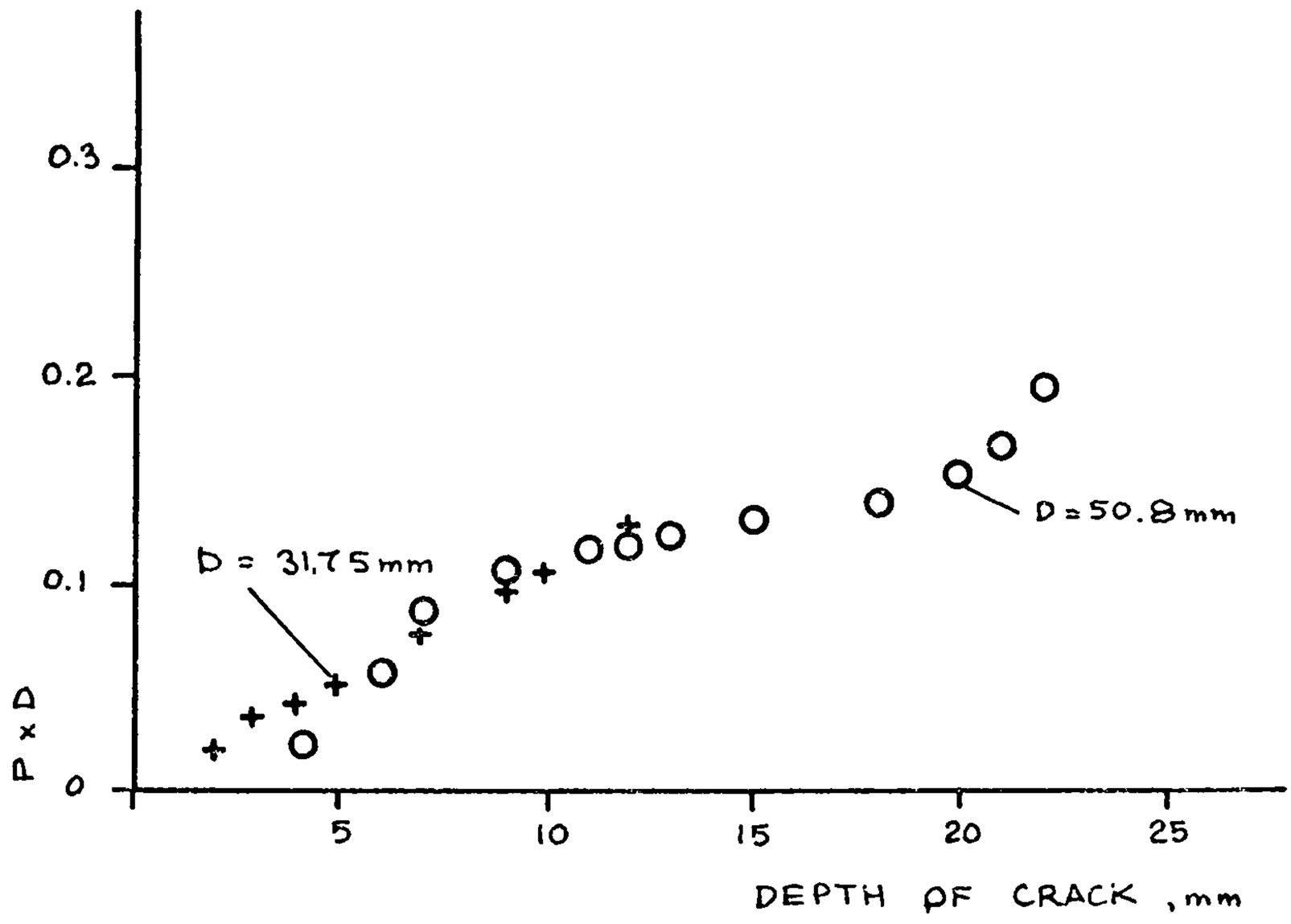

FIG. 6.33 PXD vs. CRACK DEPTH
BIAXIAL LOADING : NONE

The results on the effect of crack size will be discussed in the following section.

6.7.2 Effect of Crack Size

In tests described in this chapter three different crack sizes, namely: 19·05mm, 31·75mm and 50·08mm diameters are tested.

Fig.6.25 shows that, the depth of the crack being the same, the smaller is the size of the crack the higher is the pressure required to cause spalling.

In Fig. 6.32 the failure pressures of D=19·05mm and D=31·75mm cracks are compared with the failure pressure of D=50·08mm cracks at various depths. It is seen that at depths larger than 9mm the ratio of failure pressures are directly proportional to the ratio of crack sizes. In other words the product of failure pressure and crack diameter seem to be approximately constant for any crack size at depths in the range of 6·5 - 17mm. (Fig.6.33)

This is in agreement with the original model described in Chapter 4 (Case I and II) where it is shown that the product PD is independent of D for all practical purposes.

6.7.3 Effect of Age

In general, age of specimen did not seem to affect substantially the pressures required to cause spalling.

In fact 14 to 28 days old specimens containing cracks at a depth of 10mm from the surface required the same pressure to spall as 70 weeks old specimens.

(Fig. 6.26). However, the effect of age is gradually felt as the depth of crack increased. 70 weeks old specimens containing cracks at 20mm depth required 25% more pressure to spall than 2-4 weeks old specimens.

It is believed that the older the specimen gets the more shrinkage cracks are formed near the surface due to drying. Consequently, it is possible that at reasonably shallow depths the extra strength of the old specimens is overshadowed by the presence of these cracks.

6.7.4 Effect of Biaxial Loading

Before generalizing the conclusions reached in section 6.7.1 it is important to investigate the effect of biaxial compression on the failure of material outside the crack, because, the mechanism proposed in Chapter I assumes the existence of such compression.

The results of the Break-Out tests which involved the application of biaxial loading (Fig.6.27) show that the effect of biaxial loading is either beneficial or detrimental depending on the depth of the crack on which pressure is applied.

Biaxial loading slightly encourages spalling if cracks are less than 7mm deep. This tendency of shallow cracks to spall more easily under biaxial loading may be attributed to buckling under axial loading. On the other hand, if the cracks are deeper, biaxial loading makes spalling mo re difficult to occur.

However this effect of biaxial loading is relatively

unimportant as, say at a depth of 10mm only 33% more pressure is required under biaxial loading as opposed to tests where no loading is applied. The effect of biaxial loading gets more important as the depth of the crack increases. For instance if the crack is at a depth of 20mm, 80% more pressure is necessary to cause spalling in tests where biaxial loading is applied as compared with the ones where no loading is applied. (Fig.6.27)

This relatively small beneficial effect of biaxial loading should, however, not be exagerated, as, such loading seem to encourage spalling substantially by causing cracks parallel to the surface. (Chapter 4)

Moreover, examination of the spalled pieces showed that the surface area of the spalled pieces are larger if biaxial loading is present. (Compare Figs.6.34 to 6.41 with 6.42 to 6.48)

This may be the explanation of widespread surface damage encountered in some slabs in actual fires.

FIGS. 6.36& 6.37 SPALLED PIECES FROM SPECIMENS TESTED WITHOUT LOADING

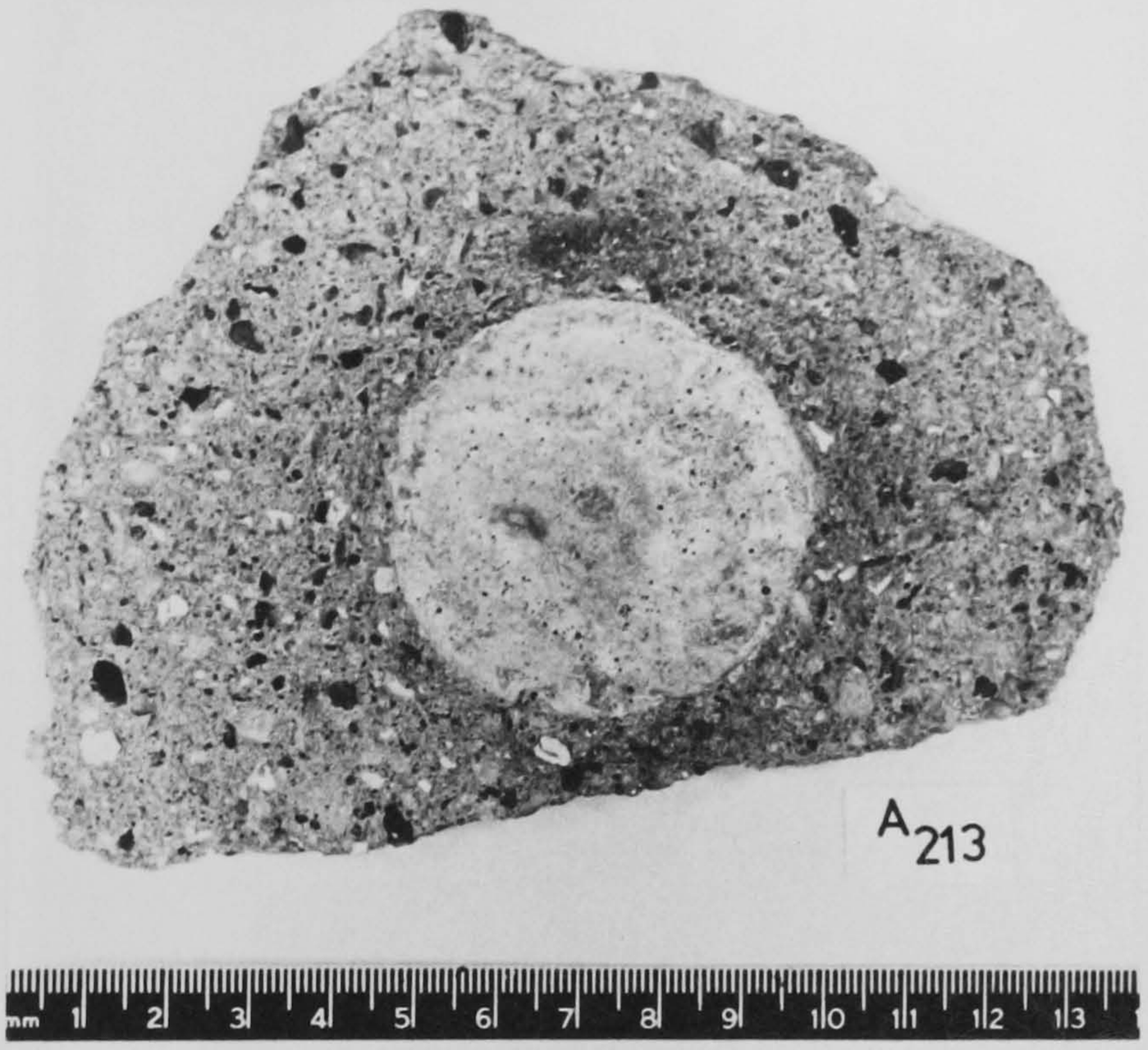

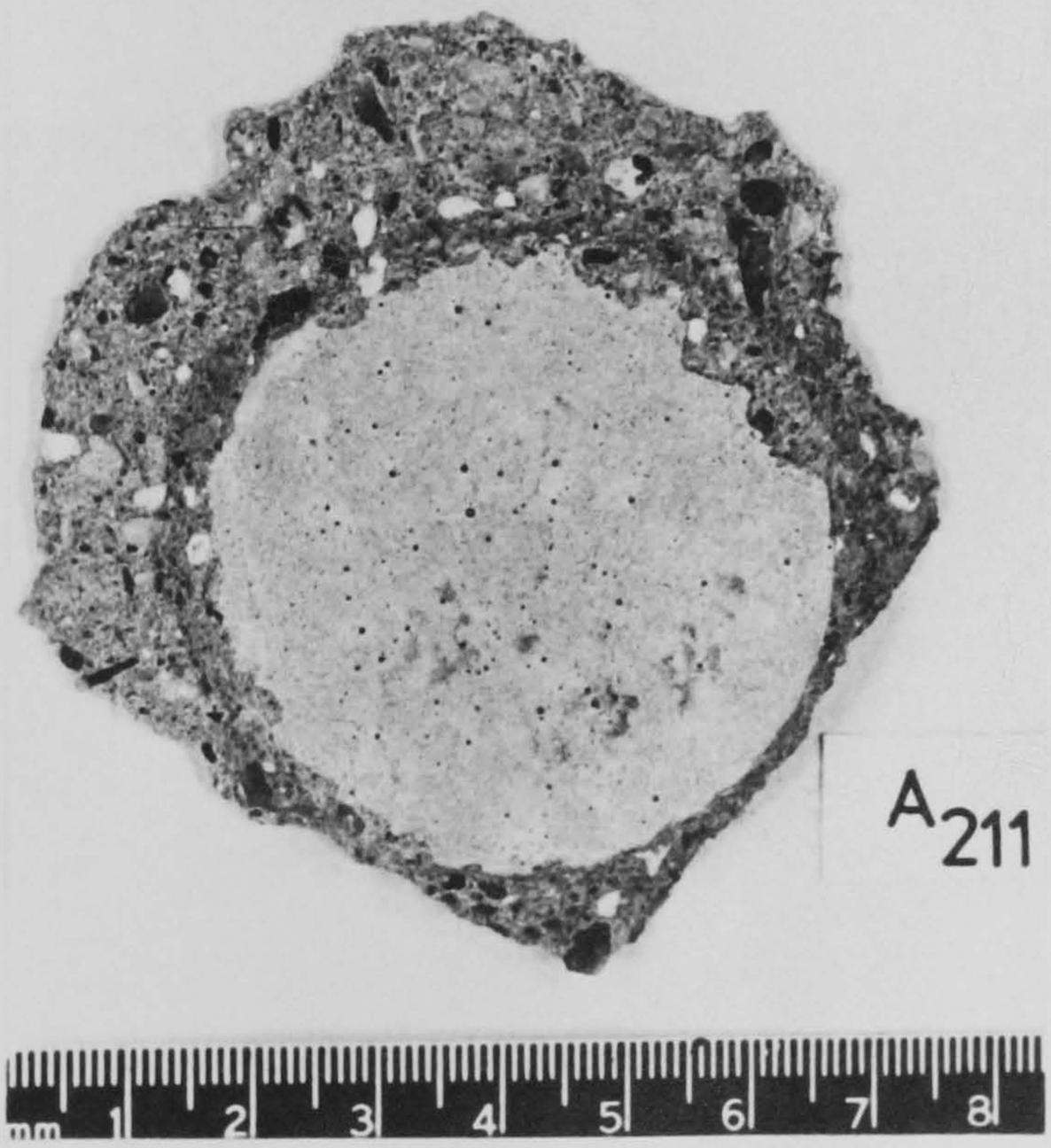

FIG. 6.38 SPALLED PIECES FROM SPECIMENS TESTED WITHOUT BIAXIAL LOADING

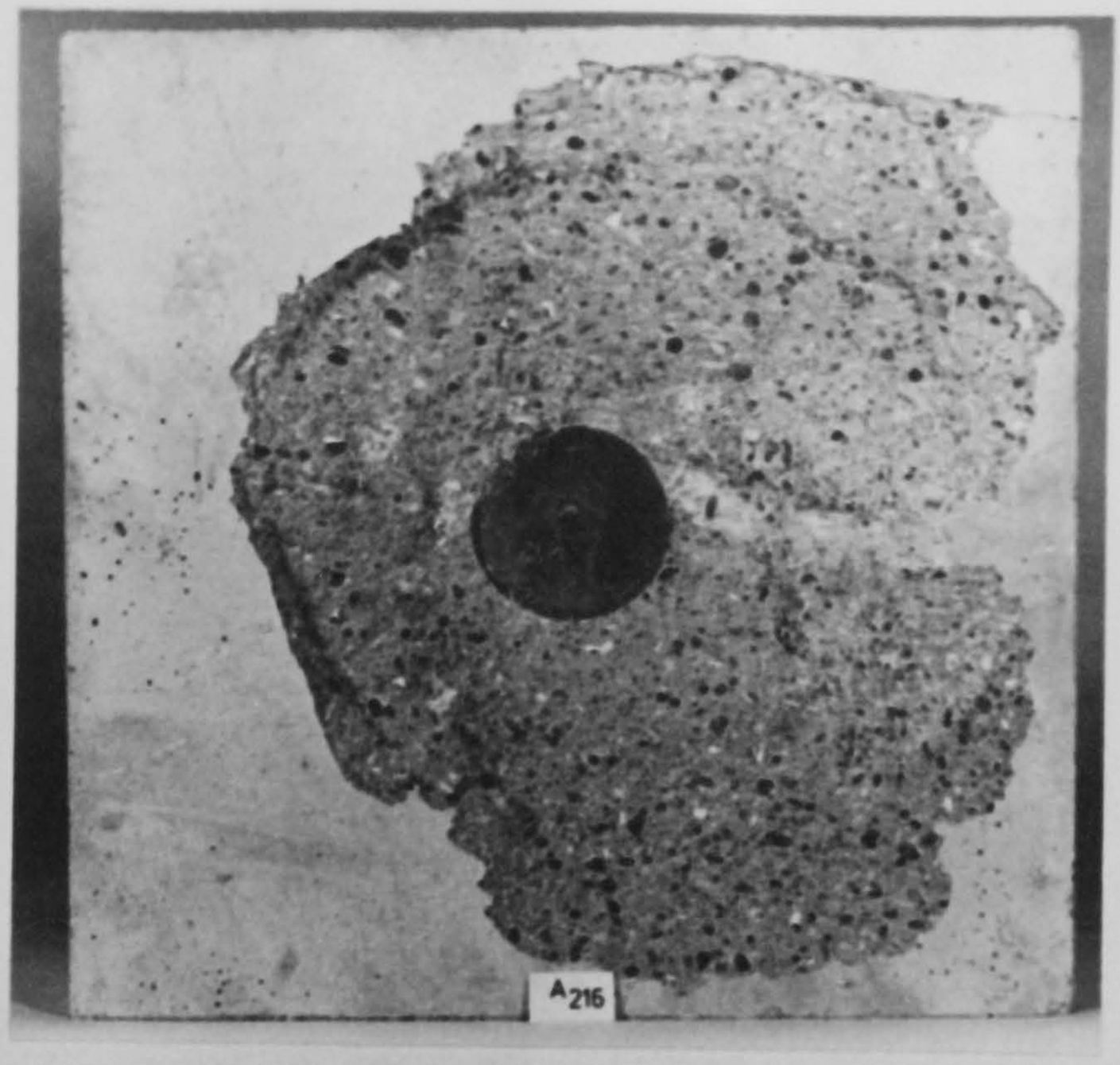

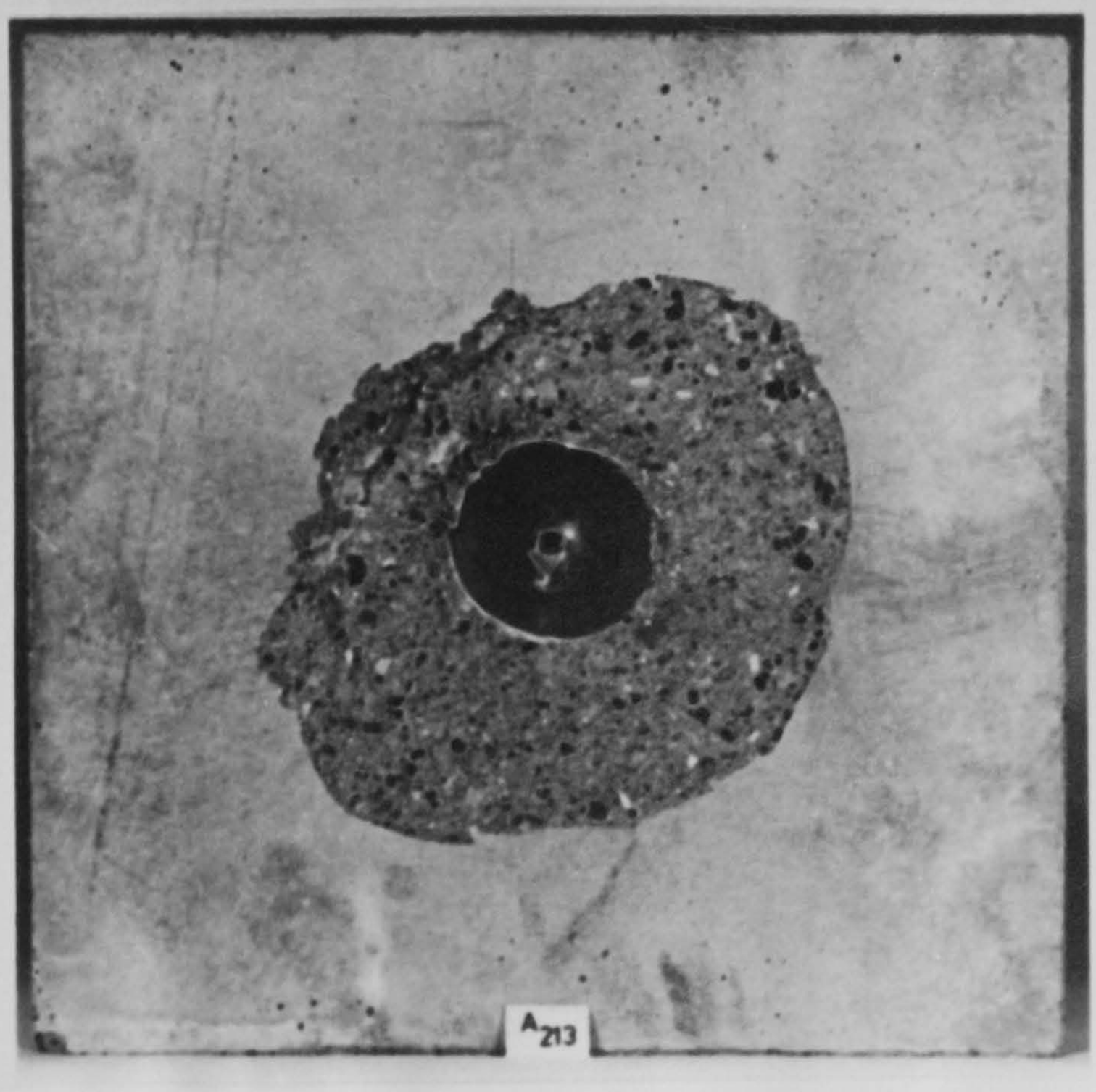

FIGS. 6.39 & 6.40 SPECIMENS AFTER TEST WITHOUT LOADING

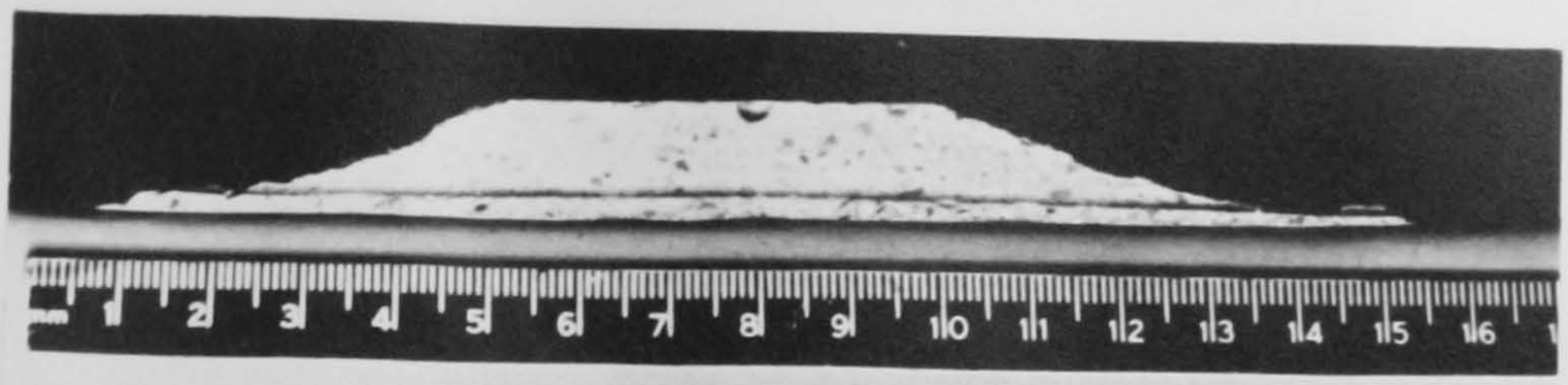

FIG. 6. 41 SPALLED PIECES FROM SPECIMENS TESTED WITHOUT LOADING

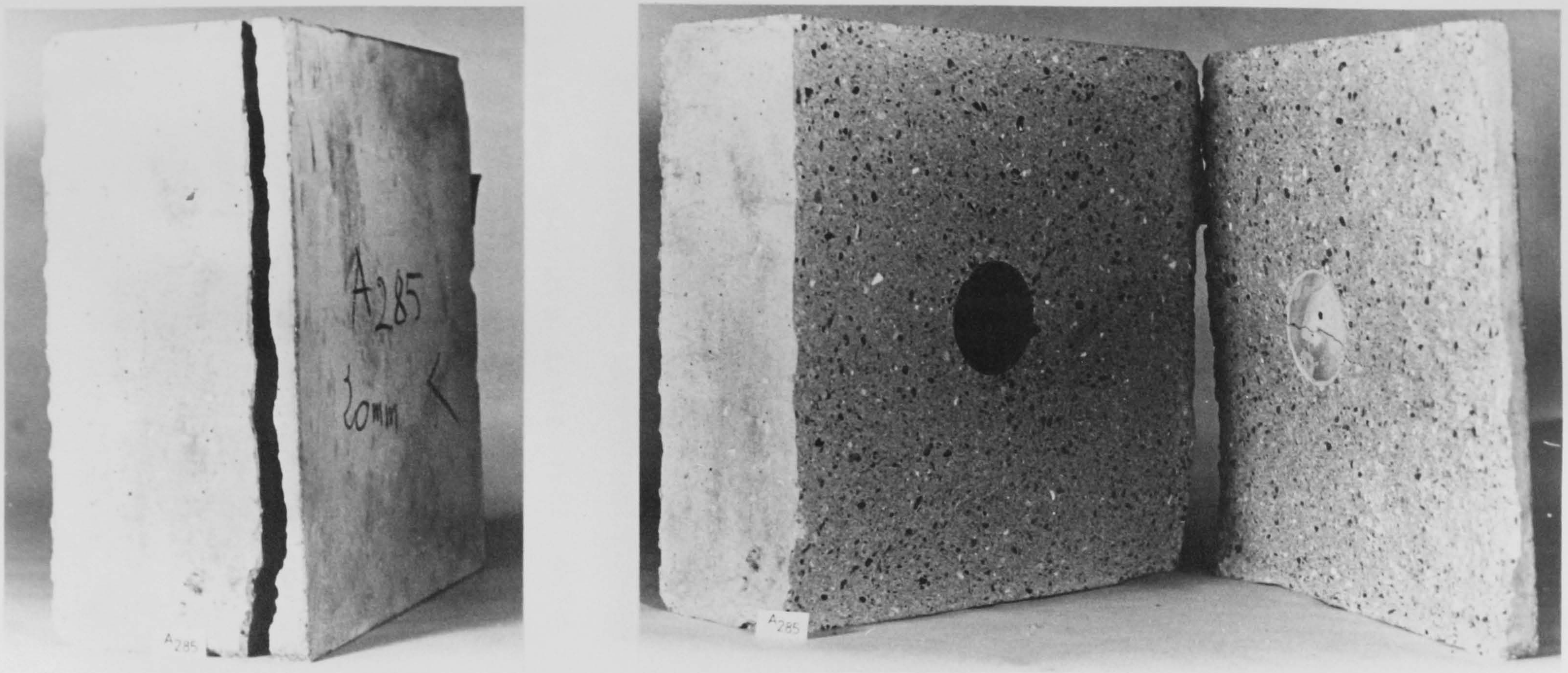

FIG. 6.42 SPECIMEN AFTER TEST WITH BIAXIAL LOADING

FIG.6.43 SPECIMEN AFTER TEST WITH BIAXIAL LOADING

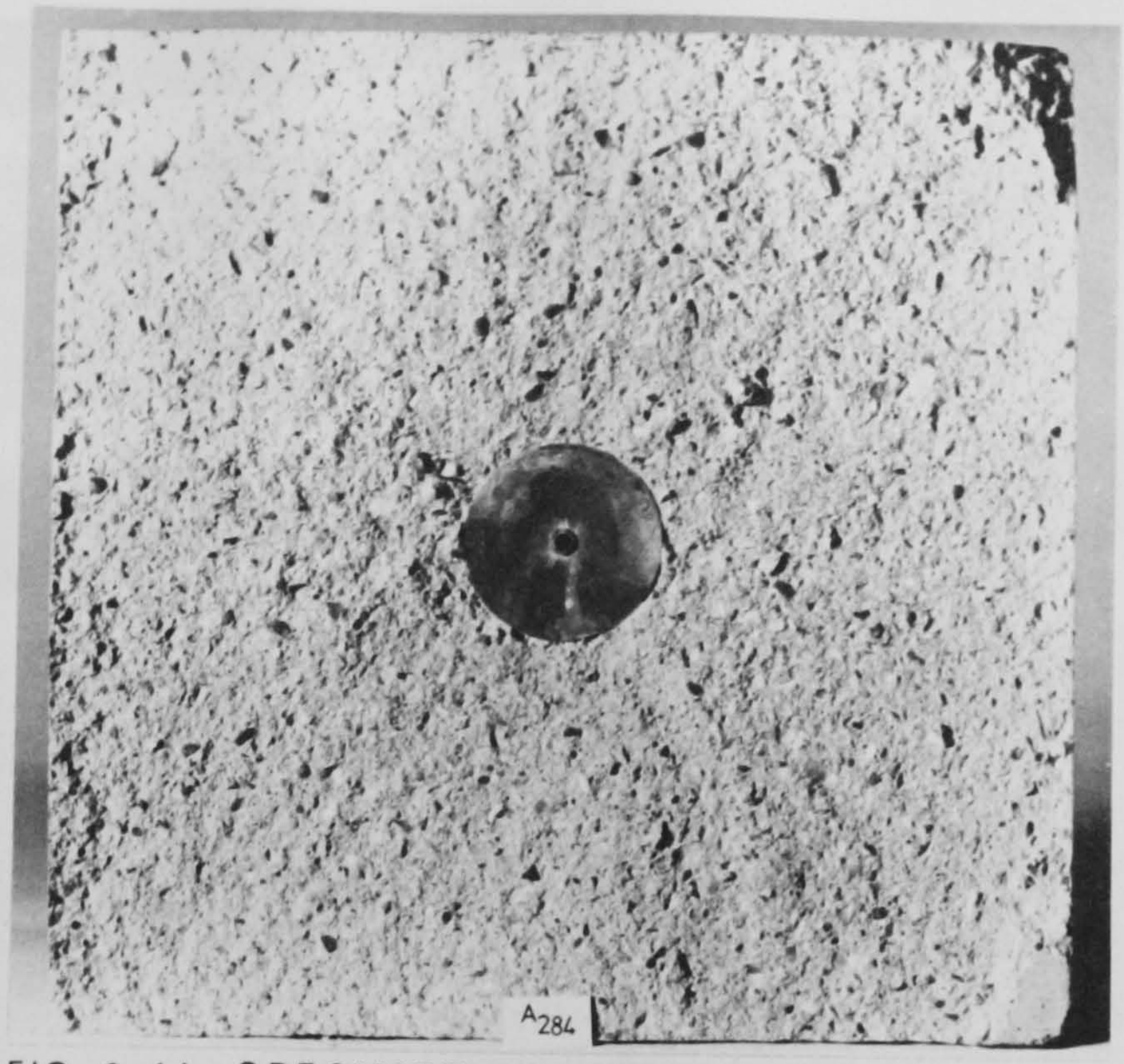

FIG. 6.44 SPECIMEN AFTER TEST WITH BIAXIAL LOADING

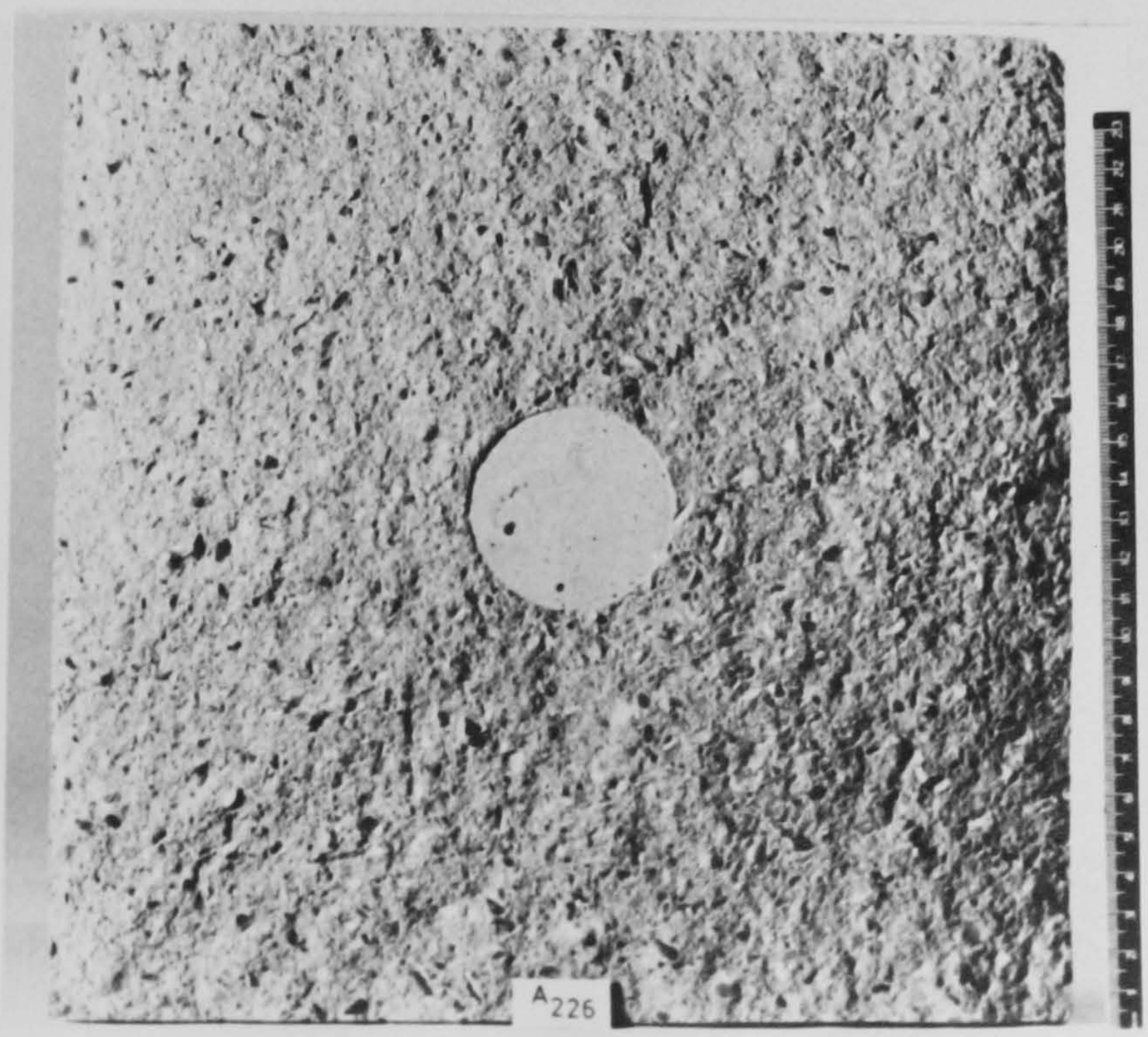

FIG. 6.45 SPALLED PIECE FROM SPECIMEN TESTED UNDER BIAXIAL LOADING

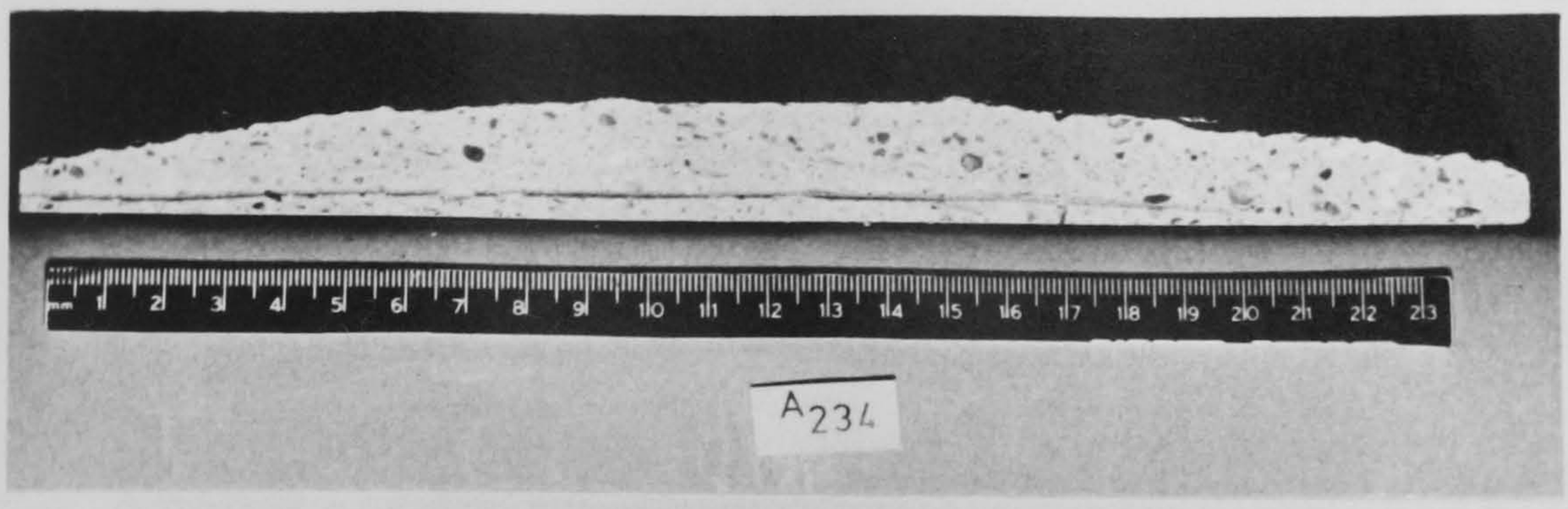

FIG. 6.46 CROSS SECTIONS OF SPALLED PIECES FROM SPECIMENS TESTED WITH BIAXIAL LOADING

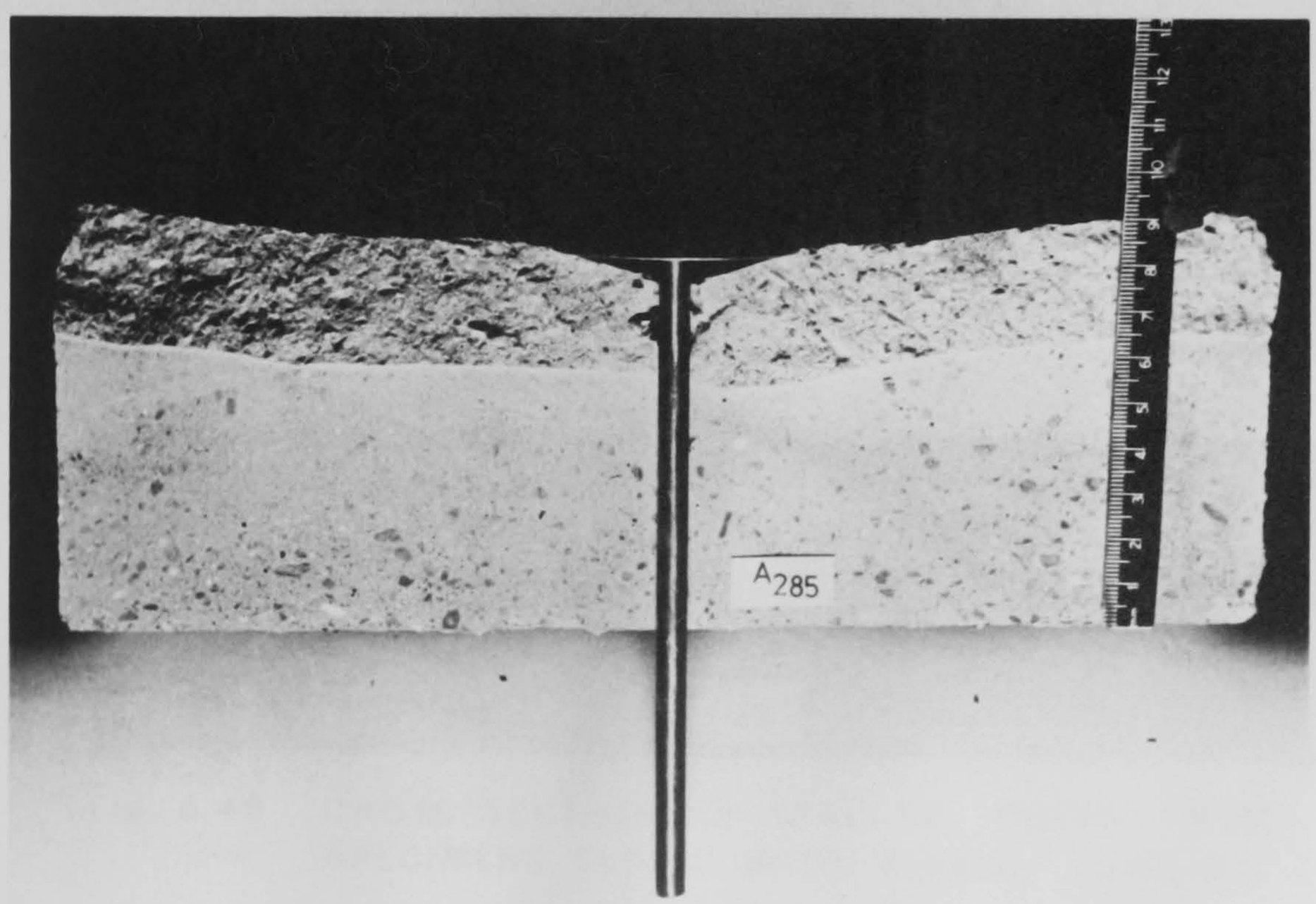

FIG. 6.47 CROSS SECTION OF THE SPECIMEN TESTED WITH BIAXIAL LOADING

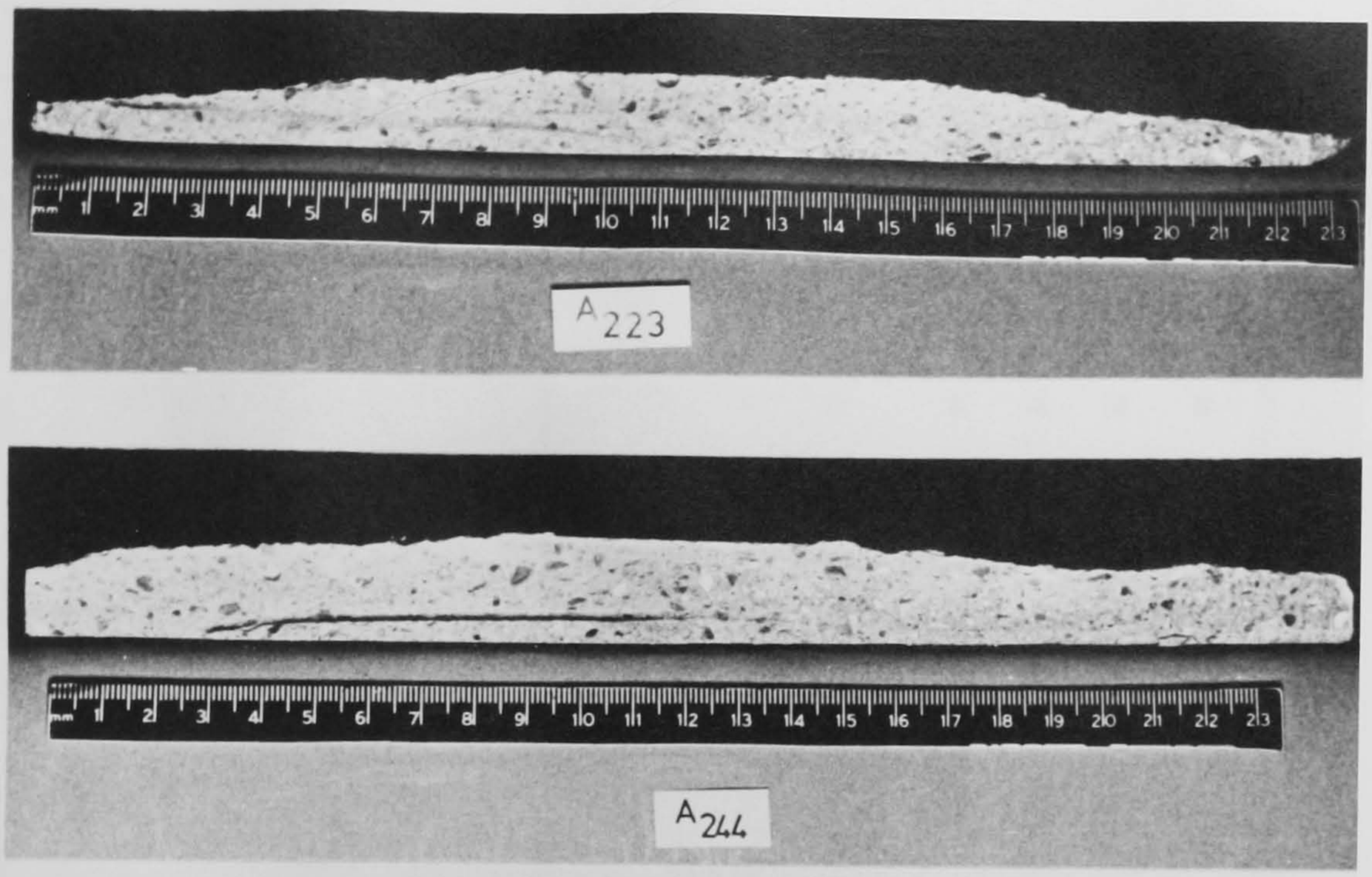

FIG. 6.48 CROSS SECTIONS OF SPALLED PIECES FROM SPECIMENS TESTED WITH BIAXIAL LOADING

Table 6.2 Break-Out test results. Loading:none.

Specimen no.	Type of pressure applied	Age, days	W/C	Curing method	Loading	Crack diameter, mm	Crack depth, mm	Applied pressure, MN/m^2	PD	S/D	Average comp. strength, MN/m^2	Average tensile strength, MN/m^2	P/σ_t
A_{I03I}	gas	I4	.50	moist	none	3I.7	I0	3.I0	98.4	.3I	39.8	2.9	I.07
A_{I032}	"	"	"	"	"	"	I0	3.27	I03.8	.3I	"	"	I.I4
A_{I033}	"	"	"	"	"	"	I2	4.I3	I3I.I	.37	"	"	I.42
A_{I034}	"	"	"	"	"	"	I2	4.00	I27.0	.37	"	"	I.38
A_{I04I}	"	"	"	"	"	"	2	.79	25.0	.06	"	"	.27
A_{I042}	"	"	"	"	"	"	6	I.72	54.6	.I9	"	"	.59
A_{I043}	"	"	"	"	"	"	5	I.59	50.5	.I5	"	"	.55
A_{I044}	"	"	"	"	"	"	I3	4.28	I35.9	.4I	"	"	I.48

Table 6.2 (Cont.) Break-Out test results. Loading:none.

Specimen shape													
P/σ_t													
Average tensile strength, , MN/m^2													
Average comp. strength, , MN/m^2													
S/D													
PD													
Applied pressure MN/m^2													
Crack depth, mm													
Crack diameter, mm													
Biaxial loading MN/m^2													
Curing type													
W/C													
Age , days													
Type of applied pressure													
Specimen no.													
A_{I09I}	gas	I4	.50	moist	none	50.8	9.0	I.72	87.4	.I8	39.8	2.9	.59	
A_{I092}	"	"	"	"	"	"	I9.0	I.72	I57.5	.37	"	"	I.07	"
A_{I093}	"	"	"	"	"	"	I4.0	2.75	I39.7	.28	"	"	.94	"
A_{I094}	"	"	"	"	"	"	I5.0	2.4I	I22.4	.30	"	"	.83	"
A_{I095}	"	"	"	"	"	"	2I.0	2.93	I48.8	.4I	"	"	I.oI	"
A_{II0I}	"	"	"	"	"	"	4.3	.52	26.4	.90	"	"	.I8	"
A_{II02}	"	"	"	"	"	"	6.0	I.38	70.I	.I2	"	"	.48	"
A_{II03}	"	"	"	"	"	"	5.8	I.04	52.8	.II	"	"	.36	"
A_{II04}	"	"	"	"	"	"	22.0	4.I4	2I0.3	.43	"	"	.I4	"

Table 6.2 (Cont.) Break-Out test results. Loading:none.

Specimen no.	Type of pressure applied	Age, days	W/C	Curing method	Loading	Crack diameter, mm	Crack depth, mm	Applied pressure, MN/m^2	PD	S/D	Average comp. strength, MN/m^2	Average tensile strength, MN/m^2	P/σ_t
A_{20II}	water	28	.40	6W + 2IM	none	50.8	5	I.06	53.8	.09	47.0	3.2	.33
A_{20I2}	"	"	"	"	"	"	I0	2.4I	I22.4	.I8	"	"	.75
A_{20I3}	"	"	"	"	"	"	I0	2.4I	I22.4	.I8	"	"	.75
A_{20I4}	"	"	"	"	"	"	I5	2.76	I40.2	.30	"	"	.86
A_{206I}	"	49I	.45	moist	"	"	9.7	2.07	I05.0	.I9	45.44	3.0	.68
A_{2062}	"	"	"	"	"	"	II.6	2.75	I42.3	.23	"	"	.90
A_{2063}	"	"	"	"	"	"	I3.7	2.76	I45.6	.27	"	"	.90
A_{2064}	"	"	"	"	"	"	I7.0	3.38	I73.9	.33	"	"	I.I2
A_{2065}	"	"	"	"	"	"	I9.5	3.62	I86.4	.38	"	"	I.I8
A_{2066}	"	"	"	"	"	"	I9.I	3.96	203.6	.38	"	"	I.30

Table 6.3 Break-Out test results. Loading:I3.8 MN/m^2

Specimen shape	P/σ_t	Average tensile strength, MN/m^2	Average comp. strength, MN/m^2	S/D	PD	Applied pressure, MN/m^2	Crack depth, mm	Crack diameter, mm	Biaxial loading MN/m^2	Curing method	W/C	Age, days	Type of pressure applied	Specimen no.
"	.34	3.04	45.4	.I3	52.3	I.03	6.4	50.8	I3.8	moist	.45	I4	gas	A_{IIII}
"	.52	"	"	.I5	80.9	I.59	7.5	"	"	"	"	"	"	A_{III2}
"	.27	"	"	.I2	42.I	.83	6.0	"	"	"	"	"	"	A_{III3}
"	.I2	"	"	.06	I7.8	.35	3.0	"	"	"	"	"	"	A_{II2I}
"	.I3	"	"	.I0	I9.3	.38	5.0	"	"	"	"	"	"	A_{II22}
"	.46	"	"	.I4	70.I	I.38	7.0	"	"	"	"	"	"	A_{II23}
"	.9I	"	"	.I8	I40.2	2.76	9.0	"	"	"	"	"	"	A_{II24}
"	.97	"	"	.22	I48.9	2.93	II.0	"	"	"	"	"	"	A_{II25}
"	I.02	"	"	.30	I57.5	3.I0	I5.0	"	"	"	"	"	"	A_{II26}
"	I.36	"	"	.34	2I0.3	4.I4	I7.0	"	"	"	"	"	"	A_{II27}

Table 6.3 (Cont.) Break-Out test results. Loading:I3.8 MN/m^2

Specimen no.	A_{I07I}	A_{I072}	A_{I073}	A_{I08I}	A_{I082}
Type of pressure applie	gas	"	"	"	"
Age , days	I4	"	"	"	"
W/C	.50	"	"	"	"
Curing type	moist	"	"	"	"
Biaxial loading MN/m^2	none	"	"	"	"
Crack diameter, MN/m^2	50.8	"	"	"	"
Crack depth, mm	I2.0	9.6	I4.0	9.7	5.3
Applied pressure MN/m^2	2.4I	2.07	2.4I	2.07	I.72
PD	I22.4	I05.I	I22.4	I05.6	87.3
S/D	.24	.I9	.28	.I9	.II
Average comp. strength, MN/m^2	39.8	"	"	"	"
Average tensile strength, MN/m^2	2.9	"	"	"	"
P/σ_t	.83	.7I	.83	.7I	.59
Specimen shape		"	"	"	"

Table 6.3 (Cont.) Break-Out test results. Loading:I3.8 $MN/_m{}^2$

Specimen shape													
P/σ_t													
Average tensile strength, $MN/_m{}^2$													
Average comp. strength, $MN/_m{}^2$													
S/D													
PD													
Applied pressure, $MN/_m{}^2$													
Crack depth, mm													
Crack diameter, mm													
Biaxial loading $MN/_m{}^2$													
Curing method													
W/C													
Age , days													
Type of pressure applied													
Specimen no.													
A_{208I}	water	I4	.45	moist	I3.8	50.8	20	6.20	3I4.9	.39	45.4	3.0	2.04	
A_{2082}	"	"	"	"	"	"	I7	4.I4	2I0.3	.34	"	"	I.36	"
A_{2083}	"	"	"	"	"	"	5	I.03	52.3	.98	"	"	.34	"
A_{2084}	"	"	"	"	"	"	II	2.76	I40.2	.22	"	"	.9I	"
A_{I05I}	gas	"	.50	"	none	3I.8	3.0	I.03	32.7	.94	39.8	2.9	.36	
A_{I052}	"	"	"	"	"	"	6.3	2.4I	76.5	.20	"	"	.83	"
A_{I053}	"	"	"	"	"	"	9.0	3.I0	98.4	.28	"	"	I.07	"

Table 6.3 (Cont.) Break-Out test results. Loading:I3.8 $MN/_m2$

Specimen no.	Type of pressure applied	Age , days	W/C	Curing method	Biaxial loading $MN/_m^2$	Crack diameter, mm	Crack depth, mm	Applied pressure $MN/_m^2$	PD	S/D	Average comp. strength, $MN/_m^2$	Average tensile strength, $MN/_m^2$	P/σ_t	Specimen shape
A_{202I}	water	28	.40	6W+2IM	I3.8	50.8	5	.69	35.I	.I2	47.0	3.2	.22	
A_{2022}	"	"	"	"	"	"	I0	3.I0	I57.5	.20	"	"	.97	"
A_{2023}	"	"	"	"	"	"	I5	3.45	I75.3	.30	"	"	I.08	"
A_{2024}	"	"	"	"	"	"	I5	4.I8	202.4	.30	"	"	I.3I	"
A_{2025}	"	"	"	"	"	"	20	5.I7	262.6	.40	"	"	I.62	"
A_{2026}	"	"	"	"	"	"	25	9.65	490.2	.49	"	"	3.02	"
A_{204I}	"	"	"	"	"	"	I0	2.74	I39.2	.20	"	"	.85	"
A_{2042}	"	"	"	"	"	"	I5	3.I0	I57.5	.30	"	"	.97	"
A_{2043}	"	"	"	"	"	"	20	3.45	I75.2	.40	"	"	I.08	"
A_{2044}	"	"	"	"	"	"	25	6.90	350.5	.49	"	"	2.I6	"

Table 6.3 (Cont.) Break-Out test results. Loading:I3.8 $MN/_m^2$

Specimen shape													
P/σ_t													
Average tensile strength, $MN/_m^2$													
Average comp. strength, $MN/_m^2$													
S/D													
PD													
Applied pressure $MN/_m^2$													
Crack depth, mm													
Crack diameter, mm													
Biaxial loading, $MN/_m^2$													
Curing method													
W/C													
Age, days													
Type of pressure applied													
Specimen no.													
A_{II4I}	gas	I4	.45	moist	I3.8	I9.05	5.0	4.9	94.5	.26	45.4	3.0	I.63	
A_{II42}	"	"	"	"	"	3I.75	5.0	2.0	65.7	.I6	"	"	.68	"
A_{II43}	"	"	"	"	"	"	I5.0	6.I	I94.2	.47	"	"	2.02	"
A_{II44}	"	"	"	"	"	50.80	3.0	.3	I7.3	.06	"	"	.II	"
A_{II45}	"	"	"	"	"	"	7.0	2.4	II8.9	.I4	"	"	.77	"
A_{II46}	"	"	"	"	"	"	II.0	3.I	I57.5	.30	"	"	I.02	"
A_{II47}	"	"	"	"	"	"	I5.0	3.9	20I.2	.30	"	"	I.30	"

Table 6.3 (Cont.) Break-Out test results. Loading:I3.8 $MN/_m{}^2$

Specimen shape	P/σ_t	Average tensile strength, $MN/_m{}^2$	Average comp. strength, $MN/_m{}^2$	S/D	PD	Applied pressure, $MN/_m{}^2$	Crack depth, mm	Crack diameter, mm	Biaxial loading, $MN/_m{}^2$	Curing method	W/C	Age, days	Type of pressure applied	Specimen no.
A_{II3I}	gas	I4	.45	moist	I3.8	I9.05	2.0	2.07	39.4	.I0	45.4	3.0	.68	
A_{II32}	"	"	"	"	"	"	3.0	2.07	39.4	.I6	"	"	.68	"
A_{II33}	"	"	"	"	"	"	5.0	4.I4	78.8	.26	"	"	I.36	"
A_{II34}	"	"	"	"	"	"	7.0	5.69	I08.4	.37	"	"	I.87	"
A_{II35}	"	"	"	"	"	"	9.0	6.03	II4.8	.47	"	"	I.98	"
A_{II36}	"	"	"	"	"	"	II.0	6.90	I3I.4	.57	"	"	2.27	"
A_{II37}	"	"	"	"	"	"	I4.6	6.90	I34.4	.76	"	"	2.27	"
A_{II38}	"	"	"	"	"	"	I7.0	9.65	I83.8	.89	"	"	3.I7	"

Chapter 7

FRACTURE MECHANICS VIEW OF THE BREAK-OUT TESTS

7.1 Introduction

It was noted in Chapters I and 4 that, in some circumstances, cracks may be present in concrete even before the start of heating. In addition, it was noted that biaxial compression induced by heating tends to produce cracks in the plane of compression, and that these cracks are known to be of appreciable size. In this chapter, we look at the stability of such cracks under internal pressure as might occur if they were filled with steam or pore water under pressure. The approach is to use the techniques of linear elastic fracture mechanics. Before doing this some background is given in the next few paragraphs.

7.2 Background Material

Pre-existing cracks have long been recognised as starters of failure. In 1913, Inglis (7.1) confirmed this view by studying the stress distribution around elliptical holes. Although his calculations showed that the stresses at the tip of an elliptical crack are much larger than elsewhere, they didnot indicate the conditions under which a crack would extend to failure. Griffith (7.2), in 1920, was the first to provide this condition. Based on the assumption that the free energy of a cracked body and the applied forces should not increase during crack extension, he derived the expression,

$$\sigma_c = A\left(\frac{\delta E}{c(1-\nu^2)}\right)^{1/2} \qquad (7.1)$$

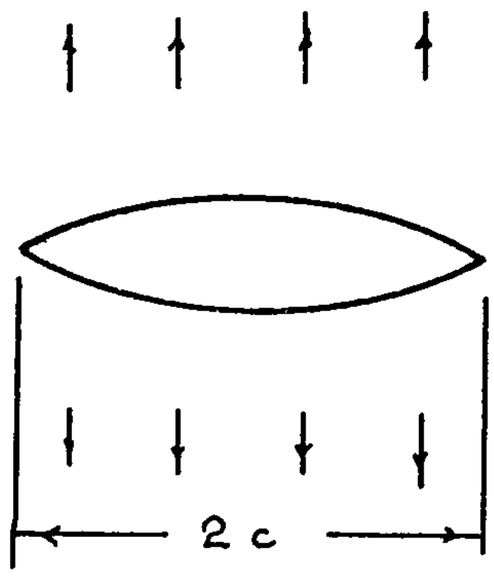

FIG. 7.1

FIG. 7.2

where, A is a numerical constant which depends on the crack geometry and location, the mode of loading, and the dimension of the body, σ_c, the measured strength, c, the size of crack, E and ν, the elastic constants, γ, the surface energy.

Griffith has effectively considered a crack of dimension c and a vertical crack extension of an amount δ_c. He based his analysis on the idea that the crack (Fig.7.1) would grow if the rate of release of strain energy $-\frac{\partial U}{\partial c}\delta_c$ was greater than the rate of work required to form new surfaces.

Thus the crack would propagate if

$$-\frac{\partial u}{\partial c}\delta c \geqslant 4\gamma\delta_c \qquad (7.2)$$

Irwin (7.3) extended this notion by taking the term on the left hand side to be the rate of release of strain energy (which he called G) from the elastic region beyond the crack tip, and by assuming that any forms of energy dissipation occurring in the crack tip region could be included on the right hand side as a kind of surface energy. This allows Griffith's purely elastic theory to be applied to materials in which there is a small amount of yielding in the vicinity of the crack tip (Fig.7.2). When the amount of yielding is small, the work done in extending the crack a unit amount can still be regarded as material constant. Thus, for this case of small scale yielding, the crack will propagate if the strain energy release rate G becomes equal to

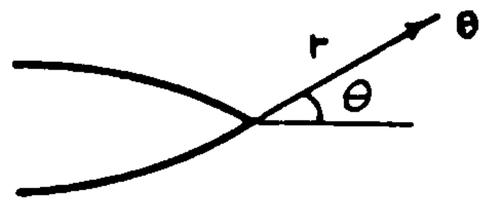

FIG. 7.3

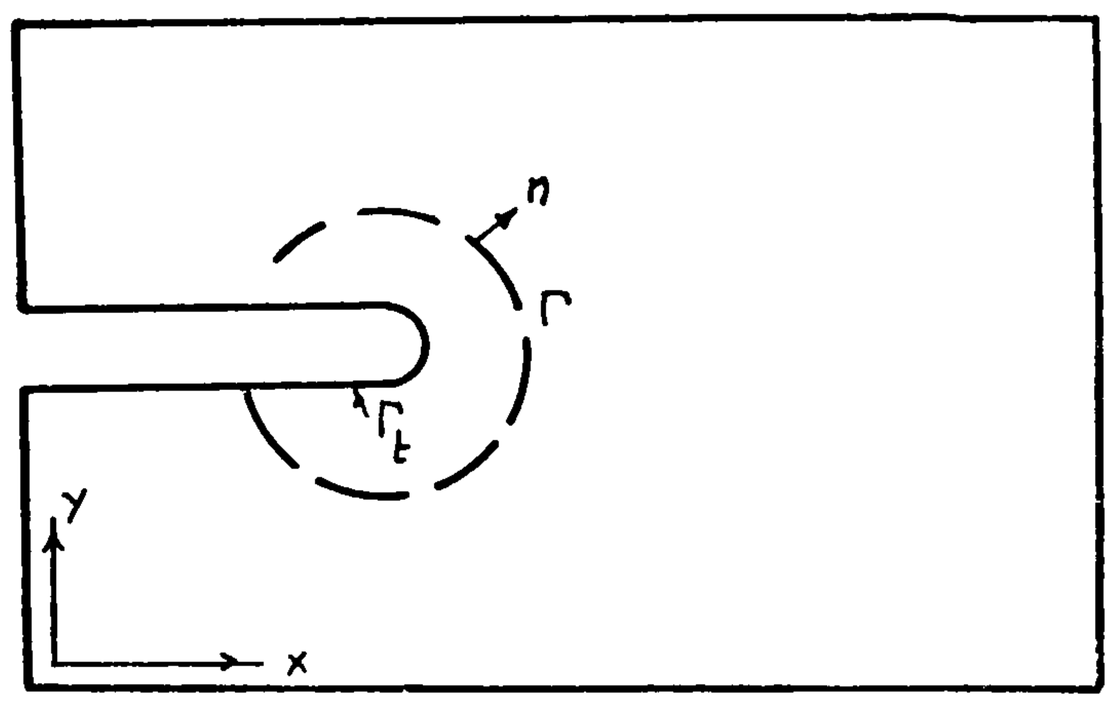

FIG. 7.4 FLAT SURFACED NOTCH
IN TWO-DIMENSIONAL DEFORMATION FIELD

[AFTER, RICE (7.4)]

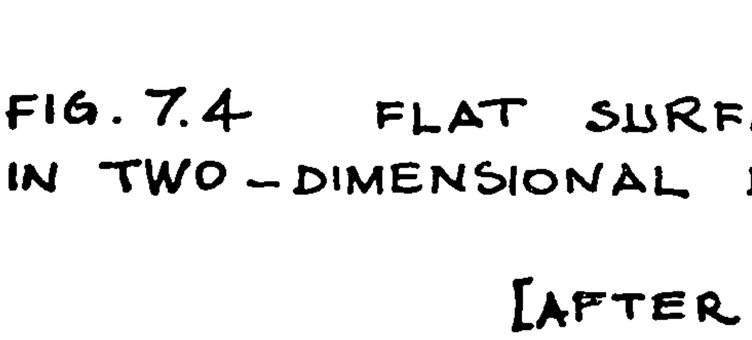

FIG. 7.5

some critical value G_c, i.e. propagation occurs for,

$$G \geqslant G_c \qquad (7.3)$$

In calculating G, the strain energy release rate, Irwin noted that the stress in the vicinity of the crack tip could be expressed in terms of a stress intensity factor K. Thus if the crack (Fig.7.3) is supposed to open as in pure tension the additional stresses due to the pressure of the crack are given by:

$$\sigma_{ij} = \frac{K_1}{(2\pi r)^{1/2}} \; f_{ij}(\theta) \qquad (7.4)$$

where, K, is the stress intensity factor. Thus G can be determined in terms of K_1 and the critical value G_c corresponds to critical value of $K = K_{1c}$

The basis of fracture mechanics is the elastic analysis of the region outside the crack tip which shows a stress-strain field with a singularity at the crack tip. One measure of the strength at the crack tip singularity is the stress intensity factor K, mentioned earlier on. Fracture occurs for a critical value of K, namely K_{1c}.

The calculation of stress intensity factor or the strain energy release rate can be considerably simplified by using the 'J integral' technique devised by Rice (7.4). This is now described in outline.

7.3 J Integral Technique

Rice (7.4) considered the integral

$$J = \int_c \left(W \, dy - T_i \frac{\partial u_i}{\partial x} \, ds \right) \qquad (7.5)$$

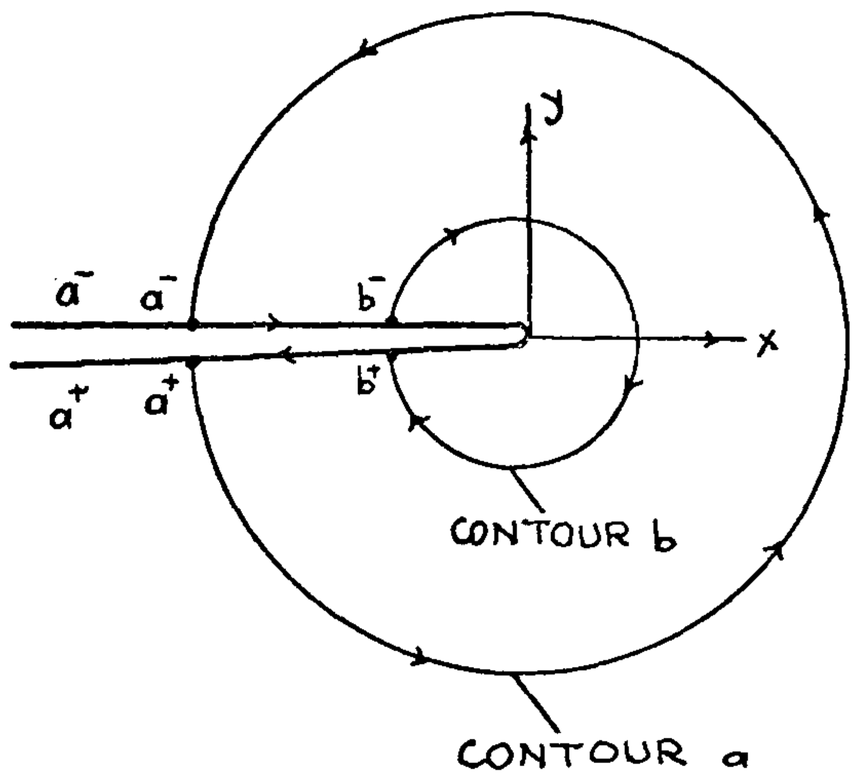

FIG. T.6

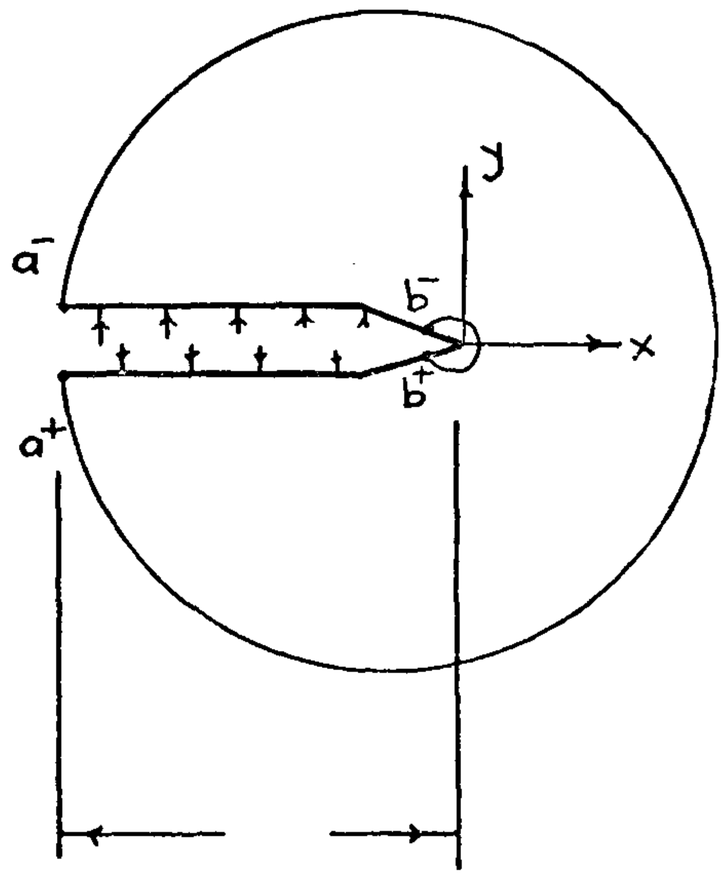

FIG. T.7

where W is the potential energy function and T_i is the surface traction vector on the contour c so that $T_i = \sigma_{ij} n_j$ u_i is the displacement vector, and ds is an element of arc length along c. (Fig.7.4).

He showed that,

$$J = 0 \qquad (7.6)$$

for any closed contour c (Fig.7.5) for which the displacement components u_i and the tractions T_i are continuous functions of the arc length s.

Now let us consider the integration path in the vicinity of the crack tip shown in Fig.7.6. This contour starts at a^+ on one side of the crack, meets the crack again on the other side at a^- and follows the upper edge of the crack to b^-. Thus the contour goes outside the crack tip to b (opposite b^-) and follows the bottom edge of the crack to its starting point a^+.

As this is a closed circuit,

$$J = J_{a^+ \to a^-} + J_{a^- \to b^-} + J_{b^- \to b^+} + J_{b^+ \to a^+} = 0 \qquad (7.7)$$

For a traction free crack, the contributions from the contours along the edges of the crack to the J integral are both zero.

Now we can write,

$$J_{a^+ \to a^-} = J_a \qquad (7.8)$$

and

$$J_{b^+ \to b^-} = J_b \qquad (7.9)$$

so that J_a is the value of the J integral computed for a contour 'a' from a point on one side of a crack to

the corresponding point on the opposite face evaluated in the anticlockwise direction. Then, for the stress free crack,

$$J_a = J_b \qquad (7.10)$$

i.e. the result is independent of the contour chosen.

Next, we note that the contour $b^+ \rightarrow b^-$ could be shrunk and taken close to the crack tip so it would have apparently a negligible length. Clearly the only terms contributing to J_b are those due to the singularity at the crack tip and the corresponding value of the integral can be found using an arbitrary contour such as 'a'. J_a is thus a measure of the crack tip singularity for a stress free crack and for the case of linear elasticity or small scale yielding, Rice showed that

$$J_a = \frac{1-\nu^2}{E} K_I^2 \qquad \text{in plain strain} \quad (7.11)$$

or

$$J_a = \frac{K_I^2}{E} \qquad \text{in plain stress} \quad (7.12)$$

This result has to be modified when the crack carries internal pressure. We recognise that we require the value of J_b when both b^+ and b^- are close to the crack tip, but note that there will be terms arising from the contours along the crack edge in this case. Thus,

$$J_{\text{crack tip}} = J_a + J_{a^- \rightarrow b^-} + J_{b^+ \rightarrow a^+} \qquad (7.13)$$

Taking a slit crack with internal pressure 'p' with

its edges in the x direction except at the tip (Fig.7.7),

$$J_{a^- \to b^-} = \int_{a^-}^{b^-} -P \frac{\partial V}{\partial x} ds = -\int_{a^-}^{b^-} P \frac{\partial V}{\partial x} dx \qquad (7.14)$$

so,

$$J_{a^- \to b^-} = -\int_{a^-}^{b^-} P\, dV = -P(V_{b^-} - V_{a^-}) \qquad (7.15)$$

similarly,

$$J_{b^+ \to a^+} = -\int_{b^+}^{a^+} -P \frac{\partial V}{\partial x} ds = \int_{b^+}^{a^+} -P \frac{\partial V}{\partial x} dx \qquad (7.16)$$

as $ds = -dx$ for this contour, we have,

$$J_{b^+ \to a^+} = \int_{b^+}^{a^+} -P\, dV = -P(V_{a^+} - V_{b^+}) \qquad (7.17)$$

now noting that V_{b^+} must equal V_{b^-}

$$J_{a^- \to b^-} + J_{b^+ \to a^+} = P(V_{a^-} - V_{a^+}) \qquad (7.18)$$

so that the result for the value of J for a contour around the crack tip is modified by term equal to the pressure times the crack opening displacement, i.e.

$$J_{\text{crack tip}} = J_a + P \text{ (crack separation at 'a')} \qquad (7.19)$$

This is used in place of J_a in equations 7.II and 7.I2 in evaluating K_1 using any convenient contour.

In the next section the J integral as defined above will be used to obtain a method of checking the experimental results obtained from 'Break Out' tests described in Chapter 7.

7.4 Method of Approach

As expressed by Irwin (7.3), K_c is a material property depending on the crack tip geometry, temperature etc. but independent of the crack depth.

Therefore, the equation,

$$P_f = \frac{K_c}{\sqrt{J}} \qquad (7.20)$$

where, P_f is the pressure causing failure, K_c, critical stress intensity factor, J, the J integral, can be expressed as,

$$P_f \sqrt{J} = \text{Constant} \qquad (7.21)$$

Thus, for different crack depths d_o and d_1, we have,

$$\frac{P_{fo}}{P_{f1}} = \frac{\sqrt{J_1}}{\sqrt{J_o}} \qquad (7.22)$$

It is therefore possible to substitute p_{fo} and p_{f1} values obtained from Break-Out tests and J_o [x] and J_1 from theoretical work, corresponding to depths d_o and d_1, and, thus, compare the experimental and theoretical results with each other.

For this purpose the values of J for various depths of crack are obtained according to the theoretical consideration presented in Appendix VIII and using finite

Footnote

x J_o and p_{fo} are J integral, and failure pressure respectively, corresponding to the crack depth d_o = 6·35mm.

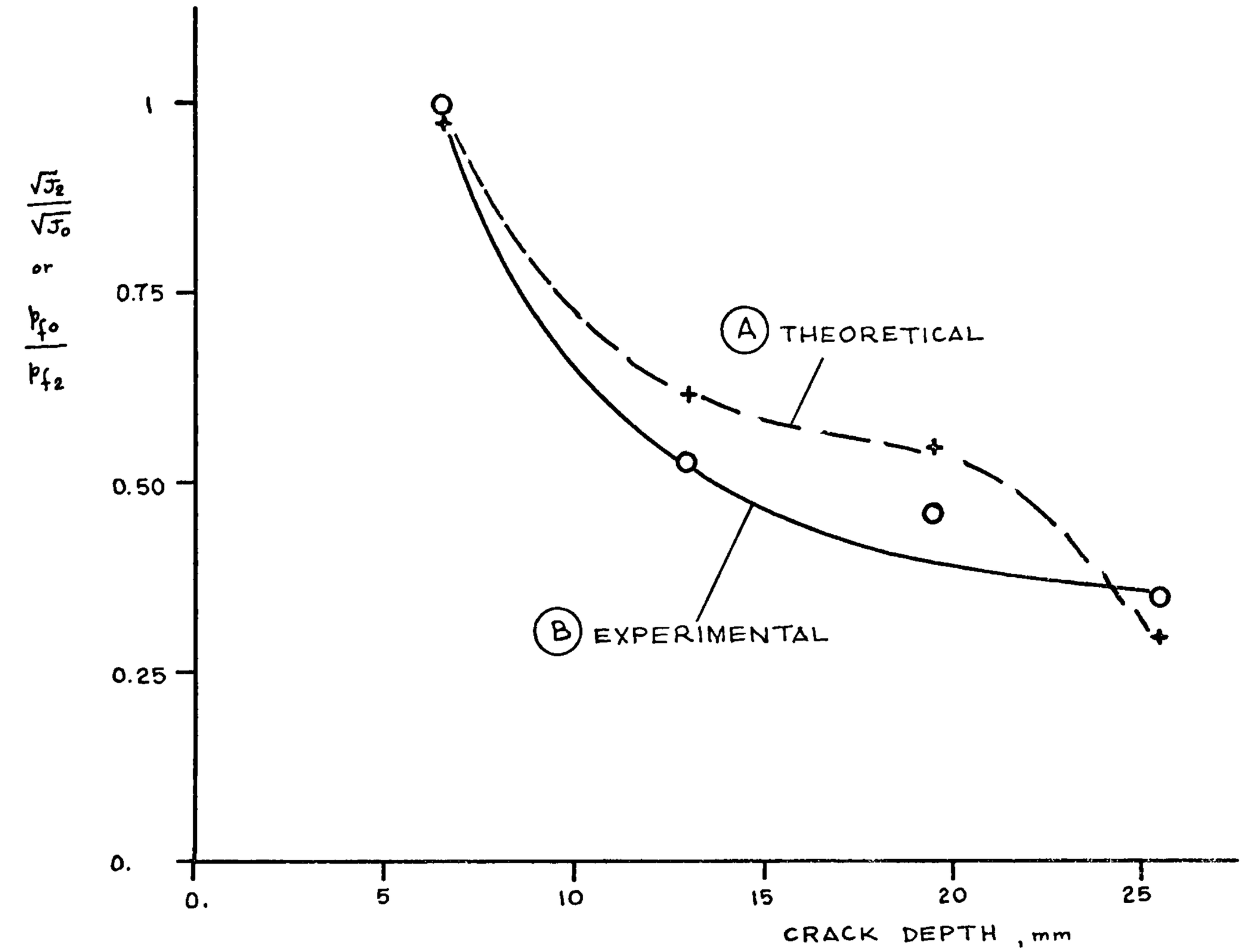

FIG. 7.8 COMPARISON OF EXPERIMENTAL AND THERETICAL RESULTS

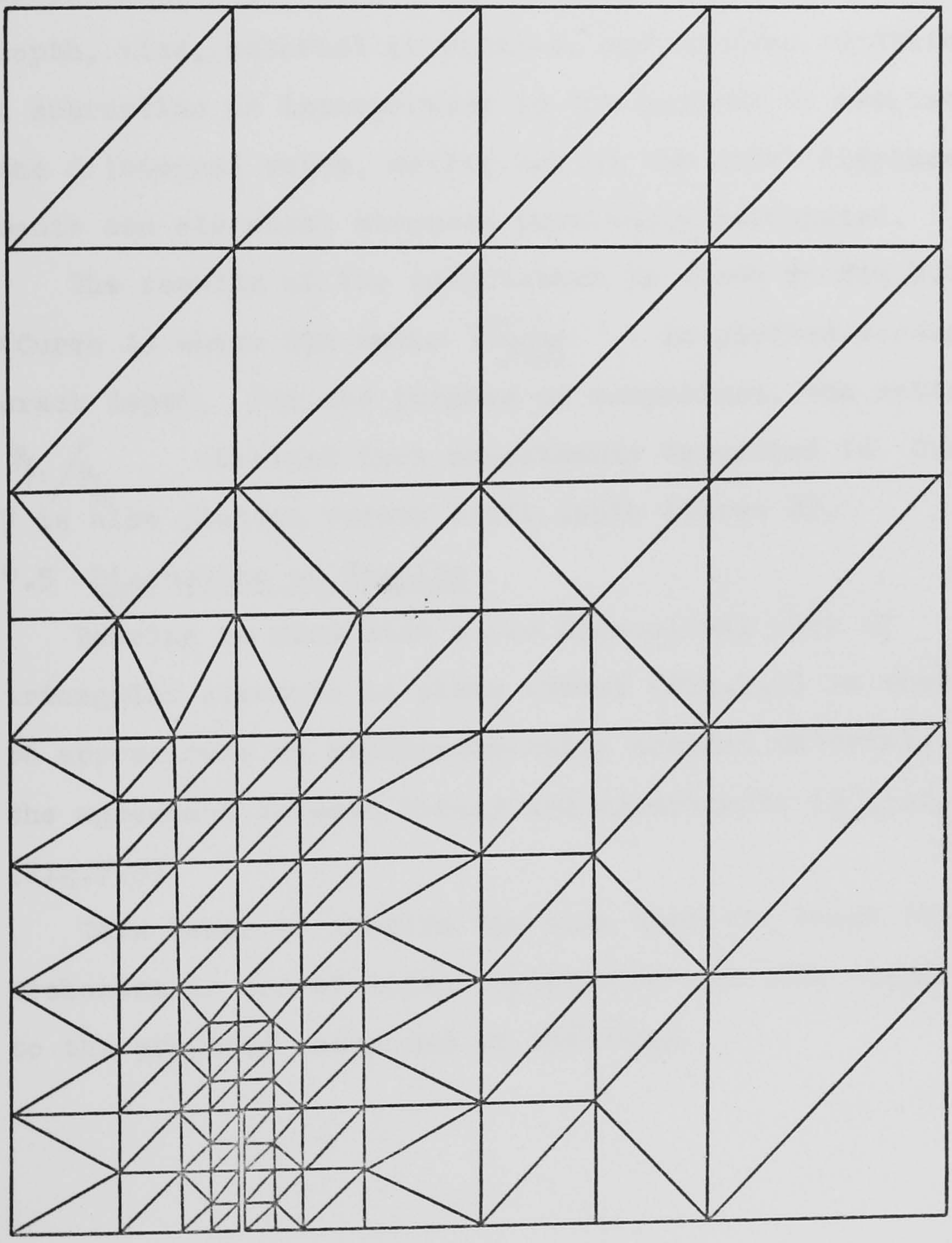

FIG. 7.9 A TYPICAL FINITE ELEMENT MESH USED IN COMPUTATION OF J INTEGRAL

element method.

A standard computer program developed at King's College, London, is used to calculate the nodal displacements and elemental stresses for given crack depth, size, material properties, and loading conditions. A subroutine is incorporated in the program to evaluate the J integral value, making use of the nodal displacements and elemental stresses previously calculated.

The results of the computation is shown in Fig.7.8 (Curve A) where the ratio $\sqrt{J_o}/\sqrt{J_1}$ is plotted versus crack depth. For the purpose of comparison, the ratio P_{f_1}/P_{f_o} obtained from experiments described in Chapter 7 is also plotted versus crack depth (Curve B).

7.5 Discussion of Results

Bearing in mind that a two dimensional mesh of triangular elements in plane stress (Fig.7.9) is used to approximate an axisymmetrically cracked material, the agreement between theory and experiments is good. (Fig.7.8)

This tends to confirm the view that the break out mechanism is one of local instability and adds support to the proposed mechanism of spalling.

Chapter 8

BREAK-OUT TESTS AT HIGH TEMPERATURES

8·1 Introduction

In Chapter 4 a mechanism for spalling of concrete was proposed. In this it was suggested that if cracks parallel to the surface were present internal pressure in these cracks might cause the failure of the material between the crack and the surface, in a similar shape as the ones observed in fire conditions.

If true, the mechanism would account for the observed effects of compressive stresses (Chapter 2) and pore pressures on spalling. Furthermore, it would explain how pressures comparatively smaller than the tensile strength of concrete could cause failure.

The mechanism seemed plausible because, firstly, there was experimental evidence of formation of cracks parallel to the surface (Chapter 4) when the material was loaded biaxially in the plane parallel to the free surface, and, secondly, there was evidence that pressure due to water vapour might be generated when concrete was exposed to heat (Chapter 3).

To show that such a mechanism may actually cause spalling it was necessary on one hand to assess the pressure necessary to cause failure of the material between the crack and the surface, and, on the other hand, to show that pressures of such magnitude can actually be generated in heated concrete.

In order to assess the pressures required to cause failure outside various cracks, 'Break-Out' tests were designed.(Chapter 6) To find out whether such pressures

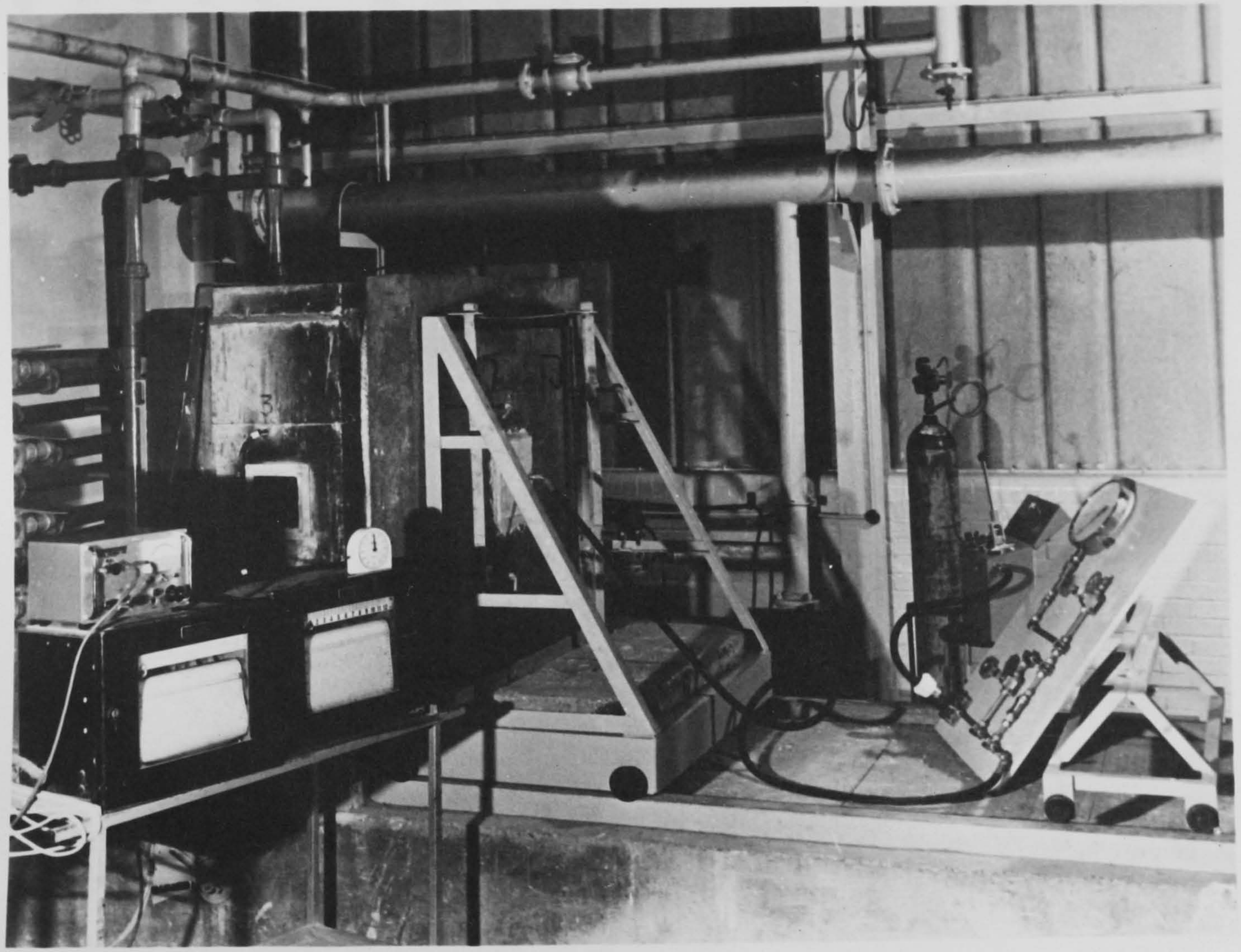

FIG. 8.1 OVERALL VIEW OF HIGH TEMPERATURE BREAK OUT TEST SET-UP

do actually exist, or not, 'Pore Pressure' tests have been planned (Chapter 5).

'Break-Out' tests described in Chapter 6 were, however, carried out at room temperature, because, the emphasis was on the pressure rather than on the source of it. This pressure could be gas or water pressure at room temperature, or, water vapour pressure due to vapourization at high temperatures as in the case of fire exposure. However, the qualitative results of 'Break-Out' tests performed at room temperature might be substantially different from the ones at high temperatures, and, unless the effect of high temperatures on these results were determined, any prediction related to fire conditions could be uncertain. Therefore it was decided to extend the range of the 'Break-Out' tests by performing some experiments with the surface of the specimen heated to high temperature.

8·2 Apparatus

8·2·1 Overall View

The basic mechanism of the 'Break-Out' tests is the same as the ones described in Chapter 6. Namely, the artificial crack in the specimen was internally pressurized from an external pressure source till the failure and separation of the material between the crack and the surface occurs. The system comprised a nitrogen bottle, a hydraulic pressure unit, a pressure control board connected to the specimen with a high pressure flexible hose. (Fig.8·1)

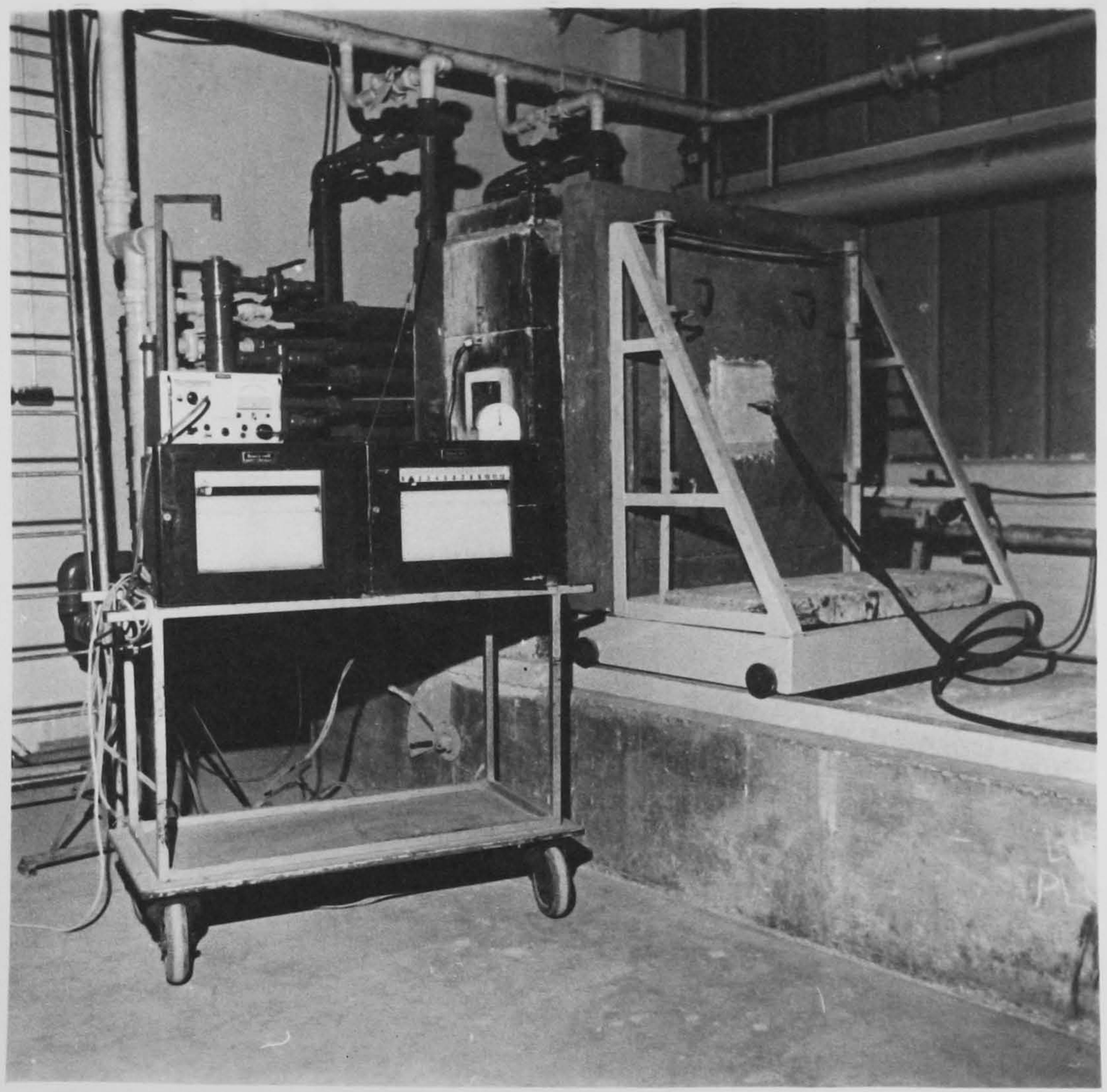

FIG. 8.2 FURNACE

The main difference, however, between the tests described in this chapter and the ones in Chapter 6 lies in the fact that the former tests are performed on specimens exposed to heating.

The technical details of the furnace and the related equipment are described in the following section.

8·2·2 The Furnace

The tests described in this Chapter were carried out at Fire Research Station, using the furnace shown in Fig.8·2.

The furnace is made up of three sections:

1. the furnace door
2. a middle section

and 3. the gas injector holder

The furnace door was mounted on a steel base sitting on four wheels running on two rails.

The door contained a concrete frame of 1m x 1m internal dimensions, thus being capable of accommodating a 1m x 1m specimen. The latter was fixed on to the frame by the pressure of two removable cross-bars.

The middle section contained 4 built-in chromel-alumel thermocouples to record the furnace temperature at four different points at 75mm from the specimen. Viewing windows were also provided in this middle section.

The gas injector holder accommodated eighty one gas injectors held in a concrete frame which received the gas pipes through the rear. The nine groups of injectors, nine in each group were held in position

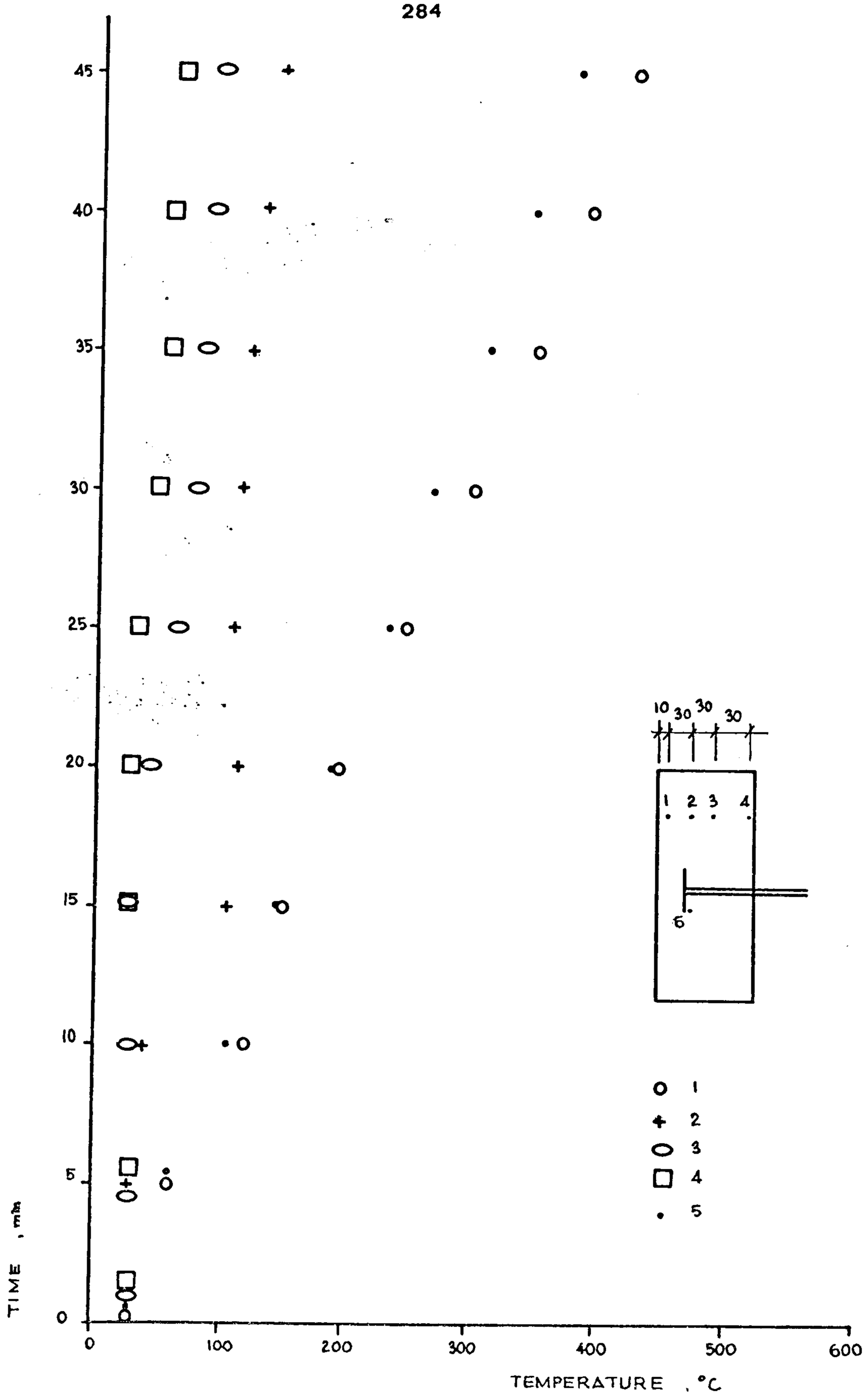

FIG. 8.4 TEMPERATURE DISTRIBUTION THROUGH THE SPECIMEN AFTER THE START OF HEATING

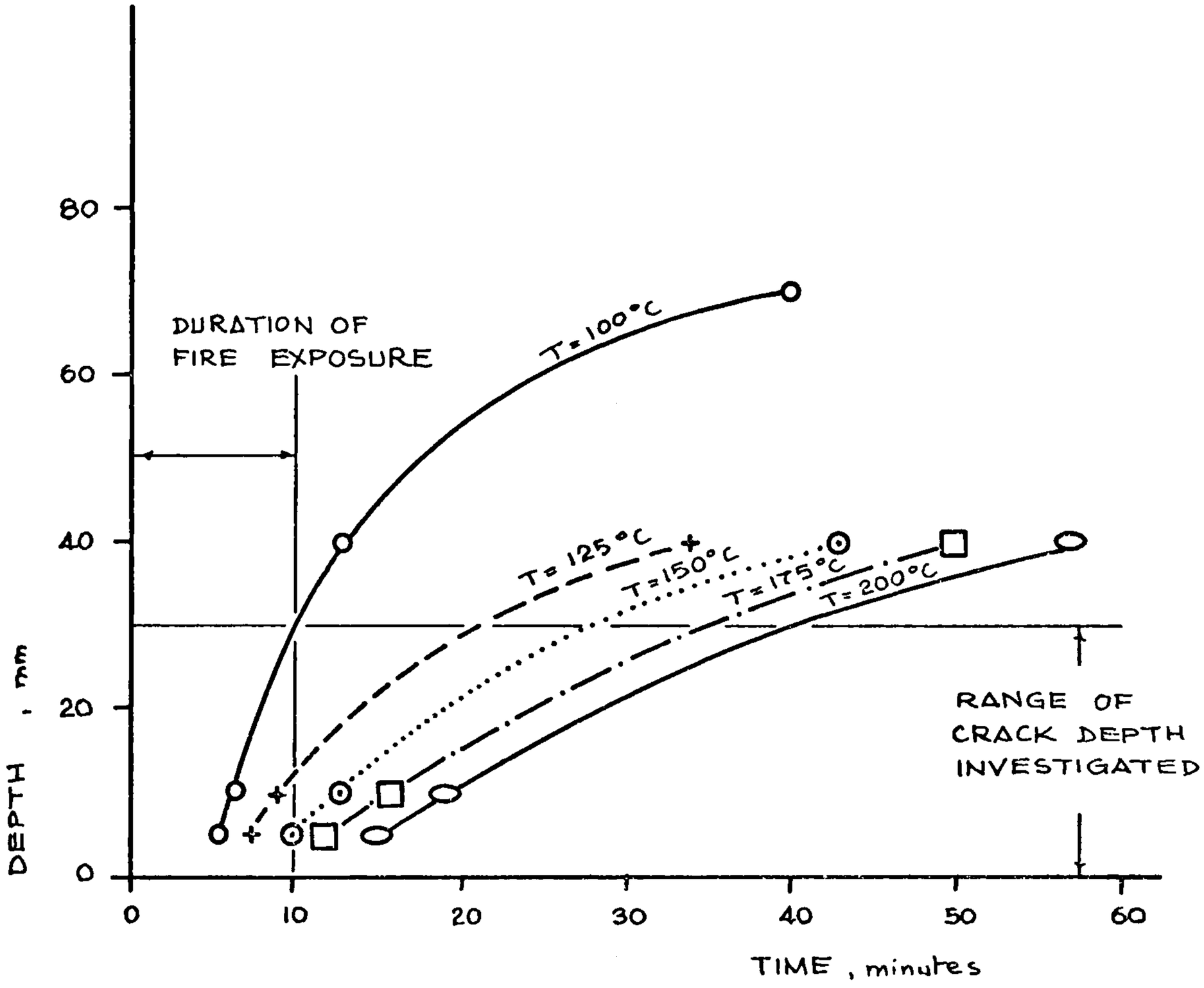

FIG. 8.5 THE MOVEMENT OF $T_{100°C}$, $T_{125°C}$, $T_{150°C}$, $T_{175°C}$ AND $T_{200°C}$ FRONTS DURING FIRE EXPOSURE (STANDARD HEATING)

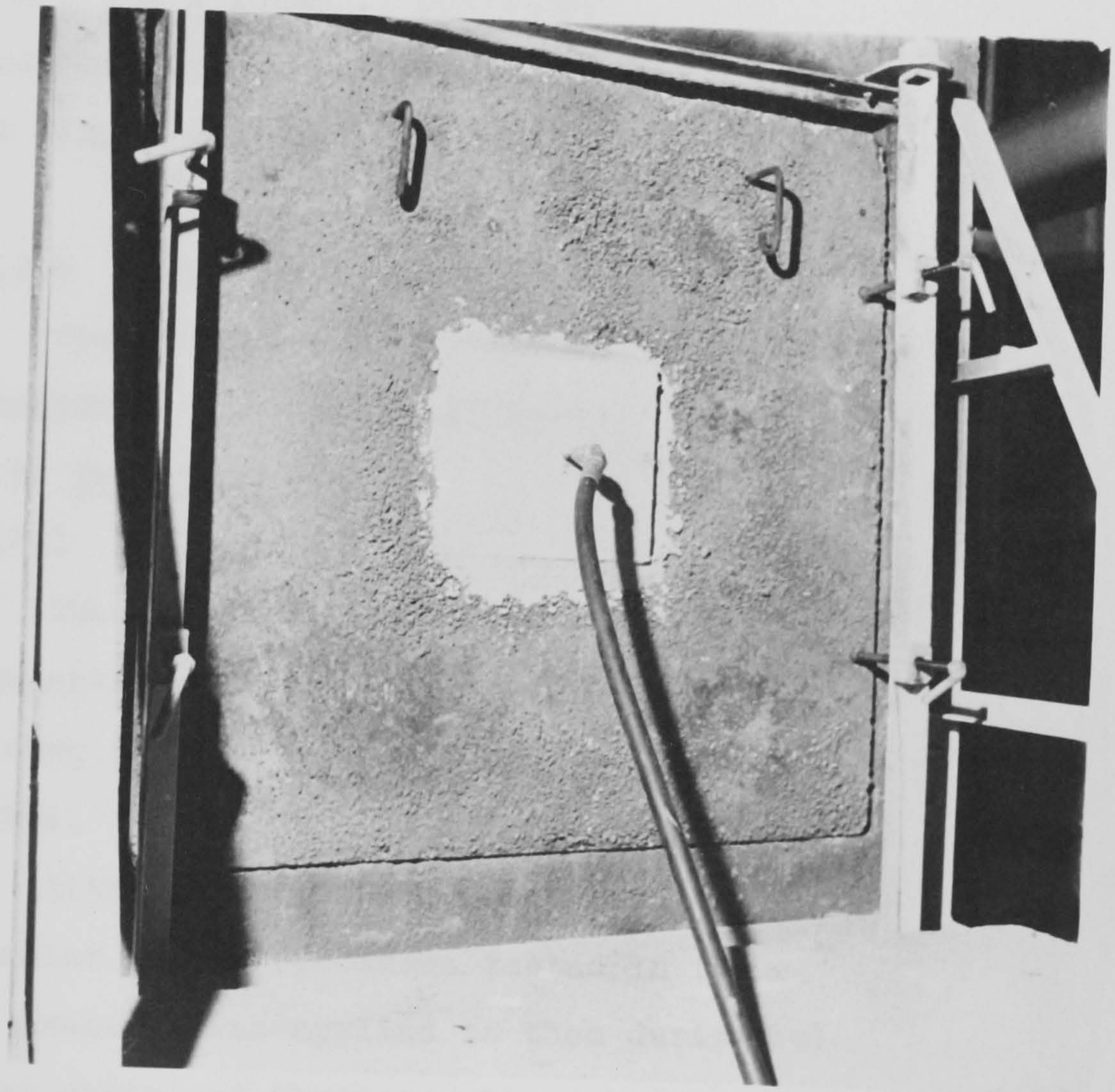

FIG.8.3 SPECIMEN HOLDER

in a metal frame bolted to the concrete frame.

8.2.3 The Specimen Holder

The furnace could only accommodate 1m x 1m specimens while the specimens mentioned in this chapter were 254 x 254 x 102mm . Consequently, two specimen holders, made of high temperature resistant concrete were built at King's College.(Fig. 8.3)

8.2.4 Specimens

The specimens were cast in steel moulds and were similar to the ones described in Chapter 6.

8.3 Test Series

8.3.1 Preliminary Tests

These tests were carried out to determine the temperature distribution in the specimens at any time during the exposure to heat following standard temp./ time curve.

Although these specimens contained artificial cracks similar to the specimens tested in the main test series, no pressure was applied to them during the heat exposure. They contained thermocouples embedded through their thickness as shown in Fig. 8.4 and continuous temperature recording was carried out during the heat exposure. The results of these tests (Fig. 8.5) gave an indication of the temperature distribution to be expected in specimens in the main test series.

The procedure used during these Preliminary tests was as follows:

1. The specimen was fixed in the central hole of the

specimen holder.

Care was exercised in this stage to fill in the gap between the specimen and the holder, with plaster.

2. The specimen,thermocouples,and the furnace thermocouples were then connected to the temperature recorders, the heating started, and the sliding furnace door closed.

3. The intensity of the fire was controlled so as to follow standard Temperature/Time curve.

Preliminary Test Results and Discussion

According to Meyer-Ottens (8.1) the vapourization temperature of the moisture in concrete is between 100°C and 150°C. The results of the preliminary tests showed that (Fig. 8.4) the range of the crack depth investigated (3-25mm) falls entirely in the 100-150°C interval at the 10th minute of fire exposure. (Fig. 8.5) Accordingly it was decided that the external pressure would be applied to the specimens 10 minutes after the start of the heat exposure.

Observations During Preliminary Tests

After twenty minutes of fire exposure some moisture on the cool face was observed. This suggested that pore pressure generated at the interface might push the moisture clog towards the cooler face in a similar manner described by Harmathy (8.2).

After 17 minutes of fire exposure vapour was observed to leave the specimen through the copper tubing. It was

however believed that vapourization around the crack started earlier, when the temperature reached vapourization temperature, but the escape of the vapour was prevented by the rubber membrane. It was only after the damage of the membrane under the pressure that vapour could escape to the atmosphere through the copper tubing. Although no attempt had been made to measure the quantity of vapour released this way, this process went on for about 10 minutes and the amount of vapour thus released seemed surprisingly large.

Ideally the pressure should be applied at different times for each specimen depending on the depth of crack present in the specimen. But, as there was no data available for the actual steam pressures developed through the thickness of concrete at various times, the vapourization temperature at various depths and times was not available. Consequently, the exact position of the interface not being known, the same period of fire exposure was applied to all specimens. This was taken to be 10 minutes.

8.3.2 Main Test Series

Procedure and Results

Following the preliminary tests, the actual specimens were tested as follows:

1. The specimen was placed in the central hole of the specimen holder and the gap between the specimen and the specimen holder was filled with plaster.
2. The copper tubing protruding from the specimen

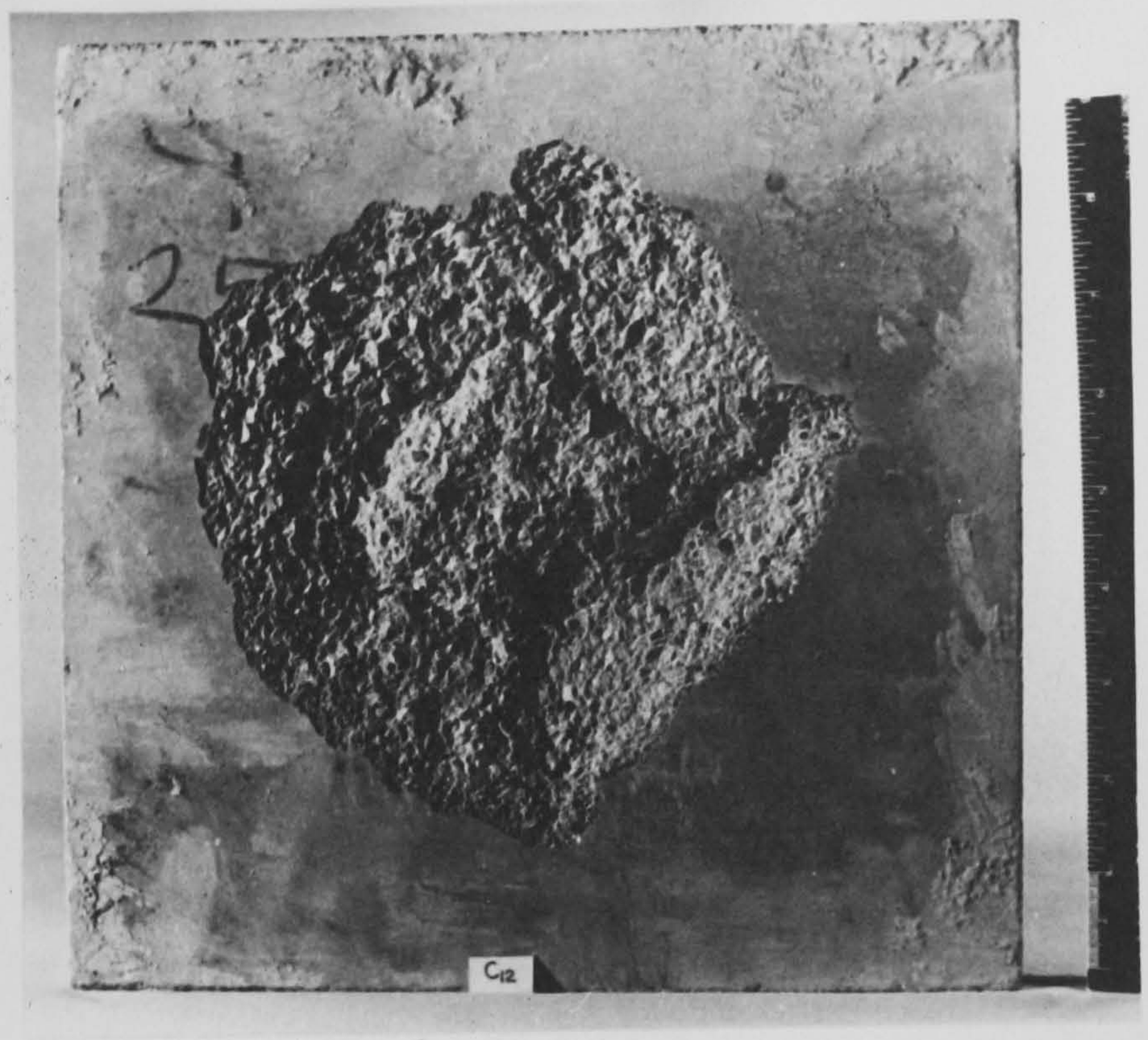

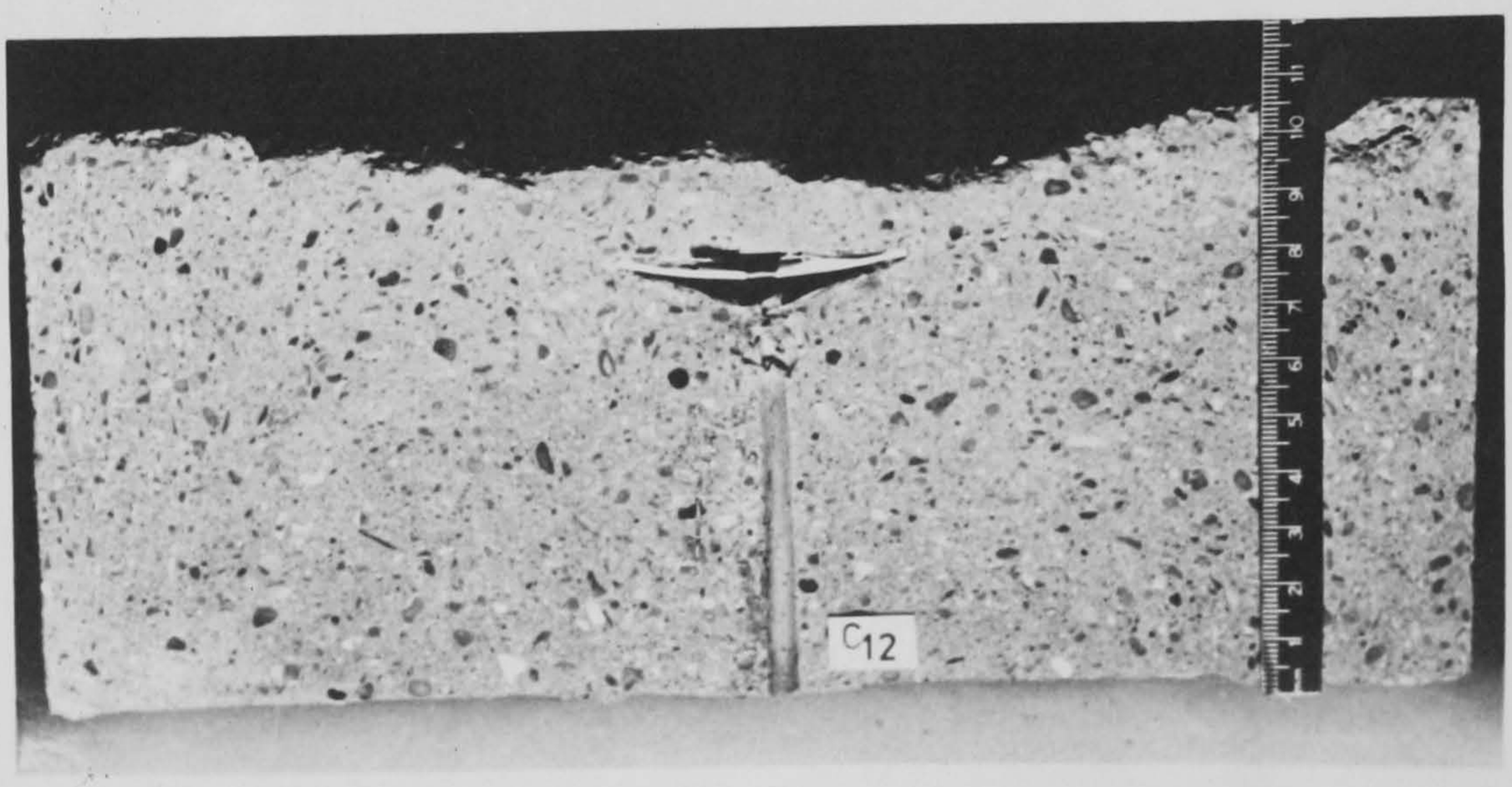

FIG. 8.6

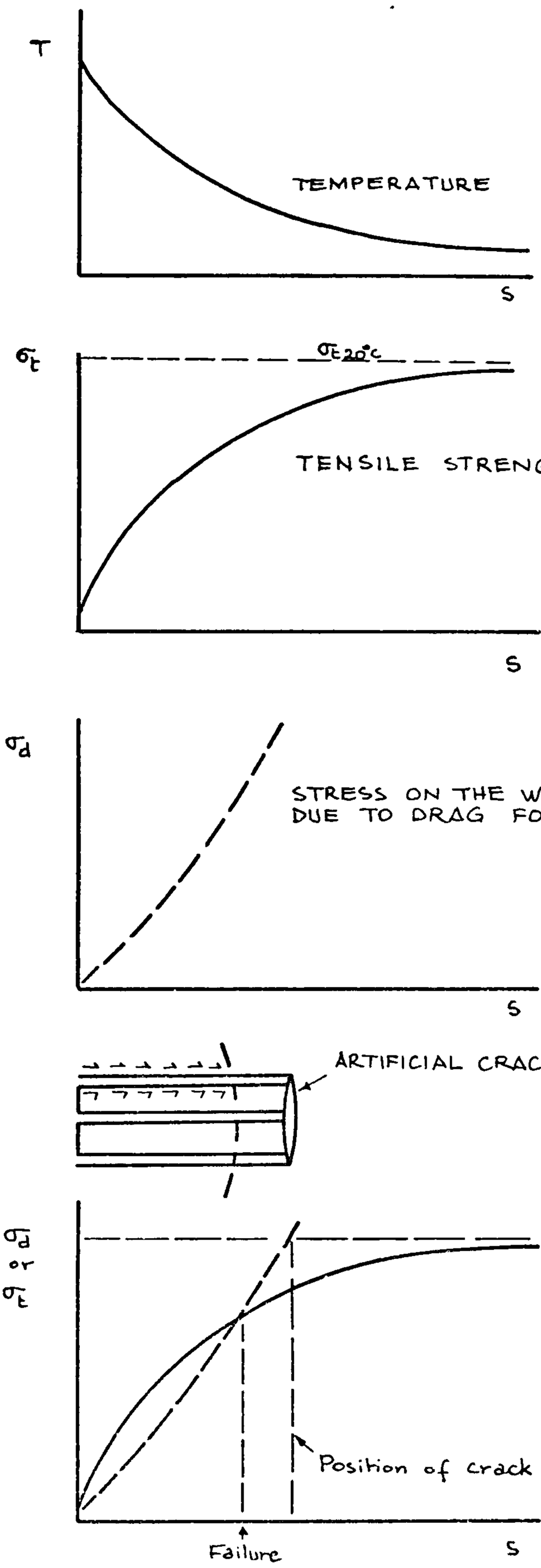
T
TEMPERATURE
S
σ_t
$\sigma_{t\,20^\circ c}$
TENSILE STRENGTH ,
S
σ_d
STRESS ON THE WALLS
DUE TO DRAG FORCE
S
ARTIFICIAL CRACK
σ_d or σ_t
Position of crack
Failure
S

FIG. 8.8

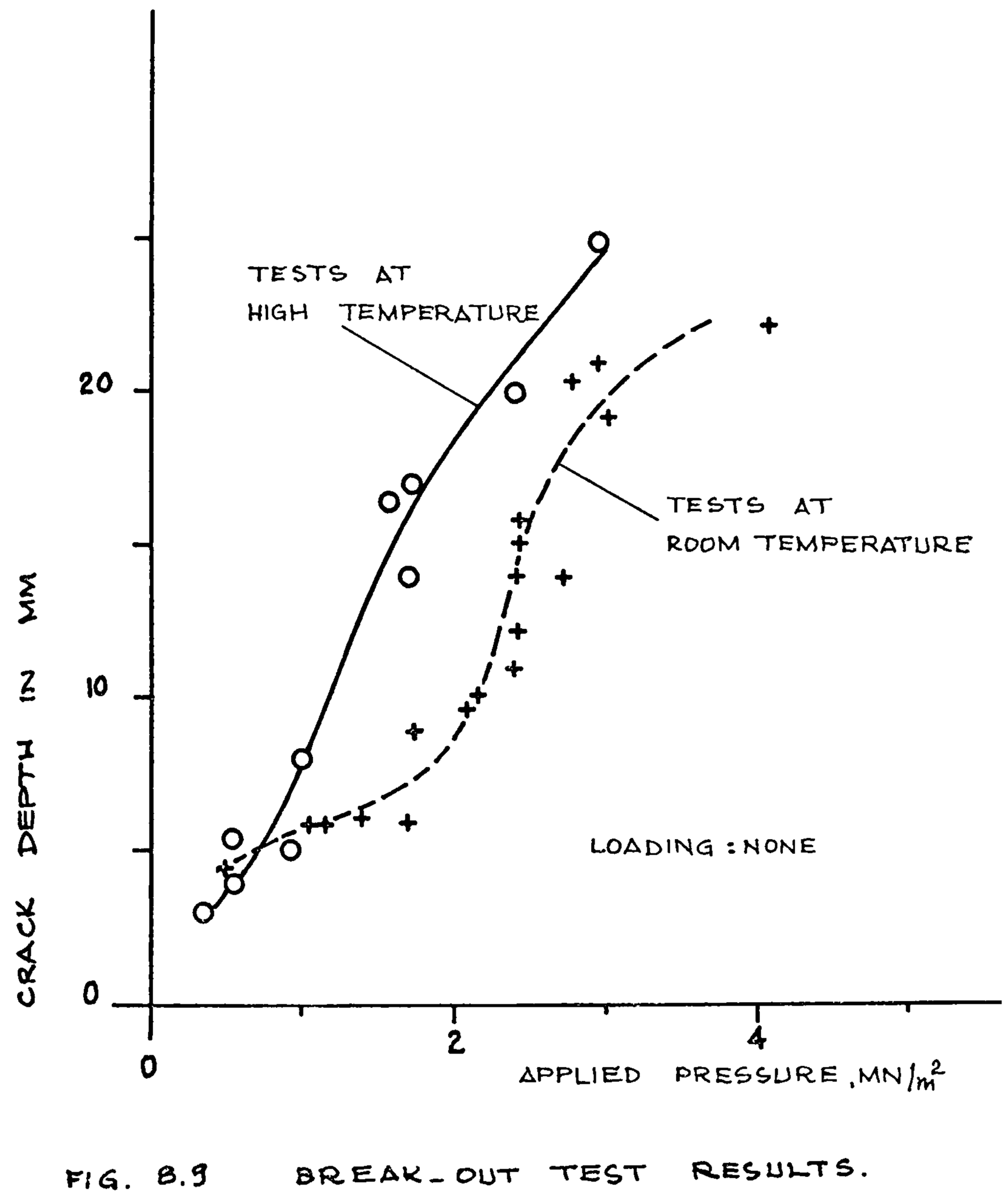

FIG. 8.9 BREAK-OUT TEST RESULTS.

was connected to the pressure application system described in Section 6.3.2

3. The heating was then started.
4. Ten minutes after the start of heating, gradual water pressure was applied until failure of the specimen occurred.

Although in the majority of the tested specimens the extent of damage was comparable to the ones tested at room temperatures, the shape of the spalling differed slightly.

At high temperatures, in some of the specimens the failure did not start at the edge of the artificial crack, as was the case in specimens tested at room temperatures, but some distance away, somewhere between the crack and the heated surface. In these specimens the metal disc that formed the artificial crack was either completely (Fig.8.6) or partially (Fig.8.7) covered with mortar even after failure occurred.

This behaviour is probably due to the reduction of the tensile strength of the material near the heated surface, thus causing failure in a manner shown in Fig.8.8.

8.4. Discussion of Results and Conclusion

Fig.8.9 shows that less pressure is required to cause spalling in fire conditions than at room temperatures.

The implication is that, although the pressures recorded in pore pressure tests described in Chapter 5 may not be high enough to cause spalling at room

temperature, they may be high enough to cause spalling under fire conditions.

In fact, the maximum pressure obtained in pore pressure tests, 2.I MN/m^2, is only enough to cause spalling if the crack depth is 8mm or less (Fig.8. 9). At high temperatures, however, the same pressure is enough to cause spalling down to a depth of 18mm . (Fig.8. 9)

It should however be remembered that the pressure in these tests was applied after 10 minutes of fire exposure. But, the maximum pressure 2.I MN/m^2 recorded in pore pressure tests, corresponds to a vapourization temperature of 210°C (Schmidt 8·3). Consequently, according to Fig.8.5 it would be more realistic to apply the pressure after 20 minutes of fire exposure rather than 10 minutes as is the case.

One can however note that the higher the temperature in the specimen the steeper would the slope of the curve in Fig.8. 9 be. This suggests that 2.I MN/m^2 of pore pressure mentioned earlier would cause spalling down to a depth much larger than 18mm.

Therefore, the results of tests described in this chapter, coupled with ones in Chapter 5 and 6 lead to the conclusion that if cracks parallel to the heated surface are present, the steam pressures could be high enough to cause spalling of concrete.

Chapter 9

CONCLUSION

The purpose of the work was to investigate experimentally the mechanism first proposed by Dougill (9.1) and presented in Chapter 4 of the present work.

The mechanism requires that in concrete panels exposed to heat, cracks parallel to the unloaded face are formed. These cracks may subsequently be filled with vapour, and, if the vapour pressure reaches certain critical limit, the material between the crack and the surface may be expelled.

The pore pressures developed in heated concrete are, only under certain conditions, high enough to cause spalling. In general these pressures are relatively small, when compared with the pressures required to cause failure of an uncracked concrete.

Therefore, pressures generated in concrete by exposure to fire conditions are rarely enough to cause spalling of the material.

Tests described in Chapter 2 show that the occurrence of spalling increases with the combination of the effects of pore pressure and compressive stresses above certain levels.

Therefore a mechanism of failure involving pore pressures and compressive stresses causing spalling is probable.

There is evidence that when concrete is subjected to biaxial compression, cracks parallel to the surface are formed (Chapter 4).

Although no direct tests have been carried out on specimens exposed to fire in order to determine the

existence of such cracks, it is known that when concrete wall panels are exposed to fire from both sides, the surfaces exposed to heat are under biaxial compression due to restriction from the relatively cool central portion. (Chapter 2)

Therefore, it seems inevitable that cracks parallel to the heated face are formed in concrete exposed to fire conditions.

If such cracks are present, pressures in the range possibly developed in heated concrete appear to be capable of causing failure. (Chapters 5,6 and 8)

Therefore, the suggested mechanism can be a possible cause of spalling.

The implications of such a mechanism will be discussed in the following section.

Conclusions Related to the Failure Mechanism:

1. Pore pressures at least up to 2·1 MN/m^2 can develop in concrete exposed to fire conditions (Chapter 5)
2. However, such pressures alone are usually not enough to cause failure of concrete even if the reduction in tensile strength[x] of the

Footnote

x Preliminary tests described in Chapter 8 showed that after exposure of a specimen to standard fire conditions for 30 mins, the temperature was only 300°C at a depth of 10mm (Fig. 8.4). Saemam and Washa (9.2) showed that at this temperature the tensile strength reduced approximately by 25%.

material with increase in temperature is taken into account.

3. The mechanism as proposed by Dougill (9.1) is possible. That is, if cracks parallel to the heated face are present in concrete, the pressures possibly generated in heated concrete can cause failure.

4. Biaxial compression which is believed to produce cracks parallel to the unloaded surface, should be avoided wherever possible.

   For this, heavy reinforcement near the axis of symmetry in concrete wall panels should be avoided, because, the relatively cool central reinforcement can create restriction to the thermal expansion of the surface layer, thus causing biaxial compression.

5. For the same crack depth and size, higher pressures are required to cause spalling of the material under biaxial compression as compared with the one with no compression.

   However, for the reason explained in item 4, biaxial compression must be avoided altogether, whenever possible.

6. The pressures required to cause failure depends on the size of the cracks. The smaller is the crack, the higher is the pressure required to cause failure. (Chapter 6)

Other Factors Affecting Spalling

1. Permeability of concrete is an important factor in causing spalling of heated concrete. In concrete with low permeability, spalling may occur even in the absence of cracks parallel to the surface.

The permeability is substantially affected by the curing method. Water curing significantly increases the occurrence of spalling.

However, there is little room for improvement in prevention of spalling as far as curing method is concerned, because, water curing is, in most cases, necessary for more complete hydration and therefore higher strength.

Nevertheless, membrane curing should be used whenever applicable because this type of curing applied after the disappearance of free moisture on the surface of concrete would lead to a weak surface layer which would provide better resistance to spalling.

Steam curing, applicable to precast concrete members, appears to be most suitable, as, this method is known to increase permeability as opposed to moist or water curing which are known to decrease permeability.

2. Age[x] of concrete does not affect spalling as significantly as curing method. (Chapter 5)

Footnote

x The highest age tested was 70 weeks.

3. As implied by Akharuzzaman and Sullivan (9.3) carbonation of the surface layer seems to increase the occurrence of spalling. This effect is, however, not as significant as the influence of the curing method.

Appendix I

EFFECTS OF RESTRAINT ON FIRE RESISTANCE

A.1.1 Introduction

According to most relevant standards (B.S. (A.1), ASTM (A.2), ISO (A.3)), fire tests should simulate the conditions in real life situations. However, with the range of equipment available in most laboratories it is not usually possible to simulate end restraint and continuity. Consequently the behaviour of an element tested under furnace conditions may be very different from that of a member that is part of a building structure.

These differences can be much more pronounced in case of spalling as there is evidence that spalling is affected by high compression.

It may therefore be useful to discuss the effect of restraint and continuity in relation to spalling of concrete.

A.1.2 Longitudinal Restraint

The statically indeterminate structures subject to fire have the characteristic property that the deformations caused by heating cannot develop freely and thereby give rise to restraining forces.

P.C.A. laboratories were probably the first to consider the effect of longitudinal restraint. For this purpose a special furnace and loading frame was built and extensive data were obtained during the period of 1960-1968. (See Selvaggio and Carlson (A.4), Carlson et al. (A.5), Issen et al. (A.6))

Gustaferro and Carlson (A.7) noted that the relation

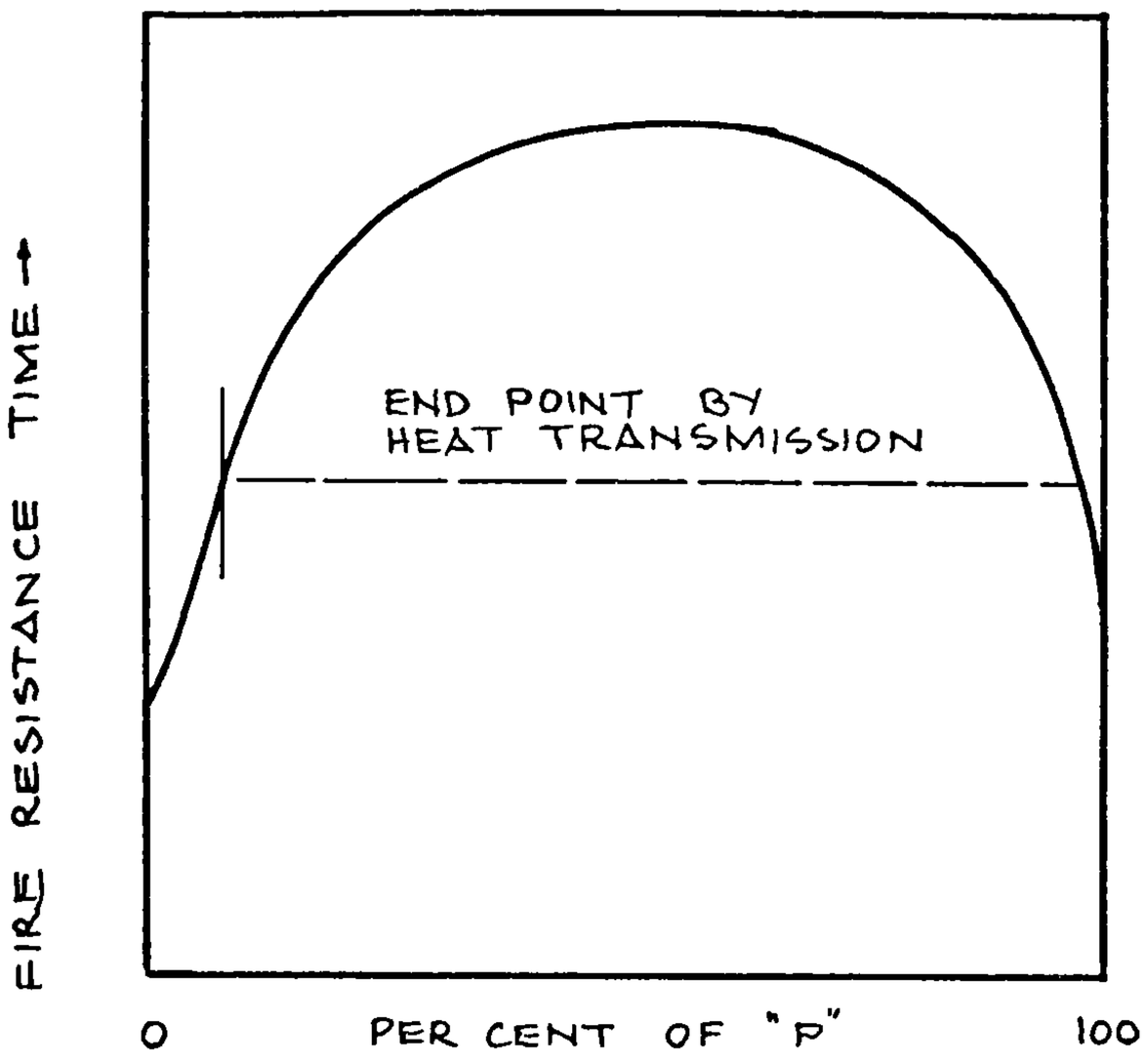

FIG. A.1 EFFECT OF END RESTRAINT ON FIRE RESISTANCE OF PRESTRESSED CONCRETE

[AFTER GUSTAFERRO & CARLSON, (A.7)]

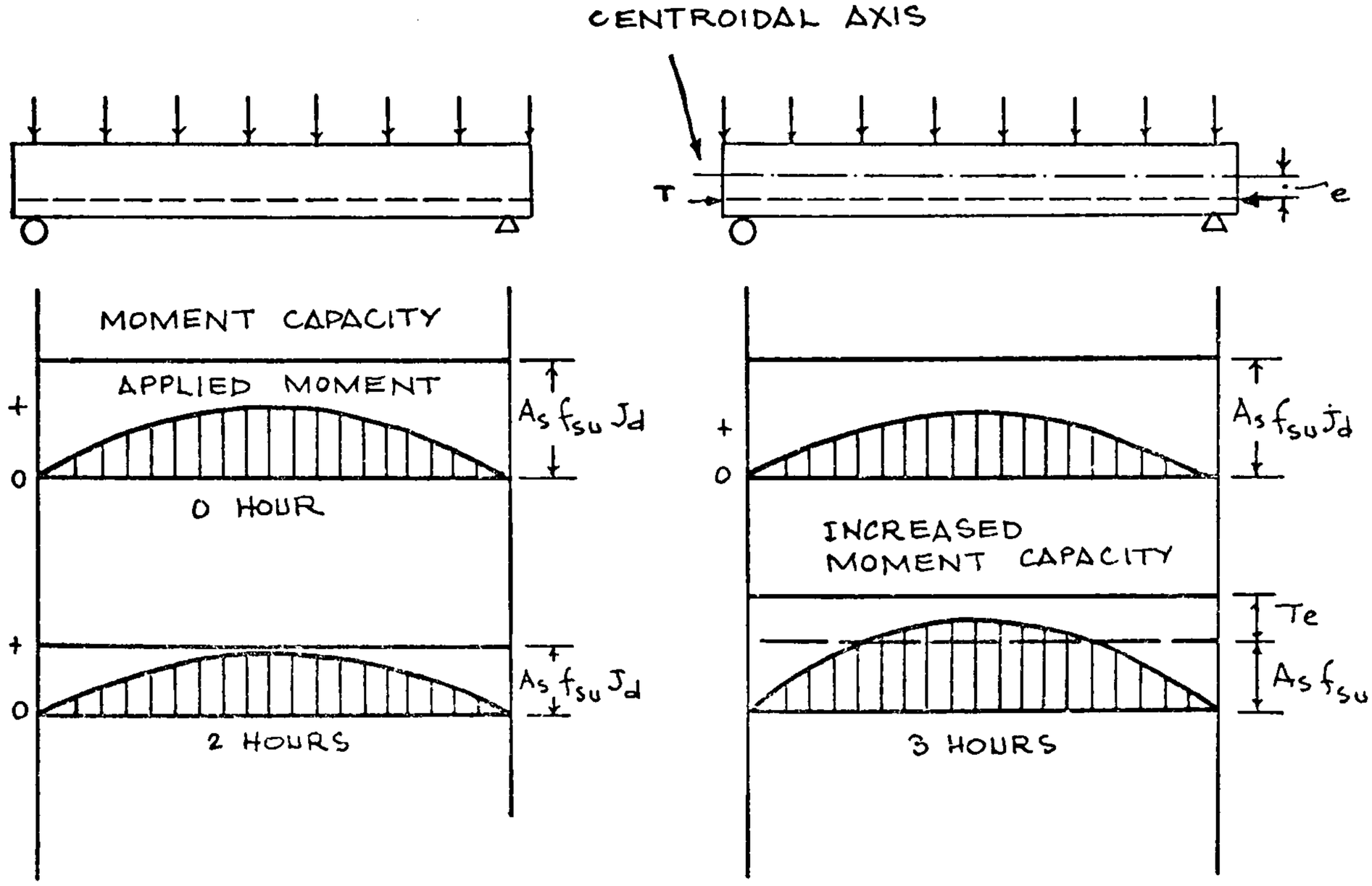

FIG. A.2 COMPARISON OF APPLIED MOMENT AND MOMENT CAPACITIES IN RESTRAINED AND UNRESTRAINED BEAMS EXPOSED TO FIRE

Tc = MOMENT FROM RESTRAINT

$A_s f_{su} J_d$ = MOMENT CAPACITY

[AFTER CARLSON et AL. (A.5)]

between fire resistance and restraint would be as shown in Fig.A.1 where it is assumed that simply supported and built-in beams should have zero restraint and 100% restraint respectively. According to Fig.A.1 only a small amount of restraint is required to provide substantial increase in the fire resistance. With high restraint there is possibility of compression failure.

However, Selvaggio and Carlson (A.4) pointed out that the forces required to create near 100% restraint during a fire test are extremely high,and therefore full restraint is probably never achieved in buildings. Accordingly they concluded that restraint increases the resistance of a member to fire and only a small amount of restraint is sufficient in order to extend the fire resistance period of a beam for several hours.

In a series of tests on 5·83m long double-tee flexural members where the allowed thermal expansion was varied from 1mm to 38mm, Selvaggio and Carlson showed that the intensity of thermal thrust was proportional to the coefficient of thermal expansion, and the modulus of elasticity, and, that at the temperatures attained during fire exposures, in-elastic deformations occur very rapidly, in terms of minutes, probably due to the increase in rate of creep at high temperatures.

Salvaggio and Carlson state that the maximum thrust also depends on the portion of the perimeter of the cross-section normal to the direction of the restraining force, referred to as 'heated perimeter.'

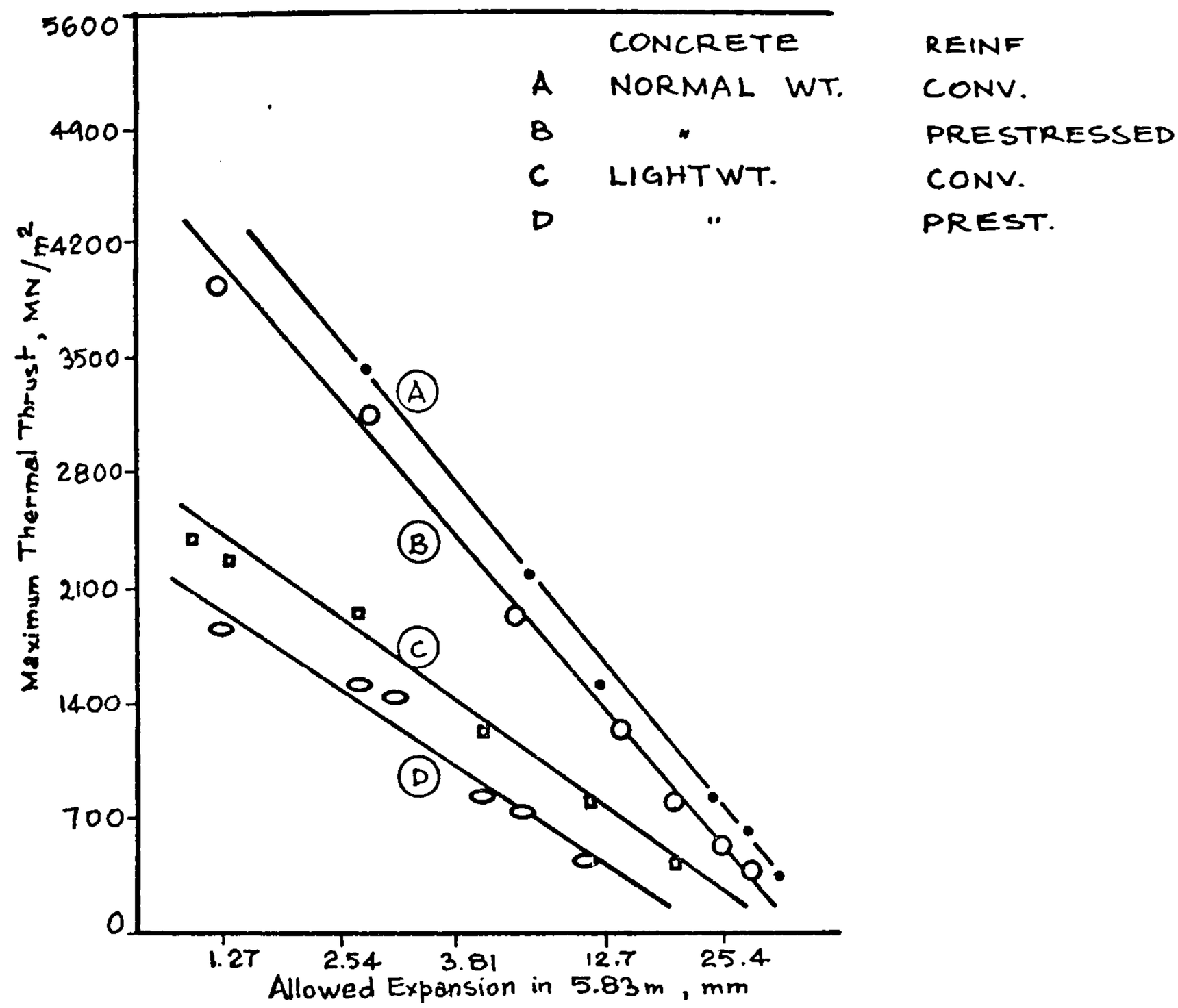

FIG. A.3 MAXIMUM THRUST FOR ALLOWED EXPANSIONS OF REFERENCE SPECIMENS

[AFTER SELVAGGIO & CARLSON, (A.4)]

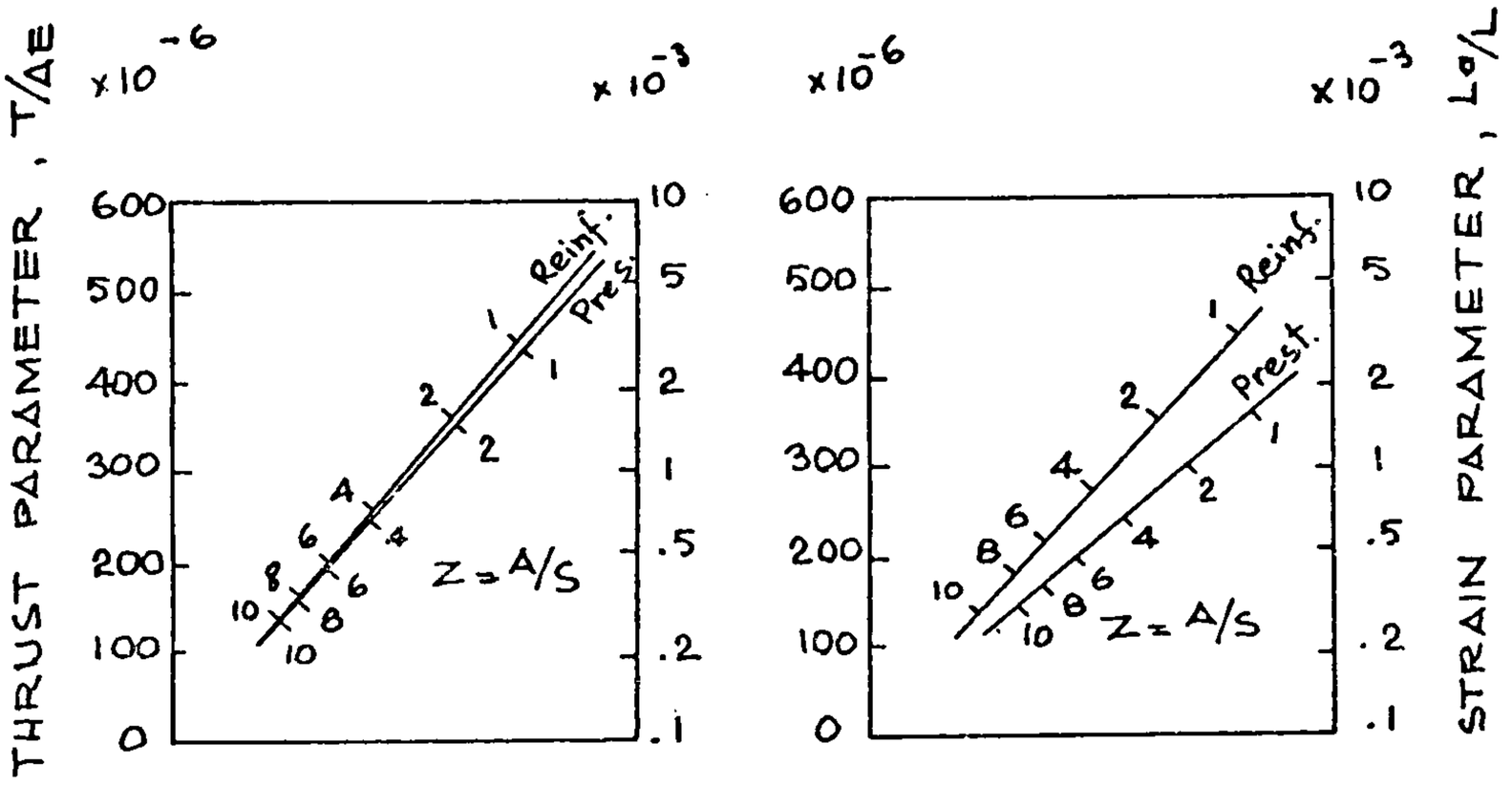

FIG. A.4 NOMOGRAMS RELATING THRUST PARAMETER, STRAIN PARAMETER, FOR NORMALWEIGHT AND LIGHTWEIGHT CONCRETE

Z = THE RATIO OF CROSS-SECTIONAL AREA TO HEATED PERIMETER

[AFTER ISSEN et AL. (A.6)]

Using this concept, the authors derived a formula, which, after improvements by Issen et al. (A.6) is expressed as,

$$\frac{T_f}{A_f E_f} = \frac{T_o Z_o}{A_o E_o Z_f} \qquad (A.1)$$

where, Z = A/s in which s is the heated perimeter, A the cross sectional area normal to the direction of thrust,

T = maximum thrust

E = elastic modulus

and the suffix 'o' referring to the reference specimen whose properties can be determined from Fig.A.3, and 'f' to the specimen whose thrust is unknown.

Using equation A.I. it is possible to estimate the thrust, T_f, for a particular allowed expansion strain.

However, Fig.A.3 is only applicable to specimens having the same cross-section and made of concrete similar to those of the reference specimens. A more general application is suggested by Issen et al. (A.6) making use of the nomograms (Fig.A.4) where the effect of size difference between the reference and the actual specimen is taken into account.

The effect of restraint should, however, be interpreted cautiously, as, in some cases it is likely to be detrimental to the structural member. Dougill (A.8) pointed out that in the absence of live load, the top flange of beams could be put under tension, due to eccentricity of the thermal thrust, and thus lead to

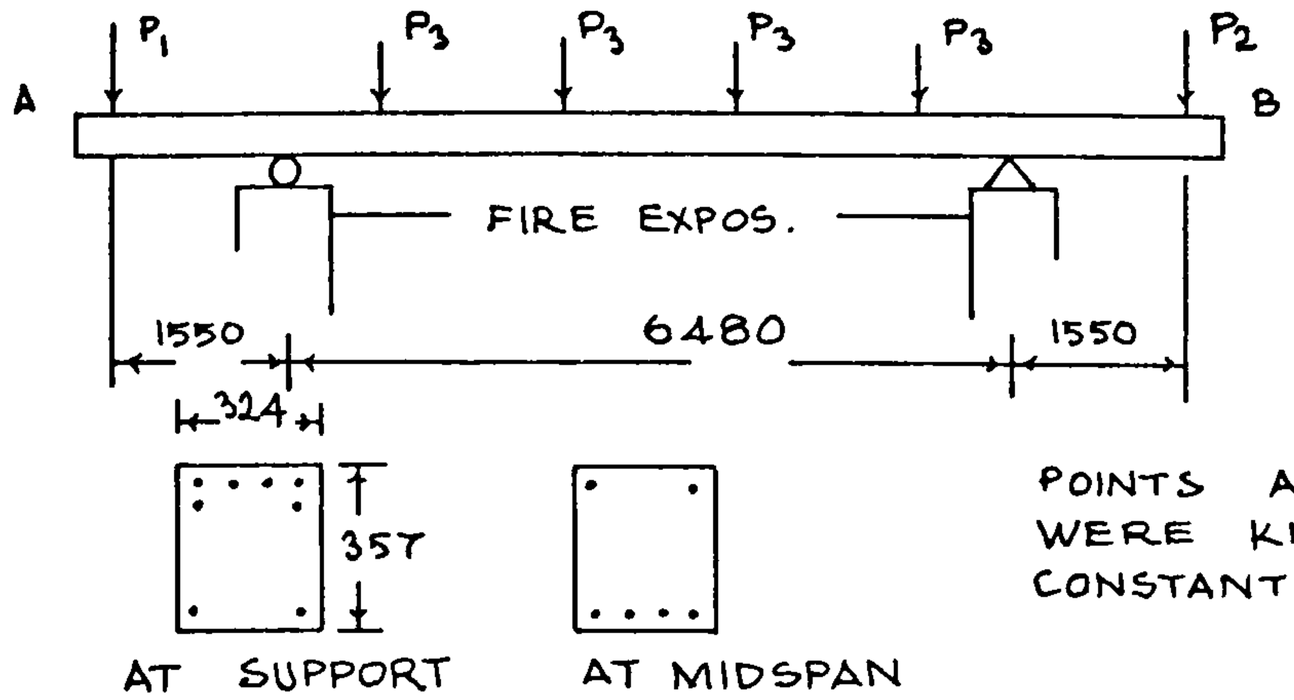

FIG. A.5 REINFORCED CONCRETE FIRE TEST SPECIMEN USED TO SIMULATE CONTINUOUS BEAM IN PCA TESTS

[AFTER GUSTAFERRO ,(A10)]

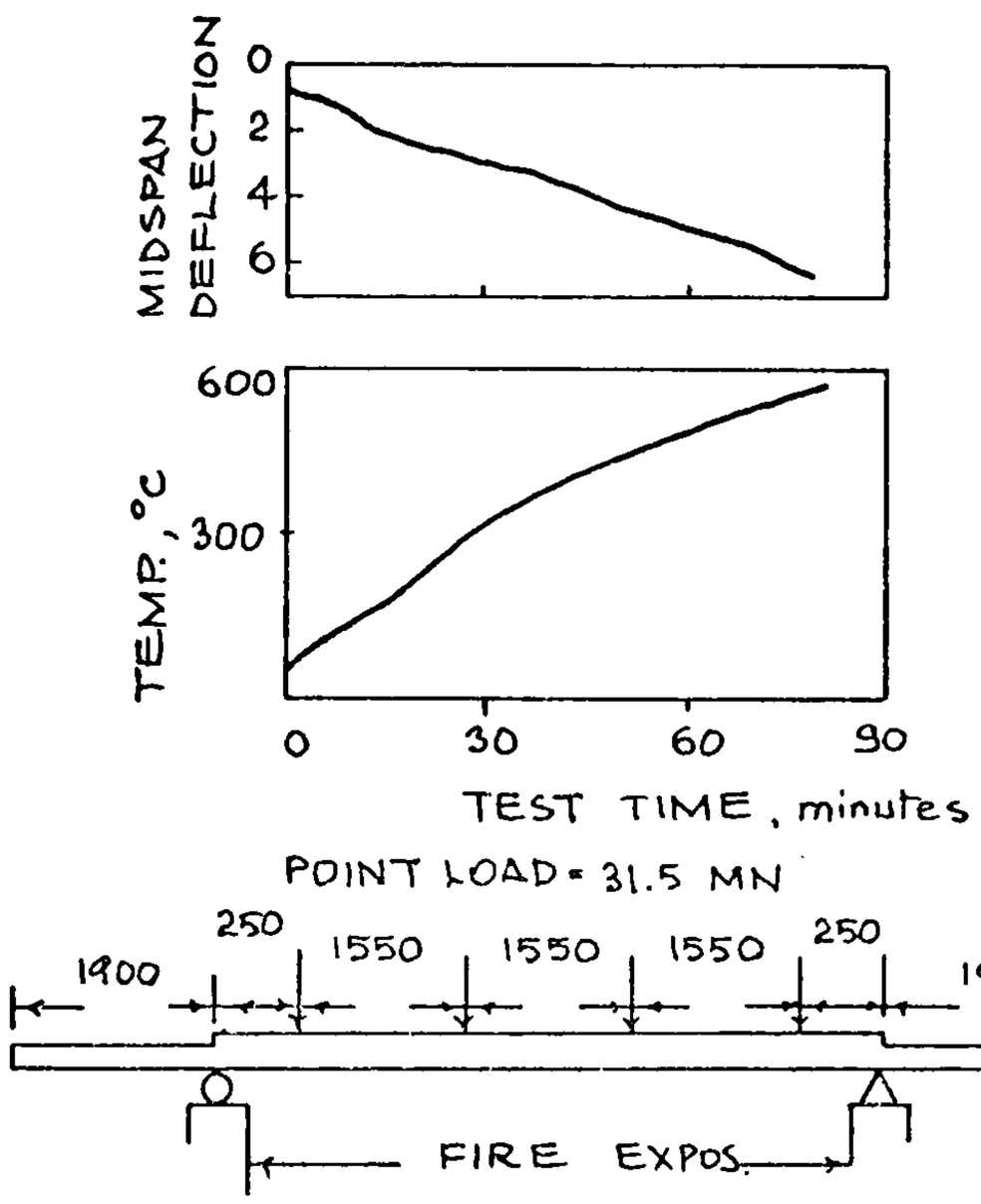

FIG. A.6 DATA ON FIRE TEST OF SPECIMEN TESTED SIMPLY SUPPORTED (PCA TESTS)

[AFTER GUSTAFERRO ,(A.10)]

failure. Supporting this view, tests on restrained steel beams reported by Bletzacker (A.9) exhibited buckling and only slight increase in fire resistance when compared with unrestrained ones. If, however, the induced compressive force is just sufficient to put the entire section in compression, the loss of strength of the reinforcement is not important. In this case the structural end point [x] will be determined by the strength and stability of the concrete member, but, not by the condition of the steel. (Gustaferro (A.10), Dougill (A.8))

A.1.3 Effect of Continuity: Flexural Restraint

Structures that are continuous or otherwise statically indeterminate behave differently, when subjected to fire, from statically determinate ones.

To study the structural behaviour of continuous reinforced concrete beams without longitudinal restraint, Portland Cement Association (PCA) tested beams similar to the one shown in Fig.A.5.

In these tests a specimen was tested as a simply supported beam, that is, the cantilever loads P_1 and P_2

Footnote

+ 'Structural end point' defined by ASTM corresponds to the 'stability criteria for failure' defined by BS 476 : Part 8 : 1972 which states that a beam should be deemed to have failed the stability requirements when the maximum deflection exceeds L/30, where L = clear span.

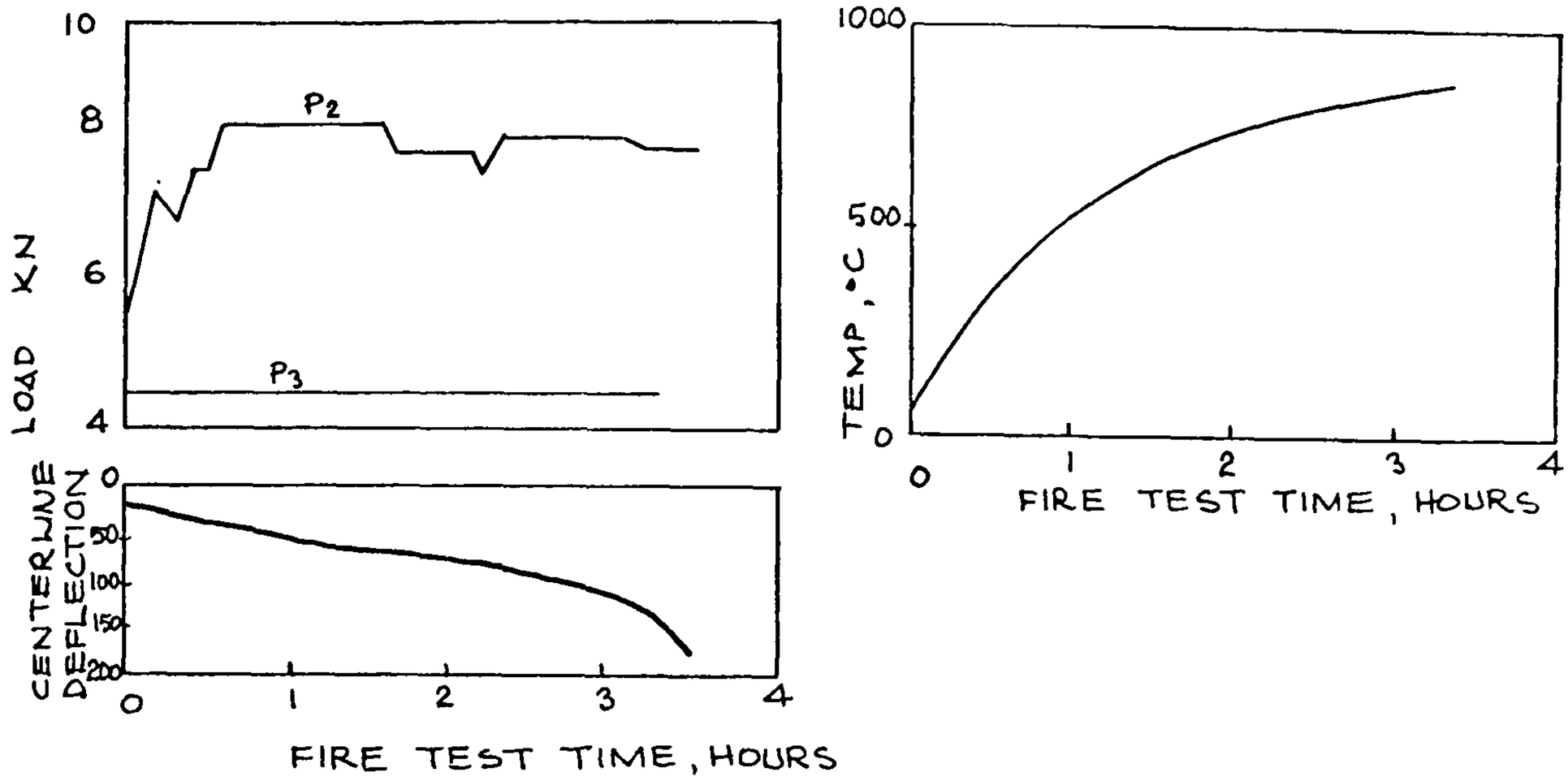

FIG. A.7 DATA ON FIRE TEST SPECIMEN TESTED AS A CONTINUOUS BEAM

[AFTER GUSTAFERRO, (A.10)]

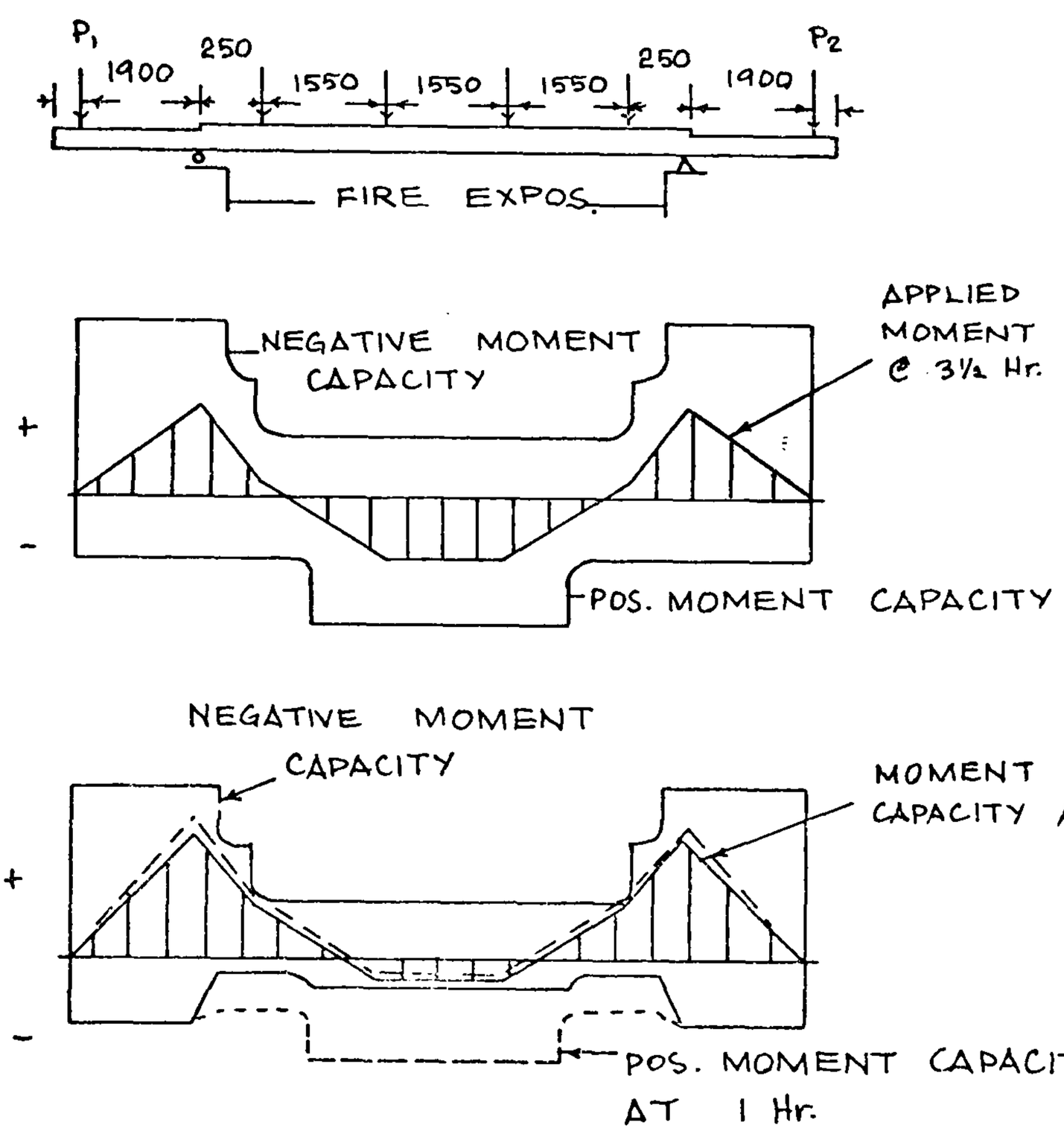

FIG. A.8 BENDING MOMENT DIAGRAMS FOR SPECIMENS TESTED AS A CONTINUOUS BEAM

[AFTER GUSTAFERRO, (A.10)]

in Fig.A.5 were omitted. In addition a similar specimen was tested in such a way as to simulate a fixed ended beam. The latter was tested by maintaining the ends (Points A and B in Fig.A.5) at constant elevation by varying the loads P_1 and P_2. In the first case the test was stopped 1hr 20min. after the start and in the second 3hr 30min. after the start, due to rapidly increasing centre line deflection (Figs, A.6 and A.7).

Bending moment diagrams for specimen 2 (Fig.A8) show how redistribution of moments during the test results in an increase in moment over the supports, and, a decrease in moment over the midspan.

This redistribution is basically beneficial because the reduction in the negative moment capacity at the supports is less than the reduction in the positive moment capacity at midspan as the reinforcement at the supports is further away from the effects of heating.

Therefore the reduction of moment at the midspan more than compensates the detrimental effect of increase of moment over the supports. The compression zone near the supports, on the other hand, should be able to resist the increased compressive stresses because the compressive strength of concrete at temperatures up to 650°C is still relatively high (Weigler and Fischer, A.II)

As a result a better performance in fire is expected from a continuous beam.

Another way of simulating continuity is exercised by Ehm and Von Postel (A.12) who used a stiff cantilever with an external variable force P, varied in such a way

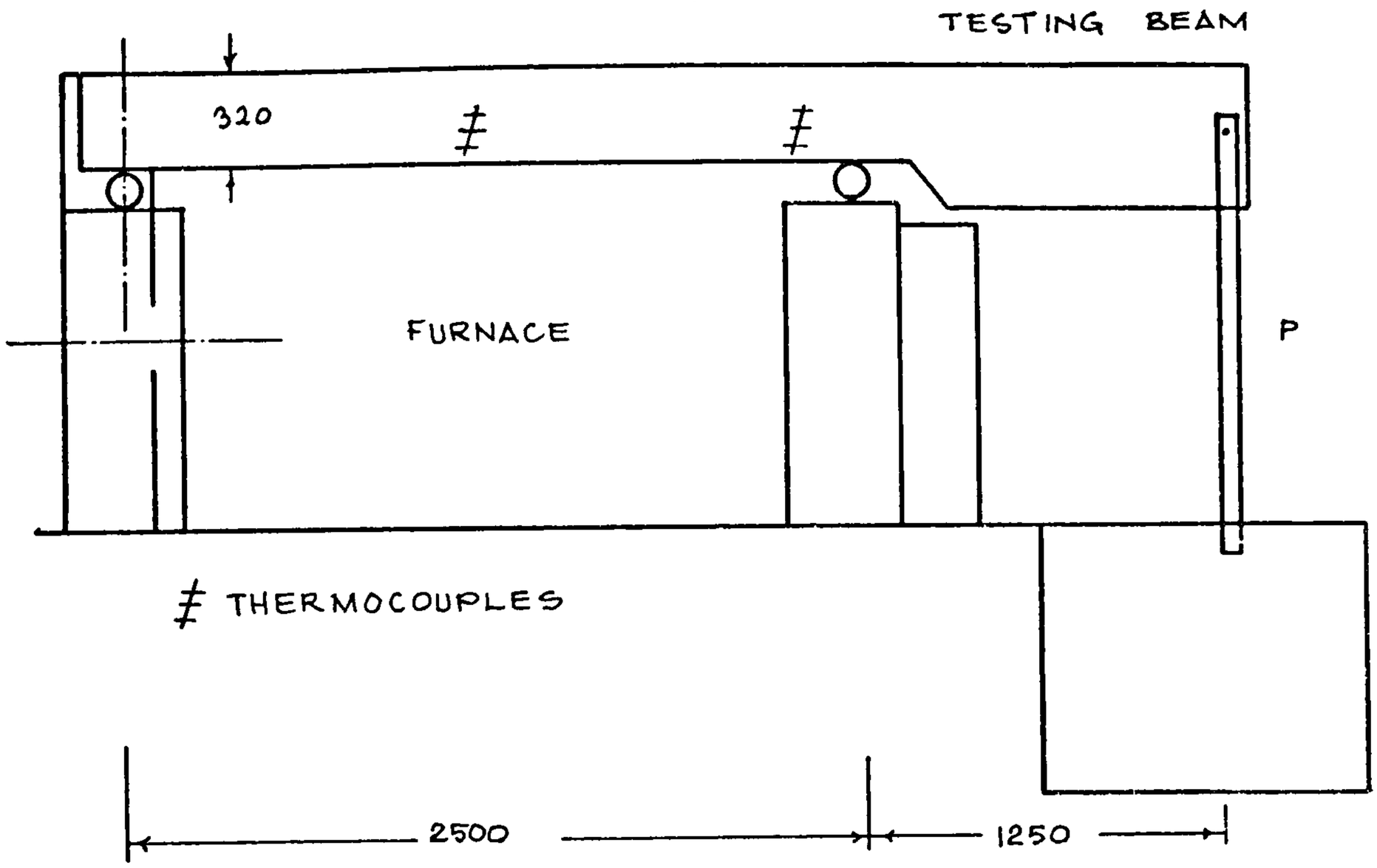

FIG. A.9 TEST ARRANGEMENT FOR A FIRE TEST
[AFTER EHM AND VON POSTEL, (A.12)]

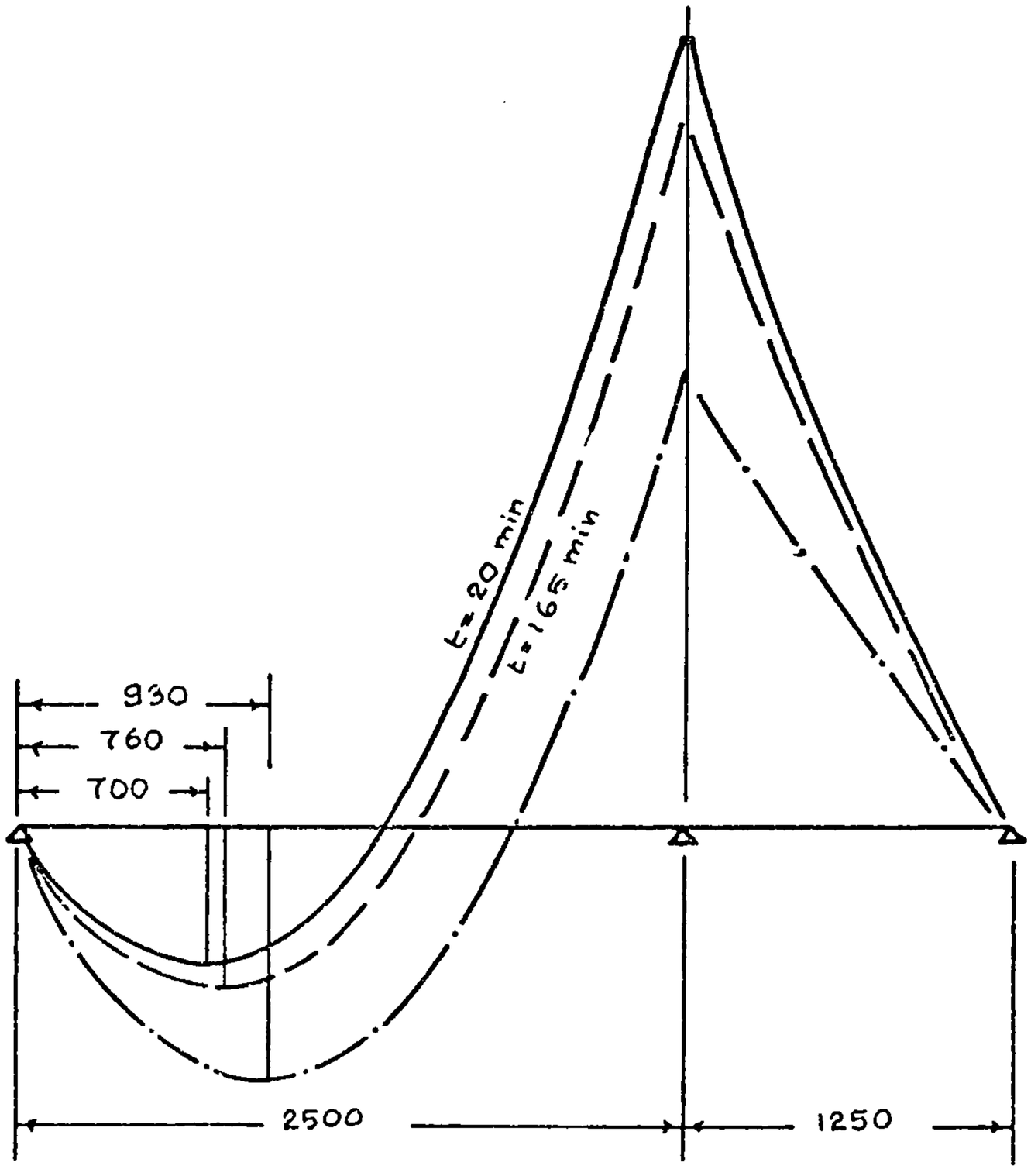

FIG. A.10 MOMENT DISTRIBUTION IN A CONTINUOUS BEAM
[AFTER EHM AND VON POSTEL, (A.12)]

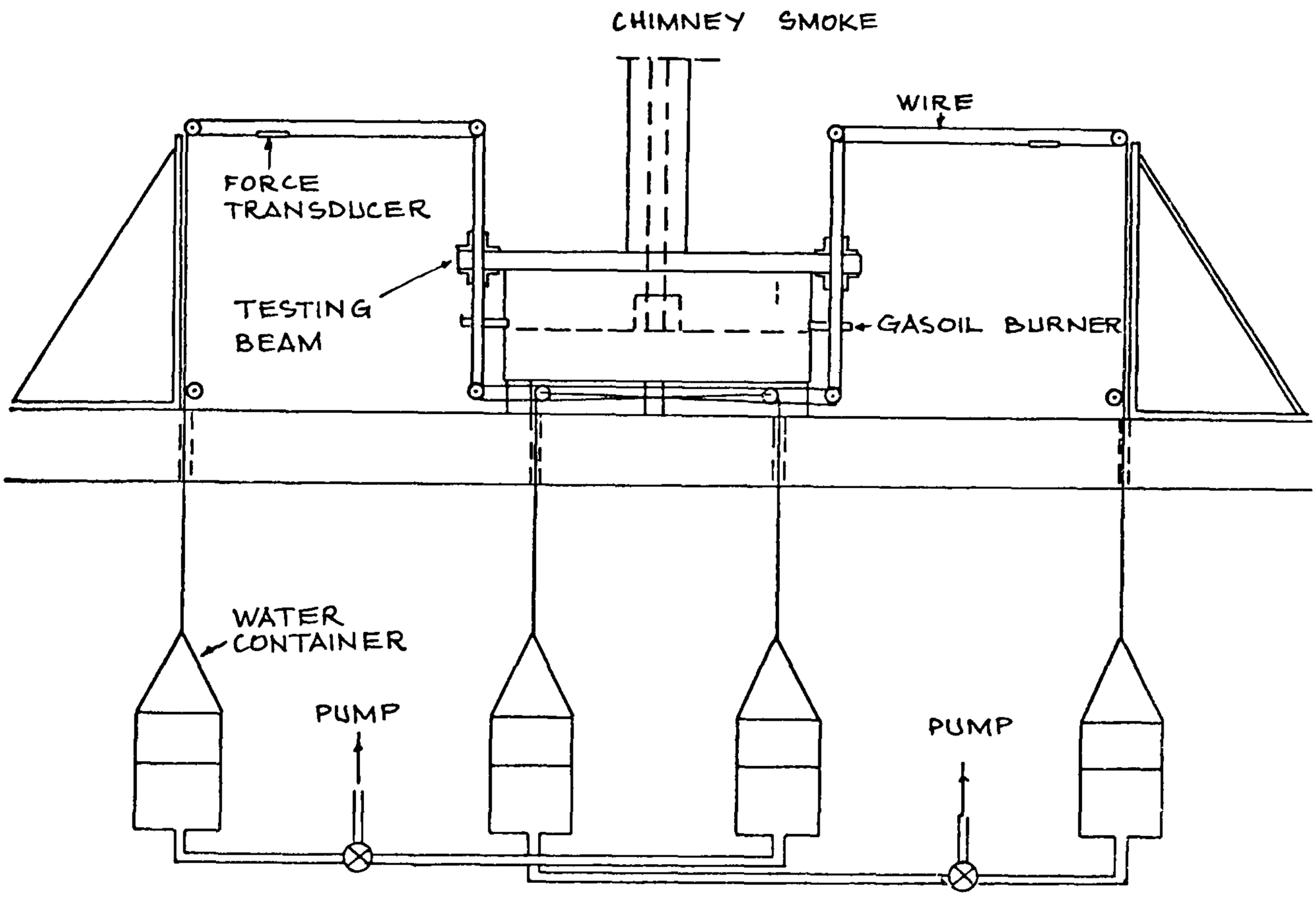

FIG. A.11 TESTING ARRANGEMENT

[AFTER ANDENBERG, (A.13)]

that angular rotation over the right support was prevented during the fire exposure (Fig.A.9). Fig.A.10 shows the reduction in bending moment at the midspan and the increase at the support which is also observed by Gustaferro (A.10). The bending moments in the figure are calculated from the P values corresponding to times 0, 20, 100, and 165 minutes of fire exposure.

Andenberg (A.14) provided continuity by preventing end rotation by the use of applied moment (Fig.A.11) and investigated the behaviour of statically indeterminate reinforced concrete members under different fire processes, loads, and material characteristics.

In none of the experimental work described above has any attempt been made to test continuous beams under longitudinal restraint.

Dougill (A.14) showed theoretically that axial restraint and flexural restraint lead to different modes of failure when applied separately, and a dangerous situation leading to sudden failure may arise if heavy axial restraint and constant flexural restraint are applied simultaneously. In reasonable amounts, however, the combination of restraint and continuity will increase the fire endurance (Gustaferro A.10).

APPENDIX II :

Pressure and Velocity Relationship in Water Flowing in a Cylindrical Tube Under a Pressure Gradient.

Let us considerwater flowing through a cylindrical tube at the ends of which there is a pressure difference p_1. (Fig.A.2.I)

For equilibrium,in steady state conditions,we have,

$$A_1\left(P+\frac{dP}{dx}\right)-PA_1 = 2\pi r\,\tau\,dx \qquad \text{(A.2.I)}$$

where A_1 is the cross sectional area of the tube ,

and,

$$A_1 P_1 = \int_0^x 2\pi r\ \tau\ dx \qquad \text{(A.2.2)}$$

But,

$$\tau = \frac{4\eta v_{cp}}{r} \qquad \text{(A.2.3)}$$

and,

$$A_1 = \pi r^2$$

Therefore ,

$$P_1 = \frac{8\eta v_{cp}}{r^2}\ L \qquad \text{(A.2.4)}$$

or,

$$v_{cp} = \frac{r^2 P_1}{8\eta L} \qquad \text{(A.2.5)}$$

But,

$$N\frac{A_1}{A} = n_s \qquad \text{(A.2.6)}$$

where,N is the number of pores per unit area,and,

n_s is the surface porosity.

Taking A=I,we obtain,

$$A_1 = \frac{n_s}{N} = \pi r^2 \qquad \text{(A.2.7)}$$

or,

$$r^2 = \frac{n_s}{n\pi} \qquad \text{(A.2.8)}$$

Substituting A.2.8 in A.2.5 we obtain,

$$v_{cp} = \frac{n_s P_1}{N\pi 8\eta L} \qquad \text{(A.2.9)}$$

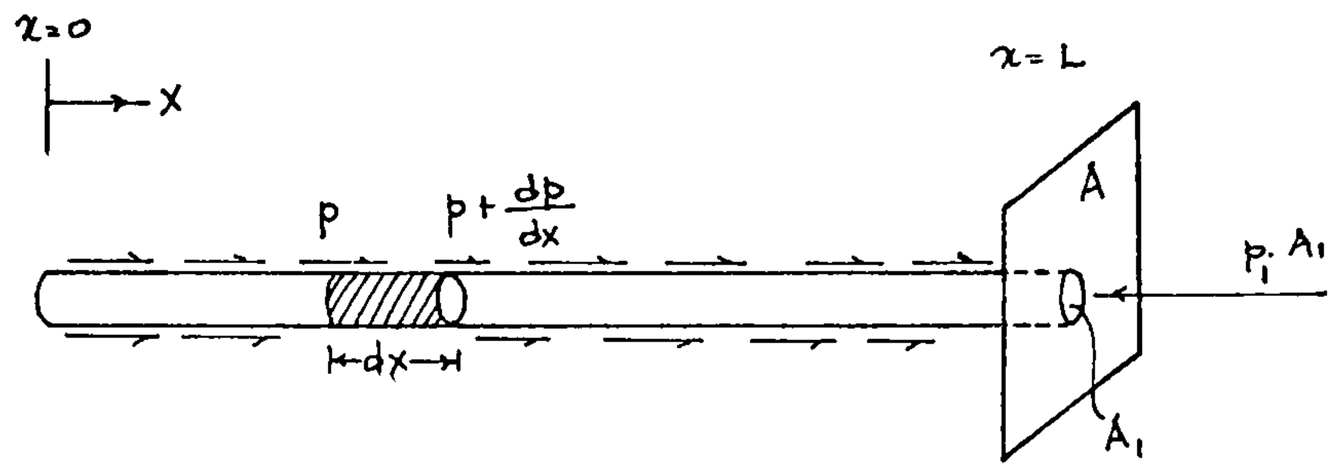

FIG. A.2.1

APPENDIX III:

Gasket Design

Check for Gasket Factor

To overcome the variations in bolt loading under working conditions due to creep and relaxation, "Gasket Factor" is introduced into the flange design to ensure that at all times the bolt loading is sufficient for the gasket to seal efficiently.

The "Gasket Factor" is the ratio of the residual stress on the gasket under operating pressure to that pressure. For design purposes the gasket factor should be taken as 2 or more.

Hence,

$$\text{Gasket factor} = \frac{\text{Total bolt load - Hydraulic pressure}}{\text{Gasket area x Internal pressure}}$$

In Appendix V bolt load is found to be 35001bs.

Therefore,

Total bolt load= (3500)(I2)=420001bs.

Hydraulic end load=Pressure x Area over which the pressure is applied

The barrel was designed for an internal pressure of I000psi and the effective gasket area was found to be I2.7 in^2 (See Appendix V).

Therefore,

$$\text{Gasket factor} = \frac{(42000) - (I000)(\frac{\pi (4.5)^2}{4})}{(I2.7)(I000)} = 2.06$$

$2.06 > 2.0$

Therefore the gasket area available is sufficient for efficient sealing.

APPENDIX IV :

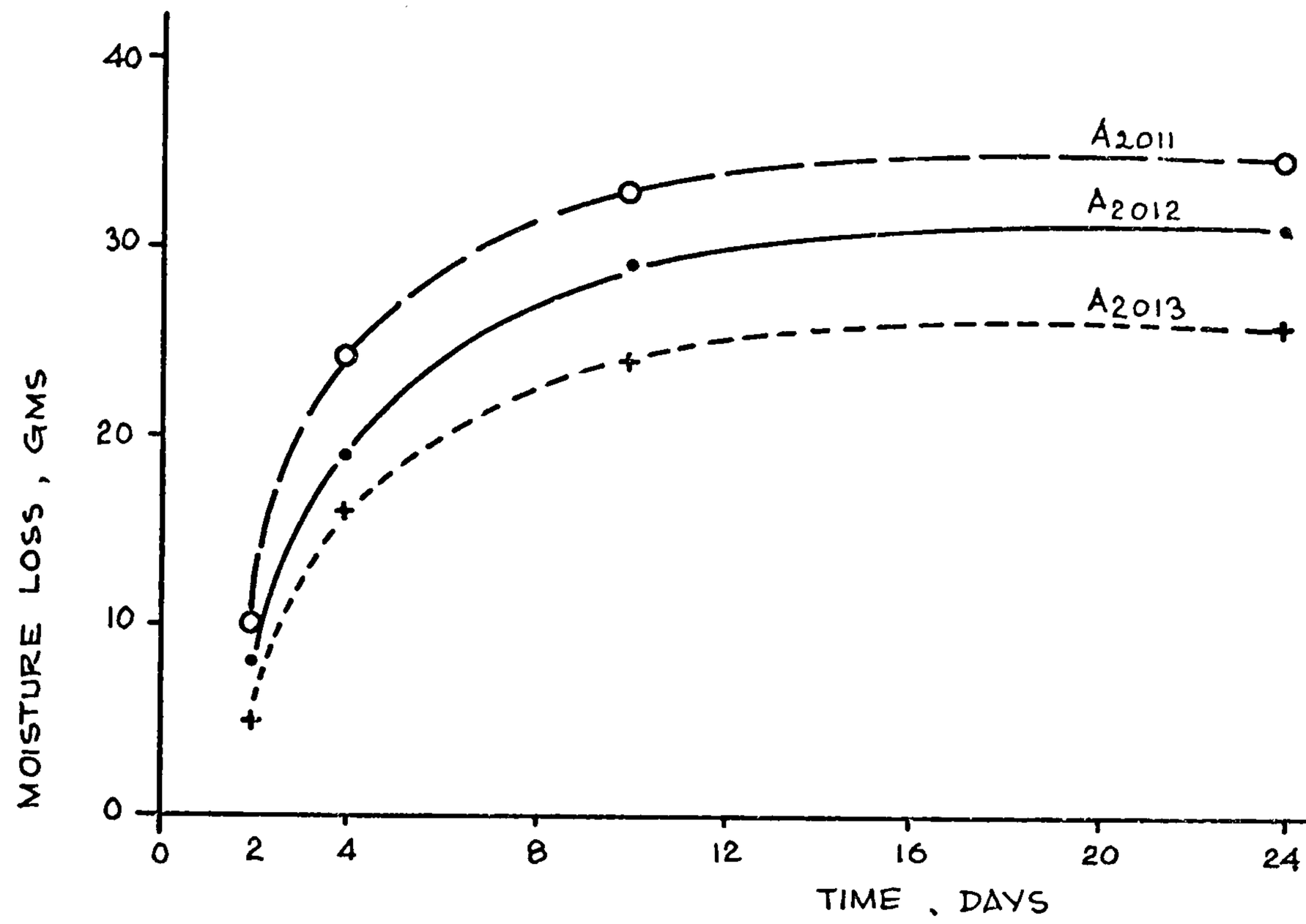

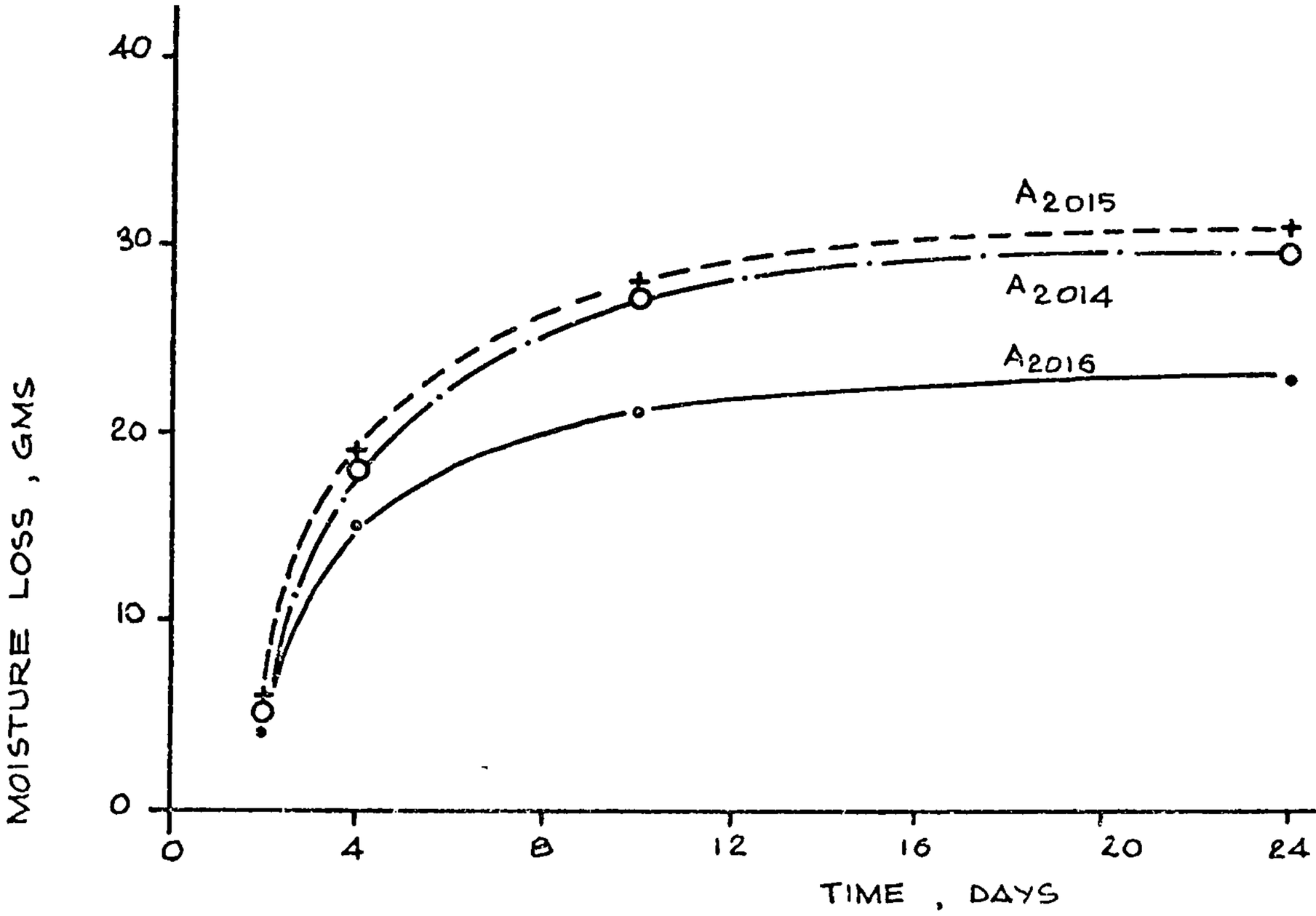

APPENDIX IV WEIGHT LOSS OF SOME TYPICAL SPECIMENS DURING MOIST CURING (BREAK-OUT TESTS)

APPENDIX V:

Determination of Initial Tension on Bolts.

Gasket thickness: I/I6 in(.063in)

Number of bolts: I2

Bolt size : I/2 in.

Method:

Gasket area : $(.92)(2\pi)(2.88) = I6.4\ in^2$

Total bolt area: $I2(.I4I) = I.69\ in^2$

Effective gasket area: $I6.4 - I.69 = I2.7\ in^2$

The load per bolt is found using the following formula as suggested by Faires(A.II):

$$F_i = \frac{S_g A_g}{N_b}$$

where, F_i is the load per bolt, s_g is the apparent flange pressure, A_g is effective gasket area, and N_b is the number of bolts.

Apparent flange pressure for asbestos base materials is s_g = 3300 psi.(Faires, A.II).

Therefore,

$$F_i = \frac{(3300)(12.7)}{12} = 3500 \text{ lbs.}$$

The relation between the applied torque T in-lb, and initial tension ,F_i,(or load per bolt) ,is given by Faires(A.II)as,

$$T = C\ D\ F_i \text{ in-lb}$$

where, D is the nominal bolt size,and C, the torque coefficient.

C is suggested to be 0.2 for nonlubricated gasket materials.(Faires , A.II).

Hence,

$$T = C\ D\ F_i = (.25)\ (.5)\ (3500) = 437 \text{ in-lb} = 54 \text{ N-m}$$

APPENDIX VI :

Sieve Analysis Result

Sieve No.	% retained	Cumulative % passing	B.S.I377
7	I7.I	82.9	60-I00
I4	I4.4	68.5	30-90
25	II.5	57.0	I5-60
52	40.0	I7.0	5-30
I00	I7.2	0.	0-I0

APPENDIX VII :

Properties of the Cement used.

Ordinary Portland Cement:

Chemical Analysis

SiO_2	I9.9
I.R.	.24
Al_2O_3	7.0
Fe_2O_3	2.3
Mn_2O_3	0.04
P_2O_5	0.I2
TiO_2	0.40
CaO	64.6
MgO	I.3
SO_3	2.7
L.O.I.	0.9
K_2O	0.58
Na_2O	0.I9
L.S.F./L.C.F.	96/94
S/A + F	2.I
A/F	3.I
Free lime	I.2

B.S.I2 Physical test results

Setting times

Water %	25.0
Initial (min)	I45
Final (min)	I90

Fineness	
Specific surface, m^2/kg	3I4
Specific gravity	3.II
Expansion ,mm	.5
Compressive strength , $MN/_m2$	
B.S.I2 concrete 3 days	20.5
7 "	29.9
28 "	4I.I

APPENDIX VIII:

Derivation of Governing Equation for "J Integral" Calculation

J^* is given by Rice (7.4) as:

$$J = \int_{\Gamma} \left(W\,dy - T_i \frac{\partial u_i}{\partial x}\,ds \right)$$

we have,

$$T_i \frac{\partial u_i}{\partial x} = T_x \frac{\partial u}{\partial x} + T_y \frac{\partial v}{\partial x}$$

But,

$$\frac{\partial u}{\partial x} = \varepsilon_x$$

Therefore,

$$T_i \frac{\partial u_i}{\partial x} = T_x \varepsilon_x + T_y \frac{\partial v}{\partial x}$$

Considering the counterclockwise path $T_2BOPQRAT$ (See Fig. A.8.1).

For the paths OP and QR there are no tractions T, and dy=0.

Therefore,

$$J_{OP} = J_{QR} = 0$$

For the path PQ, $\sigma_x = 0$, $\tau_{xy} = 0$.

Therefore,

$$W_{PQ} = \frac{1}{2} \sigma_y \varepsilon_y \longrightarrow 0 \qquad \text{as} \quad OP \longrightarrow \infty$$

or,

$$J_{PQ} = \int_P^Q \left(\frac{1}{2} \sigma_y \varepsilon_y\,dy \right) \longrightarrow 0 \quad \text{as } OP \longrightarrow \infty$$

For paths RA and BO, $T_y = 0$, $ds = -dy$, $T_x = -\sigma_x$

Hence

$$J_{RA+BO} = \int_R^A \left(W\,dy - \sigma_x \frac{\partial u}{\partial x}\,dy \right) + \int_o^B \left(W\,dy - \sigma_x \frac{\partial u}{\partial x}\,\partial y \right)$$

Footnote

* See Section 7.3 for definition of J integral.

But, $$\frac{\partial u}{\partial x} = \varepsilon_x$$

Therefore,

$$J_{RA+BO} = \int_R^A (W - \sigma_x \varepsilon_x)\, dy + \int_B^O (W - \sigma_x \varepsilon_x)\, dy$$

But, $$W = \frac{1}{2}\sigma_x \varepsilon_x + \frac{1}{2}\sigma_y \varepsilon_y$$

Therefore,

$$J_{RA+BO} = \frac{1}{2}\int_R^A (\sigma_x \varepsilon_x - \sigma_y \varepsilon_y)\, ds + \frac{1}{2}\int_B^O (\sigma_x \varepsilon_x - \sigma_y \varepsilon_y)\, ds$$

or,

$$J_{RA+BO} = \frac{1}{2}\int_R^A (\sigma_y \varepsilon_y - \sigma_x \varepsilon_x)\, dy + \frac{1}{2}\int_B^O (\sigma_y \varepsilon_y - \sigma_x \varepsilon_x)\, dy$$

$$J_{RA+BO} = \frac{1}{2E}\left(\sigma_y^2 - \sigma_x^2\right)(y_h - y_j)$$

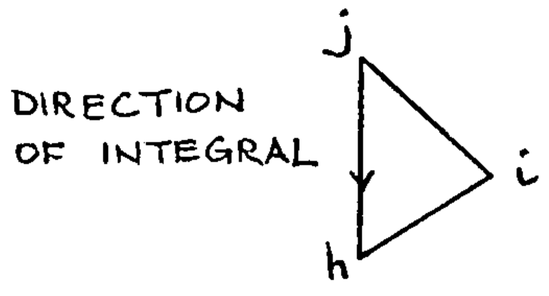

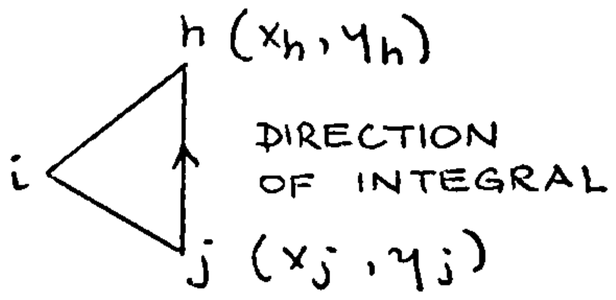

and $J = \Sigma J$ over all boundary elements in RA, BO, and PQ.

For path AT, and T_2B,

dy=0

Hence, $$J = -\int \left(T_x \frac{\partial u}{\partial x} + T_y \frac{\partial v}{\partial x}\right) ds$$

T_x is always zero.

Therefore,

$$J_{AT_1 + T_2B} = -\int T_y \frac{\partial v}{\partial x}\, ds$$

For AT_I, $$T_y = p \quad , \quad \frac{\partial v}{\partial x} = \frac{\partial v}{\partial s}$$

and,

$$J_{AT_1} = -\int_{v_A}^{v_{T_1}} p\, dv = p\,(v_A - v_T)$$

where v_{T_1} and v_A are y displacements at T_I and A respectively.

for T_2B,

$$T_y = -p \quad , \frac{\partial v}{\partial x} = -\frac{\partial v}{\partial s}$$

Therefore,

$$J_{T_2B} = -\int_{V_T}^{V_B} p\, dV = p(V_T - V_B)$$

Hence, assuming $y_{T_1} - y_{T_2} \cong 0$, we have,

$$J_{AT_1+T_2B} = p(V_A - V_B)$$

Also, $$J = J_{RA+BO} + J_{ATB}$$

Therefore,

$$J = \frac{1}{2E}(\sigma_y^2 - \sigma_x^2)(y_h - y_j) + p(V_A - V_B) \qquad \text{(A.8.I)}$$

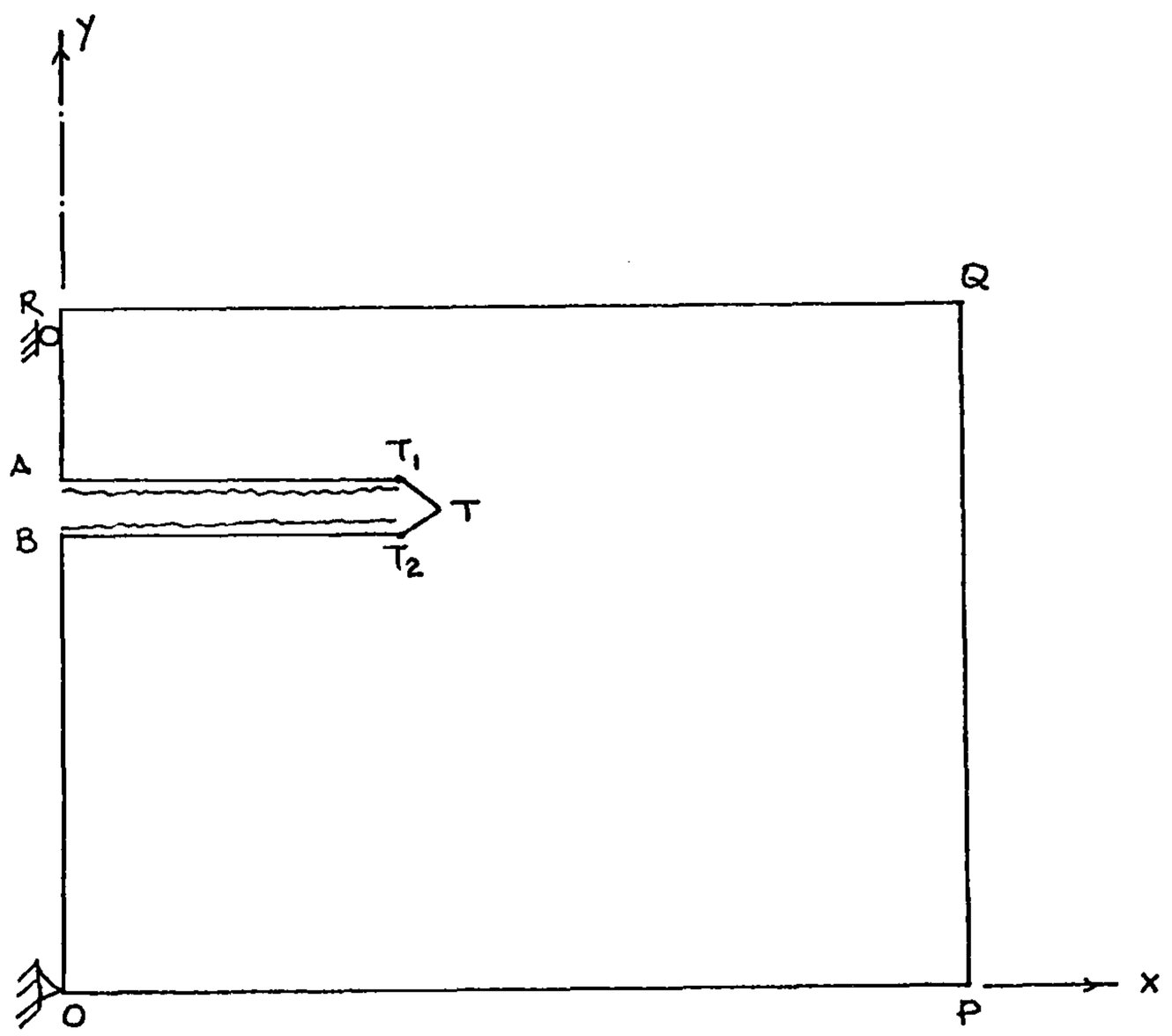

FIG. A.8.1

REFERENCES

PART I : LIST OF WORKS REFERRED TO IN THE TEXT

1.1 BS 476 Fire Tests on Building Materials and Structures. British Standard Specification for Standard Furnace Tests 1932.

1.2 BS 476: Part 8: 1972 Test Methods and Criteria for the Fire Resistance of Elements of Building Construction. 1972.

1.3 ISO/R834 Fire Resistance Tests of Structures. International Organization for Standardization Sept. 1968

1.4 Ingberg S.H., Griffin H.K., Robinson W.C. and Wilson R.E. Fire Tests of Building Columns. U.S.Dept. of Commerce, Bureau of Standards. Tech. Paper No.184 Washington 1921.

1.5 Carlson C.C. and Gustaferro A.H. A Review of Studies of the Effects of Restraint on the Fire Resistance of Prestressed Concrete. Fire Resistance of Prestressed Concrete. Proc. of a Symposium, Braunschweig, Germany pp. 32-42 June 1965.

1.6 Selvaggio S.L. and Carlson C.C. Effect of Restraint on Fire Resistance of Prestressed Concrete. Bult. 164 Research Dept. Portland Cement Assoc. 1963.

1.7 Inst. of Structural Eng. and The Concrete Society. Fire Resistance of Concrete Structures. Report of a Joint Ctte. pp.59 Aug.1975.

1.8 Fire Resistance of Prestressed Concrete. Proc. of an Int. Symposium Braunschweig Germany pp.111 1965.

1.9 Malhotra H.L. Spalling of Concrete. Results of a questionnaire by CIB Commission W14 pp.16 1972.

1.10 Harmathy T.Z. Effect of Moisture on the Fire Endurance of Building Elements ASTM STP 385, pp.74-94 1965.

1.11 Dougill J.W. The Effect of High Temperature on the Strength of Concrete with Reference to Thermal Spalling. Ph.D. Thesis submitted to the University of London pp.421 1971.

1.12 Meyer-Ottens C. Über die Ursachen und Ma Bnahmen zur Verkinderung von Abplatzungen an Beton - Stahlbeton - und Spannbetonbauteilen aus Normalbeton bei Brandbeanspruchung. Ph.D. thesis submitted to Carolo-Wilhelmina University, Germany 1972.

1.13 Saito H. Explosive Spalling of Prestressed Concrete in Fire. Proc. of a Symposium, Braunschweig, Germany pp.80-91 1965.

1.14 Shorter G.W. and Harmathy T.Z. Contribution to the discussion of a paper by L.A.Ashton and S.C.C.Bate. Proc. I.C.E. Vol.20, pp.313-315 1960.

1.15 Akhtaruzzaman A.A. and Sullivan P.J.E. Explosive Spalling of Concrete Exposed to High Temperature. Concrete Structure and Research Report. (Internal Report) Imperial College, London pp.1-24 1970.

1.16 Waubke N.V. Uber einen Physicalischen Gesichtspunkt der Portlandzementbetonen bei Temperaturen bis 1000°C. Heft 2, TU Braunschweig, Germany 1973.

1.17 Christiaange A.E.,Langhorst A. and Gerritse A. Discussion on Fire Resistance of Lightweight Concrete and Spalling. STUVO Report 12 pp.18 1972.

1.18 Dougill J.W. Proposal for Research Programme on Spalling of Concrete. Report submitted to Fire Research Station, Borehamwood 1971

1.19 Bannister J.L. Steel Reinforcement and Tendons for Structural Concrete. Part I: Steel for Reinforced Concrete. Concrete Vol.2, No.7, pp.295-306 1968.

2.1 Malhotra H.L. Spalling of Concrete. Results of a Questionnaire by CIB Commission W14 pp.16 1972.

2.2 ISO/R834 Fire Resistance Tests of Structures. Int. Organization for Standardization. Sept. 1968.

2.3 Barends J.F.B. Abplatzungen und plötzlicher Bruch. Proc. of a Symposium, Braunschweig, Germany p.58. 1965.

2.4 Kordina K. Sécurité et Résistance au Feu des Structures en Béton. Principe du Comportement au Feu du Béton Armé et du Béton Précontraint; expériences, Conséquences sur la Sécurité. Annales de l'Institut Technique du Bâtiment et des Travaux Publics. No.294, pp.22-32 June 1972.

2.5 Ashton L.A. and Bate S.C.C. The Fire Resistance of Prestressed Concrete Beams. Proc. Inst. Civil Eng., Vol.17, pp.15-38. Sept.1960.

2.6 Davey N. and Ashton L.A. Investigations on Building Fires. Nat. Building Studies. Research Paper No.12. Part V pp.273 1953.

2.7 Meyer-Ottens C. Zur Frage der Abplatzungen an Betonbauteilen aus Normalbeton bei Brandbeanspruchung. Braunschweig Technical University. Heft 23, Germany. pp.89. 1972.

2.8 Meyer-Ottens C. Über die Ursachen und Maßnahmen zur Verkinderung von Abplatzungen an Beton - Stahlbeton - und Spannbetonbauteilen aus Normalbeton bei Brandbeanspruchung Ph.D. thesis submitted to Carolo-Wilhelmina University, Germany 1973.

2.9 Christiaange A.E.,Langhorst A. and Gerritse A. Discussion on Fire Resistance of Lightweight Concrete and Spalling. STUVO Report 12 pp.18 1972.

2.10 Meyer-Ottens C. Abplatzungsversuche. Proc. of an Int. Symposium, Braunschweig,Germany pp.59-66 1965.

2.11 Meyer-Ottens C. Verhalten von Betonbauteilen im Brandfall. Beton No.4, pp.133-136 and No.5, pp175-178 1974.

2.12 Meyer-Ottens C. Die Widerstandsfahigkeit von Biegebeanspruchten Stahlbeton und Spannbeton-bauteilen gegen Feuer. Bauwirtschaft. Heft 6/17 Feb.1963.

2.13 Meyer-Ottens C. Abplatzversuche an Prufkörpern aus Beton, Stahlbeton und Spannbeton bei verschiedenen Temperaturbeanspruchungen. Deutscher Ausschuss für Stahlbeton. Heft 241 1974.

2.14 DIN 4102 Brandverhalten von Baustoffen und Bauteilen. 1970.

2.15 Dougill J.W. Modes of Failure of Concrete Panels Exposed to High Temperatures. Mag. of Concrete Research. Vol.24 No.79 pp.71-76 1972.

2.16 Dougill J.W. Conditions for Instability in Restrained Concrete Panels Exposed to Fire. Mag. of Concrete Research. Vol.24 No.80 1972.

2.17 Harmathy T.Z. Effect of Moisture on the Fire Endurance of Building Elements. ASTM, STP 385 pp.74-94 1965.

2.18 Gustaferro A.H. and Carlson C.C. An Interpretation of Results of Fire Tests of Prestressed Concrete Building Components. Journal of the Prestressed Concrete Inst. Vol.7 No.5 pp.14-22 1962.

2.19 Akhtaruzzaman A.A. and Sullivan P.J.E. Explosive Spalling of Concrete Exposed to High Temperature. Concrete Structure and Research Report (Internal Report) Imperial College, London pp.1-24 1970.

2.20 Nekrasov K.D.,Zhukov V.V. and Shevchenko V.I. Investigation of Heating Large Blocks of Refractory Concrete from one side. (in Russian) Trans. from Ognenpory No.6 pp.21-26 June 1967.

2.21 Thelandersson S. Mechanical Behaviour of Concrete under Torsional Loading at Transient High-Temperature Conditions. Bult. 46, Lund Inst. of Technology, Lund, Sweden pp.81 1974.

3.1 Shorter G.W. and Harmathy T.Z. Contribution to the discussion of a paper by L.A.Ashton and S.C.C.Bate. Proc. Inst. of Civil Eng. Vol.20 pp.313-315 1960

3.2 Harmathy T.Z. Effect of Moisture on the Fire Endurance of Building Elements. ASTM STP385 pp.74-94 1965.

3.3 Arnold E. UK Steam Tables in SI Units. pp.161 1970

3.4 Dougill J.W. The Effects of High Temperature on the Strength of Concrete with Reference to Thermal Spalling. Ph.D. thesis submitted to the University of London 1971

3.5 Nekrasov K.D.,Zhukov V.V. and Shevchenko V.I. Investigation of Heating Large Blocks of Refractory Concrete from one side. (in Russian) Trans. from Ognenpory No.6 pp.21-26 June 1967.

3.6[x] Therzaghi K. Die Wirksame Flachenporositat des Betons. Zeitschr. des Osterreicht Architektur und ingenieur Ver. pp.1-25 1934.

3.7 Leliavsky S. Uplift in Gravity Dams. McGraw-Hill Book Co. 1958.

3.8 McHenry D. The Effect of Uplift Pressure on the Shearing Strength of Concrete. Proc. of 3rd Congress on Large Dams. Stockholm, Sweden. pp.329-347 1948.

3.9 Meyer-Ottens C. Zur Frage der Abplatzungen an Betonbauteilen aus Normalbeton bei Brandbeanspruchung. Braunschweig Technical University Heft 23 Germany pp.89 1972.

Footnote

x Not read, but referred to by Leliavsky (3.7) who gave a detailed summary of the work.

3.10 Waubke N.V. Transportphanomene in Betonporen. Braunschweig Technical University Heft 6 Germany pp.76 1966.

3.11 Neville A.M. Properties of Concrete. Pitman Publishing Ltd. pp.687 1975.

3.12 Powers T.C.,Copeland L.E. and Mann H.M. Capillary Continuity and Discontinuity in Cement Pastes. Journal of PCA Research and Development Labs. pp.38-48 1959.

3.13 Zhukov V.V. Explosive Failure of Concrete During a Fire. (in Russian) Tran. held by Fire Research Station, London. Trans. No.DT 2124 pp.10 1975.

4.1 Meyer-Ottens C. Zur Frage der Abplatzungen an Betonbauteilen aus Normalbeton bei Brandbeanspruchung. Braunschweig Technical University. Heft 23 Germany pp.89 1972.

4.2 Robinson G.S. The Failure Mechanism of Concrete with Particular Reference to the Biaxial Compressive Strength. Ph.D. thesis submitted to the University of London 1964.

4.3 Bresler B. and Pister K.S. Failure of Plain Concrete Under Combined Stresses. Trans. of ASCE Vol.122 pp.1049-60 1957.

4.4 McHenry D and Karni J. Strength of Concrete Under Combined Tensile and Compressive Stress. Journal of ACI Vol.54 pp.829-839 1958.

4.5 Robinson G.S. Behaviour of Concrete in Biaxial Compression. Proc. of ASCE pp.71-85 1967.

4.6 Kupfer H.,Hilsdorf H.K. and Rusch H. Behaviour of Concrete Under Biaxial Stresses. Proc. ACI Vol.66 pp.656-666.

4.7 Hobbs D.W. Strength and Deformation Properties of Plain Concrete Subject to Combined Stress Part 3: Results Obtained on a Range of Flint Gravel Aggregate Concretes. Technical Report 42497 pp.19 1974.

4.8 Hsu T.T.C.,Slate F.O.,Sturman G.M. and Winter G. Microcracking of Plain Concrete and the Shape of the Stress-Strain Curve. Journal of the ACI Proc. Vol60 No.2 pp.209-224 1963.

4.9 Spooner D.C. Progressive Damage and Energy Dissipation in Concrete in Uniaxial Compression. Ph.D. thesis submitted to the University of London 1975.

4.10 Newman K. The Structure and Engineering Properties of Concrete. Theory of Arch Dams: Proc. of an Int. Symposium, Southampton 1964 Ed. J.R.Rydzewski, Oxford. Peramon press pp.683-712. 1965.

4.11 Spooner D.C. and Dougill J.W. A Quantitative Assessment of Damage Sustained in Concrete During Compressive Loading. Mag. of Concrete Research. Vol.27 No.92 pp151-160 1975

4.12 Dougill J.W. A Mathematical Model of the Failure of Cement Paste and Mortars. Mag. of Concrete Research Vol.19 No.60 pp.135-142 1967.

4.13 Dougill J.W. Further Consideration of a Mathematical Model for Progressive Fracture of a Heterogeneous Material. Mag. of Concrete Research Vol.23 No.74 pp.5-10 1971.

4.14 Dougill J.W. and Burt N.J. Progressive Failure of Random Network Structures. Paper presented at the Int. Conf. on Fracture Munich April 1973 Paper VI - 422.

4.15 Dougill J.W. Modes of Failure of Concrete Panels Exposed to High Temperatures. Mag. of Concrete Research Vol.24 No.79 pp.71-76 June 1972.

5.1 Harmathy T.Z. Effect of Moisture on the Fire Endurance of Building Elements. ASTM STP 385 pp.74-94 1965.

5.2 Meyer-Ottens C. Über die Ursachen und Maßnahmen zur Verhinderung von Abplatzungen an Beton-, Stahlbeton-, und Spannbeton bauteilen aus Normalbeton bei Brandbeanspruchung. Ph.D. thesis submitted to Carolo-Wilhelmina University Germany 1973.

5.3 Zhukov V.V. Explosive Failure of Concrete During a Fire. (in Russian) Tran. held by Fire Research Station London. Trans No. DT 2124 pp.10 1975.

7.1[x] Inglis C.E. Inst. Naval Architects Trans. Vol.55 No.219 1913.

7.2[x] Griffith A.A. Phil. Trans. of Royal Soc. London 221A No.163 1920

7.3 Irwin G.R. Handbuck der Physik. Vol6 p.551 Springer, Berlin 1958.

7.4 Rice J.R. A Path Independent Integral and the Approximate Analysis of Strain Concentration by Notches and Cracks. Trans. of the ASME Journal of Applied Mechanics. pp.379-386 June 1968.

Footnote

x Not read, but detailed treatment given by Lange F.F.

8.1 Meyer-Ottens C. Zur Frage der Abplatzungen an Betonbauteilen aus Normalbeton bei Brandbeanspruchung. Braunschweig Technical University Heft 23 Germany pp.89 1972.

8.2 Harmathy T.Z. Effect of Moisture on the Fire Endurance of Building Elements. ASTM STP 385 pp.74-94 1965.

8.3 Schmidt E. Properties of Water and Steam in S I Units. pp.205 1969.

9.1 Dougill J.W. Proposal for Research Programme on Spalling of Concrete. Report submitted to Fire Research Station, London 1971

9.2 Saemann J.C. and Washa G.W. Variation of Mortar and Concrete Properties with Temperature. ACI Journal Proc Vol.54 No.5 pp 385-396 Nov.1957.

A.1 BS 476: Part 8: 1972 Test Methods and Criteria for the Fire Resistance of Elements of Building Construction. 1972.

A.2 ASTM Part 18 1975 Fire Tests of Building Constructions and Materials. 1975.

A.3 ISO/R834 Fire Resistance Tests of Structures. Int. Orgn. for Standardization. Sept 1968

A.4 Selvaggio S.L. and Carlson C.C. Effect of Restraint on Fire Resistance of Prestressed Concrete. Bult. 164 Research Dept. Portland Cement Assoc. 1963.

A.5 Carlson C.C. and Gustaferro A. Review of Studies of the Effect of Restraint on the Fire Resistance of Prestressed Concrete. Proc. of Symposium at Braunschweig, Germany pp.32-42 June 1965.

A.6 Issen L.A.,Gustaferro A.H. and Carlson C.C. Fire Tests on Concrete Members: An Improved Method for Estimating Thermal Restraint Forces. Fire Test Performance ASTM STP 464 pp.153-185 1970.

A.7 Gustaferro A.H. and Carlson C.C. An Interpretation of Results of Fire Tests of Prestressed Concrete Building Components. Journal of the Prestressed Concrete Inst. Vol.7 No.5 1962.

A.8 Dougill J.W. Contribution to the discussion of a paper by Issen et al. Fire Test Performance STP 464 pp.180,182 1969.

A.9 Bletzacker R.W. Fire Resistance of Protected Steel Beam Floor and Restraint and Smoke. ASTM STP 422 pp.63-92 1966.

A.10 Gustaferro A.H. Temperature Criteria at Failure. Fire Test Performance, ASTM STP 464 pp.68-84 1970

A.11 Weigler H. and Fischer R. Behaviour of Concrete at High Temperature Above 100°C on the Compressive Strength of Concrete. (in German with English summary) Deutscher Ausschuss für Stahlbeton Heft 164 pp.1-8 1964

A.12 Ehm H. and Von Postel R. Versuche an Stahlbeton-konstruktionen mit Durchlaufwirkung unter Feuerangeriff. Proc. of an Int. Symposium Braunschweig, Germany pp. 24-32 1965

A.13 Andenberg Y. Fire Exposed Hyperstatic Concrete Structures Document DI. The Swedish Council for Building Research. Lund Inst. of Technology Lund Sweden pp. 1-76 1973

A.14 Dougill J.W. Conditions for Instability in Restrained Concrete Panels Exposed to Fire. Mag. of Concrete Research Vol.24 No.80 pp.139-148 1972

A.15 Faires V.M. Design of Machine Elements. Collier-Macmillan International editions. 4th edition. 1970

REFERENCES :PART II

Literature not referred to in the text .

Abrams M.S. and D.L.Orals. Concrete drying methods and their effect on fire resistance. ASTM , SP 385 I965.

Becker J.,B.Bresler, and H.Bizri. Reinforced concrete frames in fire environments.ASCE National structural engineering meeting. Meeting preprint 2250,April I974.

Browne R.D. Thermal movement of concrete. "Concrete", pp.5I-53, November I972.

Bucci R.J.,P.C.Paris,J.D.Landes,J.R.Rice. J integral estimation procedures. Proc. of the National Symposium on fracture mechanics,Part II, ASTM, STP 5I4,I97I.

Bushev,V.S. et al.Fire Resistance of Buildings. (translated from Russian),Edited by Fire Research Station,published by National Lending Library,pp.44-68, I966.

Cruz C.R. Elastic Properties of Concrete at High Temperatures. Journal of PCA, Research and Development Labs.,Vol.8, No.I,I966.

Dixon J.R. and L.P.Pook. Stress Intensity Factor Calculated Generally by the Finite Element Technique. "Nature", Vol.224,No.52I5,pp.I66-I67,I969.

Dougill J.W. and P.J.E.Sullivan.A Furnace and Loading Rig for Testing Small Concrete Beams at High Temperatures. MCR,Vol.25,No.82,pp.47-52, I973.

Dougill J.W. Some Effects of Thermal Volume Changes on the properties and Behaviour of Concrete. Proc.of International Conference on the structure of concrete.

Paper I2,ppI6,I965.

Dougill J.W. Fire Resistance of Concrete Structures Materials Aspects of Behaviour in Compression. Paper presented at the Jubilee Confr. on Structural Design for Fire Resistance ,University of Aston, Birmingham, September I975.

Dougill J.W. The Relevance of the Established Method of Structural Fire Testing to Reinforced Concrete. Applied Materials Research,Vol.5,No.4,pp.235-240,I966.

Figg J.W. Methods of Measuring the air and Water permeability of Concrete. MCR Vol.25.No.85,pp.2I3-2I9, I973.

Gustaferro A.H. Temperature Criteria at Failure. Fire Test Performance,ASTM STP 464,pp68-84,I970.

Hansen T. and Ericsson J. Temperature Change Effect on Behaviour of Cement Paste,Mortar,and Concrete Under Load. Proc. ACI,Vol.63,No.4,I966.

Harmathy T.Z. Determining Moisture Content and Calculating its Effect on Fire Endurance.National Research Council of Canada,Division of Building Research,Fire Study NO.I7, I967.

Harmathy T.Z. Experimental Study on Moisture and Fire Endurance . Fire Technology,Vol.2,pp.52-59,I966.

Harmathy T.Z. and J.E.Berndt. Hydrated Portland Cement and Lightweight Concrete at Elevated Temperatures. ACI Journal,Vol.63,No.I,pp.93-II2,I966.

Harmathy T.Z. Deflection and Failure of Steel Supported

Floors and Beams in Fire.Test Methods,Restraint and Smoke.ASTM STP 422,I966.

Harmathy T.Z. A Treatise on Theoretical Fire Endurance Rating. Fire Test Methods,ASTM STP 30I,p.IO,I96I.

Harmathy T.Z. Variable State Method of Measuring the Thermal Properties of Solids. Journal of Applied Physics, Vol.35,p.II90,I964.

Harmathy T.Z. and J.E.Berndt. Hydrated Portland Cement and Lightweight Concrete at Elevated Temperatures.ACI, Vol.38,Proc.63,pp.93-II2,I966.

Harmathy T.Z. and T.T.Lie. Fire Test Standard in the Light of Fire Research. Fire Test Performance,ASTM STP 464, pp.85-97,I970.

Hobbs D.W. Strength and Deformation Properties of Plain Concrete Subject to Combined Stress. Technical Report, C&CA, No.42,497,I974.

Hundt J. and P.Schimmelwitz. Heat and moisture transfer in Concrete under the Effect of a Temperature Gradient. Preprints of the 2nd International Conference on Structural Mechanics in Reactor Technology,Vol.6A Commission of the European Communities,Brussels, Paper No.h6/I,p.7,I973.

Issen L. Scaled Models in Fire Research on Concrete Structures. Journal of PCA,Research and Development Labs pp.IO-26,I966.

Kaplan M.F. Crack Propagation and the Fracture of Concrete.

Proc. ACI,Vol.58,No.5,pp.591-610,1961.

Lankard D.R. et al. Effects of Moisture Content on the Structural Properties of Portland Cement Concrete Exposed to Temperatures up to 500 °C . ACI STP 25. 1971.

Malhotra H.L. The Effect of Temperature on the Compressive Strength of Concrete. MCR, Vol.8,No.23,pp.85-93,1956.

Malhotra H.L. Fire Resistance of Structural Concrete Beams. Fire Research Note No.741,Fire Research Station, pp.1-41,1969.

Malhotra H.L. Fire Resistance of Encased Steel Stanchions. Proc. Institution of Civil Engineers,Vol.27,pp.77-98.

Malhotra H.L. The Meaning of Fire Resistance Tests. Preprints of Institution of Structural Engineers Jubilee Conference,Univ.of Aston,Birmingham,pp.92-114, September 1975.

Malhotra H.L. New Concepts in Structural Fire Protection. Preprints of Institution of Structural Engineers Jubilee Conference,Univ.of Aston,Birmingham,pp.201-213. September 1975.

Parker T.W. and R.W.Nurse. Investigations on Building Fires. Part I. The Estimation of the Maximum Temperature Attained in Building Fires from Examination of the Debris. National Building Studies,Technical Paper No.4, 1950.

Spooner D.C. and Dougill J.W. A Quantitative Assessment of Damage Sustained in Concrete During Compressive

Loading.MCR,Vol.27,No.92,pp.I5I-I6I, I975.

Sullivan P.J.E. and M.P.Poucher. The Influence of Temperature on the Physical Properties of Concrete and Mortar in the Range 20-400°C. ACI SP-25,I968.

Woodside W. Water Vapour Permeability of Porous Media. Canadian Journal of Physics,Vol.37,No.4,pp.4I3-I6, I959.